EPSC2017

TP8 abstracts

EPSC Abstracts
Vol. 11, EPSC2017-11, 2017
European Planetary Science Congress 2017

Search for HBr and bromine photochemistry on Venus

Vladimir A. Krasnopolsky (1), Denis A. Belyaev (2)
(1) Moscow Institute of Physics and Technology (PhysTech), Russia, (2) Space Research Institute, Moscow, Russia
(vlad.krasn@verizon.net)

Please make sure that your pdf conversion results in a document with a page size of 237 x 180 mm!

Abstract

Search for the strongest HBr line at 2605.8/6.2 cm^{-1} using NASA IRTF and CSHELL spectrograph with resolving power of 4×10^4 resulted in an upper limit to the HBr mixing ratio of 1 ppb at 78 km. A simplified version of the bromine photochemistry is included into the photochemical model by Krasnopolsky (2012). Photolysis of HBr and its reactions with O and H deplete the HBr mixing ratio at 70-80 km relative to that below 60 km by a factor of ≈300. Reanalysis of the observational data with the calculated profile of HBr gives an upper limit of 20-70 ppb for HBr below 60 km and the aerosol optical depth of 0.7 at 70 km and 3.84 μm. The bromine chemistry may be effective on Venus even under the observed upper limit. However, if a Cl/Br ratio in the Venus atmosphere is similar to that in the Solar System, then HBr is ≈1 ppb in the lower atmosphere and the bromine chemistry is insignificant. Thermodynamic calculations based on the chemical kinetic model (Krasnopolsky 2013) predict HBr as a major bromine species in the lower atmosphere.

1. Introduction

The high temperature near the surface of Venus stimulates reactions between the rocks and atmospheric species that release HCl and HF, which looked unexpected and exotic when they were detected by Connes et al. (1967). No attempts have been made to search for HBr, and the only relevant result is an upper limit of 0.2 ppb to Br_2 near 15 km from the Venera 11 and 12 descent probes (Moroz et al. 1981). Search for HBr is the subject of this work.

2. Observations and analysis

We chose for our study the strongest line R2 of the fundamental band of HBr at 2605.8/6.2 cm^{-1}. Though the line is strong, it is weaker than the similar HCl and HF lines by factors of 8 and 36, respectively.

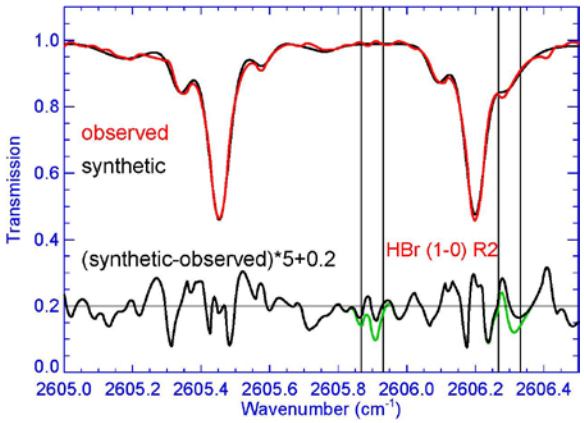

Fig. 1. Observed and synthetic spectra of Venus at the equator. Vertical lines show resolution elements at the expected positions of the Doppler-shifted HBr lines. The black line near the bottom shows a difference between the synthetic and observed spectra scaled by a factor of 5. The green line is for HBr = 10 ppb.

Venus was observed in July 2015 using NASA IRTF and a long-slit spectrograph CSHELL with resolving power of 4×10^4. We used our standard tools for observations and processing of the observed spectra. 101 spectra along the slit that crossed the bright crescent of Venus were analyzed and compared with best-fit synthetic spectra. A spectrum observed near the equator is shown in Fig. 1. The synthetic spectra were calculated in Fig. 1 for the best fit with HBr near zero and for HBr = 10 ppb, and the latter is close to the detection limit for an individual spectrum. Combinations of the HBr and CO_2 lines provide mixing ratios of HBr that refer to 78 km. Retrievals for all 101 spectra are shown in Fig. 2. The values scatter between -8 and 5 ppb with a mean value of -1.2 ppb and standard deviation of 2.5 ppb. According to the Gauss statistics, uncertainty of the mean of 101 values is smaller by a factor of 10 and equal to 0.25 ppb. Our observations result in an upper limit of 1 ppb for HBr at 78 km on Venus.

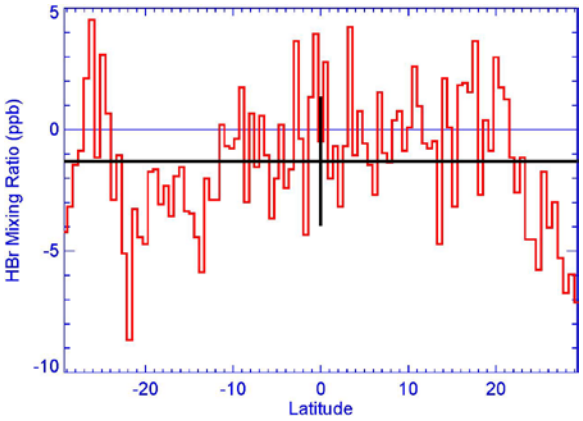

Fig. 2. HBr mixing ratio in the observed 101 spectra of Venus. The mean value and standard deviation are shown by black solid lines.

3. Possible HBr photochemistry

Quantitative assessment of the HBr chemistry on Venus is made by inclusion of ten major photochemical reactions of bromine (Table) into the photochemical model by Krasnopolsky (2012) and assuming HBr = 10 ppb below 60 km.

Table. Column rates (CR) of bromine reactions

#	Reaction	CR	CR (Cl)
1	HBr + *hν* → H + Br	3.27+10	9.46+10
2	HBr + O → Br + OH	1.15+10	1.60+9
3	HBr + H → Br + H_2	1.30+10	2.31+9
4	H + Br + M → HBr + M	1.47+10	-
5	Br + HO_2 → HBr + O_2	4.12+10	6.71+10
6	Br + O_3 → BrO + O_2	2.16+12	6.89+12
7	BrO + O → Br + O_2	4.35+11	3.50+12
8	BrO + NO → Br + NO_2	1.73+12	4.22+12
9	Br + Br + M → Br_2 + M	1.04+14	1.64+13
10	Br_2 + *hν* → Br + Br	1.04+14	3.18+13

3.27+10 = 3.27×10^{10} cm^{-2} s^{-1}. CR (Cl) is the column rate of the similar Cl reaction in the model by Krasnopolsky (2012)

Photolysis of HBr and its reactions with O and H strongly deplete the HBr mixing ratio above 65 km (Fig. 3). The fast photolysis of Br_2 and the reactions of BrO with O and NO convert these species to Br, which dominates above 67 km. The most significant effect of the bromine chemistry is in the production of H_2 (reaction 3), which exceeds that without Br by a factor of 5, and in the production of O_2, which is a third of that without Br.

Our upper limit of 1 ppb at 78 km is applicable to the uniform distribution of HBr. To constrain the HBr abundance below 60 km from our observation and the model, we use the Venus albedo of 0.028 at 3.66 μm (Krasnopolsky 2010). This low value is caused by the H_2SO_4 absorption, Single scattering approximation is reasonable for this black atmosphere in our observation at 3.84 μm. Assuming the aerosol scale height of 3 and 4 km above 70 km and a constant extinction coefficient at 60-70 km, the calculated upper limits to HBr below 60 km are 70 and 20 ppb, respectively, and $\tau \approx 0.7$ at 70 km, in accord with Cottini et al. (2015) and Fedorova et al. (2016). The bromine chemistry may be effective on Venus even under the observed upper limit. However, if a Cl/Br ratio in the Venus atmosphere is similar to that in the Solar System, then HBr ≈ 1 ppb in the lower atmosphere and the bromine chemistry is insignificant.

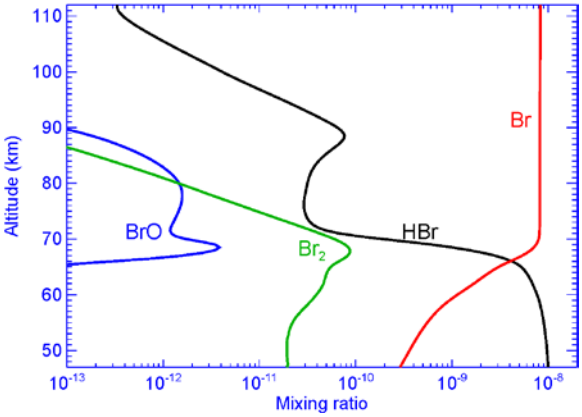

Fig. 3. Vertical profiles of bromine species in the photochemical model.

Acknowledgement

This work is supported by Grant 16-12-10559 of the Russian Science Foundation.

References

[1] Connes, P., et al., Astrophys. J. 147, 1230-1237, 1967
[2] Cottini, V., et al., Planet. Space Sci. 113-114, 219-225, 2015.
[3] Fedorova, A., et al., Icarus 275, 143-162, 2016.
[4] Krasnopolsky, V.A., Icarus 208, 539-547, 2010.
[5] Krasnopolsky, V.A., Icarus 218, 230-246, 2012.
[6] Krasnopolsky, V.A., Icarus 225, 570-580, 2013.
[7] Moroz, V.I., et al., Cosmic Res. 19, 599-612, 1981.

EPSC Abstracts
Vol. 11, EPSC2017-12, 2017
European Planetary Science Congress 2017

Annual mean mixing ratios of N_2, Ar, O_2, and CO in the martian atmosphere

Vladimir A. Krasnopolsky
Moscow Institute of Physics and Technology (PhysTech), Moscow, Russia (vlad.krasn@verizon.net)

Please make sure that your pdf conversion results in a document with a page size of 237 x 180 mm!

Abstract

The precise mixing ratios of N_2, Ar, O_2, and CO measured by the MSL Curiosity quadrupole mass spectrometer must be corrected for the seasonal variations of the atmospheric pressure to reproduce annual mean mixing ratios on Mars. The corrections are made using measurements the Viking Landers and the Mars Climate Database data. The mean correction factor is 0.899 ± 0.006 resulting in annual mean mixing ratios of (1.83 ± 0.03)% for N_2, (1.86 ± 0.02)% for Ar, (1.56 ± 0.06)×10^{-3} for O_2, and 673 ± 2.6 ppm for CO. The O_2 mixing ratio agrees with the Herschel value within its uncertainty, the ground-based observations corrected for the dust extinction, and photochemical models by Nair et al. (1994) and Krasnopolsky (2010). The CO mixing ratio is in excellent agreement with the MRO/CRISM value of 700 ppm and with 667, 693, and 684 ppm recently observed at L_S = 60, 89, and 110° and corrected to the annual mean conditions. Lifetimes of N_2 and Ar are very long in the martian atmosphere, and differences between the MSL and Viking data on these species cannot be attributed to their variations.

1. Introduction

The high-precision measurements of mixing ratios of N_2, Ar, O_2, and CO were made using the quadrupole mass spectrometer as a part of Mars Science Laboratory at the Curiosity rover (Mahaffy et al. 2013, Franz et al. 2015). These measurements must be corrected for the seasonal variations of the atmospheric pressure to reproduce annual mean mixing ratios on Mars.

2. Lifetimes of CO, O_2, N_2, and Ar on Mars

Lifetimes of long-living species are ratios of their column abundances to their column production or loss rates. The calculation is simple for CO, whose production is just the photon flux at λ < 200 nm times the disk-to-sphere area ratio of 1/4, with the lifetime of six Earth's years. O_2 recycles in some reactions, and only two processes, O + O + M → O_2 + M and OH + O → O_2 + H, result in formation of the O = O bonds and the O_2 lifetime of 60 years. N_2 is affected by outgassing from the interior and is lost by photochemical escape and sputtering (Jakosky et al. 1994). Its current lifetime is ≈1 Byr. Evolution of radiogenic ^{40}Ar was considered by Krasnopolsky and Gladstone (1996, 2005), and its current lifetime relative to sputtering is very long, 19 Byr. Here we confirm the conclusion by Mahaffy et al. (2013) that the differences between the Viking and MSL data on N_2 and Ar cannot be explained by their variations.

3. Seasonal corrections to MSL mixing ratios

Long-living species on Mars have two components of variations: (1) seasonal-latitudinal variations induced by condensation/sublimation of CO_2 on the polar caps and (2) the component related to seasonal variations of the total CO_2 amount in the atmosphere. The first component is significant at high latitudes exceeding 60° and negligible in the MSL observations at 5°S. The second component may be considered as independent of latitude, though it may be affected by weather. To correct the MSL mixing ratios for this component and get annual-mean mixing ratios, the MSL values should be scaled by p_m/p_0.. Here p_m is the atmospheric pressure at the season of the MSL measurements (L_S ≈ 184°) and p_0 is the annual mean pressure. Both values should be measured at the same conditions anywhere at lowe latitudes on Mars. The most detailed data of this type were published for the Viking Landers (Hess et al. 1980), and we will use them (Fig. 1)

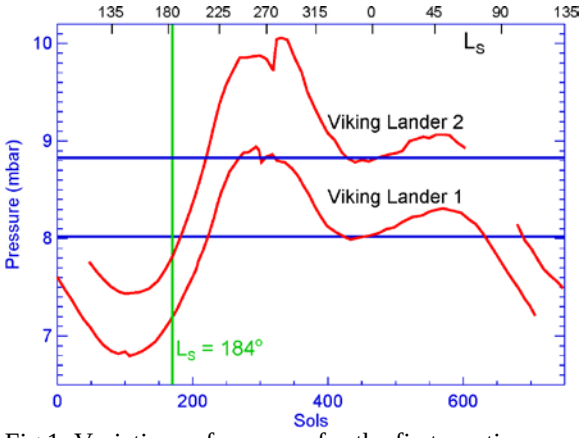

Fig.1. Variations of pressure for the first martian year (669 sols) of Viking Landers. Horizontal lines are calculated annual mean pressures p_0. Vertical line marks the season of the MSL measurements.

The peak-to-peak variation of pressure is a factor of 1.3, the Viking Landers were at the opposite longitudes and different latitudes (22°N and 48°N), and the calculated p_m/p_0 = 0.897 and 0.886 are rather similar. These calculations were also made for two points using the Mars Climate Database (Fig. 2).

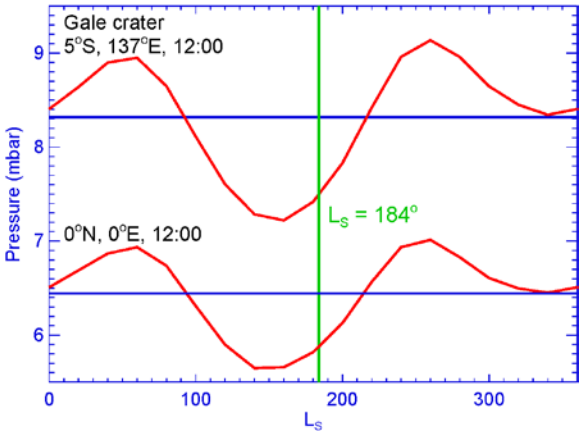

Fig. 2. Same as in Fig. 1 for two points from MCD.

Figure 2 is in the more convenient format (L_S instead sols) but requires corrections for variable angular velocity of Mars. The calculated p_m/p_0 = 0.902 and 0.911 with a mean of the four values of 0.899 ± 0.006. Annual mean mixing ratios can be obtained by scaling the MSL mixing ratios from Franz et al. (2015) by this factor (Table).

4. Comparison with other observations of O_2 and CO

Table

Species	Franz et al. (2015)	Annual mean
N_2	(2.03 ± 0.03)%	(1.83 ± 0.03)%
Ar	(2.07 ± 0.02)%	(1.86 ± 0.02)%
O_2	(1.73 ± 0.06)×10^{-3}	(1.56 ± 0.06)×10^{-3}
CO	749 ± 2.6 ppm	673 ± 2.6 ppm

The seasonally corrected Herschel observation (Hartogh et al. 2010) O_2 = (1.45 ± 0.12)×10^{-3} agrees with MSL. The mean of three ground-based observations is (1.2 ± 0.2)×10^{-3} (Nair et al. 1994). Corrected by a factor of 1.3 for dust extinction, this agrees with MSL as well. The MRO/CRISM observations of CO (Smith et al. 2009) showed the seasonally and globally averaged mixing ratio of 700 ppm. This value was 667, 693, and 684 ppm in the observations by Krasnopolsky (2015) at L_S = 60, 89, and 110°.

Acknowledgement

This work is supported by Grant 16-12-10559 of the Russian Science Foundation.

References

[1] Franz, H.B., et al., Planet. Space Sci. 109-110, 154-158, 2015.

[2] Hartogh, P., et al., Astron. Astrophys. 521, L49, 2010.

[3] Hess, S.L., et al., Geophys. Res. Lett. 7, 197-200, 1980.

[4] Jakosky, B.M., et al., Icarus 111, 271-288, 1994.

[5] Krasnopolsky, V.A., Icarus 207, 638-647, 2010.

[6] Krasnopolsky, V.A., Icarus 253, 149-155, 2015.

[7] Krasnopolsky, V.A., Gladstone, G.R., JGR 101A, 15,765-15,772, 1996.

[8] Krasnopolsky, V.A., Gladstone, G.R., Icarus 176, 395-407, 2005.

[9] Mahaffy, P.R., et al., Science 341, 263-266, 2013.

[10] Nair, H., et al., Icarus 111, 124-150, 1994.

[11] Smith, M.D., et al., JGR 114, E00D03, 2009.

EPSC Abstracts
Vol. 11, EPSC2017-17, 2017
European Planetary Science Congress 2017

Disulfur dioxide and its NUV absorption in the photochemical model of Venus atmosphere

Vladimir A. Krasnopolsky
Moscow Institute of Physics and Technology (PhysTech), Moscow, Russia (vlad.krasn@verizon.net)

Please make sure that your pdf conversion results in a document with a page size of 237 x 180 mm!

Abstract

The Venus photochemical model (Krasnopolsky 2012) is updated by the data on S_2O_2 formation and photolysis (Frandsen et al. 2016) and improved densities of H_2O, OCS, and H_2 at 47 km (Krasnopolsky 2013). The basic model and four versions with small deviations in eddy diffusion and SO_2 at 47 km are presented and agree with the observed variations of CO, H_2O, SO_2, SO, and OCS. Three methods are used to evaluate S_2O_2 abundance sufficient for the NUV absorption, and the required S_2O_2 exceeds the model prediction by a factor of 200. The SO profile by Na et al. (1994) with 12 ppb at 64-95 km significantly exceeds the model below 74 km. If SO ≈ 12 ppb at 64 km, then S_2O_2 contributes to but does not completely explain the NUV absorption.

1. Introduction

Frandsen et al. (2016) proved that S_2O_2 is formed by SO + SO + M as cis- and trans-OSSO isomers that dissociate to SO and calculated their absorption spectra. Using the SO abundances of 12 ppb at 64-95 km observed by Na et al. (1994), they calculated abundances of OSSO that appear sufficient to explain the NUV absorption of Venus at 320-500 nm. We will implement the findings by Frandsen et al. (2016) into our photochemical model (Krasnopolsky 2012, Paper I), update the model using the chemical kinetic model (Krasnopolsky 2013), and test the hypothesis of OSSO as the NUV absorber.

2. Updated photochemical model

It was assumed in Paper I that S_2O_2 is formed as the lowest energy isomer S=SO_2 that dissociates to S + SO_2. The formation of OSSO and its dissociation to SO + SO significantly affect the sulfur chemistry in the model that also adopts the OSSO formation and dissociation reaction rates from Frandsen et al. (2016). The model is updated using mixing ratios of H_2O = 26 ppm, OCS =140 ppb, and H_2 = 8.5 ppb at 47 km from the chemical kinetic model (Krasnopolsky 2013) as the lower boundary conditions. Similar to Paper I, a basic model and four versions with minor variations of eddy diffusion and SO_2 at the lower boundary were calculated (Table). Here eddy diffusion is 7300 cm^2 s^{-1} below h_e increasing to 10^7 cm^2 s^{-1}at 100 km above h_e.

Table. Some data from five versions of the model

h_e	SO_2	H_2O	SO_2	SO	S_2O_2+$h\nu$
km	47 km	70 km	70 km	90 km	cm^{-2} s^{-1}
60	9.7 ppm	3.11 ppm	128 ppb	10.1 ppb	3.91+13
57	9.7	4.38	577	43.4	5.39+13
65	9.7	2.90	57	2.44	5.99+13
60	8.7	5.36	70	6.3	2.77+13
60	10.7	1.48	342	25	5.46+13

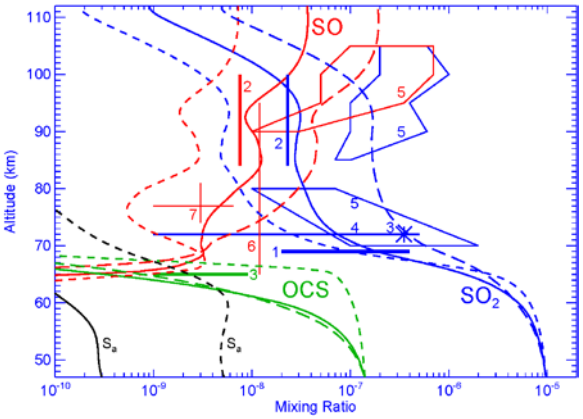

Fig. 1. Basic sulfur species: model results (solid, short and long dashes for h_e = 60, 57, and 65 km, respectively) and observations. S_a refers to total number of sulfur atoms in the aerosol. Observations of SO by Na et al. (1994) and Jessup et al. (2015) are (6) and (7).

The model results for the sulfur species SO_2, SO, OCS, and aerosol sulfur S_a are compared with the observations in Fig. 1. Minor variations of eddy diffusion induce variations of the species by a factor

of ≈30 and do not require volcanism. Variations of H_2O in the model and observations are compared in Fig. 2. Again, there is a good agreement between the model and observations.

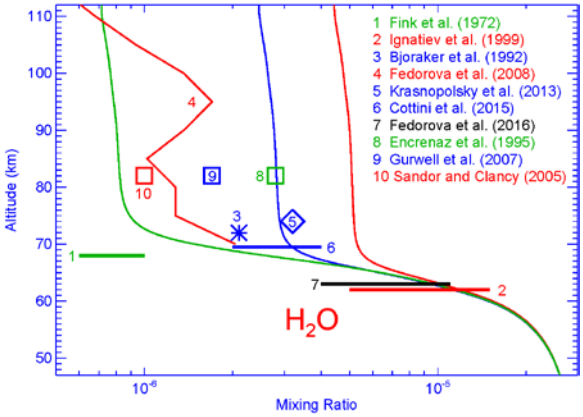

Fig. 2. Vertical profiles of H_2O for SO_2 = 8.7, 9.7, and 10.7 ppm at 47 km (red, blue, and green lines) are compared with the observations.

3. NUV absorption by OSSO

The calculated column photolysis rate of OSSO is 3.9×10^{13} cm^{-2} s^{-1} and peaks at 68 km in a layer of 4 km thick. The NUV absorption at 320-500 nm (Fig. 3) removes 1.9×10^{16} cm^{-2} s^{-1} solar photons and exceeds the OSSO photolysis in the model by a factor of 500. The calculated OSSO column is 2.13×10^{14} cm^{-2} with the cis-to-trans isomer ratio of 0.82/0.18.

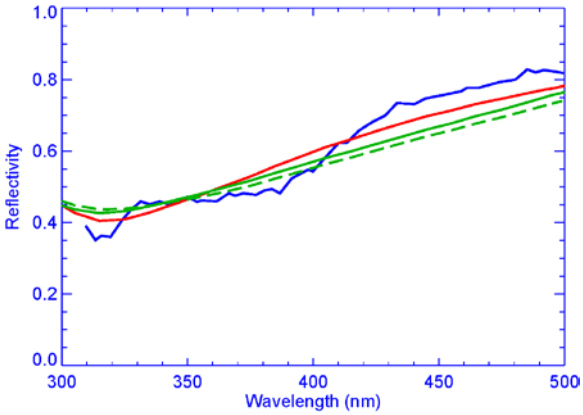

Fig. 3. Observed spectrum of Venus (blue, Barker et al. 1975) is compared with OSSO absorption in a thin layer (red) and for uniformly mixed absorber (green) with the isomer proportion 0.82/0.18 and 0.7/0.3 (solid and dashed curves, respectively). The OSSO abundances in the models are chosen to fit the observation at 350 nm.

The observed spectral reflectivity of Venus is compared with that of OSSO in Fig. 3. The red curve is for a thin absorbing layer above the clouds with OSSO = 2.8×10^{16} cm^{-2} exceeding the model value by a factor of 130. The green curve is for OSSO = 4×10^{16} cm^{-2} uniformly mixed in the upper cloud layer. (The cis-to-trans ratio is 0.7/0.3 in production and 0.82/0.18 in abundances because of the weaker photolysis of cis-OSSO.) This abundance exceeds the model value by a factor of 190. Frandsen et al. (2016) calculated the OSSO densities using SO = 12 ppb at 64-95 km observed by Na et al. (1994). This SO exceeds the recent observations by Jessup et al. (2015, 6.5, 2, and 1 ppb at 74-81 km, Fig. 1) and the model values below 74 km. Even SO from Na et al. (1994) results in an absorption that is weaker than that observed by a factor of 3. The spectral fit by OSSO to the observed NUV absorption is not perfect as well. Even if SO from Na et al. (1994) is valid below 74 km, then OSSO contributes to but does not completely explain the NUV absorption.

Na and Esposito (1997) proposed S_2O as the NUV absorber. They calculated $[S_2O] \approx 5\times10^9$ cm^{-3} at 64 km, close to that at 47-60 km in our model. However, absorption spectra of gaseous S_2O are lacking.

Strong arguments in favour of $FeCl_3$ diluted to ≈1% in the droplets of sulphuric acid in the upper cloud layer may be found in Krasnopolsky (2017). This species explains the NUV absorption, though contribution of other candidates is not ruled out.

Acknowledgement

This work is supported by Grant 16-12-10559 of the Russian Science Foundation.

References

[1] Barker, E.S., et al., J. Atmos. Sci. 32, 1205-1211, 1975.
[2] Frandsen, B.N., Wennberg, P.O., Kjaergaard, H.G., Geophys. Res. Lett. 43, 11146-11155, 2016.
[3] Jessup, K.L., et al., Icarus 258, 309-336, 2015.
[4] Krasnopolsky, V.A., Icarus 218, 230-246, 2012.
[5] Krasnopolsky, V.A., Icarus 225, 570-580, 2013.
[6] Krasnopolsky, V.A., Icarus 286, 134-137, 2017.
[7] Na, C.Y., et al., Icarus 112, 389-395, 1994.
[8] Na, C.Y., Esposito, L.W., Icarus 364-368, 1997.

EPSC Abstracts
Vol. 11, EPSC2017-29, 2017
European Planetary Science Congress 2017

Impact of Crustal Magnetic Fields on Day-to-night Plasma Transport in the Martian Ionosphere

J. Cui (1,2), Y.-T. Cao (3) and Y. Wei (4)
(1) School of Atmospheric Sciences, Sun Yat-Sen University, Zhuhai, China, (2) Lunar and Planetary Science Laboratory, Macau University of Science and Technology, Macau, China, (3) Key Laboratory of Lunar and Deep Space Exploration, National Astronomical Observatories, Chinese Academy of Sciences, Beijing, China, (4) Institute of Geology and Geophysics, Chinese Academy of Sciences, Beijing, China (cuijun7@mail.sysu.edu.cn / Fax: +86-0756-3668292)

Abstract

This study is aimed at a systematic investigation of the impact of crustal magnetic fields on day-to-night transport in the Martian ionosphere, based on the Mars Express (MEx) data in both the Active Ionospheric Sounding (AIS) mode and the Subsurface (SS) mode. Our analysis reveals noticeable differences in the variations of near-terminator topside plasma scale height and total electron content (TEC) between regions of the Martian ionosphere with and without strong crustal magnetic fields. The observed trends are fully compatible with a scenario in which strong crustal magnetic fields exert a blocking effect on day-to-night transport in the Martian ionosphere across the terminator.

1. Introduction

At the dayside, Mars contains a regular Chapman-like ionosphere mainly produced by solar EUV / X-ray ionization (Withers 2009). In contrast, the nightside ionosphere of Mars is patchy and sporadic (Gurnett et al. 2008), with impact ionization by precipitating electrons from the Solar Wind (SW) and day-to-night transport generally thought to be the two most important sources (Zhang et al. 1990, Duru et al. 2011, Withers et al. 2012, Cui et al. 2015). It has been shown extensively that the crustal magnetic fields exert a profound influence on the morphology of the Martian ionosphere deep in the nightside where electron precipitation dominates (e.g., Safaeinili et al., 2007, Lillis et al. 2009). This study is the first attempt to investigate systematically the impact of crustal magnetic fields on day-to-night transport in the near-terminator Martian ionosphere. Two independent tests have been performed, both based on the data obtained with the Mars Advanced Radar for Subsurface and Ionospheric Sounding (MARSIS) onboard Mars Express (MEx).

2. Topside plasma scale height

Based on the MARSIS data in the Active Ionospheric Sounding (AIS) mode, we derive the topside plasma scale height in the near-terminator Martian ionosphere well above the peak. We find that over regions free of crustal magnetic fields, this scale height increases progressively with time as Mars rotates into darkness. Such a feature is fully compatible with predictions from photochemical models as the upper regions of the Martian ionosphere are dominated by O^+ with a relatively long chemical timescale and the lower regions dominated by O_2^+ that are lost via dissociative recombination much faster. In contrast, the observed variation of near-terminator topside plasma scale height is inconsistent with predictions from photochemical models over regions of strong crustal magnetic fields. We attribute such a difference to the blocking of day-to-night transport by strong crustal magnetic fields.

3. Total electron content (TEC)

Based on the MARSIS data in the Subsurface (SS) mode, we further examine the time evolution of TEC at any fixed location on Mars as it passes nightward across the terminator. This part of the work is a direct extension of our early analysis of the same dataset (Cui et al. 2015) that focused on the northern hemisphere only and led to an estimated nightward plasma flow velocity of 2 km/s on average. Our analysis here, implemented to the data acquired over the entire region of the near-terminator Martian ionosphere and divided into several categories with varying magnitude of crustal magnetic fields, reveals

a clear tendency of faster decline in TEC over regions with strong crustal magnetic fields, as compared to other regions away from. Such an observation could also be understood as an outcome of blocked day-to-night transport due to strong crustal magnetic fields. Quantitative description of such an effect is then performed using a simplified one-dimensional, time-dependent photochemical model treating the horizontal plasma flow velocity as the only free parameter to be constrained by the data.

4. Summary and Conclusions

Based on the MARSIS data in both the AIS and SS modes, our analysis reveals noticeable differences in the variations of topside plasma scale height and TEC between regions of the near-terminator Martian ionosphere with and without strong crustal magnetic fields. The observed behaviors of these variations are fully compatible with a scenario in which strong crustal magnetic fields exert a blocking effect on day-to-night transport in the Martian ionosphere across the terminator.

Acknowledgements

The authors acknowledge supports from the National Science Foundation of China (NSFC) through grants 41374178 and 41525015. This work is also supported by the Science and Technology Development Fund of Macau SAR (039/2013/A2 and 082/2015/A3).

References

[1] Cui, J., et al., Day-to-night transport in the Martian ionosphere: Implications from total electron content measurements, J. Geophys. Res., 120, 2333-2346, 2015.

[2] Duru, F., et al., Nightside ionosphere of Mars studied with local electron densities: A general overview and electron density depressions, J. Geophys. Res., 116, A10316, 2011.

[3] Gurnett, D. A., et al., An overview of radar soundings of the Martian ionosphere from the Mars Express spacecraft, Adv. Space Res., 41, 1335-1346, 2008.

[4] Lillis, R. J., et a., Nightside ionosphere of Mars: Modeling the effects of crustal magnetic fields and electron pitch angle distributions on electron impact ionization, J. Geophys. Res., 114, E11009, 2009.

[5] Safaeinili, A., et al., Estimation of the total electron content of the Martian ionosphere using radar sounder surface echoes, Geophys. Res. Lett., 34, L23204, 2007.

[6] Withers, P., A review of observed variability in the dayside ionosphere of Mars, Adv. Space Res., 44, 277-307, 2009.

[7] Withers, P., et al., Observations of the nightside ionosphere of Mars by the Mars Express Radio Science Experiment (MaRS), J. Geophys. Res., 117, A12307, 2012.

[8] Zhang, M. H. G., et al., An observational study of the nightside ionospheres of Mars and Venus with radio occultation methods, J. Geophys. Res., 95, 17095-17102, 1990.

EPSC Abstracts
Vol. 11, EPSC2017-58, 2017
European Planetary Science Congress 2017

On Mars' atmospheric sputtering after MAVEN first two years

Leblanc F. (1), Modolo R. (2), Curry S. (3), Luhmann J. (3), Lillis R. (3), Chaufray J.Y. (1), Hara T. (3), McFadden J. (3), Halekas J. (4), Eparvier F. (5), Larson D. (3), Connerney J. (6) and B. Jakosky (5)
(1) LATMOS/IPSL, UPMC Univ. Paris 06 Sorbonne Universités, UVSQ, CNRS, Paris, France, (2) LATMOS/IPSL, UVSQ Université Paris-Saclay, UPMC Univ. Paris 06, CNRS, Guyancourt, France, (3) UC Berkeley Space Sciences Laboratory, Berkeley, CA, USA, (4) University of Iowa, Department of Physics and Astronomy, IA, USA, (5) Laboratory for Atmospheric and Space Physics, University of Colorado Boulder, Boulder, CO, USA, (6) NASA Goddard Space Flight Center, MD, USA (francois.leblanc@latmos.ipsl.fr, Tel: +33 (0)144273753)

Abstract

Mars may have lost a significant part of its atmosphere into space along its history, in particular since the end of its internal dynamo, 4.1 Gyr ago. The sputtering of the atmosphere by precipitating planetary picked up ions accelerated by the solar wind is one of the processes that could have significantly contributed to this atmospheric escape. We here present a two years base analysis of MAVEN observation of the precipitating flux, in particular the dependency of the precipitating intensity with solar zenith angle and used this measurement to model the expected escape rate and exosphere induced by this precipitation.

1. MAVEN measurements

In order to reconstruct the flux of precipitating picked-up ion measured by MAVEN, we used the same approach as in [1], that is, we used all available measurements of the ion mass and energy distributions realized between 200 and 350 km in altitude by SWIA (cs product) and STATIC (ca and d0 products). We selected the anodes covering the 75° cone angle oriented along the zenith direction and reconstructed the energy distribution. Figure 1 displays the average precipitating flux measured by MAVEN SWIA and STATIC during the first two years of MAVEN operations (between 12/02/2014 and 10/24/2016).

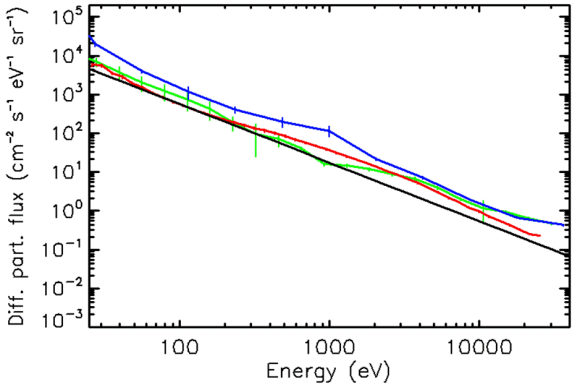

Figure 1: Differential particle flux of the precipitating pick-up ion as measured by MAVEN between 200 and 350 km in altitude during the 12/2014-10/2016 period. Red line: SWIA cs, blue line: STATIC ca, green line: STATIC d0 15-17 amu mass range, black line: theoretical predicted flux (Wang et al. 2015).

As shown in Figure 1, there is globally a good agreement between the measured flux by SWIA and STATIC, knowing that SWIA field of view allows a better coverage of the cone angle pointing towards the zenith than STATIC. Moreover, the comparison between STATIC d0 product for masses between 15 and 17 amu and SWIA cs suggests that most of the precipitating ion measured by SWIA with energy larger than few tens of eV are O^+ ions. Compared to the predicted energy flux distribution [2], Figure 1 highlighted the good agreement between prediction and measurements.

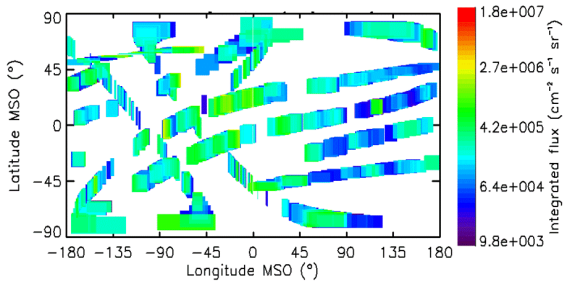

Figure 2: Integrated precipitating flux measured by MAVEN (SWIA cs) during the 12/2014-10/2016 period plotted vs MSO latitude and longitude. The subsolar point is at 0°,0°.

In Figure 2, we plotted the integrated flux in a MSO longitude/latitude frame. This shows that the precipitating flux is organized between day and night sides with a 1.7 times higher intensity of the dayside precipitating flux.

2. Induced atmospheric escape

Reconstructing the precipitating flux between day and night sides, we simulated the fate of precipitating pick-up O^+ ions into Mars' atmosphere using Exospheric Global Model (EGM) [3] coupled to LMD-GCM [4] in order to calculate the induced exosphere and atmospheric escape by the precipitating ion (Figure 1, red line). EGM is a multispecies parallelized 3D model describing, for any season and solar conditions, how energetic ion will interact with Mars' upper atmosphere (composed of CO_2, CO, O, N and N_2) by transferring energy and momentum to the atom and molecule and ejecting atmospheric species into the exosphere. To describe the collision, we used at low energy the universal collision scheme of [5] and at high energy molecular dynamic scheme [6] in order to take into account the possibility of molecular dissociation.

3. Conclusion

Based on the average measured precipitating flux during the first two years of MAVEN observations, and using a model to determine the potentially induced atmospheric escape, we concluded that 5×10^{23} O/s, 8×10^{22} CO_2/s, 4×10^{22} CO/s, 1×10^{23} C/s, 1.6×10^{24} N/s and 4×10^{23} N_2/s should have escaped Mars' atmosphere between December 2014 and October 2016.

Acknowledgements

FL, JYC and RM acknowledge the support of the ”Système Solaire” program of the French Space Agency CNES and the Programme National de Planétologie and Programme National Soleil-Terre. This work is also part of HELIOSARES Project supported by the ANR (ANR-09-BLAN-0223) and ANR MARMITE (ANR-13-BS05-0012-02). Authors also acknowledge the support of the IPSL data center CICLAD for providing us access to their computing resources and data. The results of the simulations presented in this paper can be requested to FL.

References

[1] Leblanc F., R. Modolo, S. Curry, J. Luhmann, R. Lillis, J. Y. Chaufray, T. Hara, J. McFadden, J. Halekas, F. Eparvier (2015), et al., Mars heavy ion precipitating flux as measured by Mars Atmosphere and Volatile EvolutioN, Geophys. Res. Lett., 42, doi:10.1002/2015GL066170.

[2] Wang, Y.-C., J. G. Luhmann, X. Fang, F. Leblanc, R. E. Johnson, Y. Ma, and W.-H. Ip (2015), Statistical studies on Mars atmospheric sputtering by precipitating pickup O+: Preparation for the MAVEN mission, *J. Geophys. Res. Planets*, *120*, 34–50, doi:10.1002/2014JE004660.

[3] Leblanc F., Modolo R., Chaufray J.Y. , Leclercq L., Curry S., Luhmann J., Lillis R., Hara T., McFadden J., Halekas J., Schneider N., Deighan J. and B. Jakosky, Mars' exosphere observation and modelling: HELIOSARES view of MAVEN's measurements, J. Geophys. Res., Submitted, 2017.

[4] Chaufray J-Y, Gonzalez-Galindo F., Forget, F., Lopez-Valverde M., Leblanc F., Modolo, R., Hess, S., M. Yagi, Blelly, P-L., Witasse, O. (2014), 3D Martian Ionosphere model : II Effect of transport processes without magnetic field, Journal of Geophysical Research: Planets, 119 (7), 1614-1636. doi: 10.1002/2013JE004551

[5] Lewkow N.R. and V. Kharhenko (2014), Precipitation of energetic neutral atoms and induced non-thermal escape fluxes from the Martian atmosphere, ApJ, 790, doi:10.1088/0004-637X/790/2/98.

[6] Leblanc, F., Johnson, R.E., (2002), Role of molecular species in pickup ion sputtering of the Martian atmosphere. Journal of Geophysical Research 107.

EPSC Abstracts
Vol. 11, EPSC2017-77-2, 2017
European Planetary Science Congress 2017

AKATSUKI-IR2 reveals unexpected opacity disruption affecting Venus's lower clouds every 9 days

J. Peralta [javier.peralta@ac.jaxa.jp] (1), T. Satoh (1), T. Horinouchi (2), K. Ogohara (3), T. Kouyama (4), S. Murakami (1) , T. Imamura (5), K. McGouldrick (6), T. M. Sato (1), S. Limaye (7), E. García-Melendo (8), A. Sánchez-Lavega (9), R. Hueso (9) and the AKATSUKI team.

(1) Institute of Space and Astronautical Science (ISAS/JAXA), Japan, (2) Hokkaido University, Japan, (3) University of Chiga Prefecture, Japan, (4) National Institute of Advanced Industrial Science and Technology, Japan, (5) The University of Tokyo, Japan, (6) University of Colorado, CO, USA, (7) University of Wisconsin-Madison, WI, USA, (8) Fundació Observatori Esteve Duran, Spain, and (9) Universidad del País Vasco (UPV/EHU), Spain.

Abstract

The images of AKATSUKI acquired with the camera IR2 at 1.74-2.3 μm report the discovery of an equatorial disruption or "front" in the opacity of the lower clouds of Venus at 50 km between 30ºN–30ºS. This feature appears on the night every 9 terrestrial days during more than 8 months, and introduces a dramatic and abrupt increase of the cloud opacity and reducing the thermal radiance in a factor of about 1:2 from its brightest to the darkest side.

1. Introduction

The lower clouds of Venus, located at ~50 km, can be observed on the night side, mainly through the infrared spectral bands 1.74 and 2.30 μm which allow sensing the clouds' opacity to the deep thermal emission. Observations performed by the imaging spectrometer VIRTIS-M onboard ESA's Venus Express (VEx) [1,2] set that these lower clouds have different spatial scales at different latitudes, with larger and stretched features dominating from polar to mid-latitudes, while patchy and fine-scale structures being apparent at latitudes lower than about 40º [2]. In contrast to the upper clouds, the lower clouds features keep coherent longer (up to 6–7 hours), although for timescales of more than about 1 day the cloud opacity can change dramatically [3]. The prevailing circulation consists on less variable wind speeds with a magnitude similar to that found at the dayside upper clouds' deck at ~60 km [1]. They do not exhibit a clear mean meridional component, although VEx/VIRTIS-M observations were severely constrained to mid-to-high latitudes because of the polar orbit of VEx. Finally, nor the zonal neither the meridional component of the winds display any dependence with the local time [2].

2. Instrumentation

The successful orbit insertion of AKATSUKI in December 2015 [4] has implied a unique chance to continue the study of the mid-to-low clouds of Venus since the infrared channel of VEx/VIRTIS stopped its operations at the end of October 2008 after the end of the operative lifetime of the instrument cryocoolers. AKATSUKI began its regular scientific observations in April 2016, and the infrared camera IR2 [5] has continued studying the lower clouds of Venus thanks to a set of narrow-band filters with wavelengths 1.74, 2.26 and 2.32 μm. Among its scientific objectives, we can highlight the study of the atmospheric dynamics by measuring the cloud motion vectors, characterization of the morphology of the clouds, inference of the aerosol properties by combining 1.74 and 2.26-μm images, and mapping the CO concentrated below the cloud layer by differentiating 2.26 and 2.32-μm images [5].

3. Observations and Results

Up to date, IR2 has acquired more than 1,800 images of the nightside of Venus, covering from March 2016 until December 2016. The IR2 images have revealed that at lower latitudes the nightside deeper clouds of Venus exhibit a more dynamical behavior than at higher latitudes. Even though the period of rotation for the lower clouds is about 7 terrestrial days, the cloud patterns can become unrecognizable even after just 24 hours. A variety of new cloud features have been revealed thanks to the IR2 observations, including frequent shear-like structures, features resembling slowly developing vortices, or mesoscale packets waves even more abundant that at higher latitudes [6]. During the 27 of March 2016, a striking feature became apparent at equatorial latitudes, consisting a sudden change in the lower clouds'

opacity extending between 30ºS–30ºN, and orientated with an angle of about 60º relative to the equator (Figure 1). From March to September 2016, this drastic change in the cloud opacity seems to follow the following 9-day cycle:

1. Once this disruption on the cloud opacity appears, it propagates slightly faster than the zonal flow and is followed by more opaque (darker) and homogeneous clouds.

2. The area of the darker clouds becomes gradually narrower, and its border with high-latitude brighter clouds adopts a wavy shape.

3. Finally, the equatorial dark area is invaded by turbulent patterns and small vortices. The disruption reappears again.

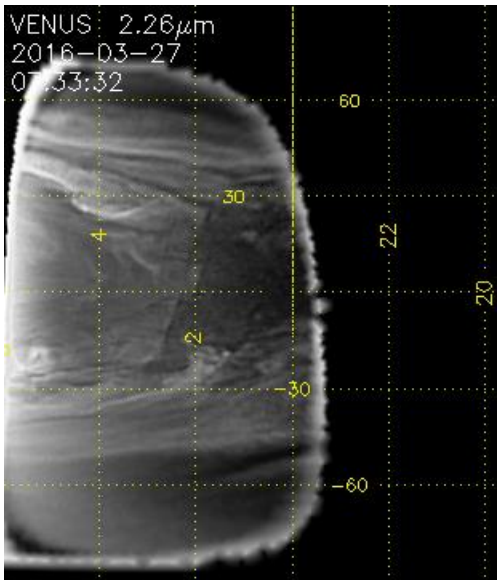

Figure 1: IR2 image of the disruption on the lower clouds' opacity during its first appearance.

4. Summary and Conclusions

Several candidates are proposed in order to explain this periodical change in the lower clouds' opacity, from the manifestation of an equatorially trapped wave to the formation of an atmospheric front from the interaction between masses of air with different properties (temperature, density). Recent analysis of past ground-based observations with telescopes has provided evidence that this phenomenon might be a recurrent cycle on the lower clouds beyond our period of observation with AKATSUKI. Also, the equatorial zonal winds experience a gradual increase in their magnitude up to a maximum of 30 m/s when the disruption is present. Both the cycle of changes in the cloud opacity and these disturbances on the zonal winds are being explored with a numerical shallow-water model [7] adapted to the conditions of Venus. Venus observations during the Galileo flyby [8] suggest that such a phenomenon might manifest also on the dayside upper clouds, so AKATSUKI/IR1 images at 900 nm will complement this work.

Acknowledgements

JP acknowledges JAXA's International Top Young Fellowship (ITYF). RH and ASL thank Spanish project AYA2015-65041-P (MINECO/FEDER, UE), Grupos Gobierno Vasco IT-765-13 and UPV/EHU program UFI11/55.

References

[1] Sánchez-Lavega A. et al.: Variable winds on Venus mapped in three dimensions. Geophysical Research Letters, 35, L13204, 2008.

[2] Hueso R. et al.: Assessing the Long-Term Variability of Venus Winds at Cloud Level from VIRTIS-Venus Express. Icarus, 217, 585-598, 2012.

[3] McGouldrick, K. et al: Venus Express/VIRTIS observations of middle and lower cloud variability and implications for dynamics. Journal of Geophysical Research: Planets, 113 (E5), 2008.

[4] Nakamura, M. et al.: AKATSUKI returns to Venus, Earth, Planets and Space, 68, 1-10, 2016.

[5] Nakamura, M. et al.: Planet-C: Venus Climate Orbiter mission of Japan. Planetary and Space Science, 55, 1831-1842, 2007.

[6] Peralta, J. et al.: Characterization of mesoscale gravity waves in the upper and lower clouds of Venus from VEX-VIRTIS images. Journal of Geophysical Research, 113, E00B18, 2008.

[7] García-Melendo, E. et al.: Shallow Water simulations of Saturn's Giant Storms at different latitudes, Icarus, 286, 241-260 (2017).

[8] Belton, M. J. S. et al.: Images from Galileo of the Venus cloud deck, Science, 253, 1531-1536, 1991.

EPSC Abstracts
Vol. 11, EPSC2017-78, 2017
European Planetary Science Congress 2017

Venus's winds and temperatures during the MESSENGER's flyby: towards a three-dimensional instantaneous state of the atmosphere

J. Peralta [javier.peralta@ac.jaxa.jp] (1), Y. J. Lee (1), R. Hueso (2), R. T. Clancy (3), B. J. Sandor (3), A. Sánchez-Lavega (2), E. Lellouch (4), M. Rengel (5,6), P. Machado (7), M. Omino (8), A. Piccialli (9), T. Imamura (8), T. Horinouchi (10), S. Murakami (1), K. Ogohara (11), D. Luz (7) and D. Peach (12).

(1) Institute of Space and Astronautical Science (ISAS/JAXA), Japan, (2) Universidad del País Vasco (UPV/EHU), Spain, (3) Space Science Institute, CO, USA, (4) LESIA/CNRS/UPMC, France, (5) Max-Planck-Institut für Sonnensystemforschung (MPS/MPEG), Germany, (6) European Space Astronomy Centre (ESAC), Spain, (7) Observatório Astronómico de Lisboa (OAL/IA), Portugal, (8) The University of Tokyo, Japan, (9) Belgian Institute for Space Aeronomy, Belgium, (10) Hokkaido University, Japan, (11) University of Shiga Prefecture, Japan, and (12) British Astronomical Association, UK.

Abstract

We present a three-dimensional global view of Venus's atmospheric circulation from data obtained in June 2007 by the MESSENGER and Venus Express (VEx) spacecrafts, together with ground-based observations [1]. Winds and temperatures were measured from 47 to 110 km from multi-wavelength images and spectra covering 40°N–80°S and local times 12h to 21h. Dayside westward winds exhibit day-to-day changes, with maximum speeds ranging 97–143 m/s and peaking at variable altitudes within 75–90 km, while on the nightside these peak below cloud tops at ~60 km. Our results support past reports of strong variability of the westward zonal superrotation in the transition region, and good agreement is found above the clouds with results from the LMD Venus general circulation model [2].

1. Introduction

The general circulation of the Venus atmosphere consists of two main regimes: a Retrograde Superrotating Zonal circulation (RSZ) dominating the cloud region 40–90 km, a strong subsolar-to-antisolar circulation (SS-AS) above 120 km, and a complex transition region within 90–120 km. New General Circulation Models (GCMs) simulate the bulk atmosphere from the surface to the thermosphere [2] and current efforts are oriented toward "data assimilation" from space missions. Thus, acquiring detailed snapshots of the Venus winds at specific moments/epochs is essential to set realistic initial conditions and top/lower boundaries in GCMs with data assimilation. Unfortunately, wind measurements on Venus have been dispersed spatially and in time, and studies of long-term data have only focused on the three best known cloud levels and provide time averages, ignoring the time evolution for a given instantaneous 3-D state [3].

2. Observations and Methods

During the VEx mission a campaign of coordinated observations was performed in June 2007 when NASA's spacecraft MESSENGER made its second flyby of Venus towards Mercury [4]. A first realistic approximation to the instantaneous dynamic state of the Venus atmosphere is performed combining new and previously published wind measurements during the flyby, using data from eight instruments of MESSENGER, VEx, and Earth-based telescopes. The wind speeds and atmospheric temperatures of Venus were calculated for the afternoon and early night during several days around the flyby (see Figure 1) using three remote sensing techniques: Cloud-tracking winds (CT), and Doppler and thermal winds derived from the atmospheric spectra and inferred temperatures, respectively. The images for CT were acquired by the cameras MESSENGER/MDIS, VEx/VMC, and the imaging spectrometer VEx/VIRTIS-M [1]. Our images were taken with different filters to sense the atmospheric motions at several atmospheric levels [5]: the dayside upper clouds at ~60 and ~70 km from the scattered sunlight (350 and 996 nm), the oxygen nightglow (1.27 μm) at 95–100 km, the thermal emission of the night upper clouds (3.8 μm) at ~65 km, and the night lower clouds' opacity to the deep thermal emission (1.74 μm) from ~50 km. Our atmospheric spectra to estimate winds and temperature cover ultraviolet-visible wavelengths (VLT/UVES), the infrared range

(VEx/VIRTIS-M and the Heterodyne Infrared Spectrometer THIS), and submillimeter spectra from the radio-telescopes IRAM, JCMT and HHSMT [1,4].

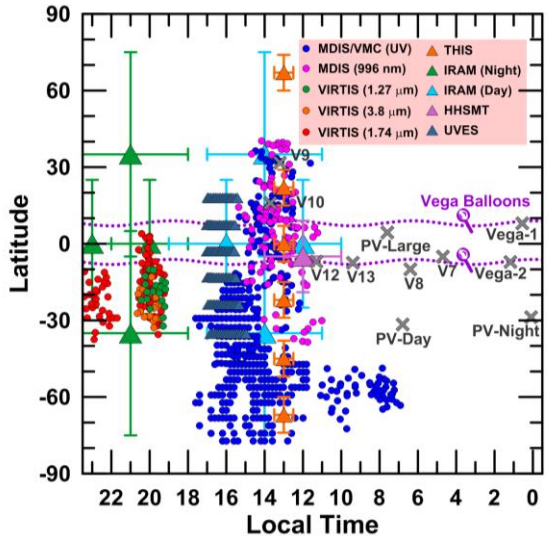

Figure 1: Spatial coverage of our measurements.

3. Results and Conclusions

Our wind measurements were combined to describe the vertical variation of the winds (Figure 2). For a coherent comparison, the zonal winds were averaged for the latitude range 0°–30°S and local times 12h–16h and 19h–21h. Figures 2A and 2B correspond to afternoon during 2–11 June 2007 and early night to 2–5 June. Thermal winds were calculated with the thermal wind equation and temperatures from JCMT and VIRTIS-M: for dayside, 3 days of JCMT thermal gradients were calculated, and only 1 day of VIRTIS-M. Zonal winds are compared with vertical profiles of VEGA, Pioneer Venus and Venera series at similar areas of latitude/local time. Zonal winds predicted by the Venus LMD GCM [2] are also exhibited. The GCM underestimates winds below 60 km, while above it predicts the dayside gradual decrease of the zonal wind towards weak eastward values and the night strong recovery up to winds faster than −140 m/s. The GCM does not predict the step decrease in the night thermal winds at the upper clouds (Fig. 2B), apparently related to a sudden breakdown of the cyclostrophic balance from ∼73 km [1]. Our results also show that both the height and maximum value of the zonal wind peak seem subject to significant changes on the dayside (Fig. 2A), with altitudes ±15 km about the cloud tops and speeds ranging from −97±8 m/s to −143±21 m/s. Regarding the nightside, the zonal wind peaks even deeper (∼60 km) with speeds weaker than on dayside. This behavior is also consistent with the interpretation of eventual vertical invasions of the SS-AS circulation down to deeper altitudes [1].

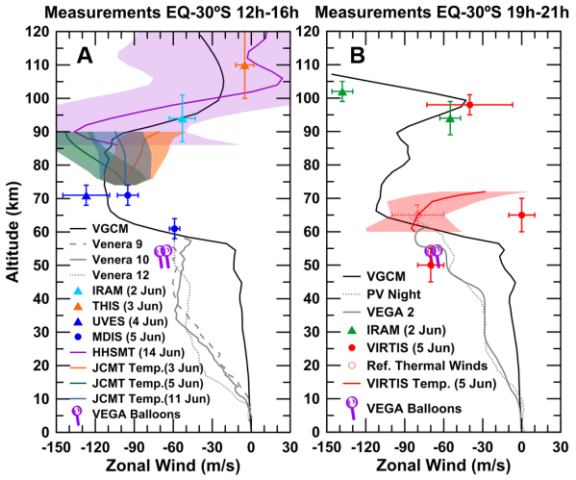

Figure 2: Vertical profiles of zonal wind in June 2007.

Acknowledgements

JP acknowledges JAXA's ITYF Fellowship. RH and ASL thank Spanish project AYA2015-65041-P (MINECO/FEDER, UE), Grupos Gobierno Vasco IT-765-13 and UPV/EHU program UFI11/55.

References

[1] Peralta, J. et al.: Venus's winds and temperatures during the MESSENGER's flyby: An approximation to a three-dimensional instantaneous state of the atmosphere, Geophys Res Lett, 44, doi: 10.1002/2017GL072900, 2017.

[2] Gilli, G. et al.: Thermal structure of the upper atmosphere of Venus simulated by a ground-to-thermosphere GCM, Icarus, 281, 55–72, 2017.

[3] Hueso, R., Peralta, J., Sánchez-Lavega, A.: Assessing the long-term variability of Venus winds at cloud level from VIRTIS-Venus Express, Icarus, 217, 585–598, 2012.

[4] Lellouch, E., and Witasse, O.: A coordinated campaign of Venus ground-based observations and Venus Express measurements, Planet. Space Sci., 56, 1317–1319, 2008.

[5] Peralta, J. et al.: Overview of useful spectral regions for Venus: An update to encourage observations complementary to the Akatsuki mission, Icarus, 288, 235–239, 2017.

EPSC Abstracts
Vol. 11, EPSC2017-80, 2017
European Planetary Science Congress 2017

Stationary waves and slow cloud features challenge Venus's night side superrotation

J. Peralta [javier.peralta@ac.jaxa.jp] (1), R. Hueso (2), A. Sánchez-Lavega (2), Y. J. Lee (1), A. García-Muñoz (3), T. Kouyama (4), H. Sagawa (5), T. M. Sato (1), G. Piccioni (6), S. Tellmann (7), T. Imamura (8) and T. Satoh (1).

(1) Institute of Space and Astronautical Science (ISAS/JAXA), Japan, (2) Universidad del País Vasco (UPV/EHU), Spain, (3) Technische Universität Berlin, Germany, (4) National Institute of Advanced Industrial Science and Technology, Japan, (5) Kyoto Sangyo University, Japan, (6) INAF-IAPS, Italy, (7) Universität zu Köln, Germany, (8) University of Tokyo, Japan.

Abstract

We present the first global measurements of the night side circulation of Venus at the upper cloud level from the tracking of individual features in thermal emission images at 3.8 and 5.0 µm during 2006-2008 (Venus Express/VIRTIS) and 2015 (IRTF/SpeX). The zonal motions range from -110 to -60 m/s, consistent with those found for the dayside but with larger dispersion6. Slow motions (-50 to -20 m/s) are also found and may indicate temporal changes in the vertical structure of the superrotation [1]. Abundant stationary wave patterns with zonal speeds from -10 to +10 m/s clearly dominate the night upper clouds.

1. Introduction

The atmosphere of Venus rotates at the cloud tops sixty times faster than the solid globe, a phenomenon called superrotation. Whereas on the dayside cloud top motions are well determined [2], the night side circulation remains poorly studied except at the polar region [3]. Night images at 3.8 and 5.0 µm sense the thermal contrasts of the upper clouds at ~65 km [4] and first images at these wavelengths were obtained during the Galileo flyby [5]. The largest dataset was acquired with the instrument VIRTIS on Venus Express (VEx), and was used to infer the winds at the southern polar region [2]. Middle and low latitudes have so far been ignored because images at these wavelengths display very low contrast.

2. Observations and Methods

We used 3.8 and 5.0 µm images obtained by VIRTIS-M from June 2006 to August 2008, and ground-based observations at 4.7 µm taken with SpeX instrument on the 3-m NASA Infrared Telescope Facility (IRTF) in July 2015 to study the motions of the night clouds of Venus. The spatial resolution of the images range from about 10 km/pix in VIRTIS-M to 400 km/pixel in the case of SpeX. Observational constraints due to the polar orbit of VEx limit the number of available images showing mid-to-low latitudes. Additional constraints (like exposure time and detector temperature) reduced our final dataset to 55 VEx orbits (~55 Earth days) which were deemed useful for cloud tracking.

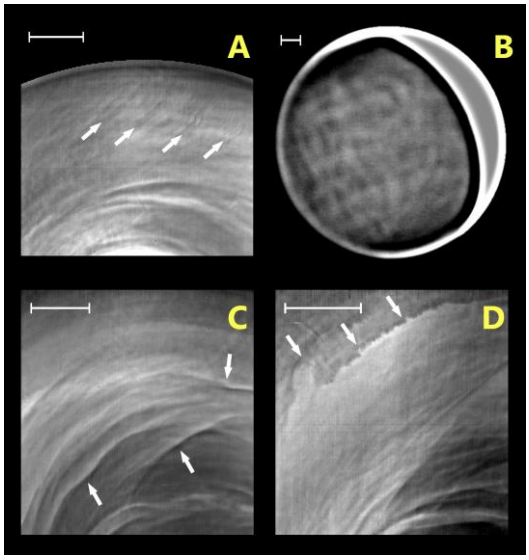

Figure 1: New upper clouds features on Venus night.

Night thermal features from the upper clouds exhibit important day-to-day changes in their appearance, revealing cloudy features unseen in dayside ultraviolet images (Figure 1). Three types of features and motions are found: wavy patterns, patchy/ irregular, and filaments or shear-like patterns. Large-scale wavy features are the most abundant (Fig. 1A), frequently seen between the equator and 60ºS and, together with a small number of the irregular structures, exhibit almost stationary motions (Figure 2). The wave trains have wavelengths 100–250 km, are oriented ±45º relative to the parallels and have packet

lengths of ~1000 km. Their properties differ from day side gravity waves observed at the same altitude. Big-scale features can be also observed in 5-µm ground-based images obtained by IRTF/SpeX (Fig. 1B). Bright stretched filaments (1C) and sheared-like features (1D) are also observed frequently.

2.1 Radiative-Transfer studies

We re-assessed previous altitude estimations using two Radiative Transfer models [4,6] which adopt a standard description of the Venus cloud particles (sulfuric acid of 75%) distributed vertically with 4 size modes with different number densities and temperature profiles from VIRA. Our calculations show that radiation is sensitive to a range of altitudes between 60 and 72 km. Since thinner clouds occur occasionally in Venus (what may result in larger contributions from lower altitudes), additional descriptions of the thermal opacity were explored reducing by a factor of 10 the number density of a size mode, while leaving the other size modes unmodified. The calculations show that even in conditions of thinner clouds the bulk of radiation at 3.8 and 5.0 µm originates at altitudes above 50 km.

3. Results and Conclusions

Figure 2 displays the latitudinal (left graph) and vertical (right) distribution of the velocities are shown. Wavy and other patterns are displayed with green and red dots, respectively. Fast filaments and shear-like features are shown with cyan dots, while eventual cases of extremely slow tracers are shown with dark yellow dots. Tracers in SpeX images are displayed as blue circles with error bars. Individual errors with VIRTIS range 5–15 m/s. Meridional profiles of zonal winds at dayside levels of the cloud tops (~70 km) and upper clouds' deck (~60 km) during the Galileo flyby [5] and VEx missions [2] are displayed with dashed and continuous black lines with shaded areas showing the dispersion of the measurements. Contrarily to the dayside motions dominated by mean super-rotating winds ranging -120 to -90 m/s, night side motions are far more variable. The abundant wave patterns with zonal speeds from -10 to +10 m/s can be interpreted as stationary gravity waves supported by the positive static stability above 60 km. VEx/VeRa radio-occultation at the geographical locations where they appear reveal vertical wavelengths ranging 4–17 km.

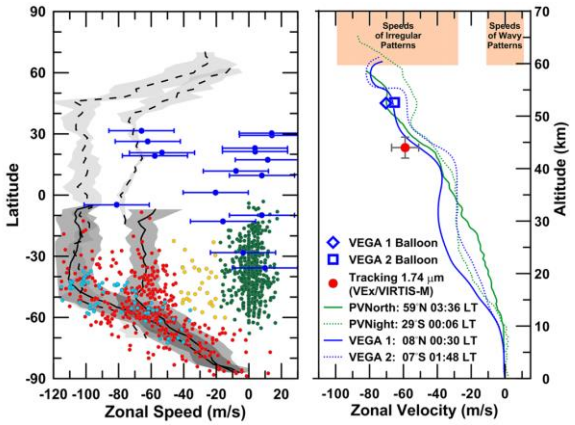

Figure 2: Meridional and vertical profiles for motions.

Acknowledgements

JP acknowledges JAXA's ITYF Fellowship. RH and ASL thank Spanish project AYA2015-65041-P (MINECO/FEDER, UE), Grupos GV IT-765-13 and UPV/EHU program UFI11/55. TMS was supported by a Grant-in-Aid for JSPS Fellows. IRTF/SpeX observations were supported by JSPS KAKENHI 15K17767. We also thank ASI and CNES for their support to the VIRTIS-Venus Express experiment.

References

[1] Peralta, J. et al.: Venus's winds and temperatures during the MESSENGER's flyby: An approximation to a three-dimensional instantaneous state of the atmosphere, *Geophys Res Lett*, 44, doi: 10.1002/2017GL072900, 2017.

[2] Hueso, R. et al.: Six years of Venus winds at the upper cloud level from UV, visible and near infrared observations from VIRTIS on Venus Express, *Planetary and Space Science*, 113-114, 78–99, 2015.

[3] Garate-Lopez, I. et al.: A chaotic long-lived vortex at the southern pole of Venus. *Nature Geo.* 6, 254–257, 2013.

[4] García-Muñoz, A. et al.: A model of scattered thermal radiation for Venus from 3 to 5 µm. *Planetary and Space Science*, 81, 65–73, 2013.

[5] Peralta, J., Hueso, R. and Sánchez-Lavega, A.: A reanalysis of Venus winds at two cloud levels from Galileo SSI images. *Icarus*, 190, 469-477, 2007.

[6] Lee, Y. J. et al.: The radiative forcing variability caused by the changes of the upper cloud vertical structure in the Venus mesosphere. *Planet Space Sci.* 113 298-308, 2015.

EPSC Abstracts
Vol. 11, EPSC2017-86, 2017
European Planetary Science Congress 2017

Generation mechanism of precessing circulation of the Venus polar vortex

H. Ando (hando@cc.kyoto-su.ac.jp) (1), N. Sugimoto (2) and M. Takagi (1)
(1) Kyoto Sangyo University, Kyoto, Japan, (2) Keio University, Yokohama, Japan

Abstract

Recent infrared measurements conducted in Venus Express showed the short-period temporal variation of the polar vortex, implying that the rotation period of the atmosphere in the polar region oscillates quasi-periodically. However, the mechanism to generate it has been unknown. Here we show the observed short-period variations are well reproduced for the first time by a Venus general circulation model. These variations are caused by short-period disturbances related to barotropic instability in the polar region. The zonally averaged zonal wind velocity changes quasi-periodically due to meridional transport of zonal momentum associated with a zonal wavenumber-1 component of the short-period disturbances; the mean zonal velocity increases (decreases) when the disturbances are inclined on the longitude-latitude plane toward northeast (northwest) direction. Our present result suggests that the vacillation of the polar vortex occurs in the Venus as well as the Earth, and shows that barotropic instability plays a crucial role to induce the vacillation in both planets.

1. Introduction

Interesting unique features are known in the Venus polar atmosphere at the cloud levels. The cold collar is a distinguishing thermal structure observed at high latitudes at about 65 km altitude, which is a local cold latitude band surrounding the warm polar region ([1], [2]). In the warm polar region, axi-asymmetric temperature disturbances with zonal wavenumbers of 1 and/or 2 have been observed by infrared measurements, which rotate around the pole with the period of ~3 Earth days ([1], [2]).

Temporal variations of the structure of the Venus polar vortex have been suggested from the recent infrared measurements in Venus Express mission ([3], [4]). It is indicated that the vortex center rotates around the pole in a precessional motion with nearly constant but temporally varying angular velocity. Interestingly, the rotational motion of the vortex center is accelerated and decelerated quasi-periodically with a period of ~3 Earth days. It is also inferred that these motions might be attributed to the axi-asymmetric eddies generated by barotropic or baroclinic instabilities. However, these infrared measurements of the Venus polar atmosphere were not performed for a long period continuously, it is difficult to investigate a mechanism of the temporal variation of the polar vortex.

Atmospheric GCM for the Earth Simulator for Venus (VAFES) ([5], [6]) succeeded in reproducing the cold collar and the warm polar region, and elucidating the generation mechanism of these thermal structures ([7]). Furthermore, it also reproduced the short-period axi-asymmetric temperature disturbances seen in the warm polar region ([7]), which is in good agreement with infrared and radio occultation measurements ([1], [2], [3], [4]), and showed their three-dimensional structures. In the present study, we used VAFES to investigate the mechanism of the short-period temporal variation of the polar vortex suggested by the previous infrared measurements ([3], [4]).

2. Results

In this study, we focus on the short-period disturbances with the period of less than 10 Earth days. Figures 1a and 1b show the latitude-time distributions of the zonally averaged zonal wind superimposed on the zonally averaged horizontal momentum flux associated with the zonal wavenumber-1 component of short-period disturbances at the latitudes of 60˚N–90˚N at 57 km and 70 km altitudes. At both altitudes, the oscillation pattern of the zonally averaged zonal wind speed is closely related to the sign of the horizontal momentum flux at latitudes poleward of 75˚N: the wind speed increases (decreases) when the sign is positive (negative) and then the horizontal momentum is transported toward the pole (low and middle latitudes). Recent work by VAFES indicated

that the short-period disturbance is related to barotropic instability in the polar region, then it is possible that the quasi-periodical oscillation of the zonally averaged zonal wind speed shown in Figures 1a and 1b is also connected with barotropic instability. Figures 1c and 1d show the latitude-time distributions of the meridional gradient of the absolute vorticity at latitudes poleward of 60˚N at 57 km and 70 km altitudes. There are a lot of timings when it is equal to zero at the latitudes poleward of 75˚N at 57 km altitude and 80˚N at 70 km altitude. This suggests that the necessary condition where barotropic instability occurs is satisfied near the pole. It is also confirmed that the short-period oscillation of the zonally averaged zonal wind speed is mainly associated with the horizontal momentum flux. Then barotropic instability seems to play an important role in generating this oscillation in our model.

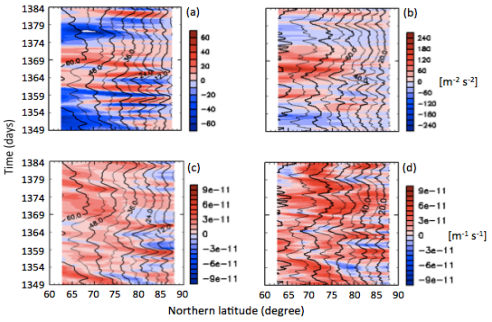

Figure 1: Latitude-time distributions of (Top) the zonally averaged momentum flux associated with zonal wavenumber-1 component of the short-period disturbances and (Bottom) meridional gradient of absolute vorticity. The black contour shown in each panel represents the zonally averaged zonal wind speed. Left (**a** and **c**) and right (**b** and **d**) columns are at 57 km and 70 km altitudes. The latitude and time ranges are 60˚N–90˚N and 1349–1384 Earth days, respectively.

3. Summary and Conclusions

Vacillation in the Earth's polar vortex, which is the quasi-periodical variation of the zonally averaged zonal wind speed in the polar region, is often observed. Our results suggest that the vacillation might also occur in the Venus polar vortex, implying that the atmospheric motion in it is unstable. In case of the Earth, it is theoretically shown that the vacillation is attributed to the short-period disturbance related to barotropic and/or baroclinic instability in a forced-dissipative polar vortex system ([8]). Our results also indicate that the quasi-periodic oscillation of the zonally averaged zonal wind speed is related to barotropic instability in the Venus polar region. Therefore, barotropic instability might be the main generation mechanism of the vacillation common to the Earth and Venus atmospheres.

Acknowledgements

This study was conducted under the joint research project of the Earth Simulator Center with title "Simulations of Atmospheric General Circulations of Earth-like Planets by AFES" and partly supported by JSPS KAKENHI Grant Number 25400470 and 00323494. Figures were produced by GNUPLOT and GFD-DENNOU Library.

References

[1] Taylor et al.: Structure and meteorology of the middle atmosphere of Venus infrared remote sensing from the Pioneer orbiter, *J. Geophys Res*., 85, 7963–8006, 1980.

[2] Piccioni et al.: South-polar features on Venus similar to those near the north pole, *Nature*, 450, 637–640, 2007.

[3] Luz et al.: Venus's southern polar vortex reveals precessing circulation, *Science*, 332, 577–580, 2011.

[4] Garate-Lopez et al.: A chaotic long-lives vortex at the southern pole of Venus, *Nat. Geosci*., 6, 254–257, 2013.

[5] Sugimoto et al.: Baroclinic instability in the Venus atmosphere simulated by GCM, *J. Geophys Res*., 119, 1950–1968, 2014a.

[6] Sugimoto et al.: Waves in a Venus general circulation model, *Geophys. Res. Lett*., 41, 7461–7467, 2014b.

[7] Ando et al.: The puzzling Venusian polar atmospheric structure reproduced by a general circulation model, *Nat. Commun*., 7:10398, doi: 10.1038/ncomms10398, 2016.

[8] Ishioka and Yoden: Non-linear aspects of a barotropically unstable polar vortex in a forced-dissipative system: flow regimes and tracer transport, *J. Meteor. Soc. Japan*, 73, 201–212, 1995.

EPSC Abstracts
Vol. 11, EPSC2017-111, 2017
European Planetary Science Congress 2017

Circulation of Venusian atmosphere at 95-100 km apparent motions of 1.27 μm nightglow of O_2 observed by VIRTIS on board Venus Express

D. Gorinov, I. Khatuntsev, L. Zasova and A. Turin
Space Research Institute RAS, Moscow, Russia (gorinov-dmitry@yandex.ru / Tel: +7-910-4741032)

Abstract

The infrared M-channel of the Visible and InfraRed Thermal Imaging Spectrometer (VIRTIS) onboard Venus Express Mission was performing observations of the atmosphere of Venus from 2006 to 2008. At 1.27 μm on the nightside it was able to monitor the $O_2(a^1\Delta)$ airglow, the distribution of which is highly variable in magnitude, location and morphology [6]. Tracking the displacement of bright features allows for measuring the wind velocities at the altitudes of the emission (95-100 km). This altitude range is located above the zonal superrotation-dominated area and below the influence of the SS-AS (subsolar-antisolar) mode of circulation, resulting in a complex behavior, therefore understanding this motion is a key aspect of the Venus atmosphere dynamics. In this work we have analyzed the entire VIRTIS-M-IR dataset of nadir images to obtain maps of the mean zonal and meridional components of the wind speed as well as analyze dependence of the motion on local time, latitude and longitude and orbit-to-orbit variation.

1. Introduction

Planet Venus possesses a thick atmosphere which demonstrates a complex combination of motions. The most distinctive dynamic feature of the atmosphere is the zonal super-rotation, a strong and consistent flow that reaches its peak velocity (~100 m s^{-1}) in the low latitudes at the altitude of 65-70 km above the surface [3] and drops in magnitude in the poleward direction. Present at much higher altitudes (> 110 km) is a subsolar-to-antisolar (SS-AS) circulation cell, which is driven by the solar heating. The two mechanisms interfere with each other in the transition region, 90-110 km, and the resulting complex dynamic pattern is not well understood [1][5].

A good indicator of the atmospheric motion on the nightside is the oxygen airglow $O_2(a^1\Delta)$ at 1.27 μm wavelength. Formed in the dayside thermosphere due to the photolysis of the CO_2 molecules, atomic oxygen travels onto the nightside with the SS-AS circulation, and recombines into molecular oxygen in the excited ($a^1\Delta$) state [2].

The "cloud-like" morphology of the oxygen nightglow allows for manually tracking the displacement of certain features in them over time, given a set of consecutive images. Previous partial analysis of the dataset revealed the wind velocities to reach 100 m/s and have a large variety of directions and the general coincidence of the apparent nightglow motion with the SS-AS mode of circulation [1].

2. Experimental data and approach

For this work we have selected 90 orbits (Table 1), where VIRTIS-M-IR obtained images, filtered by the following criteria:

- Visually identified presence of the oxygen airglow at 1.27 μm;
- Exposure time of 3 seconds and longer in order to work with an acceptable signal-to-noise ratio and minimize errors [7];
- Series of images which are spread out by 0.5 or 1 or 2 hours, focused at the same area of the disk of Venus, to allow tracking the displacement of features.

Although the lifetime of a ($a^1\Delta$) excited state is ~70 min, the large bright nightglow structures (1000-4000 km) are persistent for several hours, implying a downward flux of O_2 molecules. The smaller features, up to 100 km, which are used for wind tracking, can disappear over the course of 2 hours and more. Most wind vectors are tracked along the edges of the bright structures where the signal gradient is high, whereas areas of peak brightness are devoid of traceable markings.

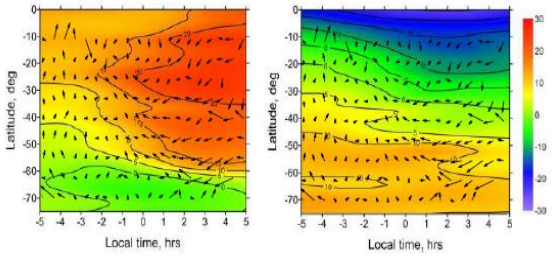

Figure 1.Average zonal (left) and meridional (right) components of $O_2(a^1\Delta)$ nightglow motion as a function of local time and latitude.

3. Results and Conclusions

We analyzed the resulting amount of 6019 vectors across the nightside in the southern hemisphere and equatorial region (no northern hemisphere due to the Venus Express orbit [8]).

The mean zonal component behaves differently before and after midnight. The 0 to +5 h local time range is dominated by the eastward motion (+10 to +70 m/s), whereas in the -5 to 0 h range the behavior is more complex, although the westward (-10 to -40 m/s) is more prevalent. Same dichotomy concerns the meridional component: it is predominantly equatorward before midnight (0 to +40 m/s), and mostly poleward after midnight (-50 to +20 m/s) (Figure 1).

No direct correlation of the wind speed with the surface was found, although the longitude-latitude range which corresponds to Aphrodite Terra, the largest surface structure was scarcely covered by nadir VIRTIS-M measurements.

The dataset of nadir images contains few series of consecutive orbits, however the available series appeared to be extremely helpful to analyze the orbit-to orbit variation. With ~24 hours between each orbit we were able to observe how the directions and the magnitudes of motions change with relation to the changing nightglow itself. Areas of circular motion with a lifetime of less than 24 hours were discovered, ranging from 1500 to 4000 km in diameter.

Acknowledgements

D. Gorinov and I. Khatuntsev were supported by the Ministry of Education and Science of Russian Federation grant 14.W03.31.0017.

References

[1] Bougher, S.W., Rafkin, S., Drossart, P.: Dynamics of the Venus upper atmosphere: Outstanding problems and new constraints expected from Venus Express. Planet. Space Sci. V. 54, P. 1371 – 1380, 2006.

[2] Connes, P., Noxon, J.F., Traub, W.A., Carleton, P.: $O_2(a^1\Delta)$ emission in the day and night airglow of Venus. Astrophys. J. 233, L29–L32, 1979.

[3] Gierasch, P.J., Goody, R.M., Young, R.E., Crisp, D., Edwards, C., Kahn, R., McCleese, D., Rider, D., del Genio, A., Greeley, R., Hou, A., Leovy, C.B., Newman, M.: The general circulation of the Venus atmosphere: an assessment. In: Bucher, J.W., Hunten, D.M., Phillips, R.J. (Eds.), Venus II — Geology, Geophysics, Atmosphere, and Solar Wind Environment. University of Arizona Press, Tucson, pp. 459–500, 1997.

[4] Hueso, R., Sanchez-Lavega, A., Piccioni, G., Drossart, P., Gérard, J.C., Khatuntsev, I., Zasova, L., Migliorini, A.: Morphology and Dynamics of Venus Oxygen Airglow from Venus Express / VIRTIS observations, J. Geophys. Res., V.113, E00B02, 2008.

[5] Lellouch, E., Clancy, T., Crisp, D., Kliore, A., Titov, D., Bougher, W.: Monitoring of mesospheric structure and dynamics, in Venus II: Geology, Geophysics, Atmospheres, and Solar Wind Environment, edited by S. W. Bougher, D. M. Hunten, and R. J. Philips, pp. 295– 324, Univ. of Ariz. Press, Tucson, 1997

[6] Piccioni, G., Zasova, L., Migliorini, A., Drossart, P., Shakun, A., García Muñoz, A., Mills F. P., Cardesin-Moinelo, A.: Near-IR oxygen nightglow observed by VIRTIS in the Venus upper atmosphere. J. Geophys. Res., 114, E00B38, 2009.

[7] Shakun, A. V., Zasova, L. V., Piccioni, G., Drossart, P., Migliorini, A.: Investigation of oxygen O2(a1Δ g) emission on the nightside of Venus: Nadir data of the VIRTIS-M experiment of the Venus Express mission. Cos. Res., Volume 48, Issue 3, pp.232-239, 2010.

[8] Svedhem, H., Titov, D.V., Taylor, F.W., Witasse, O.: The Venus Express mission. J. Geophys. Res. 114, E00B33, 2009.

EPSC Abstracts
Vol. 11, EPSC2017-121, 2017
European Planetary Science Congress 2017

Data assimilation system for the Venusian atmosphere

N. Sugimoto (1), A. Yamazaki (2), T. kouyama (3), H. Kashimura (4), T. Enomoto (2, 5), and M. Takagi (6)
(1) Keio University, Yokohama, (nori@phys-h.keio.ac.jp / Fax: +81-45-566-1320), (2) JAMSTEC, Yokohama, (3) AIST, Tsukuba, (4) Kobe University, Kobe, (5) Kyoto University, Uji, (6) Kyoto Sangyo University, Kyoto, Japan.

Abstract

A data assimilation system based on the local ensemble transform Kalman filter (LETKF) for a Venusian general circulation model (VAFES) has been developed. Two sets of data are assimilated separately to VAFES forecasts forced with the solar heating excluding the diurnal component (Qz); one is created from a VAFES run forced with the solar heating including the diurnal component (Qt) and the other is based on the observations of Venus Monitoring Camera (VMC) onboard Venus Express. Our system reduces errors between analysis and forecast quickly, and successfully reproduces the thermal tide excited by the diurnal component of the solar heating.

1. Introduction

The data assimilation is an effective tool widely used in the planetary atmospheric science. Since observation data are irregularly sampled in space and time, global and continuous analysis fields produced by general circulation models (GCMs) with the data assimilation, which are dynamically and thermodynamically consistent, are quite useful to study atmospheric dynamics.

For the Venusian atmosphere, however, the data assimilation has not been attempted so far. Recently, we developed a Venusian Atmospheric GCM named VAFES on the basis of Atmospheric GCM For the Earth Simulator (AFES) [1], which enables us to reproduce the realistic structure of the Venusian atmosphere. Using VAFES, we have succeeded in investigating barotropic/baroclinic instability waves [2, 3] and elucidating a puzzling temperature structure called “cold collar” [4]. In the present study, we develop a new data assimilation system for the Venus atmosphere based on VAFES and the local ensemble transform Kalman filter (LETKF) [5, 6], which is one of the most powerful schemes, and test it with idealized and observational data.

2. VAFES-LETKF system

VAFES is a full nonlinear Venus GCM with simplified physical processes [2-4]. The resolution is set to T42L60 (128 times 64 horizontal grids and 60 vertical levels). The vertical domain extends from the flat ground to ~120 km. In the upper atmosphere above 80 km, a sponge layer is assumed only for eddy components. The model includes vertical and horizontal eddy diffusion. Convective adjustment is applied to eliminate static instability. The infrared radiative process is simplified by a Newtonian cooling and the temperature is relaxed to a prescribed horizontally uniform temperature based on VIRA.

Vertical and horizontal distributions of the solar heating are based on previous observations and decomposed into a zonal mean component and a deviation from the zonal mean (diurnal component), which excite the mean meridional (Hadley) circulation and the thermal tide, respectively. Two cases of run are prepared as follows: Case Qt includes both components, whereas Case Qz the zonal mean component only. Other details of the model settings are described in our previous works [2-4].

The initial state is assumed to be an idealized superrotating flow in solid-body rotation. The zonal wind increases linearly with height from the ground to 70 km. The temperature distribution is in gradient wind balance with the zonal wind. Using this initial state, we perform nonlinear numerical simulations for more than 4 Earth years both for Cases Qt and Qz. The model atmospheres reached quasi-steady states within approximately an Earth year. Quasi-equilibrium data sampled at 1-hour intervals in Case Qt are used for the idealized observations, and those at 8-hour intervals in Case Qz are for initial conditions of each member of the ensemble.

In data assimilation schemes, an improved estimate (called analysis) is derived by combining observations and short time forecasts. The LETKF [5, 6] seeks the analysis solution with minimum error variance. Using an ensemble of VAFES runs, uncertainty of the model forecast is characterized. In the present VAFES-LETKF data assimilation system, 31-member

ensemble and 10% multiplicative spread inflation are employed. The localization parameters are chosen to be 400 km in horizontal and lnP = 0.4 in vertical where P is pressure. Observation errors for horizontal winds are fixed to be 4.0 m s^{-1}. A minimal interval of the data assimilation cycle is 6 hours.

We prepare several idealized observations of horizontal winds at 70 km (the cloud top level) with different intervals from Case Qt of the VAFES run. The other observation data is based on the UV images taken by the VMC (Case Vmc) [7], which includes the horizontal winds at ~70 km in a narrow dayside region. Time-intervals of the VMC horizontal wind data are approximately an Earth day. All the observations capture the thermal tide component, although the VAFES forecasts to be assimilated do not. Therefore, if the VAFES-LETKF system works, it is expected that the thermal tide is reproduced in the data assimilation with both the two observation sets.

3. Results

The VAFES-LETKF data assimilation system quickly reduces the analysis and subsequent forecast root-mean-square error. Furthermore, though the observation data are given at 70 km only, the three-dimensional structure associated with the thermal tide appears clearly even in Case Vmc, suggesting its upward propagation above 70 km (Fig.1).

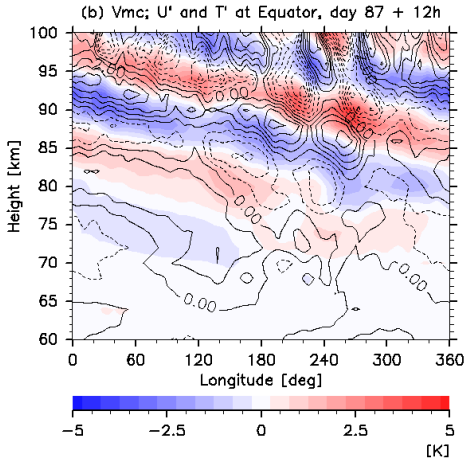

Figure 1: Vertical distributions of temperature deviation from zonally averaged temperature (color shades) for Case Vmc. Slowly varying components (thermal tide) are extracted by a low-pass filter with a cut-off period longer than 4 Earth days.

4. Summary and Conclusions

In the present work, we developed the VAFES-LETKF data assimilation system applicable to the Venus atmosphere and confirmed it works. In the presentation, we will show the impact of the data assimilation associated with the thermal tide on the general circulation. It is strongly expected that the Akatsuki data with the VAFES-LETKF data assimilation system enable us to reproduce more reliable structures of the Venus atmosphere.

Acknowledgements

This study was conducted under the joint research project of the Earth Simulator Center entitled 'Simulations of Atmospheric General Circulations of Earth-like Planets by AFES.' VAFES-LETKF data assimilation system integrations were performed on the Earth Simulator with the support of JAMSTEC.

References

[1] Ohfuchi, W., et al.: 10-km mesh meso-scale resolving simulations of the global atmosphere on the Earth Simulator: Preliminary outcomes of AFES (AGCM for the Earth Simulator), J. Earth Simulator, 1, 8–34, 2004.

[2] Sugimoto, N., Takagi, M., and Matsuda, Y.: Baroclinic instability in the Venus atmosphere simulated by GCM, J. Geophys. Res., Planets, 119, 1950–1968, 2014.

[3] Sugimoto, N., Takagi, M., and Matsuda, Y.: Waves in a Venus general circulation model, Geophys. Res. Lett., 41, 7461–7467, 2014.

[4] Ando, H., Sugimoto, N., Takagi, M., Kashimura, H., Imamura, T. and Matsuda, Y.: The puzzling Venusian polar atmospheric structure reproduced by a general circulation model, Nat. Commun., 7, 10398, 2016.

[5] Hunt, B. R., Kostelich, E. J., and Szunyogh, I.: Efficient data assimilation for spatiotemporal chaos: A local ensemble transform Kalman filter, Physica D, 230, 112–126, 2007.

[6] Miyoshi, T., and Yamane, S.: Local ensemble transform Kalman filtering with an AGCM at a T159/L48 resolution, Mon. Wea. Rev., 135, 3841–3861, 2007.

[7] Kouyama, T., Imamura, T., Nakamura, M., Satoh, T. and Futaana Y.: Long-term variation in the cloud-tracked zonal velocities at the cloud top of Venus deduced from Venus Express VMC images, J. Geophys. Res., 118, 37–46, 2013.

EPSC Abstracts
Vol. 11, EPSC2017-124, 2017
European Planetary Science Congress 2017

Atmospheric CO_2 supersaturation in the Martian polar nights: Role of large-scale atmospheric waves

K. Noguchi (1), T. Kuroda (2), S. Tellmann (3) and M. Pätzold (3)
(1) Nara Women's University, Japan(nogu@ics.nara-wu.ac.jp / Fax: +81-472-3437), (2) National Institute of Information and Communications Technology, Japan (3) University of Cologne, Germany.

Abstract

This study aims at investigating the role of large-scale atmospheric waves (stationary waves and transient waves) on CO_2 supersaturation at northern winter high latitudes on Mars. A distinct longitudinal dependence of CO_2 supersaturation was observed at high altitude levels (around 100 Pa), where a wavenumber 2 stationary wave lowered the background temperature. However, the stationary wave alone was not sufficient to cause CO_2 supersaturation. We found that additional temperature disturbances caused by transient waves, namely, superposition of both waves, had a significant role in CO_2 supersaturation.

1. Introduction

In the Martian atmosphere, the main component is carbon dioxide (CO_2). Since the air temperature often falls below the condensation temperature of CO_2 in the polar night regions on Mars, it is supposed that the supersaturation and/or condensation of CO_2 occur in the atmosphere [1].

Previous studies showed that CO_2 supersaturation is caused by small-scale atmospheric waves (e.g., gravity waves and mountain waves) and large-scale atmospheric waves such as transient waves (baroclinic waves) and stationary waves. The present study investigates the effects of transient waves and stationary waves on CO_2 supersaturation in the Martian atmosphere by using the Mars Global Surveyor (MGS) Radio occultation (RO) data [2], which are suitable for the studies of atmospheric thermal structures including CO_2 supersaturation. We show the spatio-temporal distribution of the occurrence of CO_2 supersaturation, focusing on the northern polar nights regions (60-70N), where enough profiles of temperature and pressure of the MGS RO data are available. We also compare the MGS RO results with numerical simulation results.

2. Data

In the MGS RO measurements, more than 20,000 profiles of temperature and pressure on Mars during 1998-2007 (Mars Year, MY 24-28) are available. The MGS RO data includes altitude, temperature, pressure and air number density, and are provided at the website of the Planetary Data System, NASA. For comparison, we utilized simulation results from the numerical models, Dynamics, RAdiation, MAterial Transport and their mutual InteraCtions (DRAMATIC) [3].

3. Results

At high altitudes (around 100Pa), CO_2 supersaturation appears at longitudes 90-180E and 270-360E, and no saturation can be seen in other longitude domains. The longitudinal sections where CO_2 supersaturation occurs overlap with zonal temperature minima with wave number 2 (s=2). The results from the numerical model, DRAMATIC, are consistent with the observations and suggest more frequent occurrence of CO_2 supersaturation even above 100 Pa, where much smaller number of CO_2 supersaturation events were observed by the MGS RO measurements.

At lower altitudes (around 610 Pa), CO_2 supersaturation occurs at almost all the longitude sections, although the effect of the stationary wave still remains. Past studies showed that transient waves with s=1,2 and 3 frequently appear in the mid- to high latitudes during autumn and winter [4,5]. We conducted a wavenumber analysis [5] to extract the fluctuation components of temperature caused by stationary waves and transient waves. Figure 1 shows an example of all the fluctuation components

extracted by the wavenumber analysis and CO_2 supersaturation events observed by MGS RO on the pressure level of 610 Pa in MY 27. We can see that many CO_2 supersaturation events occur in negative phases of temperature. This suggests a strong influence of stationary and transient waves on CO_2 supersaturation.

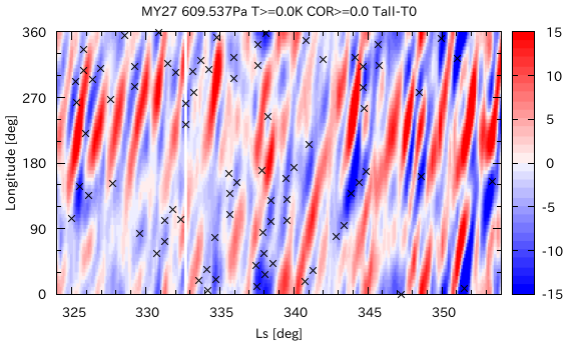

Figure 1: MGS RO temperature fluctuation components extracted by a wavenumber analysis (color shaded regions) and CO_2 supersaturation events (crosses) on the pressure level of 610 Pa in MY27.

4. Summary and Conclusions

We found the relationship between large-scale atmospheric waves including stationary and transient waves and the occurrence of CO_2 supersaturation in the northern hemisphere winter on Mars. The s=2 stationary wave played a significant role in lowering the background temperature and it was close to the CO_2 saturation temperature at around 100 Pa, where strong longitudinal dependence of CO_2 supersaturation was observed, but the stationary wave alone was not sufficient to cause CO_2 supersaturation. In addition to stationary waves, transient waves were also important and the superposition of both waves had a significant role in causing CO_2 supersaturation.

Acknowledgements

The authors are grateful to David P. Hinson and the MGS radio occultation team for providing pressure-temperature data from the radio occultation measurements. The MGS radio occultation data are available at the Atmospheres Node of the NASA Planetary Data System (http://atmos.pds.nasa.gov/MGS/tp.html). KN was supported by JSPS KAKENHI Grant Number 15K05289.

References

[1] Kieffer et al. (1977) *JGR, 82(28)*, 4249–4291.

[2] Hinson et al. (1999) *JGR, 104(E11)*, 26,997–27,012.

[3] Kuroda et al. (2005) *J. Meteorol. Soc. Japan, 83(1)*, 1–19.

[4] Banfield et al. (2003) *Icarus, 161(2)*, 319-345.

[5] Hinson et al. (2006) *JGR, 111*, E05002..

EPSC Abstracts
Vol. 11, EPSC2017-156-1, 2017
European Planetary Science Congress 2017

Simulation of the high-resolution water cycle and HDO/H_2O isotopic fractionation on Mars using DRAMATIC MGCM

T. Kuroda (1,2), (1) National Institute of Information and Communications Technology, Japan, (2) Department of Geophysics, Tohoku University, Japan (tkuroda@nict.go.jp).

Abstract

We are starting to simulate the water cycle of the present Martian environment using a Mars general circulation model (MGCM) for the investigations of the water cycle system and related material transport on Mars in collaboration with the current and future observations. We performed the horizontal high-resolution simulations with the grid intervals of ~67 km, showing the relationships between water transport and atmospheric dynamics more clearly than the previous low-resolution simulations. Our results show the consistent seasonal and latitudinal changes of zonal-mean water vapor column density and ice opacity with observations in the run without the radiative effects of water ice clouds. Also, we have implemented the HDO/H_2O isotopic fractionations, and reproduced the qualitatively consistent seasonal and latitudinal changes of the ratio with a preceding simulation.

1. Introduction

The spacecraft on the Mars orbit, such as Mars Global Surveyor (MGS), Mars Odyssey, Mars Express and Mars Reconnaissance Orbiter (MRO), have continuously observed the global distributions of water vapor and water ice clouds for these 18 years (almost a Martian decade). In parallel with the reservoir of observational data, simulations of the water cycle on Mars using Martian General Circulation Models (MGCMs) have been performed in several groups [1-3], providing a lot of improvements of the physical processes such as cloud microphysics [4] and implementation of the radiative effects of water ice clouds [5]. Also, the detailed observations of HDO/H_2O isotopic ratio are planned by the ExoMars Trace Gas Orbiter (EMTGO), for the detections of age and transport processes of water. Moreover, horizontal high-resolution simulation would be helpful for the investigations including small-scale dynamical features to support the ongoing observations by EMTGO and ground-based telescopes.

2. Model description

The DRAMATIC (Dynamics, RAdiation, MAterial Transport and their mutual InteraCtions) MGCM [6-8] used in this study is based on the dynamical core of the CCSR/NIES/FRCGC MIROC model [9]. The MGCM has a spectral solver for the three-dimensional primitive equations, and the runs are performed with the horizontal resolution of T106 (about 1.1°×1.1°, ~67 km at equator), and vertical 49 sigma-levels (the altitude of the lowest layer is ~50 m) up to ~90 km. Physical parameterizations for the present Mars environment are described in [6] with updates in [7], and the implementations of water cycle and HDO/H_2O isotopic fractionations are as described in [10]. The calculations started from the 'dry' iso-thermal state without water vapor/ice in the at-mosphere and on surface except the permanent water ice cap in the north of 80° N. The isotopic ratio of the permanent north polar water ice cap is set to 7.0 VSMOW (Vienna Standard Mean Ocean Water, $[HDO]/[H_2O]= 3.1\times10^{-4}$).

3. Results

With the run for ~10 Martian years from the isothermal state, the results of annual water cycle become in equilibrium in overall. Without the radiative effects of water ice clouds, we could reproduce the seasonal changes of water vapor column density and water ice opacity agreeing with the MGS-Thermal Emission Spectrometer (TES) observations [11]. Also, we simulated the seasonal and latitudinal changes of HDO/H_2O ratio, which were in overall consistent qualitatively with a preceding simulation [12].

Figures 1 and 2 show the snapshots of water vapor column density and HDO/H_2O ratio at L_s~9°

(northern spring), localtime of 0600 at 0° longitude. In both figures the structure of baroclinic waves with zonal wavenumbers of 1 and 2 is seen in northern mid-latitudes, as well as weaker zonal wavenumber 2 structure in southern mid-latitudes, which may transport the water vapor to polar regions. Moreover, the thermal tide may affect to strengthen the transport, as the strong flow to northeast is seen around 60° E (close to the sub-solar longitude) in northern high-latitudes. These features are more clearly seen in Figure 2, which indicates that the mapping of HDO/H_2O ratio with time sequences (for several hours or a few days) from the observations by EMTGO and/or ground-based telescopes would work to clarify the meridional transport of water.

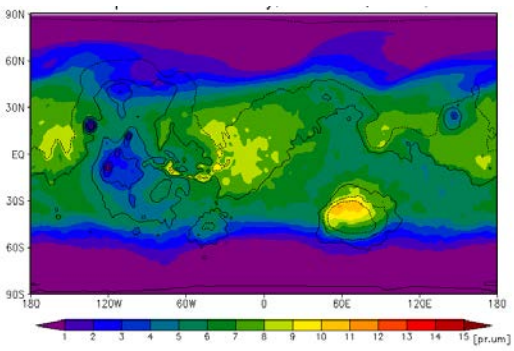

Figure 1: A snapshot of the horizontal distribution of water vapor column density in our T106 simulation, at L_s~9° at localtime of 0600 at 0° longitude.

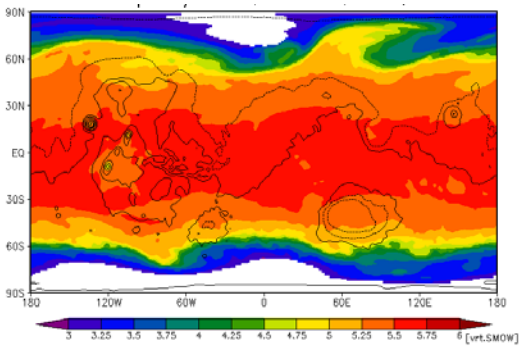

Figure 2: Same as Figure 1, except HDO/H_2O ratio in vapor column density.

4. Summary and notes

It needs to be noted that there are two main problems in our current simulation: (1) We need to make the particle size of water ice in the equatorial cloud belt unrealistically large (up to ~12 μm) to reproduce the observed cloud opacity. (2) If the radiative effects of water ice clouds are included, the atmospheric temperature becomes unrealistically high, which results in the increase of the equatorial cloud belt altitude in ~20 km and significant decrease of the opacity of equatorial cloud belt during northern summer (~1/10).

We need to improve the above points, but, nevertheless, our model has two main advantages: (1) HDO/H_2O isotopic fractionation and (2) horizontal high-resolution simulation in which the small-scale dynamical features can be reflected. With this MGCM, we intend to support the MRO and EMTGO missions which observe the water in lower atmosphere, and, moreover, the MAVEN (Mars Atmosphere and Volatile EvolutioN) mission which observe the compositions in the upper atmosphere with planned future implementation of the photochemical processes and extension of the model to the thermosphere.

Acknowledgements

This study was supported by JSPS KAKENHI Grant Number 16K05552.

References

[1] Richardson, M.I. and Wilson, R.J., J. Geophys. Res., 107(E5), 5031, doi:10.1029/2001JE001536, 2002.

[2] Richardson, M.I. et al., J. Geophys. Res., 107(E9), 5064, doi:10.1029/2001JE001804, 2002.

[3] Montmessin, F. et al., J. Geophys. Res., 109, E10004, doi:10.1029/2004JE002284, 2004.

[4] Navarro, T. et al., J. Geophys. Res. Planets, 119, 1479–1495, doi:10.1002/2013JE004550, 2014.

[5] Wilson, R.J. et al., Geophys. Res. Lett., 35, L07202, doi:10.1029/2007GL032405, 2008.

[6] Kuroda, T. et al., J. Meteorol. Soc. Jpn., 83, 1–19, 2005.

[7] Kuroda, T. et al., Geophys. Res. Lett., 40, 1484–1488, doi:10.1002/grl.50326, 2013.

[8] Kuroda, T. et al., Geophys. Res. Lett., 42, 9213–9222, doi:10.1002/2015GL066332, 2015.

[9] K-1 Model Developers, K-1 Tech. Rep., 1, Univ. of Tokyo, 1–34, 2004.

[10] Kuroda, T., Abstract book of 'Sixth international workshop on the Mars atmosphere: modelling and observations', Univ. of Granada, 2017.

[11] Smith, M.D., Annu. Rev. Earth Planet. Sci., 36, 191–219, doi:10.1146/annurev.earth.36.031207.124334, 2008.

[12] Montmessin, F. et al., J. Geophys. Res., 110, E03006, doi:10.1029/2004JE002357, 2005.

EPSC Abstracts
Vol. 11, EPSC2017-163, 2017
European Planetary Science Congress 2017

Distribution of meteoritic ions in the upper atmosphere of Mars as observed by MAVEN's mass spectrometer

M. Benna (1,2), J. M. Grebowsky (1), N. Srivastava (3), J. M. C. Plane (4), and P. R. Mahaffy (1)
(1) NASA Goddard Space Flight Center, Greenbelt, Maryland, USA, (2) CSST, University of Maryland Baltimore County, Baltimore, Maryland, USA, (3) Institute for Astrophysics and Computational Science, The Catholic University of America, Washington, District of Columbia, USA, (4) Faculty of Mathematics and Physical Sciences, University of Leeds, Leeds, UK
(mehdi.benna@nasa.gov / Fax: +1-301-6146404)

Abstract

The Mars Atmosphere and Volatile EvolutioN (MAVEN) mission made the first in situ detection of the continuous presence of Na^+, Mg^+, and Fe^+ at Mars. The measured density distributions revealed that these metal ions are well-mixed with the neutral atmosphere at altitudes where no mixing process is expected. Additionally, isolated metal ion layers mimicking Earth's sporadic E layers were regularly observed despite the lack of a strong magnetic field as required at Earth. Finally, the metal ion distributions are coherent enough to always reveal the signature of atmospheric gravity wave signatures.

1. Introduction

The formation of metal ions and their associated ionospheric layers by the ablation of meteoroids has been extensively observed in Earth's upper atmosphere, and metal ions such as Mg^+, Fe^+, Na^+, Al^+, Ca^+, and Ni^+, have been detected in the ionosphere [1, 2]. Several models mapped the chemical pathways by which these metal ions are recycled and ultimately removed [3]. Although well studied, the major characteristics of the metal ion layers are their complex structure and temporal variations. Interest in them persists because of the clues and frequent discoveries they provide for exploring meteoric properties, atmospheric dynamics, fundamental chemical processes, and ionospheric structures at low altitudes [4, 5].

Similar mechanisms were predicted to form metal ions in the Martian ionosphere as the result of the high-speed deposition and subsequent ablation of solar system dust particles. Evidence for this is based on radio occultation measurements by orbiting spacecrafts of isolated electron density layers sometimes seen below the main ionospheric peak [6]. The new in-situ observations taken by MAVEN's Neutral Gas and Ion Mass Spectrometer (NGIMS) show for the first time that the metal ions are indeed a ubiquitous ionospheric feature and do not only arise from exceptional meteoroid events like the close passage of comet Siding Spring in mid-October 2014. Several metal ion species and their isotopes have been, and are, continuously observed by NGIMS at low altitudes on most of MAVEN's orbits since the start of the mission in September 2014.

2. Observations

The NGIMS instrument has been collected data on metal ions during every other periapsis passage (every ~9 hours). While all metallic species and their ion oxides in the range of 23 – 86 Da are targeted by these observations, only Na^+, Mg^+, and Fe^+ were regularly detected. Figure 1 depicts the entire ensemble of Na^+, Mg^+, and Fe^+ measurements from MAVEN over the two years spanning from September 2014 to September 2016.

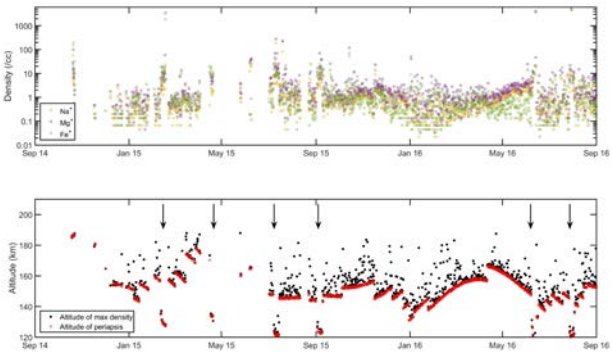

Figure 1: Orbit-by-orbit set of NGIMS measured Na^+, Mg^+, and Fe^+ maximum concentrations from September 2014 to September 2016. The altitude of each orbit's periapsis and the altitude of the maximum metal ion density of each orbit are shown on the bottom. Arrows mark the period of the deep-dip campaigns (larger figure provided in [7]).

As on Earth [8], the dominance of Mg^+ or Fe^+ on Mars changes with time. At either planet, one might expect Fe^+ to be less dominant with increasing altitude because of the mass separation from diffusion processes.

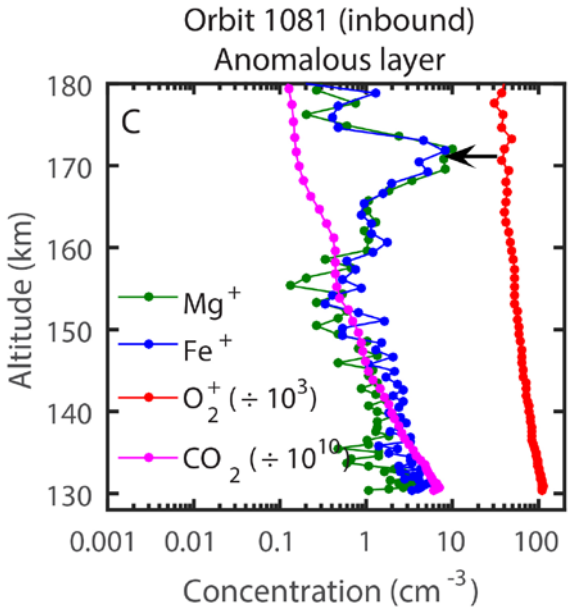

Figure 2: Characteristic structures of metal ion seen on a typical deep dip orbit. Relevant measurements of the main ionosphere ion O_2^+ and the major CO_2 neutral species are also shown. The dropoff of the metal ion concentrations follows closely the CO_2 scale heights. Isolated high-altitude metal ion peaks are pointed to. These density peaks are sometimes associated with ambient ionosphere disturbances at night and near the terminator.

Figure 2 shows samples of the metal ion altitude structures observed along orbits from "deep-dip" campaigns when periapsis was below 130 km altitude. Typically, the concentrations of metal ions at the lowest altitudes are < 10 cm^{-3} and exhibit an average orderly-like decrease with altitude. This decay of the metal ion densities with altitude tends to match closely the falloff of the neutral atmosphere concentration. The close similarity of CO_2 and metal ion scale heights indicates a well-mixed atmosphere with the metal ions behaving like inert minor atmospheric species. Such close correlation in scale heights would be expected if these data taken below the homopause (located below 130 km) where the atmosphere is well mixed through turbulent diffusion, but not well above the homopause where molecular diffusion is expected to take over, resulting in gravity mass separation of the heavy Fe^+ from the lighter Mg^+. High-altitude sporadic metal ion layers are also encountered. These layers are seen as nearly order of magnitude density enhancements above the altitude decreasing background profiles.

At Earth, the generation of isolated metal ion layers, above the main meteoric ion layer, requires the control of ions by neutral winds, or magnetospheric-induced electric fields, in a large magnetic field background [8, 9]. However, Mars has no intrinsic global magnetic field and the strength of the Martian surface remanent magnetic fields appears mostly insufficient to support any known terrestrial formation mechanism.

In addition to the well-mixing of the metal ions with the neutral atmosphere, the NGIMS observations reveal oscillations in the metal ion concentration profiles on most orbits. There is compelling evidence that these oscillations reflect the responses of the metal ions to atmospheric gravity waves. The observed waves in the metal concentrations along the MAVEN orbit have wavelengths of ~80 km along the nearly horizontal spacecraft trajectory near periapsis, which are the typical scale lengths for vertically propagating, horizontal gravity waves [10].

3. Summary and Conclusions

The in situ metal ion measurements at Mars have revealed new facets of how the ablated residues from interplanetary dust particles can interact with a planetary atmosphere. These observations leave us with several interesting puzzles to unravel. The main two being the absence of gravitational separations of the metal ions with altitude in the region where molecular diffusion is supposed to dominate; and the unknown source of the observed isolated metal ion layers in the absence of an intrinsic planetary magnetic field.

Acknowledgements

The MAVEN mission is supported by NASA through the Mars Scout program. The NGIMS data are available in a readily accessible format on the Planetary Data System at (http://atmos.nmsu.edu/data_and_services/atmospheres_data/MAVEN/ngims.html).

References

[1] Kopp, E.: On the abundance of metal ions in the lower ionosphere, J. Geophys. Res., 102, 9667–9675, 1997.

[2] Grebowsky, J. M., Goldberg, R. A., and Pesnell, W. D.: Do meteor showers significantly perturb the ionosphere?, J. Atmos. Sol. Terr. Phys., 60, 607–615, 1998.

[3] Molina-Cuberos, J. G., López-Moreno, J. J., and Arnold, F.: Meteoric layers in planetary atmospheres, Space Sci. Rev., 137, 175–191, 2008.

[4] Plane, J. M. C., Feng, W., and Dawkins, E. C. M.: The mesosphere and metals: Chemistry and changes, Chem. Rev., 115, 4497–4541, 2015.

[5] Carter, L. N., and Forbes, J. M.: Global transport and localized layering of metallic ions in the upper atmosphere, Ann. Geophysicae, 190–209, 1999.

[6] Pätzold, M., Tellmann, S., Häusler, B., Hinson, D. B., Schaa, R., and Tyler, G. L.: A sporadic third layer in the ionosphere of Mars, Science, 310, 837–839, 2005.

[7] Grebowsky, J. M., Benna, M., Plane, J. M. C., Collinson, G. A., Mahaffy, P. R., and Jakosky, B. M.: Unique, non-Earthlike, meteoritic ion behavior in upper atmosphere of Mars, Geophys. Res. Lett., 44, doi:10.1002/2017GL072635, 2017.

[8] Grebowsky, J. M., and Aikin, A. I: In-situ meteoric ion measurements, in Meteors in the Earth's Atmosphere, pp. 189–214, Cambridge Univ. Press, New York, 2002.

[9] Carter, L. N., and Forbes, J. M.: Global transport and localized layering of metallic ions in the upper atmosphere, Ann. Geophysicae, 190–209, 1999

[10] Fritts, D. C., Wang, J. L., and Tolson, R. H.: Mean and gravity wave structures in the Mars upper thermosphere inferred from Mars Global Surveyor and Mars Odyssey aerobraking densities, J. Geophys. Res., 111, A12304, 2006.

EPSC Abstracts
Vol. 11, EPSC2017-165, 2017
European Planetary Science Congress 2017

Reanalysis of the SPICAV-UV nadir spectra on the day side of Venus: SO_2, O_3 and other UV absorbers

E. Marcq, L. Baggio, F. Lefèvre, F. Montmessin, J.-L. Bertaux and the SPICAV team
LATMOS/IPSL/CNRS/UPMC/UVSQ, 11 boulevard d'Alembert, F-78280 Guyancourt, France
(emmanuel.marcq@latmos.ipsl.fr)

Abstract

1. Introduction

The ESA *Venus Express* spacecraft orbited around Venus between 2006 and 2014. During more than 14 Venusian years, its instruments, among which the UV spectrometer SPICAV-UV [1], acquired a wealth of data whose analysis has far from ended. Its nadir observations on the dayside enabled the analysis of the sunlight backscattered at Venus' cloud top in order to derive column densities of UV absorbers above the cloud top, most prominently SO_2 [2, 3].

We present here a wholly new analysis of SPICAV-UV nadir data based on a complete reprocessing of the full observational dataset. Compared to our legacy analysis, this study also take advantage of a greatly improved version of our forward radiative transfer model.

2 Improvements

2.1 Observation processing

Our pipeline has been greatly improved since our previous studies [2, 3]. A more accurate representation of the 2D instrumental PSF and spectral sensitivity has resulted in substantial improvements of the observed radiance factors. This is particularly spectacular in the wavelength range below 210 nm, where the weakness of the solar spectrum results in a poor accuracy of the spectral reflectance and therefore a large sensitivity to any parasitic light on the detector. On the other hand, the better treatment of the spectral sensitivity results in noticeable improvements for wavelengths larger than 300 nm, where the new radiance factors are more in line with other UV observations, such as those from HST [4].

2.2 Forward model

We also greatly improved our forward radiative transfer model. It is now able to take into account not only CO_2, SO_2 and SO as gaseous absorbers, but now includes O_3 as well as the new UV absorber candidate species cis- and trans-OSSO[5]. New mode 1 and mode 2 particle density profiles, based on recent SPICAV-IR data[6], are also included. It is also possible to alter the imaginary refractive index of the cloud and haze particles in order to adjust the UV brightness without resorting to a cruder multiplicative scaling factor, as it was the case in our first studies.

3 Preliminary results

The whole SPICAV-UV archive is currently (as of May 2017) being reprocessed according to the improved pipeline described hereabove. In the meantime, we were able to test out new forward model against a few selected reprocessed *VEx* orbits. Our still in progress work (Fig.1 and 2) indicates that (1) UV absorbers other than OSSO are required in order to account for the observed radiance factors, and (2) inclusion of O_3 absorption results in a statistically significant improvement of the fitting for some spectra.

Acknowledgements

This work has been supported by CNES and INSU (Programme National de Planétologie). We also wish to thank Patrick Martin ESA for their support.

References

[1] Bertaux, J.-L. et al.: SPICAV on Venus Express: Three spectrometers to study the global structure and composition of the Venus atmosphere, PSS **55**, pp. 1673-1700 (2006)

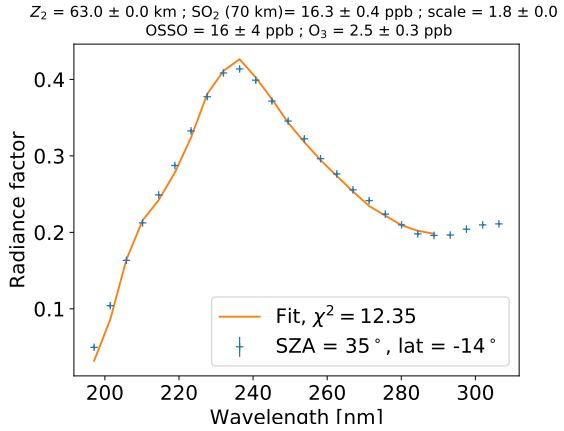

Figure 1: Preliminary fitting of a newly processed spectrum acquired during orbit # 595

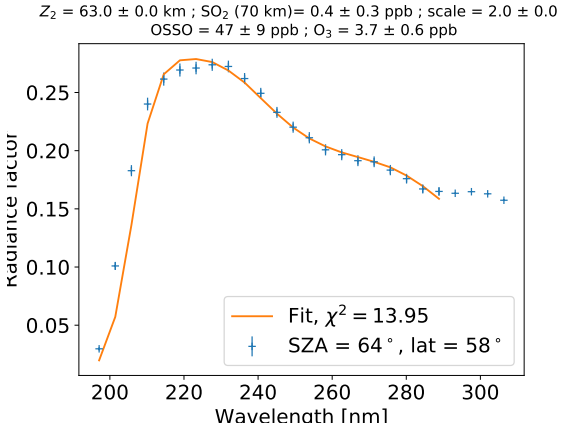

Figure 2: Preliminary fitting of a newly processed spectrum acquired during orbit # 1338

[2] Marcq, E. et al.: An investigation of the SO_2 content of the venusian mesosphere using SPICAV-UV in nadir mode, Icarus **211**, pp. 58-69 (2011)

[3] Marcq, E. et al.: Variations of sulphur dioxide at the cloud top of Venus's dynamic atmosphere, Nat. Geosci. **6**, pp. 25-28 (2013)

[4] Jessup, K. L. et al.: Variations of sulphur dioxide at the cloud top of Venus's dynamic atmosphere, Icarus **258**, pp. 309-336 (2015)

[5] Frandsen, B. N. et al.: Identification of OSSO as a near-UV absorber in the Venusian atmosphere, GRL **43**, pp. 11146-11155 (2016)

[6] Luginin, M. et al.: Aerosol properties in the upper haze of Venus from SPICAV IR data, Icarus **277**, pp. 154-170 (2016)

EPSC Abstracts
Vol. 11, EPSC2017-167, 2017
European Planetary Science Congress 2017

Ground-based thermal mapping on Venus: temperature fields and variations of SO_2 & HDO

T. Encrenaz (1), T. K. Greathouse (2), T. Widemann (1), B. Bézard (1), T. Fouchet (1), S. K. Atreya (3), H. Sagawa (4)
(1) LESIA, Paris Observatory, (2) SwRI, San Antonio, TX, USA, (3) University of Michigan, Ann Arbor, MI, USA, (4) Kyoto-Sangyo University, Kyoto, Japan (therese.encrenaz@obspm.fr)

Abstract

As a continuation of our ground-based thermal imaging campaign of Venus, we have been mapping Venus in December 2016 and January 2017 to monitor the behaviour of SO_2 and H_2O (through its proxy HDO). The SO_2 mixing ratio was at its maximum since 2012. As during our previous runs, short-term variations of SO_2 (with a timescale of a few hours) were observed. There is still no evidence for a correlation or an anti-correlation between SO_2 and HDO. The thermal maps might show some correlation with the topography, but this remains to be confirmed with further observations.

1. Introduction

Thee atmospheric photochemistry of Venus is known to be mainly driven by two minor species, SO_2 and H_2O [1, 2]. Since 2012, we have mapped the planet in the thermal infrared spectral range to monitor the behaviour of these two species [3-5], using the TEXES instrument (Texas Echelon Cross Echelle Spectrograph) at the InfraRed Telescope Facility (IRTF) at Maunakea Observatory. Our observations have shown evidence of strong spatial and temporal variations of SO_2, on both short-term and long-term. In contrast, the HDO maps are relatively uniform and show little variation with time. The origin of the SO_2 plumes is still poorly understood.

2. Observations

We observed Venus on December 16-23, 2016 and January 21-22, 2017. The planet size was 20 arcsec in December and 26 arcsec in January, with illumination factors of 60% and 46% respectively. Two spectral ranges were monitored, at 7.4 µm (1343-1348 cm^{-1}) and 19 µm (529-531 cm^{-1}). At 7.4 µm, SO_2 and HDO are probed at the cloudtop, while, at 19 µm, SO_2 is probed a few kilometers below the cloudtop [3-5].

3. Results

Figure 1 shows maps of the brightness temperature of Venus at 7.4 µm, on Dec. 22, 2016 and Jan. 21, 2017, respectively. It can be seen that the maximum radiance corresponds to a high-altitude region (Aphrodite Terra in December, Maats Mons in January) in both instances. Such correspondence, that was also observed at other wavelengths, was not found in our previous observations, which were centered on different longitudes of lower elevation. They might be associated to gravity waves as observed by Venus Express [6] and Akatsuki [7]. More observations will be needed to confirm this effect.

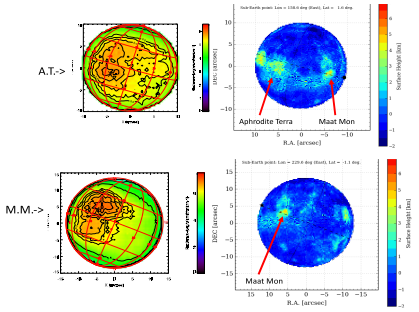

Figure 1: *Continuum maps of Venus on Dec. 22, 2016 (top) and Jan. 21, 2017 (bottom), compared with topography maps of Venus for the same observing conditions. The maximum radiance coincides with high elevations (top: Aphrodite Terra; bottom: Maats Mons).*

Figure 2 shows maps of the SO_2 mixing ratio, derived from the line depth ratio of two weak transitions of SO_2 and CO_2 at 7.4 microns, recorded on Jan. 21, 2017. Four maps are shown within a time interval of about 5 hours. They illustrate the patchy distribution of SO_2 and the short timescale of its variations. In the

present case, there is no evidence for a correlation with the zonal wind rotation. In contrast, the HDO maps inferred from the same spectra are uniform, as previously mentioned (Fig.3).

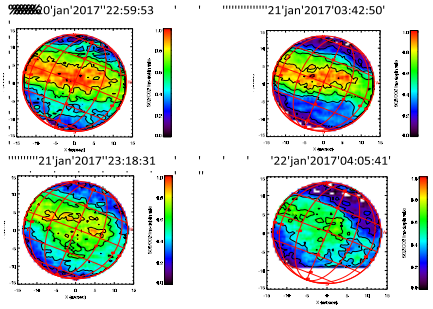

***Figure 2**: Maps of the SO_2/CO_2 line depth ratio, recorded on January 21, 2017. The SO_2 line at 1345.11 cm^{-1} and the CO_2 line at 1345.22 cm^{-1} were used (see [5]).*

Figure 4 summarizes the long-term variations of H_2O and SO_2 between 2012 and 2017, as derived from the TEXES data. It can be seen that the SO_2 abundance is strongest in January 2017, and more than 10 times its value of February 2014. The SO_2 values derived at 19 μm are usually equal or larger than the ones derived at 7.4 μm, which is expected since the 19-μm probe a few kilometres below the cloudtop observed at 7.4 μm. There is an exception in December 2016 that is presently unexplained. In contrast with SO_2, H_2O varies by less than a factor 2 as a function of time. There is no evidence for a correlation or an anti-correlation between H_2O and SO_2.

Acknowledgements

T.E. and T.K.G. were visiting astronomers at the InfraRed Telescope Facility, which is operated by the University of Hawaii under Cooperative Agreement no. NNX-08AE38A with the National Aeronautics and Space Administration, Science Mission Doctorate, Planetary Astronomy Program.

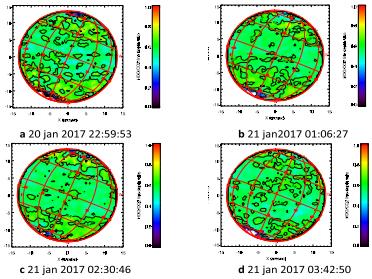

***Figure 3**: Maps of the HDO/CO_2 line depth ratio, recorded on January 21, 2017. The HDO line at 1344.90 cm^{-1} and the CO_2 line at 1345.22 cm^{-1} were used (see [5]).*

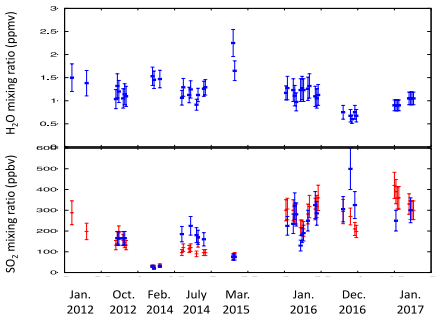

***Figure 4**: Long-term variations of the H_2O and SO_2 mixing ratios between 2012 and 2017. Top: HDO. Bottom: SO_2, 7.4-μm data (red), 19-μm data (blue).*

References

[1] Kasnopolsky, V. 1986, Photochemistry of the atmospheres of Mars and Venus (New York: Springer-Verlag)[2] Krasnopolsky, V. A. 2010, Icarus, 209, 314 ;[3] Encrenaz, T. et al. 2012, A&A 543, id.A153;[4] Encrenaz, T. et al. 2013, A&A 559, id.A65;[5]Encrenaz, T. et al. 2016, A&A 595, id.A74; [6] Bertaux, J.-L. et al. 2016, JGRE 121, 1087-1101;[7] Fukuhara, T. et al. 2017, Nature Geosc 10, 85

EPSC Abstracts
Vol. 11, EPSC2017-168, 2017
European Planetary Science Congress 2017

A new measurement of D/H on Mars using EXES aboard SOFIA

T. Encrenaz (1), C. DeWitt (2), M. Richter (2), T. Greathouse (3), T. Fouchet (1), F. Montmessin (4), F. Lefèvre (4), B. Bézard (1), S. K. Atreya (5), S. Aoki (6)
(1) LESIA, Paris Observatory, France, (2) UC Davis, CA, USA, (3) SwRI, San Antonio, TX, USA, (4) LATMOS, IPSL, Paris, France, (5) University of Michigan, Ann Arbor, MI, USA, (6) BISA, Brussels, Belgium (therese.encrenaz@obspm.fr))

Abstract

The distribution of D/H ratio on Mars is crucial for understanding the planet's water cycle including the exchange with surface reservoirs, and for estimating the amount of liquid water in the past. We have employed EXES (Echelle Cross Echelle Spectrograph) aboard SOFIA (Stratospheric Observatory For Infrared Astronomy) to map D/H on Mars in the thermal infrared, starting with the first measurement in April 2014 (Ls = 113°). Here we present a new measurement obtained in March 2016 (Ls = 127°). The disk-integrated value of D/H is found be 4.0 (+0.7, -0.6) x VSMOW, in agreement with our earlier result (4.4 (+1.0, -0.6) x VSMOW) [3]

1. Introduction

It has been known for several decades that the D/H ratio in Mars is significantly enriched relative to the terrestrial value (VSMOW, i.e. 1.556 10^{-4}), which has been interpreted as the signature of atmospheric loss due to differential escape [1]. High-resolution imaging spectroscopy now allows us to map the D/H ratio over the Martian disk, and thus provide constraints on the mechanisms responsible for deuterium fractionation through condensation/sublimation processes [2]. The high-resolution imaging spectrometer EXES, aboard the SOFIA aircraft, allows us to measure simultaneously H_2O and HDO transitions, and thus remove the contamination effect due to terrestrial atmospheric opacity. A first measurement was obtained in April 2014 during a commissioning flight of EXES [3]. At that time, Mars was close to opposition and the diameter of Mars was above 15 arcsec). The limitation of this observation was that the Doppler shift was close to zero, and the main difficulty was the removal of the terrestrial water contamination. In March 2016, we have repeated the observation with a different configuration, with a Doppler shift sufficient to separate the terrestrial water absorptions from the Martian ones, making the retrieval of the Martian water content and the D/H ratio much easier.

2. Observations

The observing run took place on March 24, 2016, between 11:43:13 UT and 12:30:27 UT. The altitude of the aircraft was 13.7 km. The diameter of Mars was 11 arcsec and the solar longitude, Ls, was 127°. We used the 1383-1392 cm^{-1} spectral range which contains both strong and weak lines of CO_2, H_2O and HDO. The spectral resolution, measured from the widths of the CO_2 Martian lines, was 0.022 cm^{-1} (Gaussian profile, R=63000). The slit of the spectrograph was moved over the planet to map the whole disk. The spatial resolution of the SOFIA is however limited to 3 arcsec.

Figure 1 shows the EXES disk-integrated spectrum of Mars, compared with a model spectrum of Mars showing the different contributions of CO_2, H_2O and HDO

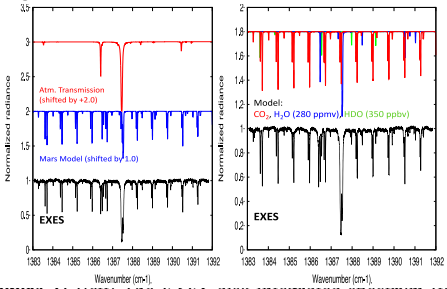

***Figure 1**: (left) The EXES disk-integrated spectrum (thick black line) compared with best-fit model of the Martian spectrum (blue) and the terrestrial opacity above 13 km (red). (right) The same EXES spectrum compared with best-fit model showing the contributions of CO_2 (red), H_2O (280 ppmv, blue) and HDO (350 ppbv, green)*

3. Data analysis and results

The terrestrial absorption spectrum dominates in the 1366-1368 cm^{-1} region. Outside this range, the Martian lines of CO_2, H_2O and HDO are mostly free of terrestrial contamination, thanks to the relatively large Doppler shift. As in the case of our previous analysis [3], we derived the H_2O and HDO mixing ratios from the line depth ratios of H_2O/CO_2 and HDO/CO_2 respectively, and we derived D/H directly from the HDO/H_2O line depth ratio. This method has the advantage of removing, to first order, the geometrical effect (airmass) and the uncertainties associated with the atmospheric thermal structure. Figure 2 shows the best disk-integrated fits obtained for the H_2O and HDO mixing ratios: H_2O = 280 +/- 20 ppbv (in very good agreement with the GCM prediction), and HDO = 350 +/-70 ppbv.

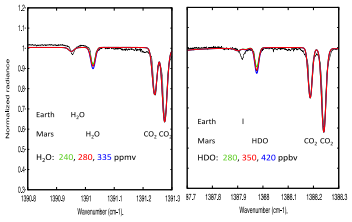

Figure 2: *Retrieval of the H_2O (left) and HDO (right) disk-integrated mixing ratios. The radiative-transfer calculations were done using the LMD-GCM thermal structure corresponding to the observing conditions.*

We have used the 1366-1368 cm^{-1} spectral range to model the terrestrial opacity (using a terrestrial model of the water vertical distribution over an altitude of 13 km), and we have multiplied this terrestrial spectrum by our best fit model for comparison with the EXES spectrum. The result is shown in Figure 3. It can be seen that the best-fit model is in excellent agreement with the EXES data in this spectral range also.

Figure 4 shows the map of D/H on Mars retrieved from the line depth ratio of the HDO and H_2O transitions shown in Figure 2. It can be seen that the H_2O mixing ratio is maximum in the northern region, as expected from the GCM for this season. The D/H map is remarkably uniform over the disk in all regions where it can be reliably measured. At high southern latitudes, the H_2O and HDO lines are too weak for their line depth ratio to be significant.

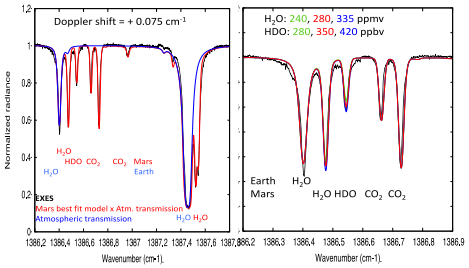

Figure3: *(left) The disk-integrated EXES spectrum compared with our best-fit model in the 1386-1388 cm^{-1} range; (right) Comparison with models including several H_2O and HDO mixing ratios in the 1386.2-1386.9 cm^{-1} range.*

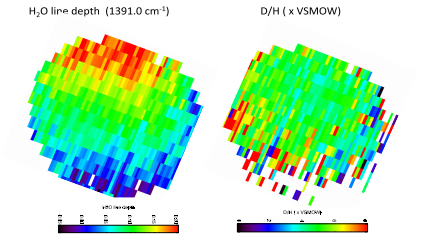

Figure 4*: (left) H_2O line line depth; (right) D/H ratio inferred from the HDO/H_2O line depth ratio.*

Our disk-integrated value of D/H is 4.0 (+0.7, -0.6) x VSMOW, consistent with but slightly lower than our 2014 estimate of 4.4 (+1.0, -0.6) VSMOW [3]. A possible reason for this difference is that, in the case of our 2016 observation, the Tharsis region is in the center of our field of view, and the D/H ratio is known to decrease with altitude above this location [2, 3]. Our result is also consistent with the ground-based map of Villanueva et al. 2015 [4], although our map appears globally more uniform. We should point out, however, that our spatial resolution is strongly limited (3 arcsec) due to the image quality of the SOFIA telescope.

Acknowledgements: This work is based on observations made with the NASA/DLR Stratospheric Observatory for Infrared Astronomy (SOFIA). SOFIA is jointly operated by USRA, under NASA contract NAS2-97001, and DSI, under DLR contract 50 OK 0901 to the University of Stuttgart.

References: [1] Owen, T. et al. 1988, Science 316,92; [2] Montmessin, F. et al. 2005, JGR 110, E03006; [3] Encrenaz, T. et al.2016, A&A 586, A62; [4] Villanueva, G. et al. 2015, Science 348, 318

EPSC Abstracts
Vol. 11, EPSC2017-175, 2017
European Planetary Science Congress 2017

Seasonal and interannual variations of H_2O_2 on Mars

T. Encrenaz (1), T. K. Greathouse (2), F. Lefèvre (3), F. Montmessin (3), T. Fouchet (1), B. Bézard (1), S. K. Atreya (4), B. Gondet (5), A. Fedorova (6), P. Hartogh (7)
(1) LESIA Paris Observatory, France, (2) SwRI, San Antonio, TX, USA, (3) LATMOS, IPSL, Paris, France, (4) University of Michigan, Ann Arbor, MI, USA, (5), IAS, University Paris-Sud, Orsay, France, (6) IKI Space Science Institute, Moscow, Russia, (7) Max-Planck Institute for Solar System Research, Göttingen, Germany (therese.encrenaz@obspm.fr)

Abstract

Following a long-term monitoring campaign on the abundance and distribution of hydrogen peroxide on Mars, we present a new observation near summer solstice which corresponds to a maximum of the seasonal abundance of H_2O_2. Our result is in full agreement with GCM predictions (Lefèvre et al. 2008; [1]). We also analyse previous measurements of H_2O_2 in the vicinity of aphelion which seem to indicate the existence of interannual variations, and we discuss their possible origin.

Introduction

Hydrogen peroxide is an important tracer of Martian photochemistry, possibly responsible for the absence of organics at the surface of Mars [1, 2]. For over ten years, we have been monitoring its abundance and distribution over the disk of the planet along the seasonal cycle using ground-based high-resolution imaging spectroscopy. Comparison with global climate models has favoured the GCM model of the Laboratoire de Météorologie Dynamique based on heterogeneous chemistry [3, 4, 5].

In this abstract, we present a new observation of Mars obtained on May 7, 2016, near opposition, under an especially favourable geometry. The disk diameter was 17″ and the solar longitude was 148.5°.

1. Observations

Our observation was performed using the TEXES instrument (Texas Echelon Cross Echelle Spectrograph; [6]) at the IRTF (InfraRed Telescope Facility), at Maunakea Observatory. As for our previous observations, we aligned the slit of the spectrograph along the North-South celestial axis and we moved the slit in the East-West direction from one limb to the other. As the slit length is about 10″, the northern and southern hemispheres of Mars were recorded sequentially. The observations took place on May 07, 2016, starting from 08:31:25 UT and lasting for 30 minutes. We used the 1230-1238 cm^{-1} spectral interval (previously observed in 2003) that contains an H_2O_2 doublet (at 1234.00 and 1234.05 cm^{-1}) with nearby weak CO_2 transitions. As in our previous analyses, our H_2O_2 map was obtained by dividing the line depth of the H_2O_2 doublet by the line depth of a nearby weak CO_2 line.

2. The H_2O_2 map for Ls = 148°

Figure 1 shows the TEXES disk-integrated spectrum between 1232.5 and 1234.2 cm^{-1}, with a nominal synthetic model including CO_2 and H_2O_2. It can be seen that the H_2O_2 doublet at 1234.0 cm^{-1} is barely detectable on the disk-integrated spectrum.

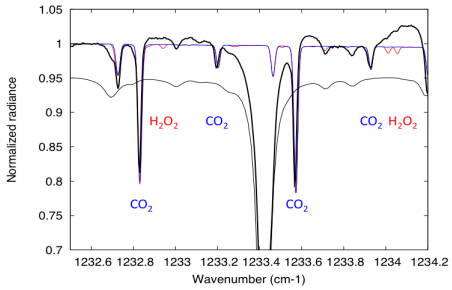

Figure 1: The disk-integrated TEXES spectrum between 1232.5 and 1234.2 cm^{-1} (rest frequencies, thick black line). Models: CO_2 (blue), H_2O_2 with a mixing ratio of 60 ppbv (red). Thin black line: standard atmospheric opacity at Maunakea Observatory, shifted vertically by 0.01 for clarity.

Figure 2 shows the H_2O_2 map retrieved from our observation, compared with the GCM prediction. It can be seen that, as expected by the model, there is a clear dichotomy between the northern and southern

hemispheres, even stronger in the TEXES data than predicted by the GCM.

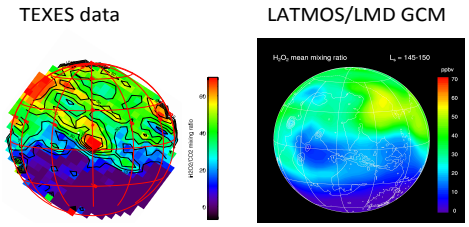

Figure 2: (left)Map of the H_2O_2 mixing ratio, in ppbv, inferred from the H_2O_2/CO_2 line depth ratio, using a summation of the two H_2O_2 doublet lines at 1234.0 cm^{-1} and the CO_2 transition at 1233.2 cm^{-1}. (right) GCM model corresponding to the same observing conditions. The Martian North pole is at the top of both figures.

Figure 3 shows the observed seasonal variations of H_2O_2 on Mars including all published measurements, compared with several models. It can be seen that the present TEXES measurement is the highest value ever measured, and is in good agreement with both GCM models (homogeneous and heterogeneous).

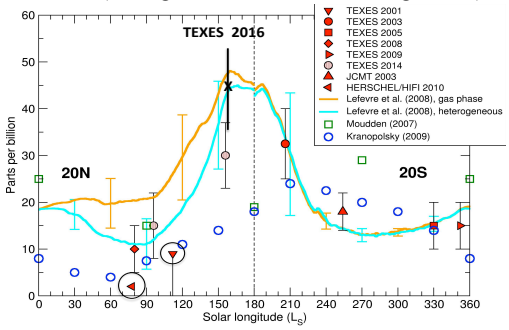

Figure 3: Seasonal variations of H_2O_2 on Mars (observations and models), for a mean latitude of 20N for Ls = 0 -180°, and 20S for Ls = 180-360°.The figure is adapted from [7].

Possible interannual variations around aphelion

A special situation appears in the region of Ls = 70 – 120°, i.e. in the vicinity of northern summer and near aphelion. There are two upper limits, measured in 2001 by TEXES and in 2010 by Herschel/HIFI, that are significantly below the expected values, while two other TEXES measurements, in 2008 and 2014, are in good agreement with the GCM. In contrast, all measurements corresponding to other seasons are consistent with the model. This anomaly suggests that interannual variations might be present at the time of aphelion.

At the time of the first H_2O_2 detection by Clancy et al. (2004), at Ls = 256°, the authors suggested that the absence of detection by TEXES in 2001 (Ls = 110°) might be due to the fact that the height of the hygropause is known to be very low near aphelion [8, 9], because of a combination of a large water vapour content and a low temperature. Indeed, in 1995 and 1997, the altitude of the hygropause, measured from millimetre observations, was found to be only a few kilometres [9, 10]. This might affect the H_2O_2 formation process which is expected to take place at higher levels. While the H_2O column density has been well monitored and is known to show little interannual variations, the height of the hygropause is less well known and might be more variable, due possibly to different dust conditions. Such variations would have little effect on the total H_2O column density. In order to test this hypothesis, it will be interesting to investigate whether a correlation exists between the H_2O_2 content and the altitude of the hygropause. This can be tried using different means: the H_2O vertical profiles of SPICAM/Mars Express [11,12], the millimetre and submillimetre spectra of H_2O and HDO [13], or the OMEGA/Mars Express data showing the altitude of the H_2O cloud.

References:

[1] Oyama,V. I. et al. 1977. Nature 265, 100
[2] Bullock, M. A. et al. 1994. Icarus 107, 142
[3] Lefèvre, F. et al. 2008. Nature 454,971
[4] Encrenaz, T. et al. 2004. Icarus 170, 424
[5] Encrenaz, T. et al. 2012. Plan. Space Sci. 68, 3
[6] Lacy, J. H. et al. 2002. Pub. Astron. Soc. Pac. 114, 153
[7] Encrenaz, T. et al. 2015. Astron. Astrophys. 578, A127
[8] Clancy, R. T. et al. 2004. Icarus 168, 116
[9] Clancy, R. T. et al. 1996. Icarus 122, 36
[10] Encrenaz, T. et al. 2001. Plan. Space Sci. 49, 731
[11] Maltagliati, L. et al. 2011. Science 333, 1868
[12] Maltagliati, L. et al. 2013. Icarus 233, 942
[13] Jarchow, C. et al. 2011. EPSC-DPS Joint Meeting, Nantes, October 2011

EPSC Abstracts
Vol. 11, EPSC2017-189, 2017
European Planetary Science Congress 2017

Still unexploited atmospheric OMEGA/Mex observations

B. Gondet, J.-P. Bibring, M. Vincendon
Institut d'Astrophysique Spatiale, Université Paris-Sud, Orsay, France,
(Brigitte.gondet@ias.u-psud.fr)

Introduction: Since the beginning of the mission (January 2004) OMEGA, the VIS-NIR hyperspectral imager onboard Mars Express has acquired regular limbs observations in conjunction with others instruments (HRSC, PFS, SPICAM and VMC). Scattering by clouds and dust was detected at different Ls, altitude, locations and local time, as well as specific emission (O2, H2O, CO2, CO). Composition and grain sizes can be derived from these measurements. Atmospheric detections are also made in nadir mode. This constitutes an important database largely unexploited at this point. We will present examples of detections concerning clouds, dust and emissions, and identify themes of potential collaborations.

Examples of available observations:

Atmospheric observations acquired by OMEGA include :
- nadir spectral images of the morphology, grain size and composition of ice clouds (Figure 1)
- vertical sampling of the atmosphere above the limbe (Figure 2-6) at various spatial resolutions, from local studies above rovers (Figure 6) to global overview at a given time (Figure 3).

All observations of the spatial distribution of clouds, either lateral of vertical, come with compositional spectral measurments covering the 0.4 to 5.1 microns range for most observations (Figures 1 ; 4-6).

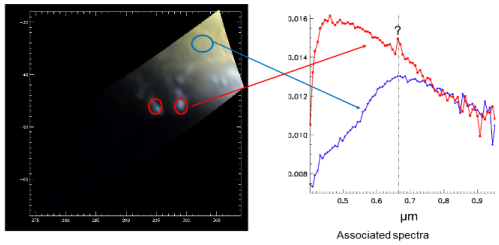

Fig 1: Clouds observed at sunset (SEA -2°) in visible

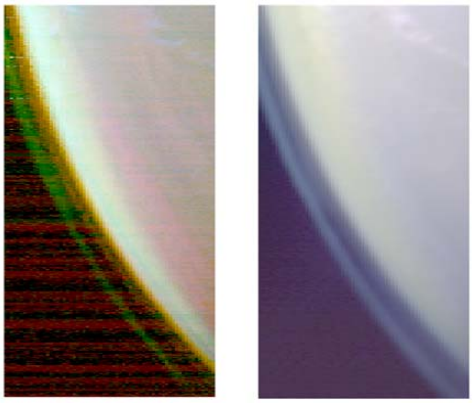
Fig 2 : deteched layer observed in IR and visible

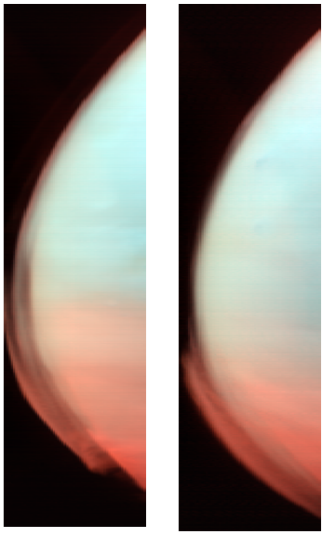

Fig 3 : Dust storm observed in december 2014

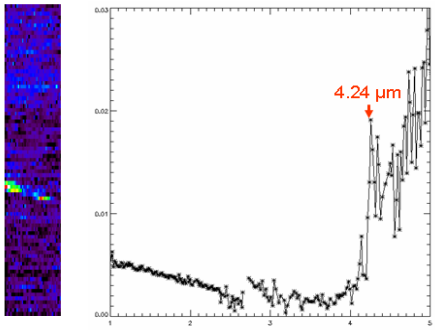

Fig 4 : CO2 clouds detected during limb observation. The grain size can be derived fom the shape of the visible part of the spectra.

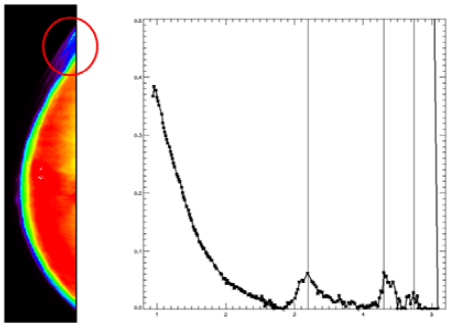

Fig 5: detached layer and associated spectrum (H2O and CO2 emissions)

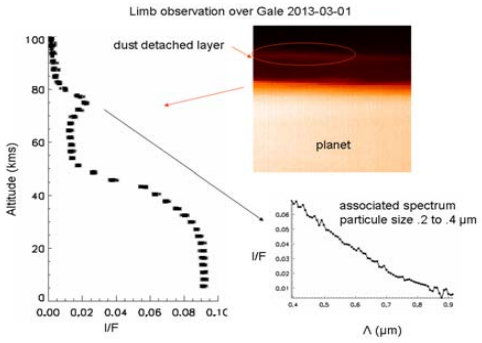

FIG 6 : Detached layer observation over Gale crater

Discussion and Conclusion:

OMEGA measurements gathered over more than 12 years offer an opportunity to explore the yearly variability of the Martian atmosphere, with sufficient time sampling or spatial coverage to put constrains on several aspects of the atmospheric dynamic. OMEGA still provides unique aerosols compositional characterization capabilities that enable detailed analyses of CO2 clouds and other poorly known high altitude aerosols layers. Ongoing and upcoming collaborations with the Martian atmospheric community will further reveal the richness of this dataset for atmospheric studies.

EPSC Abstracts
Vol. 11, EPSC2017-194, 2017
European Planetary Science Congress 2017

Martian atmospheric O_3 retrieval development for the NOMAD-UVIS spectrometer.

W. Hewson (1), J.P. Mason(1), M. Leese(1), B. Hathi(1), J. Holmes(1), S.R. Lewis(1), P.G.J Irwin(2), and M.R. Patel(1).
(1) School of Physical Sciences, Faculty of Science, Technology, Engineering and Mathematics, The Open University, Walton Hall, Milton Keynes, U.K., (2) Atmospheric Physics, Clarendon Laboratory, Parks Road, Oxford, U.K.
(will.hewson@open.ac.uk)

Abstract

The composition of atmospheric trace gases and aerosols is a highly variable and poorly constrained component of the martian atmosphere, and by affecting martian climate and UV surface dose, represents a key parameter in the assessment of suitability for martian habitability. The ExoMars Trace Gas Orbiter (TGO) carries the Open University (OU) designed Ultraviolet and VIsible Spectrometer (UVIS) instrument as part of the Belgian-led Nadir and Occultation for MArs Discovery (NOMAD) spectrometer suite. NOMAD will begin transmitting science observations of martian surface and atmosphere back-scattered UltraViolet (UV) and visible radiation in Spring 2018, which will be processed to derive spatially and temporally averaged atmospheric trace gas and aerosol concentrations, intended to provide a better understanding of martian atmospheric photo-chemistry and dynamics, and will also improve models of martian atmospheric chemistry, climate and habitability. Work presented here illustrates initial development and testing of the OU's new retrieval algorithm for determining O_3 and aerosol concentrations from the UVIS instrument.

1. Introduction

UVIS is part of the NOMAD instrument suite [1, 2] on board the joint ESA–Roscosmos ExoMars mission orbiting Mars, and is an UV / visible imaging spectrometer operating in nadir and solar occultation modes between 200–650 nm, with $<$2 nm spectral resolution. The main objectives of UVIS are to improve the O_3 climatology and deliver information on the aerosol content and variability of the martian atmosphere. O_3 is a highly reactive gas in the martian atmosphere, and through assimilation of O_3 measurements made by UVIS into martian chemical transport models, understanding of martian atmospheric chemistry is set to be greatly improved.

2. Retrieval model

The back-scattered signal sensed by UVIS is composed of solar light scattered by surface and atmospheric constituents of Mars, with absorbing signatures of trace gases imprinted on this signal. The simultaneous contribution of these factors in varying quantities make the separation of each scattering and absorbing component (e.g. aerosols and trace gases) a complex procedure. To estimate atmospheric quantities of components contributing to sensed radiation in this manner, the NEMESIS radiative transfer model [3] is employed in an iterative least squares fitting procedure to simulate martian atmospheric radiances and provide a best-fit against UVIS observed values. Modelled radiances take into account the instrument's viewing geometry, together with *apriori* profiles of atmospheric parameters.

Using this method, the new OU optimal estimation O_3 retrieval is being developed for application to data from the UVIS instrument. In addition to nadir soundings of the martian atmosphere, the retrieval will be applied to solar occultations with the instrument looking at the Sun through the atmosphere perpendicular to the martian surface, presenting an opportunity for novel insights into atmospheric chemistry, and therefore of particular interest to the modelling community.

3. Development results

NEMESIS was originally developed for simulation of radiances in the near infra-red, and requires further work, presented here, to allow operation in the UV. Initial development and validation of the retrieval will be illustrated, using several experimental atmospheric scenarios for upper bounds of the retrieval's intended operating range, incorporating a variety of atmospheric chemical and aerosol loads. For proof of concept whilst awaiting operational UVIS L1B data, we also apply the retrieval to SPICAM data from the

Mars Express instrument to derive O_3 concentrations spatially and temporally. These data will then be applied to an inter-comparison against existing martian O_3 and aerosol retrievals, as well as model fields from OU colleagues.

4. Future work

The OU retrieval will be extended to simulate UV multiple scattering in the martian atmosphere, offering the ability to retrieve limb occultation soundings and better characterise the aerosol load to significantly improve estimates of martian O_3 and other trace gases. In further work the retrieval model will be coupled to data from the Mars Climate Database, providing an improved *apriori* for the retrieval.

Acknowledgements

The authors gratefully acknowledge the support of the UK Space Agency and the Science and Technology Funding Council.

References

[1] M.R. Patel et al. "NOMAD spectrometer on the ExoMars trace gas orbiter mission: part 2—design, manufacturing, and testing of the ultraviolet and visible channel". In: *Appl. Opt.* 56.10 (2017), pp. 2771–2782. DOI: 10.1364/AO.56.002771.

[2] A.C. Vandaele et al. "Science objectives and performances of NOMAD, a spectrometer suite for the ExoMars TGO mission". In: *Planetary and Space Science* 119 (2015), pp. 233–249. DOI: 10.1016/j.pss.2015.10.003.

[3] P.G.J. Irwin et al. "The NEMESIS planetary atmosphere radiative transfer and retrieval tool". In: *Journal of Quantitative Spectroscopy and Radiative Transfer* 109.6 (2008), pp. 1136–1150. DOI: 10.1016/j.jqsrt.2007.11.006.

EPSC Abstracts
Vol. 11, EPSC2017-217, 2017
European Planetary Science Congress 2017

Unveiling Mars nightside mesosphere dynamics by IUVS/MAVEN global images of NO nightglow

A. Stiepen[1], S.K. Jain[2], N.M. Schneider[2], Z. Milby[2], J.I. Deighan[2], F. Gonzàlez-Galindo[3], J.-C. Gérard[1], F. Forget[9], S. Bougher[5], A.I.F. Stewart[2], E. Royer[2], M.H. Stevens[4], J.S. Evans[6], M.S. Chaffin[2], M. Crismani[2], W.E. McClintock[2], J.T. Clarke[7], G.M. Holsclaw[2], F. Montmessin[8], F. Lefèvre[8], D.Y. Lo[10], B.M. Jakosky[2]

(1) Laboratoire de Physique Atmosphérique et Planétaire, Space sciences, Technologies and Astrophysics Research (STAR), University of Liège, Liège, Belgium, (2) Laboratory for Atmospheric and Space Physics (LASP), University of Colorado, USA, (3) Instituto de Astrofisica de Andalucia, CSIC, Granada, Spain, (4) Space Science Division, Naval Research Laboratory, (5) Climate and Space Sciences and Engineering Department, University of Michigan, Ann Arbor, Michigan, (6) Computational Physics, Inc., Springfield, Virginia, USA, (7) Center for Space Physics, Boston University, Boston, MA, USA, (8) LATMOS/IPSL, Guyancourt, France, (9) Laboratoire de Météorologie Dynamique (LMD), Paris, France, (10) Lunar and Planetary Laboratory, University of Arizona,Tucson, Arizona, USA

Abstract

We analyze the morphology of the ultraviolet nightglow in the Martian upper atmosphere through Nitric Oxide (NO) δ and γ bands emissions observed by the Imaging Ultraviolet Spectrograph instrument on the Mars Atmosphere and Volatile EvolutioN spacecraft. The seasonal dynamics of the Martian thermosphere-mesosphere can be constrained based on the distribution of these emissions. We show evidence for local (emission streaks and splotches) and global (longitudinal and seasonal) variability in brightness of the emission and provide quantitative comparisons to GCM simulations.

1. Introduction

On the dayside thermosphere of Mars, solar extreme ultraviolet radiation partly dissociates CO_2 and N_2 molecules. O(^{3}P) and N(^{4}S) atoms are carried by the day-to-night hemispheric transport. They preferentially descend in the nightside mesosphere in the winter hemisphere, where they can radiatively recombine to form NO($C^2\Pi$). The excited molecules promptly relax by emitting photons in the UV δ bands and in the γ bands through cascades via the $A^2\Sigma$, v' = 0 state. These emissions are thus indicators of the N and O atom fluxes transported from the dayside to Mars' nightside and the winter descending circulation pattern from the nightside thermosphere to the mesosphere (e.g. Bertaux et al., 2005 ; Bougher et al., 1990 ; Cox et al., 2008 ; Gagné et al., 2013 ; Gérard et al., 2008 ; Stiepen et al., 2015, 2017).

2. Observations

Observations of these emissions have been accumulated into a large dataset of nightside disk images and limb profiles obtained by the Imaging Ultraviolet Spectrograph (IUVS, McClintock et al., 2015) instrument when the Mars Atmosphere and Volatile EvolutioN (MAVEN) spacecraft is at its apoapsis phase along its orbit. An example of observation during winter in the southern hemisphere is illustrated in Figure 1. Complementary information is obtained from limb profiles collected when the MAVEN spacecraft is near periapsis (Stiepen et al., 2017).

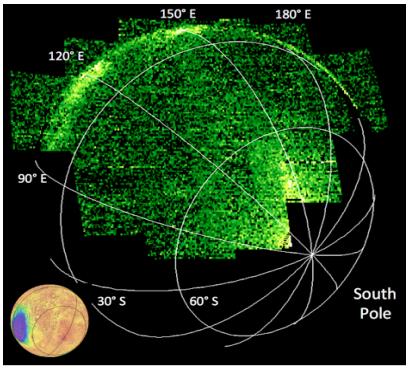

Figure 1 – IUVS observation of the NO Nightglow in disk image mode during winter in the southern hemisphere. The green color code indicates the brightness of the emission. Adapted from Jakosky et al., 2017.

IUVS ultraviolet domain ranges from 110 nm to 340 nm and therefore fully covers the range of the NO δ and γ emission bands. Disk images are accumulated during winter in the southern hemisphere.

3. Waves and tides in the Martian nightside mesosphere

Disk images and limb profiles data both show longitude sectors of enhanced brightness close to the equator during summer and winter conditions. Observations also reveal spots and streaks, indicating irregularities in the wind circulation pattern and possible impact of waves and tides.

The unexpected longitudinal variability of the NO nightglow brightness suggests the importance of dynamical impact of waves on the emission. We note that the observed variations cannot be caused by tides, as they are observed at all nightside local times and during a long period of time. Impact of geographic structure on the nightside mesosphere was not observed so far using the NO nightglow as a tracer of propagating waves in this region of Mars's atmosphere.

4. Seasonal control of the emission and global dynamics

The brightest emission is observed close to the winter pole. Stiepen et al., (2017) showed that the LMD-MGCM globally reproduces the main global seasonal trends observed, especially during equinox. The model however overestimates the altitude of the observed emission and strongly underestimates its brightness at winter. This suggests that the model dynamics transports N atoms to the nightside thermosphere at higher (polar) latitudes than observed toward the winter pole but correctly reproduces the dynamics in southern fall equinox.

5. Summary and conclusions

We make here the first use of disk images showing large and sudden variability in the NO nightglow emission, and thus the nightside mesosphere dynamics.

This dataset addresses pending questions raised by the observations of NO Nightglow at Mars by the SPICAM instrument on Mars Express (e.g. Bertaux et al., 2005 ; Cox et al., 2008 ; Gagné et al., 2013 ; Stiepen et al., 2015) and limb observations of NO Nightglow by the IUVS instrument (Stiepen et al., 2017).

The disk images and limb profiles are compared to those calculated with the LMD-MGCM model (Gonzàlez-Galindo et al., 2009 ; Lopez-Valverde et al., 2011) and the M-GITM model (Bougher et al., 2015) to focus on the seasonal, local time and geographical influences on the NO Nightglow emission. We will also provide a statistical study of the regions of enhanced brightness and discuss possible interpretation from the comparison to the GCM simulations.

Acknowledgements

A.Stiepen is supported the Fund for Scientific Research (F.R.S.-FNRS). Contact: arnaud.stiepen@ulg.ac.be. The MAVEN mission is supported by NASA through the Mars Exploration Program in association with the University of Colorado and NASA's Goddard Space Flight Center. M. Stevens is supported by the NASA MAVEN Participating Scientist program. F.G.-G. is funded by the European Union Horizon 2020 Programme (H2020 Compet-08-2014) under grant agreement UPWARDS-633127. The LMD-MGCM results used in this paper are available under request to F.G.-G. (ggalindo@iaa.es).

EPSC Abstracts
Vol. 11, EPSC2017-221, 2017
European Planetary Science Congress 2017

Synergistic retrieval of H_2O vapor in Mars' atmosphere: the path to a systematic 3D exploration of H_2O vapor

F. Montmessin (1) and S. Ferron (2)
(1) CNRS, LATMOS, Guyancourt, France (franck.montmessin@latmos.ipsl.fr), (2) ACRI-ST, Guyancourt, France (stephane.ferron@latmos.ipsl.fr)

Abstract

Understanding the contemporary water cycle on Mars is a major goal in Mars' climate research. Our study has been conducted with the motivation of optimizing the scientific return of nadir observing instruments which have performed water vapor analysis at various wavelengths on Mars. First, we have evaluated the theoretical performances of jointly analyzing water vapor retrieval in both Thermal Infrared (TIR) and Short Wavelength Infrared (SWIR) ranges (*i.e.* less than 3 μm). We then proved, by applying our method to actual Mars Express data, that a simultaneous retrieval in the TIR and SWIR of the water vapor abundance is susceptible to provide a very strong constraint on the shape of the water vapor profile. Up to now, only a column-integrated abundance has been derived from nadir observing instruments whereas it appears now possible to derive a second information on water vapor vertical confinement, opening the path to a 3D exploration of water vapor on Mars.

1. Introduction

Synergistic retrieval of trace gases (such as CO or CH_4) in the Earth atmosphere has proven very effective for constraining the vertical partitioning of these gases and might be used to identify potential sources at the surface [1,2]. Guided by this innovation, we have decided to apply a similar approach to the retrieval of water vapor when observed a nadir looking mode on Mars. A number of orbital assets have accomplished the detailed exploration of the nadir column abundance of water vapor on Mars, allowing the continuous monitoring of the water vapor temporal and horizontal distribution for almost 15 consecutive terrestrial years [3,4,5]. This dataset so far has only delivered an information on the vertically integrated amount of water, yet this information was obtained with a variety of instruments operating at different wavelengths. Indeed, it is possible to "see" water vapor through its absorption/emission in the thermal infrared with the Planetary Fourier Spectrometer (PFS) and through its absorption in the SWIR domain with three different instruments (SPICAM, OMEGA and PFS). We undertook an examination of the contribution of a SWIR / TIR synergy to the restitution of water vapor in the atmosphere of Mars. This approach is an important task in view of cross-comparing the various climate series which have been produced for water vapor to date. Our work was divided in two stages: first, establish the theoretical relevance of this method for currently operating instruments on Mars, and second test and validate the performances predicted at completion of stage 1.

2. SWIR-TIR Synergy methodology

The work presented below is limited to the cases of the SPICAM, OMEGA and PFS-LW instruments. We relied on a simplified instrumental model that we designed according to the spectral resolutions and mean SNR of the different sensors. Synthetic spectra were produced from atmospheric modeling extracted from a Martian climate database. A direct model has been developed to account for molecular absorption and aerosol diffusion. It enabled us to estimate the sensitivities of the radiances to the various geophysical parameters. We have implemented a statistical approach to combine these sensitivities with the noise models of each instrument and to estimate errors and resolutions on the vertical steam and temperature profiles. It emerged from this study that the number of pieces of information on the vertical profile of water vapor is around 1 for SWIR bands below 1 for TIR bands taken independently. The synergy of the entire band offers an increase by about 50%. This increase is highly dependent on the aerosol opacity estimated in the TIR. It has also been demonstrated that the sounded portions of altitude are different between the SWIR bands, which give access to the layer immediately above the surface, while the TIR band is sensitive to the highest altitudes (> 10 km).

On this basis, we have undertaken a statistical characterization of an estimator of the water vapor column and we have evaluated its robustness with respect to the *a priori* knowledge of aerosols. A preliminary approach, based on a maximum

likelihood estimate, allowed us to show that the synergy, in order to be significant, requires to have spectra averages to increase SNR. The synergy is shown to render information from an atmospheric portion that extends from the surface up to more than one height scale, and also reduces the error on the column-integrated abundance estimate. It requires a prior knowledge of aerosols in order to limit estimation bias.

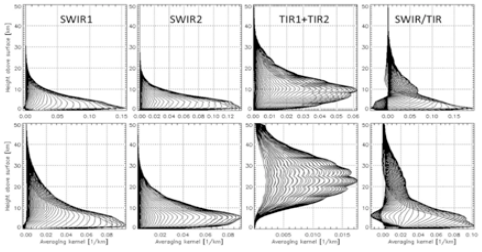

Figure 1: averaging kernels of water vapor in various configurations (from left to right: SWIR1-from SPICAM SWIR range, SWIR2-from OMEGA SWIR range, TIR1+2-PFS TIR ranges, and synergy SWIR/TIR).

3. SWIR-TIR Synergy Validation

The dataset used for testing and validating has been established from spectra acquired during Martian Year (MY) 27 by the SPICAM-IR and PFS-LW spectrometers. It consists of an ensemble of L1 products (calibrated spectra with wavelength assignment) designed specifically for our needs. Each product corresponds to an ensemble of collocated spectra satisfying the following criteria: (i) a high quality of the individual measurements; (ii) a good geographical and seasonal coverage of the final dataset encompassing various dust or water ice cloud opacity situations; and (iii) a low error modeling due to surface inhomogeneity (albedo and emissivity)

The results obtained with these tests using actual data confirmed the predictions of our theoretical investigation: the number of independently retrieved parameter increase non-linearly when adding SWIR and TIR together, by an amount of more than 20%, reaching 50% and up.

4. Summary and Conclusions

In this study, we defined and implemented a Bayesian approach to estimate water vapor in the Mars atmosphere from SWIR and TIR spectra obtained in nadir geometry. An analysis of the measurements information content showed that, on average, the spectral synergy allows the increase of retrieved information on water vapor (which can be represented by the number of independent parameters) by 20 or 50% depending on the reference case (SWIR or TIR). We also demonstrated that the SWIR/TIR synergy makes it possible to unbiasedly estimate the partial column on the 5 km section above the surface and give (a correlated) information on the total column.

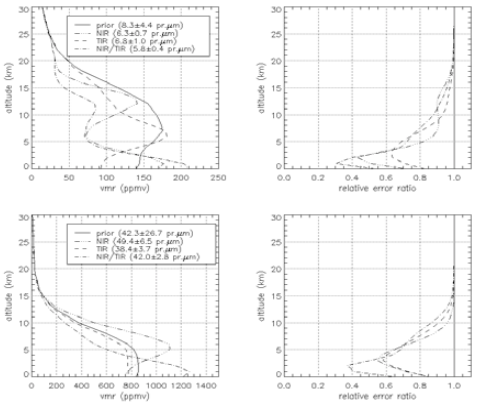

Figure 2: Left to right: H_2O vmr estimations, posterior to prior errors ratio. Upper figures for the "dry" case atmosphere, the lower figures show the "wet" case atmosphere.

Acknowledgements

This work has been entirely funded by the UPWARDS project, within Horizon 2020 program of the European Union.

References

[1] Worden, H. M., M. N. Deeter, D. P. Edwards, J. C. Gille, J. R. Drummond, and P. Nédélec (2010), Observations of near-surface carbon monoxide from space using MOPITT multispectral retrievals, J. Geophys. Res., 115, D18314, doi:10.1029/2010JD014242.

[2] Worden, H. M., M. N. Deeter, D. P. Edwards, J. C. Gille, J. R. Drummond, and P. Nédélec (2010), Observations of near-surface carbon monoxide from space using MOPITT multispectral retrievals, J. Geophys. Res., 115, D18314, doi:10.1029/2010JD014242.

[3] Smith, M.D., 2004. Interannual variability in TES atmospheric observations of Mars during 1999–2003. Icarus 167, 148–165

[4] Fedorova, A., Korablev, O., Bertaux, J.L., Rodin, A., Kiselev, A., Perrier, S., 2006. Mars water vapor abundance from SPICAM IR spectrometer: Seasonal and geographic distributions. J. Geophys. Res. 111

[6] A. Trokhimovskiy, A. Fedorova, O. Korablev, F. Montmessin, J.-L. Bertaux, A. Rodin, M. D. Smith (2015), Mars' water vapor mapping by the SPICAM IR spectrometer: Five martian years of observations, Icarus 251, 50–64

EPSC Abstracts
Vol. 11, EPSC2017-229-2, 2017
European Planetary Science Congress 2017

A singular double baroclinic vortex on Mars

A. Sánchez-Lavega [agustin.sanchez@ehu.eus] (1), A. Garro (1), T. del Río-Gaztelurrutia (1), R. Hueso (1), I. Ordoñez-Etxeberria (1), H. Chen Chen (1), A. Cardesín-Moinelo (2), D. Titov (3), S. Wood (4), M. Dias Almeida (5)

(1) Dpto. Física Aplicada I, Escuela de Ingeniería de Bilbao, UPV/EHU, Bilbao, Spain, (2) European Space Agency, ESAC, Madrid, Spain, (3) European Space Agency, ESTEC, Noordwijk, Netherland, (4) European Space Agency, ESOC, Darmstadt, Germany, (5) Dias Almeida Data Processing and Systems, Ittigen, Switzerland

Abstract

We report on a singular double vortex observed in Mars from June 6 to July 9, 2012 (L_s ~ 125°) using images obtained by the Visual Monitoring Camera (VMC) and MARCI onboard Mars Express and Mars Reconnaissance Orbiter, respectively. The vortex pair was placed at latitude ~60°N and moved northeast with a velocity ~ 3 ms^{-1}. The sizes of both vortices were in the range 600-800 km, showing a well developed central region free of clouds with a radius ~ 250-350 km where the tangential velocity reached values in the range of 5-20 ms^{-1}. Their whitish color indicates that they are formed by water-ice with their cloud density decreasing with local time. Both vortices are cyclonic, in gradient wind balance, and we interpret them as a wavenumber 5 baroclinic wave, typically found during the Martian northern summer season.

1. Introduction

Spiral and annular synoptic weather systems have been reported in Mars images since the first convincing observations by Viking orbiter in 1979 [1]-[3]. They occur during the regression of the North Polar hood in the summer season (northern hemisphere) when the meridional temperature gradient becomes large at latitudes close to the ice cap deposits [4]-[5]. These vortices have been identified as transient extratropical baroclinic eddies formed by a mixture of dust and water-ice clouds [1]-[3]. A particular yearly recurrent "annular" cloud system was observed in 1999 using Hubble Space Telescope images and then in 2001 using MOC-Mars Global Surveyor images, exactly at the same aerographical location and epoch [2]. Here we report observations of a similar system in 2012, when it developed a singular double annular ring. We base our analysis on images obtained with the Visual Monitoring Camera (VMC) [6] and MARCI [7] instruments onboard Mars Express and Mars Reconnaissance Orbiter respectively (Figure 1).

2. Measurements

The VMC-MEx and MARCI-MRO images showing the double vortex were orthographic polar projected and navigated using the methods and techniques described in Sánchez-Lavega et al. [8]. They correspond to the period from June 6 to July 9, 2012 (L_s =120.8°-136.6°, MY = 31).

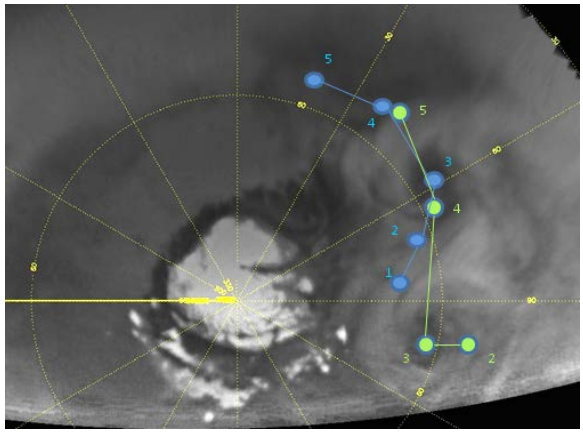

Figure 1: The double annular vortex is shown in a VMC-MEx image taken on June 18th, 2012. The track of the two storms is indicated by blue and green dots in June from 15th (position 1) to 23rd (position 5).

The size of the vortices, as traced by the clouds at their approximate circular outer edge, was in the range 600-800 km, with both vortices showing a well developed central region, free of clouds, that had a radius ~ 250-350 km. It is worth noticing that the cloud structure of the vortices changed with Martian Local Time, as had been observed previously for the single vortex case [2]. Cloud density was high and extended in area in early morning (~6 hr LT), then dissipated and broken in fragments during the

afternoon (~16 hr LT). We have tracked the motion of the center of both annulus vortices (i.e. the center of the area devoid of clouds) and we find that the pair moves northeast with a speed of ~3 ms^{-1}. In addition, we have identified and measured the motions of individual clouds in image pairs on VMC and MARCI images, retrieving the wind vectors relative to the center of the vortices. We used visual cloud identification and tracking and a supervised brightness cross-correlation method [9] to measure the cloud displacements. The velocity vectors reveal the cyclonic rotation of both vortices with tangential velocities in the range 5 to 20 ms^{-1} and peak vorticities of ~ $4x10^{-5}$ s^{-1}.

3. Interpretation

The VMC and MARCI color images show that both vortices are whitish and thus made mainly of water-ice condensate clouds instead of dust, that would show a yellowish color in these images [2], [8].

Adopting that distances between the cyclone vortices centers ~45° is half wavelength the resulting wavenumber is 4. If we assume that the vortices are in gradient wind balance [1], it follows that [10]

$$\frac{V^2}{r} + fV = \left| \frac{1}{\rho} \frac{\partial P}{\partial r} \right|$$

where V is the tangential velocity (15 ms^{-1}), r is the vortex radius (300 km), $f=2\Omega \sin\varphi$ = 1.2×10^{-3} s^{-1} is the Coriolis parameter (Ω = 7.08×10^{-4} s^{-1}, Martian angular rotation) for latitude φ (60°N), and ρ is the mean density (0.018 kgm^{-3}). We derive a radial gradient pressure $\partial P/\partial r \sim 6\times10^{-4}$ mbar km^{-1}, which is about one-two orders of magnitude lower than the standards of Earth's extratropical cyclones [10].

4. Conclusions

We are exploring baroclinic models to explain the nature of this vortex pair and its evolution, the recurrent formation of vortices in the same region and compare their behavior with similar vortex pairs observed on Earth. The models under exploration are based on the available temperature data from different space missions and from predictions by a GCM [11].

Acknowledgements

This work has been supported by the Spanish project AYA2015-65041-P (MINECO/FEDER, UE) and Grupos Gobierno Vasco IT-765-13. HCC and IO-E were supported in part by Aula EspaZio Gela under contract from Diputación Foral de Bizkaia. AG was supported by ESA Contract No. 4000118461/16/ES/JD, Scientific Support for Mars Express Visual Monitoring Camera.

References

[1] Hunt, G. E., James, P. B.: Martian extratropical cyclones, Nature, 531-532, 1979.

[2] Cantor, B., Malin, M., Edgett, K. S.: Multiyear Mars Orbiter Camera (MOC) observations of repeated martian weather phenomena during the northern summer season. J. Geophys. Res. Planets 107, E35014, 2002.

[3] Wang, H., Ingersoll, A. P.: Martian clouds observed b Mars Global Surveyor Mars Orbiter Camera, J. Geophys. Res., 107, E10, 5078, 2002.

[4] Barnes, J. R.: Linear Baroclinic Instability in the Martian Atmosphere, J. Geophys. Res., 41, 1536-1550, 1984.

[5] Barnes, J. R. et al: Mars Atmospheric Dynamics as Simulated by the NASA Ames General Circulation Model 2. Transient Baroclinic Eddies, J. Geophys. Res., 98, 3125-3148, 1993.

[6] Ormston, et al: An ordinary camera in an extraordinary location: Outreach with the Mars Webcam, Acta Astronautica 69, 703-713, 2011.

[7] Bell, J. F., et al. Mars Reconnaissance Orbiter Mars Color Imager (MARCI) : Instrument description, calibration and performance, J. Geophys. Res. 114, E08S92, 2009.

[8] Sánchez-Lavega A., et al: Limb clouds and dust on Mars from images obtained by the Visual Monitoring Camera (VMC) onboard Mars Express, Icarus (submitted).

[9] Hueso, R. et al: The jovian anticyclone BA. II. Circulation and interaction with the zonal jets, Icarus, 203, 499-515, 2009.

[10] Sánchez-Lavega A., An Introduction to Planetary Atmospheres, Taylor-Francis, CRC Press Boca Raton, Florida, 2011.

[11] Forget, F., et al: Improved general circulation models of the Martian atmosphere from the surface to above 80 km, J. Geophys. Res., 104, 24155–24175, 1999.

EPSC Abstracts
Vol. 11, EPSC2017-252-1, 2017
European Planetary Science Congress 2017

Effect of the lateral exospheric transport on the horizontal hydrogen distribution at the exobase of Mars

J-Y. Chaufray (1), R. Yelle (2), F. Gonzalez-Galindo (3), F. Forget (4), M.A. Lopez-Valverde (3), F. Leblanc (1), and R. Modolo (1)

(1) LATMOS-IPSL, CNRS, France, (2) University of Arizona, USA, (3), Instituto de Astrofisica de Andalucia, Spain (4), Laboratoire de Météorologie Dynamique, France (contact : chaufray@latmos.ipsl.fr)

Abstract

We describe the horizontal distribution of hydrogen density at the exobase of Mars as simulated by coupling a 3D GCM with an exospheric balistic model, taking into account the flight balistic time of the exopheric hydrogen atoms. Such a description is more realistic than the assumptions used in our past study [4]. We simulate 4 Martian rotations at three different seasons. The horizontal variations of the hydrogen density at the exobase are reduced when the exospheric balistic transport is included compared to our previous simulations.

1. Introduction

The Martian hydrogen corona is not spherically symmetric [1, 3]. Such asymmetry results, for example, from the differential heating between the dayside and the nightide leading to local time variations of the exospheric temperature and driving thermospheric winds [6]. Chaufray et al. 2015 [4], simulated the 3D hydrogen corona using the Global Circulation Model of Laboratoire de Météorologie Dynamique (GCM-LMD) to study the possible local time and latitude variations of the hydrogen density. These simulations show the presence of hydrogen bulge in the downwelling regions resulting from the "wind-induced diffusion" [2] that could be responsible of recent helium bulges observed by MAVEN [5]. For light species like atomic hydrogen, the horizontal distribution should be also affected by the balistic motion in the exosphere [7] due to the large horizontal motion during one balistic trajectory (typically 1000 km for a temperature of 200K at the exobase). This effect was not included in Chaufray et alal. 2015 and is investigated in this study.

2. Models

To investigate the effect of the exospheric balistic motion on the hydrogen density at the exobase, we couple the GCM-LMD to an exospheric balistic motion of hydrogen atoms, assuming no loss process and no collisions above the exobase. The upward velocity used as the upper boundary conditions in the molecular diffusion scheme in the GCM-LMD is computed by

$$w_{top} = \frac{\Phi_{bal,up} + \Phi_{esc} - \Phi_{bal,down}}{n},$$

Where n is the local hydrogen density $\Phi_{bal,up}$ and Φ_{esc} are the balistic upward and escape flux depending only on the local conditions, and $\Phi_{bal,down}$ the balistic downward flux computed with the balistic exospheric model by integration over the flux coming from all regions of the exobase.

This assumption differs from our previous simulations [4] where the vertical velocity at the upper boundary was assumed to be the effusion velocity (Φ_{esc}/n). The simulations have been performed at different seasons.

3. Results

The horizontal distribution of the temperature at Ls = 180° is displayed in Fig.1. The horizontal hydrogen density obtained after 4 martian days without and with the exospheric balistic coupling is displayed in Fig. 2 and show that the effect of the exospheric balistic motion is to reduce the simulated nightside bulge of hydrogen at this season and to redistribute the hydrogen towards the dayside as well as to lead to a smoother distribution of the hydrogen density.

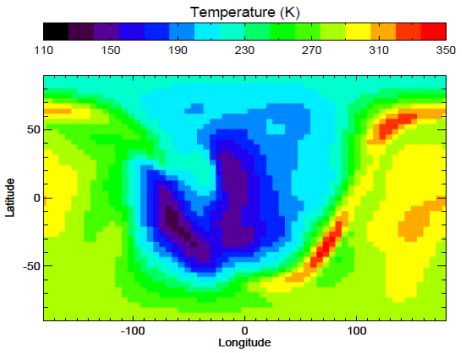

Fig. 1 Temperature at the exobase simulated with the GCM-LMD for solar average conditions at Ls = 270°. The subsolar longitude is 180°.

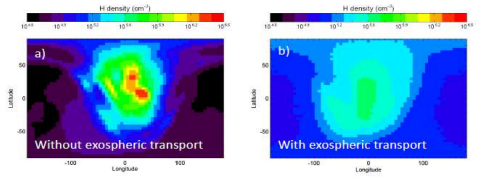

Fig. 2 Horizontal distribution of the hydrogen density at the Martian exobase without (a) and with (b) exospheric balistic coupling.

4. Summary and Conclusions

The effect of the exospheric balistic transport plays an important role in the horizontal distribution of hydrogen at the exobase of Mars. Compared to simulations presented by [4], the main effect of the exospheric balistic transport is to reduce the hydrogen density at the nightside and increase the hydrogen density at the dayside. The hydrogen density is also smoother when this effect is included. In the future, the coupling of this model with a 3D radiative transfer model, will help us to compare with the local time variations of the Lyman-α brightness performed by MAVEN/IUVS [3].

Acknowledgements

We thank the Programme National de Planetology and Programme National Soleil-Terre for their support in this study. This work has been partially funded by the European Union Horizon 2020 Programme (H2020 Compet -08-2014) under grant agreement UPWARDS-633127.

References

[1] Bhattacharyya et al. (2017), Icarus, 281, 264-280, [2] Bougher et al. (2015), JGR, 120, 311-342, [3] Chaffin et al., (2015), GRL, 42, 9001-9008, [4] Chaufray et al., (2015), Icarus, 245, 282-294, [5] Elrod et al. (2017), JGR, in press, [6] Gonzalez-Galindo et al. (2015), JGR, 120, 2020-2035, [7] Hodges (1973), JGR, 78, 31.

EPSC Abstracts
Vol. 11, EPSC2017-257, 2017
European Planetary Science Congress 2017

Three-dimensionnal turbulent-resolving modeling of the Venus cloud convective layer.

M. lefèvre, A. Spiga and S. Lebonnois
Laboratoire de Météorologie Dynamique, CNRS, UPMC, Paris, France (maxence.lefevre@lmd.jussieu.fr)

Abstract

1. Introduction

Venus hosts a global sulfuric acid cloud layer between 45 and 70 km which has been investigated in detail by the Venus Express mission. One of the main questions that remains unclear about the dynamics of the Venusian atmosphere, and its interaction with the photochemistry is how this convective cloud layer mixes momentum, heat, and chemical species and generates gravity waves. Gravity waves emitted by the convection have been proposed to promote a significant contribution to the maintenance of the super-rotation [1]. However, these waves develop from regional to local scales and cannot be resolved by global circulation models (GCM) developed so far to study Venus' atmospheric dynamics.

2. Model

Therefore we developed an unprecedented 3D turbulence-resolving Large-Eddy Simulations (LES) Venusian model with the Weather Research and Forecast terrestrial model [2]. Following the idealized LES model [3] using prescribed vertical profile of heating rates from the GCM, we coupled the Venus LMD physics to the dynamical core. Instead of constant interpolated profile, the solar and IR heating rates are directly calculated on the pressure level. The solar rate is computed with short waves radiation fluxes from Haus et al [4]. The radiative transfer is based on Eymet et al [5], using NET matrix with latitudinal varying cloud model from Haus et al [6]. As shown with the previous model, the general circulation has a strong impact on the convective layer. Therefore a third heating rate is added with an interpolated vertical profile from the LMD Venus GCM [7].

3. Results

The results shown here are for the Equator at midnight with no wind shear. Fig 1 shows the convective layer.

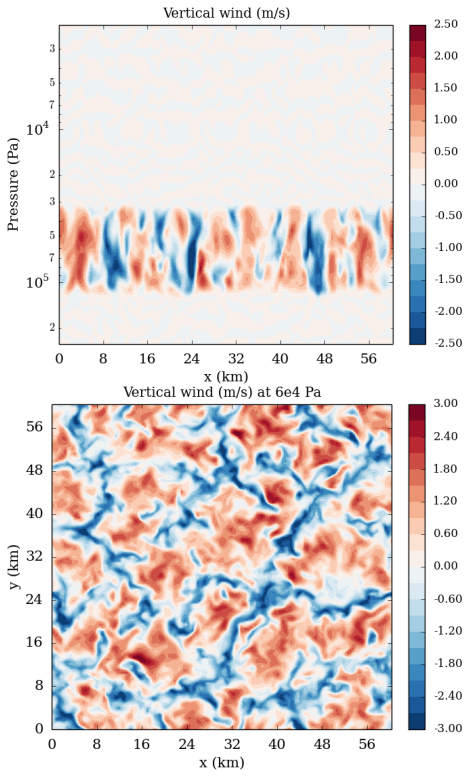

Figure 1: The convective layer. Top : vertical cross-section of the vertical wind (m/s). Bottom : horizontal cross-section of the vertical wind (m/s) at 6.0 10^4 Pa.

The convective layer extends from 1.2 10^5 Pa to 3.2 10^4 Pa (i.e. 46 to 55 km) against a 5 km thick for the idealized LES model. These values are consistent with the radio occultation by Venus Express instrument VeRa [8]. The amplitude of the vertical wind, about $\pm$ 3.5 m/s is also consistent with the VEGA balloon measurement [9].

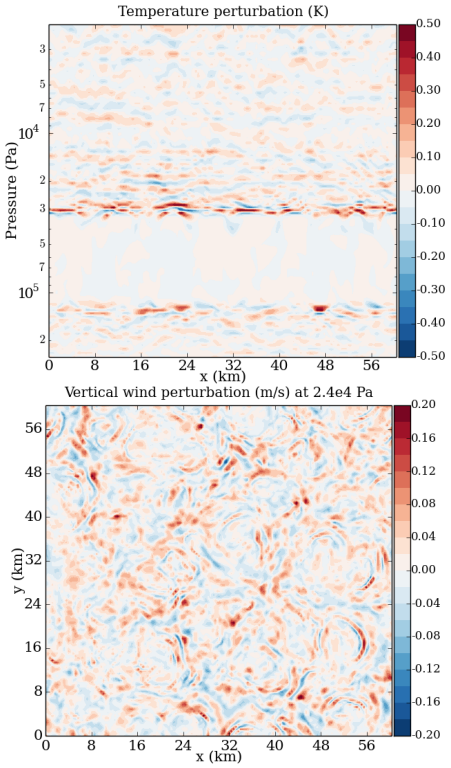

Figure 2: The induced gravity waves. Top : vertical cross-section of the temperature perturbation (K). Bottom : horizontal cross-section of the vertical wind perturbation (m/s) at 2.4 10^4 Pa.

Fig 2 shows the induced gravity waves through the temperature perturbation (top) and the vertical wind perturbation (bottom). The amplitude of the waves, $\pm$ 0.9 K, is the same order of magnitude as the observations [10]. The vertical wavelength is about 2.5 km and the horizontal wavelength between 1 and 5 km which is on lower part of the spectra [11].

4. Summary and Conclusions

The coupling with the LMD Venus physics engender a thicker convective layer with stronger gravity and therefore more consistent with the observations. The variability of the convective layer with latitude and local time will be discuss as well as the impact of wind shear and the impact of the latitudinal variation of the cloud mdel. Convective activity at cloud top will also be discuss.
We are currently working on the modeling of the deep atmosphere, especially the planetary boundary layer, as well as the implementation of the topography.

References

[1] Hou, A. Y., and Farrell, B. F., J. of Atm. Sc., 44:1049–1061, 1987.

[2] Skamarock, W. C. and J. B. Klemp, J., Comput. Phys., 227, 3465-3485, 2008

[3] Lefèvre, M., Spiga, A. and Lebonnois, S., J. of Geophys. Res. (Planets), 122, 134–149., 2017.

[4] R. Haus et al., Icarus, 272, 178-205, 2016.

[5] Eymet, V et al, J. of Geophys. Res. (Planets), 114, 2009.

[6] Haus R., and Kappel D. and Arnold G., Icarus, 232, 232–248, 2014.

[7] Lebonnois S., Sugimoto N. and Gilli G., Icarus, 278, 38–51. 2016.

[8] Tellamn S., et al.,J. of Geophys. Res. (Planets), 114, 2009.

[9] Linkin., V. M., et al., Science, 231, 1417-1419, 1986.

[10] Tellamn, S., et al., Icarus, 221, 471–480, 2009.

[11] Piccialli, A., et al., Icarus, 227, 94-111., 2014

EPSC Abstracts
Vol. 11, EPSC2017-259, 2017
European Planetary Science Congress 2017

Mars proton aurora: energy deposition and Lyman-α line profile

J.-C. Gérard (1), B. Hubert (1), D.V. Bisikalo (2) and V.I. Shematovich (2)
(1) LPAP, STAR Institute, Université de Liège, Belgium, (2) Institute of Astronomy, Russian Academy of Sciences, Moscow, Russian Federation (jc.gerard@ulg.ac.be / Fax: +32 43669729)

Abstract

We present the result of a model calculation of the brightness and line shape of Lyman-α emission produced in the Martian proton aurora recently discovered with the IUVS instrument on board MAVEN. This emission is produced by the interaction of solar wind protons with the Martian upper atmosphere.

1. Introduction

Two types of electron aurora have been observed on the Mars nightside. One is the discrete aurora confined to regions with residual magnetic field. The second one is the diffuse aurora (Schneider et al., 2015) which is more widespread and extends to lower altitudes, below the homopause. They occur during outbursts of highly energetic solar electrons. In addition, enhancements of the Lyman-α emission have been occasionally observed in the Mars dayside atmosphere with the Imaging UltraViolet Spectrograph (IUVS) instrument on board MAVEN (Deighan et al., 2016). This excess emission superimposes on the Ly-α resonance scattering background and is located between 100 and 140 km with a maximum near 120 km. It reaches as much as a 50% increase over the background level. These enhancements are generally coincident with periods of increased solar wind activity and last up to a few hours (Connour et al., 2017). They are likely caused by penetration of a fraction of solar wind protons into the Mars corona where they charge exchange with the ambient particles and produce fast neutral H_f atoms. The H^+/H_f population ratio in the auroral beam is controlled by the equilibrium between charge transfer and electron stripping during collisions with the ambient atoms and molecules. Measurements made with the SWIA instruments (Halekas et al., 2016) illustrated in the following figure indicated that the peak of the energy spectrum of protons penetrating the atmosphere is similar to that in the enhanced solar wind.

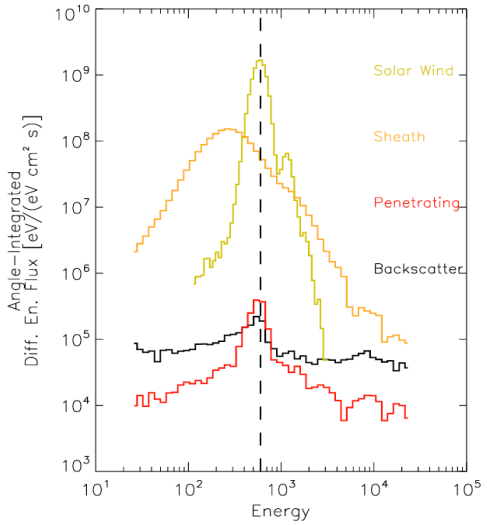

Figure 1 : angle-integrated energy spectra of protons measured by the SWIA instrument on board MAVEN in the solar wind, the sheath and those penetrating the atmosphere. Note the similarity in the peak energy suggesting the solar wind origin of the energetic protons. Energies are given in eV (from Halekas et al., 2015).

2. Monte Carlo model

The Monte Carlo code, based on the Direct Simulation Method (DSM), has been applied under different versions to calculate the interaction between a H^+- H beam with the neutral gas in the atmosphere of the Earth (Gérard et al., 2000), Jupiter (Bisikalo et al., 1996) and Mars (Shematovich et al., 2011). It is used here to calculate the energy degradation of the energetic H^+/H incident beam as it penetrates into the Martian upper atmosphere. The processes describing

the interactions of energetic H^+ and H and the atmosphere may be written as:

$$H^+(H) + M \rightarrow \begin{cases} H_{f'}^+(H_{f'}) + M^* \\ H_{f'}^+(H_{f'}) + M^+ + e \\ H_{f'}\left(H_{f'}^+\right) + M^+(M) + (e) \end{cases}$$

where M denotes CO_2, N_2 or O, and M* an excited state of species M. Part of the fast H hydrogen atoms $H_{f'}$ may be in the H(2p) excited state which radiates Doppler shifted Lyman-α photons. The vertical temperature and the neutral density profiles of CO_2, CO, N_2 and O are taken from the Mars Global Ionosphere-Thermosphere Model (M-GITM) for mid-latitude dayside conditions. The cross sections used in these calculations to calculate the H^+/H interactions with the atmosphere have been described in Shematovich et al. (2011).

3. Model simulations

We simulate the Lyman-α line profile excited by proton and H atom precipitation from the magnetosheath. For this purpose, we first calculate the altitude distribution of the velocity distribution function of the fast H(2p) atoms in the Martian proton aurora. The Lyman-α line profile is obtained by integrating the projection of the H atom velocity vector along the line of sight to simulate a limb observation. Since the line is optically thick in the central core, we use the resonance line radiative transfer model developed by Gladstone (1985) that is based on the Feautrier method with angle-averaged partial frequency redistribution and taking the atmospheric curvature into account. We show that only the central core of the line is optically thick but that most of the broader line profile remains optically thin. We then calculate the line profile of the emerging auroral Lyman-α radiation and the fraction of the Ly-α photons emerging from the atmosphere for a given viewing geometry.

Finally, we quantitatively discuss the relationship between the observed intensity enhancement caused by the aurora and the proton energy deposition.

4. Conclusions

Observations of transient dayside enhancements of Ly-a limb intensity have been interpreted as signatures of energetic H+ and H precipitation. We describe the results of calculations of the interaction of the incident beam with the Mars upper atmosphere. The altitude of the emission peak and the emerging intensity are discussed.

Acknowledgements

This research was funded by the PRODEX program of the European Space Agency, managed The PRODEX program is managed in collaboration with the Belgian Federal Science Policy Office (BELSPO). B.H. is supported by the National Fund for Scientific Research (FNRS).

References

Bisikalo, D.V. et al., The distribution of hot hydrogen atoms produced by electron and proton precipitation in the Jovian aurora, J. Geophys. Res., 101, 21157-21168, 1996.

Connour, K. et al., Three types of aurora observed by MAVEN/IUVS implications for Mars' upper atmosphere energy budget, Sixth International Workshop on the Mars Atmosphere: Modelling and observation, Granada, Spain, 2017.

Deighan, J.I. et al., Discovery of proton aurora on Mars, P13D-01, AGU Fall meeting 2016, San Francisco, USA

Gérard, J.-C. et al., A model of the Lyman-α line profile in the proton aurora, J. Geophys. Res., 105(A7), 15795-15805, 2000.

Gladstone, G.R., Radiative transfer of resonance lines with internal sources, J. Quant. Spectrosc. Radiat. Trans., 33, 453–458, 1985.

Halekas, J. S., et al., MAVEN observations of solar wind hydrogen deposition in the atmosphere of Mars, Geophys. Res. Lett., 42, 2015.

McClintock, W.E., Schneider, N.M., Holsclaw, G.M. et al. The imaging ultraviolet spectrograph (IUVS) for the MAVEN mission, Space Sci. Rev., 195, 75-124, 2015.

Schneider, N. M. et al., Discovery of diffuse aurora on Mars, Science, 350(6261), 2015.

Shematovich, V.I., et al., Proton and hydrogen atom transport in the Martian upper atmosphere with an induced magnetic field, J. Geophys. Res., 116, A11320, 2011.

EPSC Abstracts
Vol. 11, EPSC2017-294, 2017
European Planetary Science Congress 2017

Meteorological properties of Martian Dust Devils as observed by MSL

H. Kahanpää (1,2), M. T. Lemmon (3), E. Mason (3) and M. Battalio (3)
(1) Finnish Meteorological Institute, Helsinki, Finland (henrik.kahanpaa@fmi.fi), (2) Aalto University / School of Electrical Engineering, Espoo, Finland, (3) Texas A&M University / Department of Atmospheric Sciences, Texas, USA

Abstract

The Mars Science Laboratory rover (MSL) has observed dust devils simultaneously by imaging and by meteorological measurements. We use this data to determine central pressure drops and maximum wind speeds inside these Martian dust devils.

1. Introduction

Dust devils on Mars were first detected in images taken by the Viking orbiters [14]. Since then dust devils have been imaged by several Mars orbiters and landers (reviews of these observations are given in [2] and [10]). In addition, Mars landers with meteorological instrumentation have detected abrupt changes in wind direction and transient pressure dips interpreted as being caused by passing convective vortices [1][5][9][11][12][13]. However, the connection between the vortices detected in the wind and pressure data and the optically detected dust devils and has remained unclear. For example, it has not been known if the vortices detected by meteorological means lifted dust or not. As a consequence, the meteorological properties of Martian dust lifting vortices have been poorly constrained. The reason for this is that dust devils have not been observed simultaneously by both imaging and by meteorological measurements, until now.

2. Methods

2.1 Instrumentation

The MSL rover Curiosity [4] carries a suite of environmental sensors called REMS (Rover Environmental Monitoring Station) [3]. REMS includes sensors for measuring atmospheric pressure, wind speed and direction, air temperature, ground temperature, relative humidity and UV radiation flux. Nominally REMS performs 5-minute long measurement sessions with 1 Hz sampling rate, starting on every Martian hour. Furthermore, one hour long "extended measurement sessions" are performed by REMS at varying times of the sol. MSL is also equipped with cameras capable of filming atmospheric "movies", i.e. sequences of images aimed to survey varying atmospheric phenomena.

2.2 Measurement strategy

A campaign of imaging Dust Devil Search Movies was initiated soon after Curiosity landed in Gale crater on August 6, 2012 [8]. These movies consist of 4 to 24 frames pointed towards North. 249 such movies had been taken up till sol 1520 but only two dust devil had been detected in them [6][8]. However, a dust devil was identified in South/South-West direction in a multispectral sequence taken by Curiosity's Mast Camera (Mastcam) on sol 1520 [6]. Since then Navcam dust devil surveys have been performed in all directions. In these surveys two images are taken in each direction to identify moving features. In addition, "movies" with durations up till 30 minutes, comprising of 21 to 45 frames, have been taken by Navcam in directions where dust devils have been detected in the surveys. REMS extended measurement sessions have been scheduled to cover these movies whenever possible.

2.3 Determining the central pressure drops of imaged vortices

We analyze the REMS atmospheric pressure data measured during Navcam movies that contain identified dust devils. If a pressure dip is detected concurrently with the passing of a dust devil, then we model the pressure field of the dust devil by the

Lorentzian vortex model [1][5][7]. In this model, the pressure p at distance d from vortex center is given by

$$p(d) = p_\infty - \frac{\Delta p_{centre}}{(2d/D)^2 + 1}, \quad (1)$$

where p_∞ is the background pressure level, D is the half-maximum diameter of the pressure depression of the vortex and Δp_{centre} is the magnitude of the pressure depression at the center of the vortex. The pressure curve detected by a stationary measurement station, as a function of time t, can be calculated from eq. 1 by assuming that the vortex moves along a straight line and passes by the measurement station at distance $d_{\min}$ at time point t_0 [1]:

$$p_{obs}(t) = p_\infty - \frac{\Delta p_{obs}}{(2(t-t_0)/\Gamma)^2 + 1}, \quad (2)$$

where Γ is the half-maximum duration of the detected pressure dip and Δp_{obs} is the magnitude of the detected pressure drop at time point t_0. The ratio of the detected pressure drop Δp_{obs} and the central pressure drop Δp_{centre} can be solved from geometry:

$$\frac{\Delta p_{centre}}{\Delta p_{obs}} = \frac{(\Gamma U)^2}{(\Gamma U)^2 - 4d_{\min}^2}, \quad (3)$$

where U is the translation velocity of the vortex. We use eq. 3 to determine the central pressure drops of dust devils detected simultaneously in the movies and pressure data. The detected pressure drop duration Γ and the detected pressure drop magnitude Δp_{obs} are solved from the pressure data, and the distance of the closest encounter $d_{\min}$ with the dust devil and its translation velocity U are determined from the images, leaving Δp_{centre} the only unknown factor in eq. 3. Further, when the central pressure drop of a dust devil has been solved, then the maximum tangential wind velocity of the dust devil can be solved by assuming that the vortex is in cyclostrophic balance. We estimate the maximum wind velocities inside the dust devils by summing the calculated maximum tangential wind velocities and the observed translation velocities.

3. Results

We have identified 214 unique dust devils in the dust devil surveys and movies imaged over sols 1545 through 1660. The great majority of these dust devils have been detected in the foothills of Aeolis Mons, the central mountain of Gale crater. Apparently the explanation why only two dust devils were detected in the original Dust Devil Search Movies is that these movies faced North, i.e. towards the plains on the crater floor and away from the central mountain [6]. The REMS instrument recorded environmental variables, including atmospheric pressure, concurrently with 56% of the images in Navcam dust devil surveys and movies. We are currently investigating the dust devils detected in these images using the methods described in section 2. First results of the inferred central pressure drops and maximum wind speeds inside these Martian dust devils will be shown in this presentation.

4. Summary and Conclusions

This is the first study where central pressure drops of Martian dust devils are determined using in situ data. The results will be used to constrain the threshold pressure drop and/or threshold wind velocity required for dust lifting in a Martian convective vortex. Knowledge on these threshold values helps in parametrizing the amount of dust lifted by dust devils in numerical models of the Martian atmosphere.

Acknowledgements

The contribution of H. Kahanpää in this study was funded by The Finnish Cultural Foundation (grant number 00170395), and the travel expenses of H. Kahanpää were granted by the Emil Aaltonen foundation.

References

[1] Ellehoj, M. D. et al.: Convective vortices and dust devils at the Phoenix Mars mission landing site, J. Geophys. Res., Vol. 115, E00E16, 2010.

[2] Fenton, L. et al.: Orbital Observations of Dust Lofted by Daytime Convective Turbulence, Space Sci. Rev., Vol. 203(1), pp. 89-142, 2016.

[3] Gómez-Elvira, J. et al.: REMS: The Environmental Sensor Suite for the Mars Science Laboratory Rover, Space Sci Rev, Vol. 170, pp. 583-640, 2012.

[4] Grotzinger, J. P. et al.: Mars Science Laboratory mission and science investigation, Space Sci. Rev., Vol. 170, pp. 5-56, 2012.

[5] Kahanpää, H. et al.: Convective vortices and dust devils at the MSL landing site: Annual variability, J. Geophys. Res. Planets, Vol. 121(8), pp. 1514-1549, 2016.

[6] Lemmon, M. T., Newman, C. E., Renno, N., Mason, E., Battalio, M., Richardson, M. I., and Kahanpää, H.: Dust devil activity at the Curiosity Mars rover field site, 48th Lunar and Planetary Science Conference, 20–24 March 2017, The Woodlands, Texas, USA, 2017.

[7] Lorenz, R. D.: Heuristic estimation of dust devil vortex parameters and trajectories from single-station meteorological observations: Application to InSight at Mars, Icarus, Vol. 271, pp. 326-337, 2016.

[8] Moores, J. E. et al.: Observational evidence of a suppressed planetary boundary layer in northern Gale Crater, Mars as seen by the Navcam instrument onboard the Mars Science Laboratory rover, Icarus, Vol. 249(15), pp. 129-142, 2015.

[9] Murphy, J., and Nelli, S.: Mars Pathfinder convective vortices: Frequency of occurrence, Geophys. Res. Lett., Vol. 29(23), pp. 2103, 2002.

[10] Murphy, J. et al.: Field Measurements of Terrestrial and Martian Dust Devils, Space Sci. Rev., Vol. 203(1), pp. 39-87, 2016.

[11] Ringrose, T. J., Towner, M. C., and Zarnecki, J. C.: Convective vortices on Mars: A reanalysis of Viking Lander 2 meteorological data, sols 1–60, Icarus, Vol. 163(1), pp. 78-87, 2003.

[12] Ryan, J. A., and Lucich, R. D.: Possible dust devils, vortices on Mars, J. Geophys. Res., Vol. 88(C15), pp. 11005-11011, 1983.

[13] Steakley, K., and Murphy, J.: A year of convective vortex activity at Gale crater, Icarus, Vol. 278, pp. 180-193, 2016.

[14] Thomas, P., and Gierasch, P. J.: Dust devils on Mars, Science, Vol. 230(4722), pp. 175-177, 1985.

EPSC Abstracts
Vol. 11, EPSC2017-303-1, 2017
European Planetary Science Congress 2017

Venus upper atmospheric dynamics inferred from the Doppler-shift observations of submm CO line: Comparison with GCM experiments

H. Sagawa (1), M. Takagi (1), H. Maezawa (2) and K. Saigo (3)
(1) Kyoto Sangyo University, Faculty of Science, Kyoto, Japan (sagawa@cc.kyoto-su.ac.jp), (2) Osaka Prefecture University, Osaka, Japan, (3) National Astronomical Observatory of Japan, Chile Observatory (ALMA), Tokyo, Japan

Abstract

Atmospheric dynamics of Venus middle and upper atmosphere is still not fully understood. In early days, the atmospheric circulation at the altitude of ~95–110 km was considered as a combination of two globally uniform circulations: super-rotating retrograde zonal flow and subsolar-to-antisolar flow. However, recent observations have pointed out the presence of further complicated spatial variation of the wind field at the middle and upper atmosphere of Venus. In this study, we summarize the recent observations of Venus submm CO lines, which Doppler-shifted line frequency provides the information about the atmospheric dynamics of the interested altitudes, and compare them with numerical simulations using a Venus atmospheric general circulation model.

1. Introduction

Atmospheric dynamics of Venus middle and upper atmosphere (altitude region of ~70–110 km) is often discussed with two different kinds of circulation regime. One is the super-rotating retrograde zonal flow (RZ) which is well known as the global circulation in the lower atmosphere. Another one is the subsolar-to-antisolar flow (SSAS) that is a wind blowing from the dayside to nightside due to the strong thermal gradient in the thermosphere.

Several remote-sensing techniques have been applied for studying the atmospheric circulations in this middle and upper atmosphere (Lellouch et al., 1997). One is the application of the cyclostrophic-wind equation to the thermal structures obtained by infrared spectrometers (e.g., Piccialli et al., 2008). This method always postulates the validity of the cyclostrophic approximation, which becomes less appropriate at the equatorial region. Another approach is the Doppler-shift measurements of CO absorption lines at the millimeter and submillimeter wavelength using a very high frequency resolution heterodyne instrument ($\lambda/\Delta\lambda$ of ~10^7) (e.g., Lellouch, et al. 2008; Clancy, et al. 2012; Moullet, et al. 2012). This technique enables us to measure the line-of-sight velocity of wind (hereafter denoted as Doppler-wind) at ~95–110 km altitude. Most of the early observations of Doppler-winds made an attempt to describe the atmospheric circulation with a linear combination of globally uniform RZ and SSAS flows. However, the observed Doppler-winds, particularly the spatially-resolved Doppler-wind maps obtained by interferometers, cannot be sufficiently explained by such a simple combination of the two circulation regimes [**Figure 1 (a, b, c)**].

A new interpretation was proposed by Hoshino et al. (2012; 2013) based on a theoretical study using their newly developed Venus atmospheric general circulation model. Their model includes the momentum transport by gravity waves, and has shown the qualitative representation of one of the previously measured Doppler-wind maps [**Figure 2**].

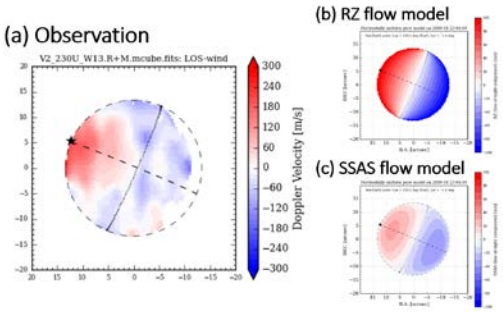

Figure 1: Doppler-wind map of Venus. (a) Observed result obtained from CO (J = 2–1) using the SMA interferometer. Blue color represents the blue-shift i.e. winds blowing toward the observer, while the red color is the red-shift. The point marked with a star symbol is the antisolar point (midnight), and the central

meridional line is the day-night terminator, thus the left-side of the apparent disk is the nightside, and the right-side is the dayside. (b) Theoretical Doppler-wind map of a globally uniform RZ flow. (c) Theoretical Doppler-wind map of a globally uniform SSAS flow. **Note that neither of (b) and (c) can explain the observed blue-shift in the nightside.**

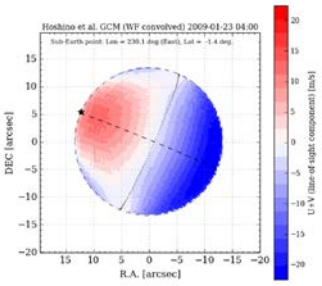

Figure 2: Theoretical Doppler-wind map calculated with the GCM developed by Hoshino et al. (2013). The blue-shit is shown in the nightside, which agrees with the observed result shown in Figure 1(a).

2. Aim of this study

The aim of this study is to expand the comparison between the previously observed Doppler-wind maps (including both single-dish and interferometric observations) with those calculated with the GCM of Hoshino et al. (2013). We collect the observational results from all available past literatures and also our own recent observations. In fact, the observation data provide a wide coverage of the solar phase angles. The detail comparison between the GCM numerical experiments will be discussed in the presentation.

References

[1] Lellouch, E., et al.: Monitoring of mesospheric structure and dynamics, in *Venus II*, edited by S. W. Bougher et al., Univ. of Arizona Press., pp. 295–324, 1997.

[2] Piccialli, A. et al.: Cyclostrophic winds from the Visible and Infrared Thermal Imaging Spectrometer temperature sounding: A preliminary analysis, JGR 113, E00B11, 2008.

[3] Lellouch, E., et al.: Monitoring Venus' mesospheric winds in support of Venus Express: IRAM 30-m and APEX observations, PSS 56, pp. 1355–1367, 2008.

[4] Clancy, R. T., et al.: Circulation of the Venus upper mesosphere/lower thermosphere: Doppler wind measurements from 2001–2009 inferior conjunction, sub-millimeter CO absorption line observations, Icarus 217, pp. 794–812, 2012.

[5] Moullet, A., et al.: Wind mapping in Venus' upper mesosphere with the IRAM-Plateau de Bure interferometer, A&A 546, A102, 2012.

[6] Hoshino, N., et al.: Characteristics of planetary-scale waves simulated by a new Venusian mesosphere and thermosphere general circulation model, Icarus 217, pp. 818–830, 2012.

[7] Hoshino, N., et al.: Effects of gravity waves on the day-night difference of the general circulation in the Venusian lower thermosphere, JGR 118, pp. 1–12, 2013.

EPSC Abstracts
Vol. 11, EPSC2017-308-3, 2017
European Planetary Science Congress 2017

Modelling the transport of trace gases in the Martian atmosphere

P. Wajer (1), P. Witek (1), M. Banaszkiewicz (1), W. Kofman (1,2), A. Pommerol (3) and P. Wolkenberg (4,1)

(1) Space Research Centre PAS, Warsaw, Poland (wajer@cbk.waw.pl), (2) Institut de Planetologie et d'Astrophysique de Grenoble CNRS/UJF, Grenoble, France, (3) Physics Institute, Space Research and Planetary Sciences - University of Bern, Bern, Switzerland, (4) Istituto di Astrofisica e Planetologia Spaziali (IAPS) – Istituto Nazionale di Astrofisica (INAF), Rome, Italy.

Abstract

The European-Russian ExoMars Trace Gas Orbiter (TGO) is set to reach its scientific orbit at the end of 2017 after the aerobraking campaign. The data returned by the probe will help to understand the origin and evolution of trace gases, especially methane (CH_4), in the Martian atmosphere. To analyze the data sent back by the probe we have developed a model of the photochemistry in the atmosphere of Mars. The model follows a few dozen molecules that are present or expected to exist in the atmosphere due to a few hundred considered chemical and photochemical reactions. The radiative transfer equation is solved by using two-stream approximation to calculate solar photon flux that determine the photochemistry at different altitudes above the surface. The model takes into account the role of dust, ice clouds as well as the densities and fluxes of considered gases at the surface as a result of their transport from subsurface/surface sources.

1. Introduction

In 2003 and 2004, a few groups of scientists by using Earth ground based observations and Mars Express Orbiter observations announced the discovery of methane (CH_4) in the atmosphere of Mars [2][3] then other observation were made by the Curiosity rover [6]. Since then, the debate has been carried out on several unexplained issues: (i) fast (seasonal) variability of CH_4 that is in contradiction with the long photochemical lifetime (a few hundred years) of this molecule in the atmosphere, (ii) sources of CH_4 that could quickly increase the concentration, (iii) sinks of methane that could reduce its concentration to the background level in several months.

Analysis of the sources and sinks of CH_4 on Mars will be an important step to understand the history, the evolution and a possible existence of life (current or past) on this planet. The biological origin of CH_4 could be explained by activity of bacteria called methanogeneses. The bacteria can exist deep under surface of Mars, or they lived in the past and CH_4 is stored in the permafrost as clathrates. There exist alternative explanation of its origin based on chemical processes called serpentinisation. It implies that if the methane is produced in this reaction, its presence is related to subsurface hydrothermal activity [1].

We plan to study propagation of CH_4 and other trace gases (e.g. hydrocarbons as C_2H_6, C_2H_4 and species containing sulphur as H_2S and SO_2 that should be observed in the atmosphere at very low concentration levels) in the Martian atmosphere by using chemical and photochemical modelling. This kind of modeling is an important step to understand observational data taken by the space instruments (for example NOMAD from TGO mission [5]) as well as to distinguish between different hypothesis that concern potential surface and subsurface sources of CH_4 and other trace gases (CaSSIS [4]).

2. Research methodology

To model photodissociation and chemical processes in the atmosphere of Mars we develop 1D model to compute the steady-state chemical composition of the atmosphere. In our study we solve one-dimensional time-dependent transport equations:

$$\frac{\partial n_i}{\partial t} = -\frac{\partial \Phi_i}{\partial z} + P_i - n_i L_i \qquad (1)$$

Where n_i means i-molecule concentration, Φ_i describes a vertical transport of molecules ($cm^{-2}s^{-1}$), P_i – production rate ($cm^{-3}\ s^{-1}$), L_i means the loss rate (s^{-1}), z - altitude over planet's surface.

The separated code was constructed to simulate the interaction of species with radiation. Since the photochemical destruction of the atmospheric

molecules depends on the solar flux, thus including absorption, Rayleigh scattering, scattering on small particles as dust or ice crystal is an important part of our simulation (see fig. 1 where we plotted the exemplary results where we modelled downstream solar photon flux in case when only absorption is present in the atmosphere. We restricted the plot to 300nm in order to show differences between the two fluxes in the part of the spectrum below about 200nm that is important for CO_2 absorption).

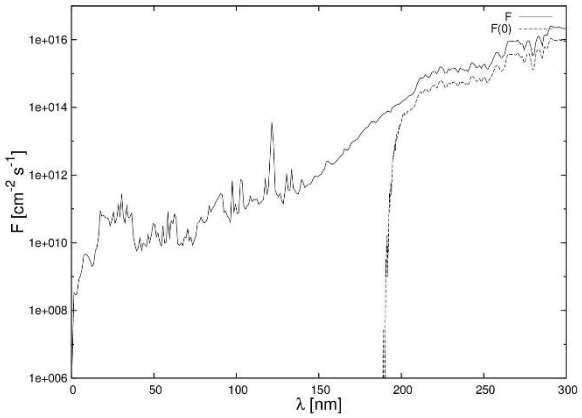

Figure 1: The solar photon flux in UV part of the spectrum at the top, F, and bottom, F(0), of the Martian atmosphere.

Both upper and lower boundaries that must be fixed in the photochemical model depend on the given molecule. The upper boundary conditions describe the atmospheric escape of molecules, for example H or H_2 [7]. Conditions at the lower boundary are determined by the chemically active surface (surface emission and deposition) and potential transport of species from subsurface sources.

To verify our numerical modelling we plan to use images obtained from stereoscopic camera CaSSIS [4], that should give us the mineralogical description of the surface from where the methane originates, and another instruments, especially instruments on TGO.

3. Summary and Conclusions

The origin of sources and sinks of methane in the atmosphere of Mars is not fully understood, although many hypotheses have been proposed [1]. In this work in progress we aim to develop a photochemical model of the Martian atmosphere. This model helps us to better understand the origin and evolution of trace gases, especially CH_4. We also plan to use the data of computer simulations of gases transport from subsurface to the surface and the data obtained from the spacecraft instruments to describe the lower boundary conditions (at the surface) for the atmospheric photochemical model, which results will later be confronted with measurements.

Acknowledgements

This research is grounded on the involvement of the Space Research Centre (SRC) in ESA's ExoMars TGO mission. The power supply unit for the ExoMars camera, CaSSIS was built in the SRC (in the project "Zasilacz Cassis/Cassis Power Supply Unit", Um. 4000111561, funded by the European Space Agency) and the CaSSIS Science Team includes members in SRC.

References

[1] Atreya S., K., Mahaffy P., R., Wong A. Methane and related trace species on Mars: Origin, loss, implications for life, and habitability. Planetary and Space Science 55 (3), 358 – 369, 2007.

[2] Formisano, V., Atreya, S., Encrenaz, T., Ignatiev, N., Giuranna, M. Detection of Methane in the Atmosphere of Mars. Science, Vol. 306, pp. 1758-1761, 2004.

[3] Mumma, Michael J.; Villanueva, Geronimo L.; Novak, Robert E.; Hewagama, Tilak; Bonev, Boncho P.; DiSanti, Michael A.; Mandell, Avi M.; Smith, Michael D. [3] Author, F. Strong Release of Methane on Mars in Northern Summer 2003. Science, Volume 323, Issue 5917, pp. 1041-1045, 2009.

[4] Thomas, N. et al., 2016. 47th LPSC, Abstract # 1306.

[5] Vandaele, A. C. et al., 2015. Science objectives and performances of NOMAD, a spectrometer suite for the ExoMars TGO mission. Planetary and Space Science, Volume 119, p. 233-249.

[6] Webster, C., R., et al., 2015. Mars methane detection and variability at Gale crater. Science, Volume 347, Issue 6220, pp. 415-417.

[7] Zahnle, K., R. M. Haberle, D. C. Catling, and J. F. Kasting. Photochemical instability of the ancient Martian atmosphere. Journal of Geophysical Research, Volume 113, Issue E11, 2008.

EPSC Abstracts
Vol. 11, EPSC2017-347, 2017
European Planetary Science Congress 2017

Stochastic Models of Lightning and Lightning Observation on Venus

R. D. Lorenz (1)
(1) Space Exploration Sector, Johns Hopkins Applied Physics Laboratory, Laurel, MD 20723, USA

Abstract

Many observations regarding lightning on Venus are mutually discrepant, with widely varying rates and intensities and many negative reports. A model of lightning as a purely random process with a uniform rate appears to be incompatible with the observation set. While a plausible thesis is that one or more observations are 'wrong' in asserting an interpretation, here I explore models of possible temporal and/or spatial variability of lightning in an attempt to maximize agreement with observations while minimizing the number of model parameters.

1. Introduction

The first-order analysis of any phenomenon not unreasonably posits a Poisson process with a single, uniform occurrence rate λ. An observation is then a set T of Bernouilli trials (detect ? Y/N) which attempt to constrain λ as ~Y/T. A major challenge in reconciling observations to date is that the detection threshold (typically, a top-of-atmosphere light flash energy) is not always accurately quantified, and is typically different for different searches, and without taking this into account (wherein the population of lightning events has some distribution that yields different counts for different thresholds) the comparisons are largely meaningless.

Some progress has been made in recent years in addressing analogous challenges in planetary meteorology, namely assessing the population of dust devils on Earth and Mars. A simple and physically based observation- dependent threshold detection with a plausible (power law) distribution of dust devil diameters [1] was able to reconcile reported dust devil occurrence rates (devils/km2/day) which differed by four orders of magnitude! These surveys were all conducted, however, at locations/times expected a priori to have dust devils, and typically with long enough periods that day-to- day variations were averaged out. Inspection of dust devil occurrences (e.g. the number of devils in single orbital Mars images) shows a strongly non-Poisson distribution, with the number of 'many-devil' images disproportionate to an extrapolation given the number of single- and few-devil images.

In other words, there is at least one 'hidden variable' determining whether conditions are favorable for dust devils or not (typically the ambient wind speed).

This paradigm seems appropriate for lightning on Venus, if it exists, as indeed it seems to be true for lightning on Earth. Casual observation indicates that if one sees one lightning flash, one is likely to see many, because there is a storm, whereas overall storms are rare.

Even with very poor statistics (7 flashes), the optical survey by Hansell et al. [3] found '*an indication that Venus undergoes quiet times and noisy times*' since on four nights (3.75 hours) of observation the counts were [2,2,0,3], with the last 3 occurring within 10 minutes of each other. On the other hand, in part such stochasticity may also be due to variations in the detection efficiency (such as the claimed dependence of Venus Express magnetometer signatures of lightning on the geometry of the magnetic field lines) : Russell et al. [4] note only 61 detections in some 12,223s of observation, but consider that the observations only access Venus 1/4 of the time, and over only a few hundred km (0.027% of the planet's area) : their extrapolation of a 18/s global flash rate (20% of Earth) based on the wholly unsupported assumption that the flash rate is uniform.

Although ultimately it may be necessary to develop a spatial variability model to explicitly track the migration of "storms" and the intersection of those lightning-favorable regions with an observation process, a first step is simply to posit two additional variables – a characteristic duration S of a storm, and an occurrence rate R, and to adopt λ as a conditional quantity (i.e. λ=λo during a storm, λ=0 otherwise). If

(as is presently the case) the observation duty cycle is small, it is possible to find many nondetections that are not inconsistent with a few high-rate detections.

2. Summary and Conclusions

Efforts are underway to develop a reasonably parsimonious model of lightning variability and detection on Venus to reconcile at least some observation claims. This modeling will help interpret results from the Lightning and Airglow Camera (LAC) on the Akatsuki Venus Climate Orbiter.

Acknowledgements

This work was supported by NASA Venus Climate Orbiter Participating Scientist Grant NNX16AC78G.

References

[1] Lorenz, R. (2009), Power Law of Dust Devil Diameters on Earth and Mars, Icarus, 203, 683-684

[2] Lorenz, R., and B. Jackson (2016) Dust Devil Populations and Statistics, Space Science Reviews, 10.1007/s11214-016-0277-9

[3] Hansell, S. et al., (1995) Optical Detection of Lightning on Venus, Icarus, 117, 345-351

[4] Russell, C. et al. (2008) Whistler mode waves from lightning on Venus: Magnetic control of ionospheric access, J. Geophys. Res., 113, E00B05, doi:10.1029/2008JE003137

EPSC Abstracts
Vol. 11, EPSC2017-358, 2017
European Planetary Science Congress 2017

Simulation of the early Martian climate using a general circulation model, DRAMATIC MGCM: Impacts of thermal inertia

A. Kamada (1), T. Kuroda (1,2), Y. Kasaba (1), N. Terada (1) and T. Akiba (1)
(1) Planetary Atmospheric Physics Laboratory, Department of Geophysics, Graduate School of Science, Tohoku University, Japan, (2) National Institute of Information and Communications Technology, Japan.

Abstract

We use a Mars General Circulation Model (MGCM) named DRAMATIC (Dynamics, RAdiation, MAterial Transport and their mutual InteraCtions) to reveal the nature of early Martian climate, "warm and wet" or "cold and icy". With high thermal inertia assuming the wet soil, the surface temperature greatly increased in comparison with the dry soil simulations. Under the assumption of ancient ocean which covers up to one third of Martian surface, the surface temperature could be maintained above 273 K throughout the year in low-mid latitudes of northern hemisphere in that case.

1. Introduction

Mars receives only 43% of the solar flux of Earth. And the solar intensity before ~3.8Ga is thought to be ~75% of today. However, there have been found many fluid traces and aqueous minerals such as phyllosilicate, sulfate, and chloride on the Martian surface paradoxically. Such evidences should indicate that the convincing action and effects of liquid water on the ancient Martian surface. Solutions to this paradox can be classified into two scenarios, "warm and wet" [1,2] and "cold and icy" [3,4]. The former scenario assumes the long-term warm and wet environments allowing the existence of permanent liquid water. The latter one assumes that the planet was mainly frozen and seasonal or impulsive melting of snow. Ice deposits due to volcanoes and meteorites would provide massive liquid water for forming fluid morphology.

2. Methods

The DRAMATIC MGCM is based on the dynamical core of CCSR/NIES/FRCGC MIROC model [5], and the implementations of physical processes for the current Mars environment have been done by [6,7]. In this study, to simulate the early Martian climate, we assume a pure CO_2 atmosphere with pressure of 2 bars, and solar flux is set to be 75% of the present-day value along with the standard stellar evolution model. Also, to provide the cooling effects in high-pressure conditions accurately, we have implemented the radiative effects of CO_2 gas assuming the sub-Lorentzian profile [8] for the far-line absorption and collision-induced absorption [9].

At first, for simplification, we compared the simulation results with globally uniform thermal inertia of between 250 and 3,000 (J $s^{-1/2}$ m^{-2} K^{-1}, hereafter the unit is omitted). Larger value supposes the wet soils, which is expected to prevent the dissipation of ground heat and strengthen the greenhouse effect. Second, we implemented the virtual ocean and lakes with the sea level of -2.54 km altitude (Figure 1) covering about one-third of the Martian surface. Thermal inertia and albedo of ocean and lakes were set to 2,000 and 0.07, respectively, where the surface temperature went above 273 K. In the locations where the surface temperature was below 273K, those parameters were set to 2800 and 0.5, respectively, assuming the icy ocean. Albedo in other areas was set to 0.22 assuming rocky surface.

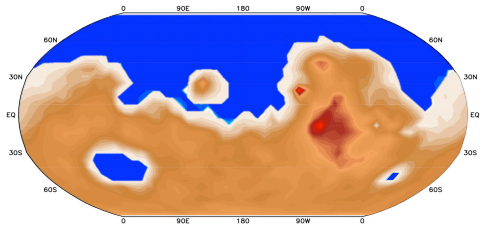

Figure 1: Martian topography with ocean and lakes with the sea level of -2.54 km altitude.

3. Results

In the "wet soil" simulation with globally-constant thermal inertia of 3,000, surface temperature increased up to ~260 K, which was higher than that with globally-constant thermal inertia of 250 (~240 K). In addition, annual mean surface temperature in equators and Hellas-basin went above 273 K (283 K on the equator and 279 K in Hellas-basin) (Figure 2). In this case, the temperature on the equator was kept to be above 273 K for a whole year. In the simulation putting virtual ocean and lakes with wet soil condition, the surface temperature went about 273 K, throughout the year in low- and mid- latitudes of northern hemisphere and half of the year in Hellas-basin. The results suggest that the surface conditions should be the key of the existence of liquid water in early Mars. The surface conditions with high thermal inertia could produce the high surface temperature enough to make liquid water even with the pure CO_2 atmosphere and solar insolation of only 75% of today.

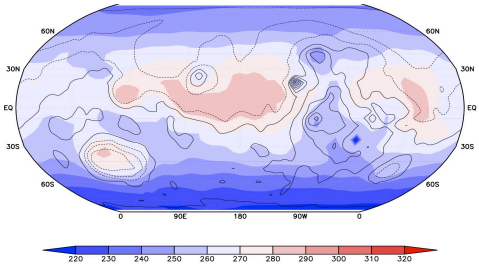

Figure 2: Annual mean temperature in thermal inertia of 3,000 (J $s^{-1/2}$ m^{-2} K^{-1}) at surface pressure of 2 bars.

4. Summary and Conclusions

Our simulation study showed that the early Martian climate under the "wet soil" condition could keep warm and wet conditions with radiative effects of CO_2 gas and clouds only, without considering other greenhouse gases such as SO_2 and H_2. Our results indicated a new direction in the research of early Martian climate, showing that the high thermal inertia would likely make warmer environment (allowing the existence of liquid water seasonally and spatially) than the studies before.

References

[1] J. B. Pollack, J. F. Kasting, S. M. Richardson, and K. Poliakoff: The Case for a Wet, Warm Climate on Early Mars, Icarus 71, 203-224, 1987.

[2] F. Forget, R. Wordsworth, E.Millour, J. B. Madeleine, L. Kerber, J. Leconte, and E. Marcq, R. M. Haberle: 3D modeling of the early martian climate under denser CO_2 atmosphere: Temperature and CO_2 ice clouds, Icarus 222, 81-99, 2013.

[3] S. W. Squyres, and J. F. Kasting: Early Mars: How Warm and How Wet?, Science 265,744-749, 1994.

[4] R. Wordsworth, F. Forget, E. Millour, and B. Charnay: Global modelling of the early martian climate under a denser CO_2 atmosphere: Water cycle and ice evolution, Icarus 222, 1-19, 2013.

[5] K-1 Model Developers: K-1 coupled GCM (MIROC) description, K-1 Tech. Rep., 1, Univ. of Tokyo, Tokyo, 1–34, 2004.

[6] T. Kuroda, N. Hashimoto, D. Sakai, and M. Takahashi: Simulation of the Martian atmosphere using a CCSR/NIES AGCM, J. Meteor. Soc. Japan 83, 1–19, 2005.

[7] T. Kuroda, A. S. Medvedev, Y.Kasaba, and P. Hartogh: Carbon dioxide ice clouds, snowfalls, and baroclinic waves in the northern winter polar atmosphere of Mars , Geophys. Res. Lett. 40, 1484-1488, 2013.

[8] M. Fukabori, T. Nakazawa, and M.Tanaka: Absorption properties of infrared active gases at high pressures – I. CO_2, J. Quant. Spectro. Rad. Trans. 36, 265-270, 1986.

[9] M. Gruszka, and A. Borysow: Roto-transitional collision-induced absorption of CO_2 for the atmosphere of Venus at frequencies from 0 to 2500 cm^{-1}, at temperatures from 200 to 800K, Icarus 129, 172-177, 1997.

EPSC Abstracts
Vol. 11, EPSC2017-376-1, 2017
European Planetary Science Congress 2017

SPICAM observations of thermospheric airglow during the 2007 dust storm

N. Schneider (1), M. Chaffin (1), D. Everding (1), F. Leblanc (2), J. Y. Chaufray (2), F. Montmessin (2), J.-L. Bertaux (2) and the SPICAM team
(1) Laboratory for Atmospheric and Space Physics, Boulder, Colorado, USA (nick.schneider@lasp.colorado.edu), (2) LATMOS/IPSL, Guyancourt, France

Abstract

In 2007 (Mars Year 28), Mars experienced a global dust storm. Previous studies have reported large changes in the H Lyman alpha coronal airglow during this period, corresponding to a large decrease in H escape fluxes during the declining phase of the dust storm. Here we present airglow measurements of CO Cameron band and CO_2^+ UV Doublet emission in the thermosphere from 2007 data gathered by the SPICAM (SPectroscopy for the Investigation of the Characteristics of the Atmosphere of Mars) instrument on Mars Express. During the dust storm period in late 2007, lower atmospheric temperatures were enhanced, pushing the thermosphere to higher altitudes. At the same time, more intense UV heating resulting from the perihelion passage of Mars resulted in extended upper atmospheric scale heights. We compare our retrievals and techniques to previous studies, which found no enhancement in thermospheric scale heights during this period.

1. SPICAM Observations of the Thermosphere

The SPICAM instrument on Mars Express is an imaging ultraviolet spectrograph that observes in the far and mid UV from $118-320$ nm (Bertaux et. al. 2006). The instrument has a focus on stellar occulations, but also performs thermospheric limb scans and nadir observations. In limb mode, the instrument observes the characteristic airglow spectrum of Mars (Figure 1), whose most conspicuous features in the mid-UV are the CO Cameron bands (180-260 nm), and the CO_2^+ UV doublet (289 nm). These features reveal thermospheric properties, with the UV Doublet diagnosing the neutral CO_2 scale height and the CO Cameron bands reflecting a larger scale height that is a blend of thermal and nonthermal emission sources. Previous studies, including most recently Stiepen et. al. (2015), have examined the time evolution of the scale height and peak altitude of these features. Unfortunately, the need to share observing time with other Mars Express instruments, and difficulties in the instrument data analysis introduced by stray light and detector high voltage spikes often limit the useful dataset, making observations sparse. As a result, these previous studies have extracted limited information about the thermosphere, particularly in the 2007 dust storm year. In addition, these previous studies found no large differences between 2007 and other years, despite the presumably large influence of the dust storm. This motivates our independent study of the dataset.

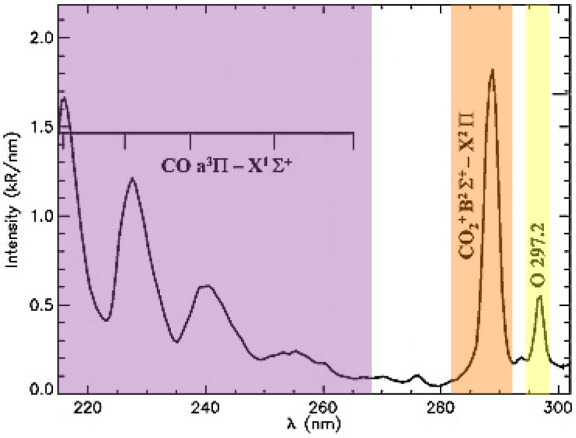

Figure 1: Mid-UV airglow of Mars, adapted from Leblanc et. al. (2006).

2. Retrieving Thermospheric Properties

To extract thermospheric peak altitudes and scale heights from the dataset, we employ a multiple linear regression technique. In this method, individual

reduced spectra are fit by scaling input model spectra by linear coefficients, and summing the models together. For model spectra we use a Cameron band model convolved and binned to the instrument resolution (Stevens et. al. 2015), a solar spectrum extracted from nadir observations made by SPICAM, and Gaussians at the location of the UV Doublet and OI 297.2 nm feature. We also include a linear component to account for dark subtraction offsets and large-scale stray light features.

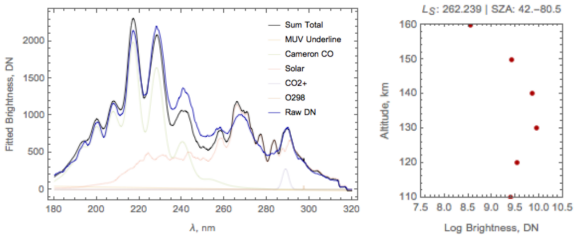

Figure 2: (a) Example SPICAM spectrum and multiple linear regression fit, showing composite fit and fitted components. (b) Retrieved altitude profile of CO Cameron band emission for a single limb scan. Each point represents the Cameron band fit component to the average SPICAM spectrum for surrounding altitudes.

An example fitted spectrum is shown in Figure 2a. Our method does a resonable job of reproducing the data, with offsets in the vicinity of $240 - 260$ nm potentially caused by poor knowledge of the solar stray light at this location. Applying this technique to multiple spectra from a given limb scan produces intensity altitude profiles (Figure 2b), which can then be fit to extract a peak altitude and scale height.

3. Response of the Thermosphere in 2007

By applying our fit procedure across 2007, we produce peak altitudes and scale heights for both the Cameron bands and the CO_2^+ UVD, shown in Figure 3. We see an increase of the peak altitude by over 10 km, centered on Southern summer solstice and declining approximately linearly on either side of the peak. Scale heights are more peaked, with a linear increase from 15 km near L_s 200 to 30 km near L_s 300, and a steep decline following the peak. These observations have implications for the structure and variability of the thermosphere and the upper atmospheric environment underlying the large variability in the H corona, which we will discuss more fully in our presentation.

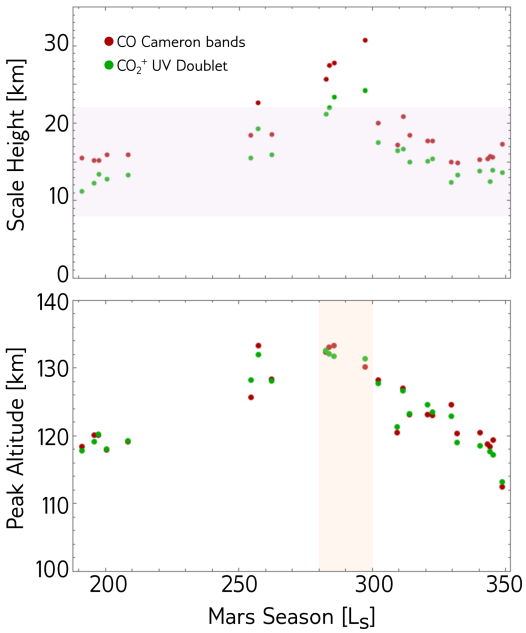

Figure 3: Retrieved peak altitudes and scale heights of thermospheric emissions at Mars in 2007.

References

[1] Bertaux, J.-L., Korablev, O., Perrier, S., Quémerais, E., Montmessin, F., Leblanc, F., Lebonnois, S., Rannou, P., Lefèvre, F., Forget, F., Fedorova, A., Dimarellis, E., Reberac, A., Fonteyn, D., Chaufray, J. Y., and Guibert, S.: SPICAM on Mars Express: Observing modes and overview of UV spectrometer data and scientific results, JGR, Vol. 111, E10S90, 2006.

[2] Stiepen, A., Gérard, J.-C., Bougher, S., Montmessin, F., Hubert, B., and Bertaux, J.-L.: Mars thermospheric scale height: CO Cameron and CO_2^+ dayglow observations from Mars Express, Icarus, Vol. 245, pp. 295-305, 2015.

[3] Leblanc, F., Chaufray, J. Y., Lilensten, J., Witasse, O., and Bertaux, J.-L.: Martian dayglow as seen by the SPICAM UV spectrograph on Mars Express, JGR, Vol. 111, E09S11, 2006.

[4] Stevens, M. H., Evans, J. S., Schneider, N. M., Stewart, A. I. F., Deighan, J., Jain, S. K., Crismani, M., Stiepen, A., Chaffin, M. S., McClintock, W. E., Holsclaw, G. M., Lefèvre, F., Lo, D. Y., Clarke, J. T., Montmessin, F., Bougher, S. W., Jakosky, B. M.: New observations of molecular nitrogen in the Martian upper atmosphere by IUVS on MAVEN, GRL, Vol. 42, pp. 9050-9056, 2015.

EPSC Abstracts
Vol. 11, EPSC2017-385, 2017
European Planetary Science Congress 2017

Variability of the cloud-top altitude deduced from radio occultation experiments and thermal mapping obtained by LIR onboard Akatsuki

T. Fukuhara (1), H. Ando (2), T. Imamura (3), M. Takagi (2), M. Taguchi (1), and LIR/RS project team
(1) Rikkyo University, Japan, (2) Kyoto Sangyo University, Japan, (3) The University of Tokyo, Japan

Abstract

The thermal infrared images acquired by LIR onboard Akatsuki have been compared with result of the radio occultation experiments which have been synchronously acquired with LIR. We have derived variability of the cloud-top altitude from the comparison. The result shows that the cloud-top altitude has been mostly ~67 km in the southern low latitude. Whereas, the altitude seems slightly increased with the mid latitude. Previous observations by Vera, VIRTIS, and VMC onboard Venus express indicated the altitude was stable in the latitude. The aspect seen in the result by the collaboration may represent a feature which is independent from the results previously observed. We are carefully considering the result obtained by our observation.

1. Introduction

Venus climate orbiter called Akatsuki which failed to be inserted into Venus orbit in 2010 has been successfully re-orbited on December 2015 [1], and instruments onboard the spacecraft has finally started observation of Venus. The longwave infrared camera (LIR) detects thermal emission with wavelengths of 8 - 12 μm from Venus disk regardless of day or night side, and represents horizontal distribution of the brightness temperature at the cloud top [2]. LIR has continuously archived more than eight thousands images without serious fault for two Venusian years. Meanwhile, the radio occultation experiment termed Radio Science (RS) retrieves the atmospheric pressure, the temperature, the sulfuric acid vapor mixing ratio, and the electron density [3]. Akatsuki RS mainly probes the low and middle latitude regions with the near-equatorial orbit in contrast to the previous radio occultation experiments using polar orbiters. It obtained 19 vertical profiles of the Venusian atmosphere by April 2017. Temperature profiles were successfully obtained at altitude of 38 - 85 km and show distinct atmospheric structures depending on the altitude.

The cloud-top altitude observed by LIR would be roughly ~65 km in accordance with the contribution function of Venus atmosphere under situation of typical cloud distribution [4]. However, it is difficult to retrieve precisely the variability of cloud-top altitude except for the comparing with the vertical temperature profile synchronously observed. LIR images have been synchronously acquired with most of RS observations as a basic strategy for Akatsuki observation. We could successfully acquire 6 data sets in which LIR and RS observations have observed completely same region.

2. Image data processing

LIR image included background variance depending on baffle temperature at observation; it brings an image brighter than our expectation. Hence, it has been canceled firstly by using deepspace images which have been acquired on orbit with different baffle temperature. Furthermore, limb-darkening effect which is generally seen in the thermal infrared images has been eliminated from the image by the approach previously developed [5]. Absolute brightness temperature of the cloud-top on Venus could be finally deduced from LIR observation.

3. Result and Discussion

The temperature of the region synchronously observed with RS has been compared with the vertical temperature profile retrieved by RS to

deduce the altitude LIR observed. The data set covers latitude of 7°S - 35°S with local time of ~5:00 except for one which has been observed at 50°N degrees with local time of ~19:00. The emission angle at the time of observation is mostly ~15 degrees in southern hemisphere. The cloud-top altitude has indicated mostly ~67 km in the southern area. Whereas, the altitude seems slightly increased with the mid latitude. In contrast, previous observations by Vera, VIRTIS, and VMC onboard Venus express (VEX) indicated the altitude was stable in the latitude [e.g., 6, 7]. The aspect seen in the result by the collaboration may represent a feature which is independent from the results observed by VEX. We are carefully considering the result obtained by our observation.

References

[1] Nakamura et al., EPS, doi 10.1186/s40623-016-0457-6, 2016.

[2] Fukuhara et al., EPS, Vol. 63, 1009-1018, 2011.

[3] Imamura et al., EPS, Vol. 63, 493–501, 2011.

[4] Taguchi et al., ASR, Vol. 40, 861–868, 2007.

[5] Taylor et al., JGR, Vol. 85, No. A13, 7963–8006, 1980.

[6] Ignatiev et al., JGR, VOL. 114, E00B43, 2009.

[7] Lee et al., Icarus, Vol. 217, 599–609, 2012.

EPSC Abstracts
Vol. 11, EPSC2017-392-2, 2017
European Planetary Science Congress 2017

Venus cloud top structure seen by the coordinated Subaru and Akatsuki observations

T.M. Sato (1), H. Sagawa (2), T. Kouyama (3), M. Taguchi (4), Y.J. Lee (1), J. Peralta (1), M. Takagi (2), G.L. Hashimoto (5), T. Satoh (1), Y. Kasaba (6), S. Aoki (7), T. Fukuhara (4), A. Yamazaki (1), T. Imamura (8), and M. Nakamura (1)
(1) Institute of Space and Astronautical Science, Japan Aerospace Exploration Agency, Sagamihara, Japan, (2) Kyoto Sangyo University, Kyoto, Japan, (3) National Institute of Advanced Industrial Science and Technology, Tokyo, Japan, (4) Rikkyo University, Tokyo, Japan, (5) Okayama University, Okayama, Japan, (6) Tohoku University, Sendai, Japan, (7) Institut d'A éronomie Spatiale de Belgique, Brussels, Belgium, (8) The University of Tokyo, Kashiwa, Japan (takao@stp.isas.jaxa.jp / Fax: +81-42-759-8178)

Abstract

We carried out the coordinated observations of Venus cloud top with Subaru Telescope and Japanese Venus orbiter, Akatsuki, in January 2017. In this presentation, we will present the observational results and discuss the interpretation of them.

1. Introduction

The first sequential mid-infrared images taken by Longwave Infrared Camera (LIR) onboard Akatsuki after its insertion into Venus orbit on December 7, 2015 [1] revealed that a planetary-scale bow-shaped structure exists at Venus cloud top and has been fixed in a position above Aphrodite Terra for at least four Earth days. This stationary structure has been suggested to result from an upward-propagating mountain gravity wave generated by the interaction of atmospheric flow with the topography [2]. Up to the present, small and large stationary bow-shaped structures possibly originated from similar mechanism have been detected above various highlands in not only mid-infrared but also UV images. Here, we report the coordinated Subaru and Akatsuki observations conducted to obtain a better understanding of the atmospheric dynamics at the cloud top including the newly discovered stationary structure.

2. Observations

We observed Venus at the solar phase angle of ~90˚, with evening terminator in view, with the Cooled Mid-infrared Camera and Spectrometer (COMICS) mounted on the 8.2-m Subaru Telescope atop Mauna Kea, Hawaii, during the period of January 11-14, 2017 (UT). The narrow band imaging (8.66 μm and 11.34 μm) and N-band (8-13 μm) low spectral resolution (R~250) spectroscopy were carried out to investigate the cloud top morphology and several atmospheric parameters such as cloud top temperature and altitude, etc. During the period, Akatsuki was approaching to the periapsis and the local solar time at the sub-spacecraft point shifted from 13 h to 15 h. LIR and Ultraviolet Imager (UVI) took Venus images at intervals of one and two hours, respectively.

3. Results

The obtained COMICS images with good signal-to-noise ratio and with high spatial resolution (~200 km at the sub-observer point) provide several observational findings.

- As seen in Figure 1, the images at both wavelengths after high-pass filtering clearly show that a stationary bow-shaped structure distributed in the equatorial region appears above the highland named Maat Mons (0.5˚N and 194.6˚E) in the early night and survives through the observation period. It is noteworthy that a stationary structure similar to those discovered by LIR was also observed by another different instrument, COMICS.

- Several streaks are also found to be distributed over the entire disk and some of them are not fixed to the topography.

- The images on January 14 have a horizontal Y-shape feature resembling that seen in UV.

- Venus mid-infrared images in 2007 showed the possibility that the westward rotation of the

polar features is synchronized between the northern and southern hemisphere [3]. However, we could not see such phenomenon this time.

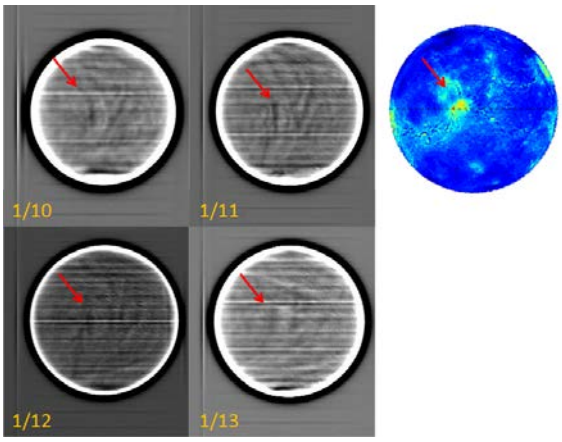

Figure 1: Day-to-day variations of residual patterns at 11.34 μm after high-pass filtering. The upper right image illustrates the topography seen from the Earth during the observation period.

4. Summary and Future work

The coordinated Subaru and Akatsuki observations of Venus cloud top were conducted during the period of January 11-14, 2017. By using a large-aperture ground-based telescope, we could confirm a stationary bow-shaped structure fixed in a position above the highland (Maat Mons). As a next step, we will compare the morphologies seen in images taken by COMICS, LIR, and UVI. The absolutely calibrated COMICS images can also be helpful to validate the absolute calibration of LIR images.

Acknowledgements

This study is based on data collected at Subaru Telescope and obtained from the SMOKA, which is operated by the Astronomy Data Center, National Astronomical Observatory of Japan. This work is supported by JSPS KAKENHI Grant Numbers JP16K17816 and JP16H02231. JP thanks JAXA's International Top Young Fellowship.

References

[1] Nakamura, M., et al.: AKATSUKI returns to Venus, Earth, Planets and Space, 68:75, doi 10.1186/s40623-016-457-6, 2016.

[2] Fukuhara, T., et al.: Large stationary gravity wave in the atmosphere of Venus, Nature Geoscience, 10, pp. 85-88, 2017.

[3] Sato, T.M., et al.: Cloud top structure of Venus revealed by Subaru/COMICS mid-infrared images, Icarus, 243, pp. 386-399, 2014.

EPSC Abstracts
Vol. 11, EPSC2017-403, 2017
European Planetary Science Congress 2017

Initial results of the radio occultation experiment in the Venus orbiter mission Akatsuki

T. Imamura (1), H. Ando (2), K. Noguchi (3), S. Tellmann (4), M. Pätzold (4), B. Häusler (5), and Akatsuki RS Team
(1) The University of Tokyo, Japan (t_imamura@edu.k.u-tokyo.ac.jp), (2) Kyoto Sangyo University, Japan, (3) Nara Women' s University, Japan, (4) Universität zu Köln, Germany, (5) Universität der Bundeswehr München, Germany

Abstract

Akatsuki radio occultation observation of the Venusian atmosphere has started in March 2016. Temperature profiles were obtained down to 38 km altitude and show distinct atmospheric structures depending on the altitude. The overall structure is close to the previous observations, suggesting a remarkable stability of the thermal structure. The H_2SO_4 vapor profiles suggest condensation above ~47 km altitude. The ionospheric electron density profiles are also retrieved, showing a distinct day-night contrast.

1. Introduction

Radio occultation measurement in the Venus orbiter mission Akatsuki, termed RS (Radio Science), aims at exploration of the vertical structure of the Venusian atmosphere [1]. The main goal of Akatsuki is to understand the mechanisms driving the atmospheric circulation and maintaining the cloud layer [2]. For this purpose, five cameras onboard take images of Venus at different wavelengths to observe the distributions of clouds and minor constituents at different heights. RS is complementary to those imaging observations: radio occultation can precisely determine the vertical structure of the atmosphere, while cameras map the horizontal structure.

2. Observations

One-way downlink at X-band is used in the experiment. Akatsuki is equipped with an ultra-stable oscillator as the onboard frequency source. The primary ground station used so far is the 64-m antenna of Usuda Deep Space Center (UDSC) of JAXA. In addition to UDSC, for increasing the number of observation opportunities, we started to use the 32-m antenna of Indian Deep Space Network (IDSN) of Indian Space Research Organization (ISRO) in 2017. The received signals are down-converted to several hundred kHz by an open-loop heterodyne system and 8-bits digitized.

The orbit around Venus is a 10.5 day-period elliptical orbit near the equator. The apoapsis altitude is ~360,000 km, or 59 Venus radii, and the periapsis altitude is variable in the range 1000-8000 km. Thanks to the near-equatorial orbit, Akatsuki RS mainly probes the low and middle latitude regions in contrast to the previous radio occultation experiments using polar orbiters. The first observation was conducted on March 3, 2016, and 10 occultation experiments, including 10 ingress (entry) and 9 egress (exit) measurements, have been conducted by April 2017.

3. Atmospheric profiles

The temperature profiles obtained at latitudes < 65° by February 2016 using UDSC are shown in Figures 2. They are close to VIRA [4], suggesting a remarkable stability of the Venusian atmosphere over decades. The profiles clearly show differences in the stratification characteristics among the altitude regions. Almost constant lapse rate of ~10 K/km, which is close to the adiabatic lapse rate, is observed in the middle and lower cloud region (50-58 km); this region is considered as a convective layer driven by the heating of the cloud base by the thermal infrared flux from below. The region below the cloud (< 50 km) is weakly stable. The region above 58 km is also stable, and is dominated by short-vertical scale fluctuations, being consistent with the previous observations [5].

Figure 2 shows an example of the H_2SO_4 vapor profile obtained from the intensity time series. About 50% of supersaturation is seen around 46-48 km altitudes. At higher altitudes the vapor profile roughly follows the saturation pressure, suggesting equilibrium with the condensed cloud particles.

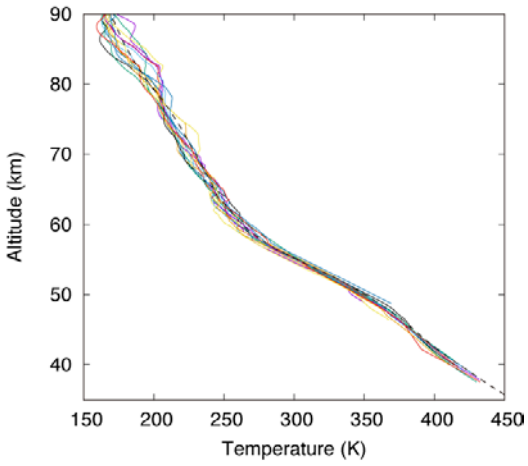

Figure 1: Temperature profiles obtained by the radio occultation experiments. The VIRA temperature profile for the low latitude (< 30°) is also plotted by a dashed curve for comparison [4].

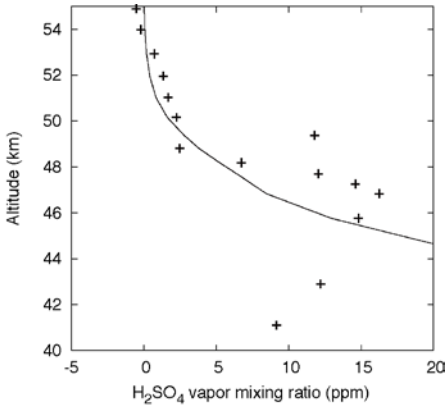

Figure 2: An example of the H_2SO_4 vapor mixing ratio profile obtained from the ingress occultation at 10°N conducted on May 6, 2016 (crosses). The mixing ratios corresponding to the saturation vapor pressure for the observed temperature are also plotted for comparison (solid).

Figure 3 shows examples of the ionospheric electron density profile in an illuminated region and an unilluminated region. The peak electron density of ~3 x 10^5 cm^{-3} and the peak altitude of ~140 km in the illuminated region are typical of the dayside ionosphere [3]. Above 200 km altitude in the illuminated region, the electron density gradually decreases with height and merges into the background noise floor. The electron density in the unilluminated region is marginally detectable at 100-400 km altitudes.

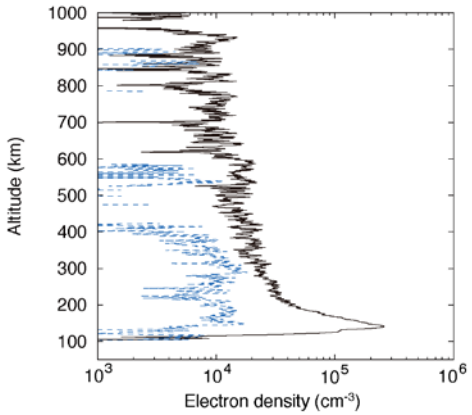

Figure 3: Electron density profiles obtained from the ingress occultation (solid) that sampled an illuminate region (SZA = 78°) and the egress occultation (blue dashed) that sampled an unilluminated region (SZA = 102°) conducted on May 6, 2016.

References

[1] Imamura, T., A. Nabatov, N. Mochizuki, T. Iwata, H. Hanada, K. Matsumoto, H. Noda, Y. Kono, Q. Liu, Y. Futaana, H. Ando, Z. Yamamoto, K.-I. Oyama, and A. Saito: Radio occultation measurement of the electron density near the lunar surface using a subsatellite on the SELENE mission, J. Geophys. Res. 117, A06303, doi:10.1029/2011JA017293, 2012.

[2] Nakamura, M., et al.: AKATSUKI returns to Venus, Earth, Planets and Space 68, 75, DOI:10.1186/s40623-016-0457-6, 2016.

[3] Pätzold, M., Häusler, B., Bird, M. K., Tellmann, S., Mattei, R., Asmar, S. W., Dehant, V., Eidel, W., Imamura, T., Simpson, R. A., and Tyler, G. L.: The structure of Venus' middle atmosphere and ionosphere, Nature, 450, 657-660, 2007.

[4] Seiff , A., Schofield, J. T., Kliore, A. J., Taylor, F. W., Limaye, S. S., Revercomb, H.E., Sromovsky, L.A., Kerzhanovich, V.V., Moroz, V.I., and Marov, M.Ya.: Models of the structure of the atmosphere of Venus from the surface to 100 kilometers altitude, Adv. Space Res., 5, (11), pp.1-305, 1985.

[5] Tellmann, S., B. Häusler, D. P. Hinson, G. L. Tyler, T. P. Andert, M. K. Bird, T. Imamura, M. Pätzold, and S. Remus: Small-scale temperature fluctuations seen by the VeRa Radio Science Experiment on Venus Express, Icarus 221, 471–480, 2012.

EPSC Abstracts
Vol. 11, EPSC2017-404, 2017
European Planetary Science Congress 2017

Nightside temperature measurements at 95 km from OH nightglow in the Venus atmosphere

A. Migliorini (1), M. Snels (2), J.-C. Gérard (3), L. Soret (3), G. Piccioni (1) and P. Drossart (4)

(1) IAPS-INAF, Rome, Italy, (2) ISAC-CNR, Rome, Italy, (3) LPAP, Université de Liége, Belgium, (4) LESIA, Observatoire de Paris, PSL Research University, CNRS, Sorbonne Universités, UPMC Univ. Paris 06, Univ. Paris-Diderot, Sorbonne Paris Cité, 5 place Jules Janssen, 92195 Meudon, France

Corresponding author: Alessandra.Migliorini@iaps.inaf.it

Abstract

In the present work, temperature estimations at an altitude of about 95 km on the night side of Venus are provided. They are derived from hydroxyl nightglow emissions, observed in the infrared spectral range at 2.7-3.5 μm, using the Visible and Infrared Thermal Imaging Spectrometer on board Venus Express.

1. Introduction

The Venus atmospheric region from 90-100 km is dominated by a permanent warm layer, according to stellar occultation measurements with the SPICAV instrument on board Venus Express (Bertaux et al., 2007; Piccialli et al., 2015). The same is partly reproduced by the VTGCM model (Bougher et al., 2015). However, the atmospheric temperature in the upper mesosphere of Venus is still uncertain, showing a very high variability, and values from 170 K (Krasnopolsky 2010) to 250 K (Bertaux et al., 2007; Piccialli et al., 2015), obtained from ground- and space-based observations.

Independent measurements of the atmospheric temperature at about 95 km, obtained by taking advantage of the hydroxyl nightglow observations, are presented in this work. The retrieved temperature is on average on the order of 176 ± 5 K, which is in good agreement with previous space observations, and temperature measurements obtained by taking advantage of the high resolution ground-based observations of $O_2(^1\Delta_g)$ nightglow emissions.

2. Method

Infrared spectral images, acquired with the Visible and Infrared Thermal Imaging Spectrometer (VIRTIS) on board Venus Express, are analysed in this framework. The idea is to use the hydroxyl complex structure observed in the Venus nightside in the spectral range 2.7-3.5 μm, where bands from the Δv=1 sequence are clearly identified (Piccioni et al., 2009; Migliorini et al., 2011; Soret et al., 2012), to derive the atmospheric temperature, provided that the atmosphere is in Local Thermodynamic Equilibrium (LTE). In the Venus case, this condition has been demonstrated to be valid for the rotational energy levels. Hence the intensity distribution of the rotational levels can be used to estimate the local atmospheric temperature.
The band structure of the Δv=1 OH transitions is simulated with the PGOPHER code (pgopher.chm.bris.ac.uk) for different rotational temperatures (130-250 K). The simulations are then compared to the VIRTIS spectra, obtained as the average of data collected in the altitude range 90-100 km, observed in limb mode. The atmospheric temperature is finally the one that minimizes the difference between the synthetic and the observed spectrum.

3. Results

Figure 1 shows an example of best fit, for the VIRTIS image 317-06 (2007-03-04). The best fit is achieved for a rotational temperature of 172.6 ±5 K.

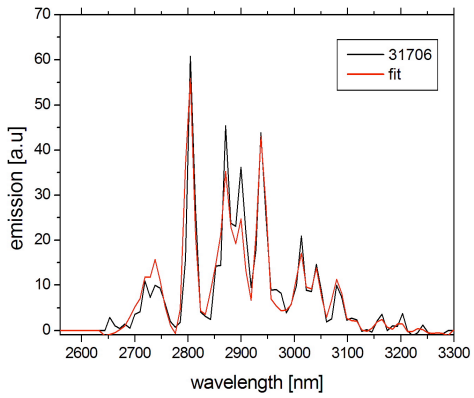

Figure 1. VIRTIS spectrum (in black) compared to the simulated spectrum (in red). The best fit is obtained for a rotational temperature of 172.6 ± 5 K.

VIRTIS measurements cover the latitude range from equator to about 70° N, and the local time interval 19 h – 5 h in the night.

Variability with respect to the latitude is investigated, while no important variations with respect to the local time are observed.

The obtained results are in good agreement with the previous measurements, as observed in Figure 2.

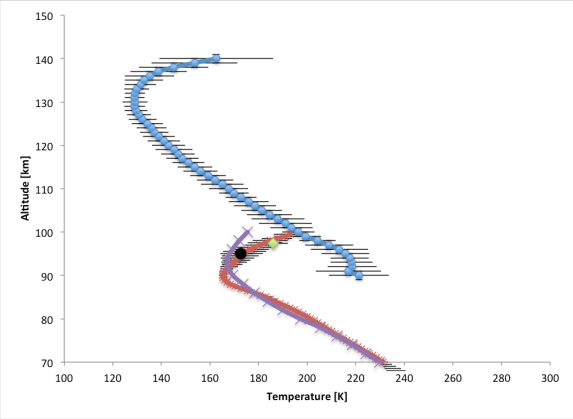

Figure 2. Comparison between mean value in this work (in black) and previous Venus Express and ground-based temperature measurements. In blue, Venus Express/SPICAV thermal profile; in red Venus Express/VeRa profile; VIRA profile is in violet; in green ground-based temperature estimate using $O_2(^1\Delta_g)$ nightglow emissions at 97.4 ± 2.5 km (Gérard et al., 2017).

4. Summary and Conclusions

Hydroxyl nightglow emissions are used to investigate the atmospheric temperature in the Venus upper mesosphere. The temperature estimation is on average equal to 176 ± 5 K, from the VIRTIS data analyzed in this framework.

The applied method is an effective alternative to derive temperatures at an altitude not well investigated with other remote sensing or occultation measurements obtained with the instruments on board Venus Express. In this way, the present work contributes with independent data to the temperatures estimation of the upper mesosphere – lower thermosphere of Venus, providing new constraints on the aeronomy of Venus

Acknowledgements

The authors wish to thank ESA, ASI, CNES and the other national space agencies, which supported the Venus Express mission. This work was funded by ASI (grant n. ASI-INAF I/050/10/2). JCG and LS acknowledge support from the PRODEX program managed by the European Space Agency with the help of the Belgian Federal Science Policy Office (BELSPO).

References

[1] Bertaux et al., 2007, Nature, 187, 247-259.
[2] Bougher et al., 2015, Planet. Space Sci, 113-114, 336-346.
[3] Gérard et al., 2017, submitted to Icarus.
[3] Krasnopolsky, 2010, Icarus, 207, 17-27.
[4] Migliorini et al., 2011, Planet. Space Sci., 59, 974-980.
[5] Piccialli et al., Planet. Space Sci., 113-114, 321-335.
[6] Piccioni et al., 2009, A&A, 483, L29-L33.
[7] Soret et al., 2012, Planet. Space Sci., 73, 387-396.
[8] Tellmann et al., 2009, J. Geophys. Res., 114, E00B36.

EPSC Abstracts
Vol. 11, EPSC2017-409, 2017
European Planetary Science Congress 2017

Cloud tracking of the Venus atmosphere with Akatsuki: High-quality wind snapshots, jets, and instabilities

Takeshi Horinouchi (1,2), Shin-ya Murakami (2), Takehiko Satoh (2), Shigeto Watanabe (3), Toru Kouyama (4), Kazunori Ogohara (5), Takeshi Imamura (6), Masahiro Takagi (7), Hiroki Kashimura (8), Javier Peralta (2), Sanjay S. Limaye (9), Takao M. Sato (2), Masato Nakamura (2), Manabu Yamada (10), Atsushi Yamazaki (2), Eliot F. Young (11)

(1) Faculty of Environmental Earth Science, Hokkaido University, Sapporo, Japan (horinout@ees.hokudai.ac.jp), (2) JAXA/ISAS, (3) Hokkaido Information University, (4) AIST, (5) University of Shiga Prefecture, (6) University of Tokyo, (7) Kyoto Sangyo University, (8) Kobe University, (9) University of Wisconsin, (10) Chiba Institute of Technology, (11) Southwest Research Institute

Abstract

We have conducted cloud tracking using image data from Akatsuki, a Venus orbiting satellite, at multiple wavelengths. Our method provides cloud-motion vectors with unprecedented high quality. Obtained cloud top winds exhibit rich spatial and temporal variability. In the lower cloud layer, it is observed that a jet stream was formed in the equatorial region in 2016, which persisted at least over a few months. Occasionally, batropically unstable vortices are found to develop to erode the shear associated with the jet.

1. Introduction

The Akatsuki spacecraft was inserted into an orbit of Venus on 7 December 2015. Since then, it has been providing images of Venusian clouds at multiple wavelengths. Here, we present the current status and scientific achievement of the dynamical study of the Venus atmosphere based on cloud tracking, which is one of the main objectives of the Akatsuki project.

2. Data and Method

We use data from Akatsuki's ultraviolet imager UVI, which conducts dayside imaging at 283 and 365 nm, and the near-infrared imager IR2, which conducts both dayside and nightside imaging at multiple wavelengths near 2 μm. (We also use data from the other near-infrared imager IR1 at ~1 μm, but it is not treated in this presentation.)

We conduct sophisticated automated cloud tracking [1, 2]. In this method, multiple images are combined to increase the accuracy and reduce erroneous template match. It also uses an error correction-rejection algorithm based on a revised relaxation method [2]. Our study also provides

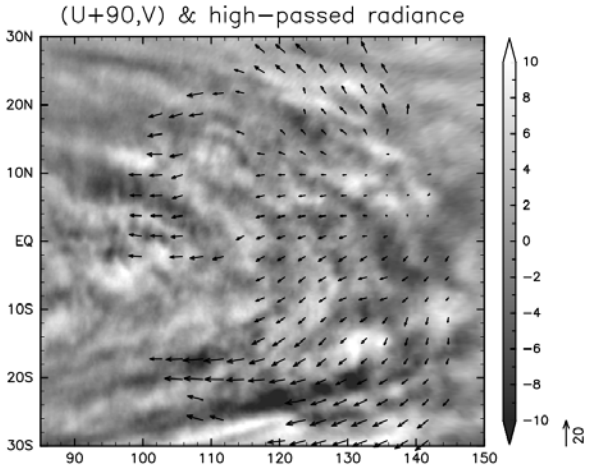

Figure 1: Horizontal winds at the cloud top derived from three UVI 365-nm images obtained on 7 Dec 2015 (arrows: here, a uniform zonal wind of 90 m/s is added to visualize spatial variation) and high-passed radiance at the beginning of tracking (W m^{-2} sr^{-1} μm^{-1}).

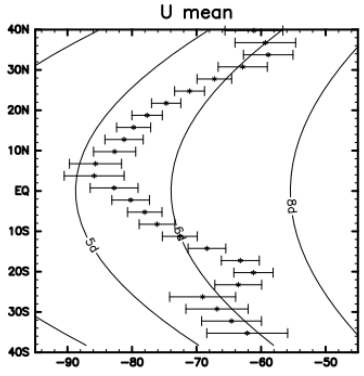

Figure 2: Longitudinally averaged zonal wind in the lower cloud layer derived from four IR2 2.26 μm images obtained on 11 Jul 2016. Error bars indicate the range of uncertainty. Curves show corresponding rotation periods (5, 6, and 8 days).

objective error estimation based on the shape of cross-correlation surfaces [1]. We apply the automated cloud tracking carefully, conducting comparison among various parameter settings and human-eye verification as in the manual tracking

3. Results

Dayside cloud-top (~70 km) motion is derived from UVI images with unprecedented high-quality. Figure 1 shows an example, which is obtained from three UVI images at 365 nm on the day of Akatsuki's orbital insertion (7 December 2015). The motion vectors are shown only where the estimated error measure [1] is smaller than 10 m/s and the difference from the 283-nm results is smaller than 5 m/s. The overall feature is consistent with the known tidal flow with divergence. The figure also indicates smaller-scale motion. The results for multiple days suggest rich temporal variability (not shown).

IR2 provides a unique opportunity to derive winds in the lower cloud layer (45-50 km). Zonal winds obtained in July, 2016 and later at low latitude are much faster than previously reported (Figure 2). Since it exhibits a jet like feature with a maximum rotational speed, we call it as the equatorial jet [3]. The equatorial zonal wind was slightly slower in March, 2016 and did not exhibit a rotational speed maximum. Subsequent observation was focused on the dayside until June, and hence the lower-cloud-layer winds cannot be derived, so we can only guess that the jet was formed in this period.

Previous near-infrared cloud tracking studies have reported mid-latitude jets. Cloud tracking with IR2 provides consistent results.

The nightside cloud images from IR2 suggest a variety of dynamical features. Figure 3 shows the radiance at 2.26 μm exhibiting features like overturning vortices as in the barotropic instability. The cloud tracking reveals that their motion is actually consistent with the unstable eddies. Also, comparison of mean zonal winds on this day and 5 days earlier (at one rotation period before) suggests the erosion of shear associated with equatorial jet, which is consistent with barotropic instability. We argue that there is a mechanism to create the jet, and the instability acts to horizontally diffuse the angular momentum associated with the jet.

4. Conclusions

Cloud tracking with Akatsuki images has been conducted successfully, and some novel features have been found such as sub-planetary-scale cloud-top features, and equatorial jets and instabilities in the lower cloud layer. Further studies are ongoing.

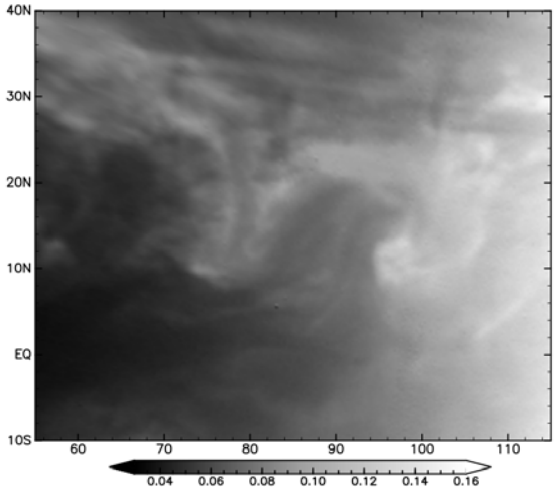

Figure 3: Unstable vortices captured by nightside imaging of IR2: 2.26-μm radiance (W m^{-2} sr^{-1} μm^{-1}) obtained by IR2 on 25 Aug 2016.

Acknowledgements

We deeply thank numerous (countless!) people who contributed to Akatsuki. This study is partially supported by the following grants: JSPS KAKENHI 15K17767, 16H02225, and 16H02231, 16K17816; NASA Grant NNX16AC79G; JAXA's International Top Young Fellowship (ITYF).

References

[1] Ikegawa, S., and T. Horinouchi (2016) Improved automatic estimation of winds at the cloud top of Venus using superposition of cross-correlation surfaces. Icarus, 271, 98-119.

[2] Horinouchi, T., S. Murakami T. Kouyama, K. Ogohara, A. Yamazaki, M. Yamada, and S. Watanabe (2017) Image velocimetry for clouds with relaxation labeling based on deformation consistency. Measurement Science and Technology, in press.

[3] Horinouchi et al. (2017) Equatorial jet in the lower cloud layer of Venus revealed by Akatsuki. Nature Geosci., submitted

EPSC Abstracts
Vol. 11, EPSC2017-460, 2017
European Planetary Science Congress 2017

Sensitive search of CH_4 on Mars by SOFIA/EXES

S. Aoki (1,2,3), M. J. Richter (4), C. DeWitt (4), A. Boogert (5), T. Encrenaz (6), H. Sagawa (7), H. Nakagawa (3), A. C. Vandaele (1), M. Giuranna (8), T. K. Greathouse (9), T. Fouchet (6), A. Geminale (8), G. Sindoni (8), M. McKelvey (5), M. Case (4), and Y. Kasaba (3)

1 Planetary Aeronomy, Belgian Institute for Space Aeronomy, 3 av. Circulaire, B-1180 Brussels, Belgium (E-mail: shohei.aoki@aeronomie.be)
2 Fonds National de la Recherche Scientifique, rue d'Egmont 5, B-1000 Brussels, Belgium
3 Department of Geophysics, Tohoku University, Sendai, Miyagi 980-8578, Japan
4 Physics Department, University of California, Davis, CA 95616, USA
5 Universities Space Research Association, Stratospheric Observatory for Infrared Astronomy, NASA Ames Research Center, MS 232-11, Moffett Field, CA 94035, USA
6 LESIA, Observatoire de Paris, PSL Research University, CNRS, Sorbonne Universités, UPMC Univ. Paris 06, Univ. Paris Diderot, Sorbonne Paris Cité, 5 place Jules Janssen, 92195 Meudon, France
7 Faculty of Science, Kyoto Sangyo University, Motoyama, Kamigamo, Kita-ku, Kyoto 603-8555, Japan
8 Istituto di Astrofisica e Planetologia Spaziali, Istituto Nazionale di Astrofisica, Via del Fosso del Cavaliere 100, 00133 Roma, Italy
9 Southwest Research Institute, Div. #15, San Antonio, TX 78228, USA

Abstract

We present the results of our sensitive search of CH_4 on Mars using the Echelon-Cross-Echelle Spectrograph (EXES) onboard the Stratospheric Observatory for Infrared Astronomy (SOFIA).

Discovery of CH_4 in the Martian atmosphere has led to much discussion since it could be a signature of biological/geological activities on Mars [1,2,3]. However, the presence of CH_4 and its temporal and spatial variations (0-60 ppb) are under discussion because of the large uncertainties embedded in the previous remote-sensing observations [4]. Although Tunable Laser Spectrometer onboard Curiosity rover detected CH_4 signal and showed strong variability of the amount (0-9 ppb), sensitive remote-sensing observation is still important to search for the source since TLS can measure CH_4 variation only on the Gale crater.

SOFIA/EXES has unique capabilities to perform a sensitive search for CH_4 from Earth. The high altitude of SOFIA (~12-14 km) enables us to significantly reduce the effects of terrestrial atmosphere. Thanks to this, it improves the chance to detect Martian CH_4 lines because it reduces the impact of telluric CH_4 on Martian CH_4, and allows us to use CH_4 lines in the 7.5 μm band which has less contamination.

We performed sensitive measurements of Martian CH_4 by using SOFIA/EXES on 16 March 2016 and 25 January 2017, which corresponds to summer (Ls = 123.2°) and winter (Ls = 305.2°) in the northern hemisphere on Mars (see Table 1). We selected the 1325-1340 cm^{-1} (7.45 - 7.55 μm) interval considering the availability of multiple strong CH_4 lines, and used the high-spectral resolution mode (R~90,000) to improve the possibility of detecting the narrow Martian CH_4 lines. We observed the planet at three separate slit positions (center, right, and left of the Martian disk with an offset of 2.5") on 16 March 2016, and two positions (right and left of the Martian disk with an offset of 1") on 25 January 2017.

We have analyzed the data taken on 16 March 2016 [6]. We confined our analysis to three CH_4 lines at 1327.074219, 1327.409783 and 1332.546743 cm^{-1} because they have no contamination from other lines (i.e., terrestrial CH_4 and H_2O, and Martian CO_2 and H_2O lines) and stronger intensities than the other CH_4 lines. Table 2 summarizes the retrieved CH_4 volume mixing ratios (the weighted averages using the ones retrieved from three CH_4 lines independently), and the corresponding locations (latitude and longitude) and local times. As shown in this Table, there are no definitive detections of CH_4. The Martian disk was spatially resolved into 3 x 3 areas, and the upper limits on the CH_4 volume mixing ratio range from 1 to 6 ppb, which are more stringent than those by the previous remote-sensing observations.

In the presentation, the results from the other data taken on 25 January 2017 will be discussed as well.

Tables

Table 1: Overview of the SOFIA/EXES observations.

Observation Date (UT)	16 March 2016	25 January 2017
Observation Time (UT)	9:59-10:32	1:40-2:11
MY	33	33
Doppler shift (km/s)	-16.2	11.7
Diameter of Mars (″)	10	5.2
Aircraft Altitude (km)	13.7	11.9
Sub Earth longitude (°W)	247-253	347-353
Spectral range (cm^{-1})	1326.57 -1338.66	1325.87 -1337.96

Table 2: CH_4 volume mixing ratio (VMR) on Mars retrieved from the SOFIA/EXES observation carried on 16 March 2016 (Ls = 123.2°) [6]. The Martian disk was spatially resolved into 3 x 3 areas, and the upper limits on the CH_4 volume mixing ratio range from 1 to 6 ppb. Note that EXES spectra were spatially binned over ~2.7 arcsec, which corresponds latitudinal/longitudinal resolution of about ±27° at the sub-Earth point.

Slit position	Lat (°)	East Lon (°)	LT	CH_4 VMR (3σ)
Mars Center #1	-17	179	16	2 ± 3 ppb
Mars Center #1	13	149	14	1 ± 1 ppb
Mars Center #1	40	113	12	1 ± 2 ppb
Mars Left	-42	155	15	0 ± 4 ppb
Mars Left	-8	123	13	0 ± 3 ppb
Mars Left	13	90	11	2 ± 4 ppb
Mars Right	0	192	18	0 ± 2 ppb
Mars Right	30	171	16	0 ± 2 ppb
Mars Right	56	126	13	0 ± 1 ppb
Mars Center #2	-17	172	16	1 ± 3 ppb
Mars Center #2	13	143	14	0 ± 1 ppb
Mars Center #2	40	107	12	1 ± 3 ppb

Acknowledgements

This work has been supported by the FNRS "CRAMIC" project under grant agreement n° T.0171.16 and based on observations made with the NASA/DLR Stratospheric Observatory for Infrared Astronomy (SOFIA). SOFIA is jointly operated by the Universities Space Research Association, Inc. (USRA), under NASA contract NAS2-97001, and the Deutsches SOFIA Institut (DSI) under DLR contract 50 OK 0901 to the University of Stuttgart. MJR, CD, and MC of the EXES team are supported by NASA award NNX13AI85A. YK and NH are supported by a Grant-in-Aid for Scientific Research (15H05209; 16K05566) from the Japanese Society for the Promotion of Science (JSPS). HN was supported by the Astrobiology Center Program of National Institutes of Natural Sciences (NINS) (Grant Number AB281003).

References

[1] Formisano, V., Atreya, S.K., Encrenaz, T., Ignatiev, N., Giuranna, M., 2004. Detection of methane in the atmosphere of Mars. Science 306, 1758–1761.

[2] Mumma, M.J., Villanueva, G.L., Novak, R.E., Hewagama, T., Bonev, B.P., DiSanti, M.A., Mandell, A.M., Smith, M.D., 2009. Strong release of methane on Mars in northern summer 2003. Science 323 (5917), 1041–1045.

[3] Atreya, S.K., Mahaffy, P.R., Wong, A., 2007. Methane and related trace species on Mars: Origin, loss, implications for life, and habitability. Planet. Space Sci. 55, 358–369.

[4] Zahnle, K., Freedman, F.S., Catling, D.C., 2010. Is there Methane on Mars?, Icarus, 212, 493–503.

[5] Webster, C.R., et al, 2015. Mars methane detection and variability at Gale crater, Science, 347, 415–417.

[6] Aoki, S., Richter, M.J., DeWitt, C., Boogert, A., Encrenaz, T., Sagawa, H., Nakagawa, H., Vandaele, A.C., Giuranna, M., Greathouse, T.K., Fouchet, T., Geminale, A., Sindoni, G., McKelvey, M., Case, M., Kasaba, Y,: Stringent upper limit of CH_4 on Mars based on SOFIA/EXES observation, Astron. Astrophys. *submitted*.

EPSC Abstracts
Vol. 11, EPSC2017-472, 2017
European Planetary Science Congress 2017

Meridional and Zonal winds at Venus' atmosphere from Cloud-tracking, Doppler techniques and comparison with modelling

P. Machado (1), T. Widemann (2), J.Peralta (3), Ruben Gonçalves (1), G. Gilli (1) and M. Silva (1)
(1) Institute of Astrophysics and Space Sciences, Observatório Astronómico de Lisboa, Ed. Leste, Tapada da Ajuda, 1349-018 Lisboa, Portugal, (2) LESIA-Laboratoire d'Etudes Spatiales et d'Instrumentation en Astrophysique, Observatoire de Paris, France, (3) Institute of Space and Astronautical Science - Japan Aerospace Exploration Agency (JAXA), JAPAN.

Abstract

We present final results of the meridional wind in both Venus' hemispheres and spatial and temporal variability of the zonal wind, based on coordinated observations at Venus cloud-tops based with two complementary techniques: Ground-based Doppler velocimetry and cloud-tracked winds using ESA Venus Express/ VIRTIS-M imaging at 0.38 μm. Cloud-tracked winds trace the true atmospheric motion also responsible for the Doppler-Fizeau shift of the solar radiation on the dayside by super-rotating moving cloud-tops with respect to both the Sun and the observer (Machado et al., 2014). Based on this complementarity, we performed a new coordinated campaign in April 2014 (Machado et al., 2017) combining both Venus Express observations and ground-based Doppler wind measurements on the dayside of Venus' cloud tops at Canada-France-Hawaii telescope at a phase angle $\Phi = (76 \pm 0.3)^\circ$. We also present final results based on observations of Venus' bottom of the cloud deck, carried out with the Near Infrared Camera and Spectrograph (NICS) of the *Telescopio Nazionale Galileo* (TNG), in La Palma, on July 2012. We observed for periods of 2.5 hours starting just before dawn, for three consecutive nights. We acquired a set of images of the night side of Venus with the continuum K filter at 2.28 microns, which allows to monitor motions at the lower cloud level of the atmosphere of Venus, close to 48∼km altitude. Our objective is to measure the horizontal wind field in order to characterise the latitudinal zonal wind profile, to study variability, to help constrain the effect of large scale planetary waves in the maintenance of superrotation, and to map the cloud distribution. We will present results of cloud tracked winds from ground-based TNG observations and winds retrieved from coordinated space-based VEx/VIRTIS observations. The observational results will be compared with the ground-to-thermosphere 3D model developed at the Laboratoire de Meteorologie Dynamique in Paris (Gilli et al. 2017), whose zonal wind predictions above 60 km seem to be consistent with available measurements (Peralta et al. this issue).

1. Winds at cloud tops

With the high-resolution spectrograph ESPaDOnS at Canada-France-Hawaii Telescope (CFHT), the complete optical spectrum, from 370 to 1050 nm, is collected over 40 spectral orders in a single exposure at a resolution of about 80,000. Our choice of observing dates offers the best compromise between observability at Mauna Kea and the need to (i) maximize the angular diameter of Venus and spatial resolution on the disk, and (ii) minimize Venus phase angle and illuminated fraction as only the dayside hemisphere is observed. In the single scattering approximation, the Doppler shift measured in solar light scattered on Venus dayside is the result of two instantaneous motions: (1) a motion between the Sun and Venus upper clouds particles, which scatter incoming radiation in all directions including the observer's [4, 5, 6]; this Doppler velocity is minimal near Venus subsolar point; (2) a motion between the observer and Venus clouds, resulting from the topocentric velocity of Venus cloud particles in the observer's frame; this effect is minimal near Venus sub-terrestrial point. The measured Doppler shift is the sum of those two terms. It therefore varies with planetocentric longitude [11, 12].

Venus Express cloud top wind measurements based on tracking using images taken with the VIRTIS instrument [3, 9] indicate nearly constant zonal winds in the Southern hemisphere between 0 and 55 deg S. The analysis and results show (1) additional confirmation of the the coherence, and complementarity, in the re-

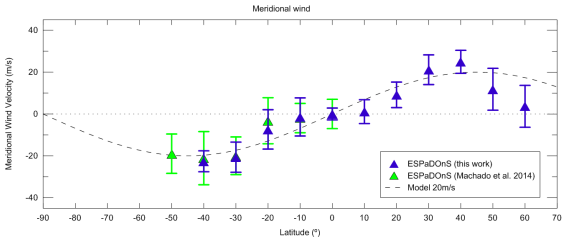

Figure 1: Meridional wind measured along both hemispheres at cloud top level (∼70 km).

sults provided by these techniques, on both spatial and temporal time scales of the two methods; (2) first-time estimation of the meridional component of the wind in other planet using the Doppler velocimetry technique, with evidence of a symmetrical, poleward meridional Hadley flow in both hemispheres; (3) spatial and temporal variability of the zonal flow with latitude and local time, with a significant increase of wind amplitude near morning terminator.

2. Winds at the bottom of the cloud layer

The lower Venusian atmosphere is a strong source of thermal radiation, with the gaseous CO_2 component allowing radiation to escape in windows at 1.74 and 2.28 μm. At these wavelengths radiation originates below 35 km, and unit opacity is reached at the lower cloud level, close to 48 km. Therefore, in these windows it is possible to observe the horizontal cloud structure, with thicker clouds seen silhouetted against the bright thermal background from the low atmosphere [1, 8]. We carried on observations at TNG telescope with the near-infrared camera (NICS). Our objective is to provide direct absolute wind measurements and a map of cloud distribution at the lower cloud level in the Venus troposphere, in order to complement Venus Express (VEX) and other ground-based observations of the cloud layer wind regime. By continuous monitoring of the horizontal cloud structure at 2.28 μm (NICS Kcont filter), it is possible to determine wind fields using the technique of cloud tracking [3, 7]. Cloud displacements in the night side of Venus were computed taking advantage of a phase correlation between images technique [6].

The absolute spatial resolution on the disk was $\sim$ 100 km/px at disk centre, and the (0.8-1") seeing-limited resolution was $\sim$ 400 km/px. By co-adding

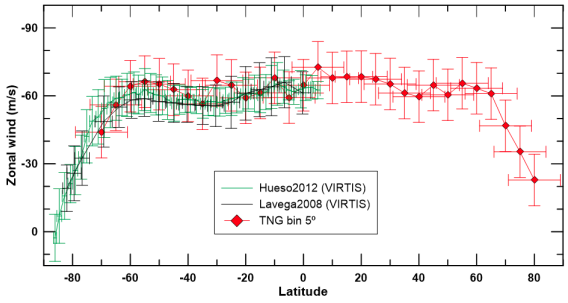

Figure 2: Zonal wind measured at the bottom of the cloud layer (∼48 km) and comparison with previous measurements in the southern hemisphere [3, 9].

the best images and cross-correlating regions of clouds the effective resolution was significantly better than the seeing-limited resolution [7]. In order to correct for scattered light from the (saturated) day side crescent into the night side, a set of observations with the Br_γ filter [10, 13] were performed.

Acknowledgements

We gratefully acknowledge the collaboration of the TNG staff at La Palma (Canary Islands, Spain). We thank the VIRTIS/Venus Express team for support with coordinated observations. This work was supported by FCT (ref. UID/FIS/04434/2013) through national funds and by FEDER through COMPETE2020 (ref. POCI-01-0145-FEDER-007672).

References

[1] Esposito, L. et al., Venus III, Bougher, Hunten and Philips Eds., Sp. Sci. Ser., Arizona U. Press, pp. 415, 1997.

[2] Gilli G. et al. 2017, Icarus, Vol. 281, pp. 55-72.

[3] Hueso, R., Peralta, J., Sànchez-Lavega, A., Icarus, Vol. 217, pp. 585-598, 2012.

[4] Machado, P., Luz, D. Widemann, T., Lellouch, E., Witasse, O, Icarus, Vol. 221, pp. 248-261, 2012.

[5] Machado, P., Widemann, T., Luz, D., Peralta, J., Icarus, 2014.

[6] Machado, P., Widemann, T., Luz, D., Peralta, J., Icarus, 2017.

[7] Peralta, J., Hueso, R. and Sanchez-Lavega, A., Icarus, Vol. 190, pp. 469, 2007.

[8] Rossow, W. B., Del Genio, A. D. and Eichler, T., Journal of Atmospheric Sciences, Vol. 47, pp. 2053, 1990.

[9] Sanchez-Lavega et al., Geophys. Res. Lett., Vol. 35, L13204, 2008.

[10] Tavenner, T. et al., Planetary Space Sciences, Vol. 56, pp. 1435, 2008.

[11] Widemann, T. et al., Planetary and Space Science, Vol. 55, pp. 1741-1756, 2007.

[12] Widemann, T. et al., Planetary and Space Science, Vol. 56, pp. 1320-1334, 2008.

[13] Young, E. et al., Bull. Am. Ast. Soc., Vol. 40, pp. 513, 2008.

EPSC Abstracts
Vol. 11, EPSC2017-476, 2017
European Planetary Science Congress 2017

Characteristics of the Venus Boundary Layer, as modeled by the IPSL Venus GCM

S. Lebonnois (1) and G. Schubert (2)
(1) Laboratoire de Météorologie Dynamique (LMD/IPSL), Sorbonne Universités, UPMC Univ. Paris 06, CNRS, 4 place Jussieu, Paris 75252, France (sebastien.lebonnois@lmd.jussieu.fr), (2) Department of Earth, Planet. and Space Sci., UCLA, CA, USA

Abstract

The deepest region of Venus' atmosphere is still fairly unknown. The temperature structure was probed in-situ by the Pioneer Venus descent probes down to 12 km above the surface, and only the VeGa-2 probe measured the temperature accurately down to the surface [1]. The Planetary Boundary Layer (PBL) interacting with the surface plays a key role in the exchanges of energy and angular momentum between the atmosphere and the surface. To characterize this layer, we use the latest numerical simulations obtained with the IPSL Venus GCM to study the convective activity near the surface: diurnal cycle, vertical extent, dependence on latitude and topography. This behavior is analysed through energy balance and stability discussion.

Between around 20-km altitude and around 7-km altitude, the atmosphere appears to be stable, according to the temperature profiles of the VeGa-2 and Pioneer Venus probes. This feature is reproduced in the modeled temperature structure. Below this altitude, the simulations show that the deep atmosphere tends to be mixed by the mean meridional circulation. The PBL, with convective activity, is limited to daytime hours and extends from the surface to 1 to 2 km altitude, except above low-latitude high topography features, where convection can reach up to 8 km around noon (Figure 1).

The interpretation of the VeGa-2 temperature profile below 7-km altitude suggests that the atmosphere may not be uniformly mixed in that region. This hypothesis is also discussed and its consequences on the PBL behavior analysed.

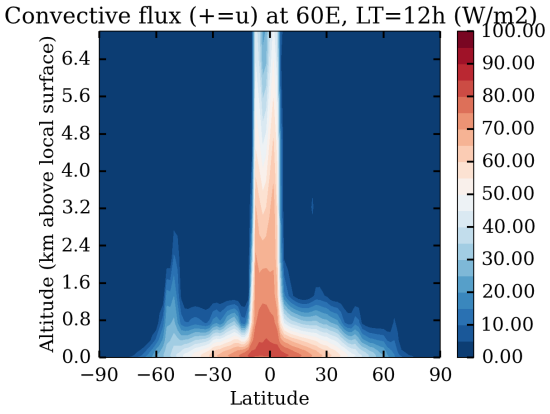

Figure 1: Convective flux modeled at noon at 60°E (positive flux is upward). The western edge of Aphrodite Terra is located around the equator.

References

[1] Zasova, L. V., Ignatiev, N. I., Khatuntsev, I. A. and Linkin, V.: Structure of the Venus atmosphere, Planet. & Space Sci., Vol. 55, pp. 1712–1728, 2007.

EPSC Abstracts
Vol. 11, EPSC2017-490, 2017
European Planetary Science Congress 2017

Interannual variation of wind properties in the Martian planetary boundary layer

M. Paton (1), A. -M. Harri (1) and H. Savijärvi (2)
(1) Finnish Meteorological Institute, Helsinki, Finland, (2) University of Helsinki, Finland (mark.paton@fmi.fi)

Abstract

The Martian winds transport dust and volatiles across the planet, sculpt the landscape and are important for the spacecraft landing studies, e.g. [1]. Martian winds, particularly those aloft, are poorly characterised as they are out of reach of in situ measurements by landed spacecraft. To address this deficit of knowledge we determine the wind speed and direction using trajectory modelling of jettisoned hardware for most spacecraft landing sites since Viking, i.e. Viking landers 1 and 2, Beagle 2, Spirit, Opportunity, Phoenix, Curiosity and Schiaparelli.

1. Introduction

The MetNet mission [2] has been designed to characterise the local and global properties of the Martian climate. This would be achieved by performing simultaneous atmospheric measurements at various locations on Mars ideally with a network covering the whole globe. The meteorological properties aloft can then be characterised using high resolution atmosphere models verified against in situ measurements and observations. Ideally however meteorological properties aloft should be measured in situ to check the models.

2. Method

Here we determine the speed, direction and limited information on the vertical structure of winds from trajectory modelling of jettisoned spacecraft hardware [3]. These results are compared to the Mars Climate Database (MCD). The MCD default settings of the online version were used which produces mean values for atmospheric properties.

3. Results

We found, when comparing our results to the MCD, that there was a tight 1:1 correlation for wind direction whereas for wind speed the correlation was weak partly due to a large uncertainty in knowing the aerodynamic properties of the spacecraft and its jettisoned components. In a small number of cases the wind speed profile appears to be disturbed by small-scale circulations not resolved in the MCD data as we found for the Phoenix case.

Figure 1 shows the best fit trajectories found so far for the Phoenix lander and its jettisoned hardware. A Monte Carlo approach was used where a large number of trajectories (1000) were run. For each trajectory a function representing the wind profile was used whose parameters were randomly selected from a probability function. The resulting best fit wind direction, blowing from the north-west, and speed closely follow that of the MCD except for a layer, a few hundred metres thick, blowing from the north and centred at an altitude of 500 m.

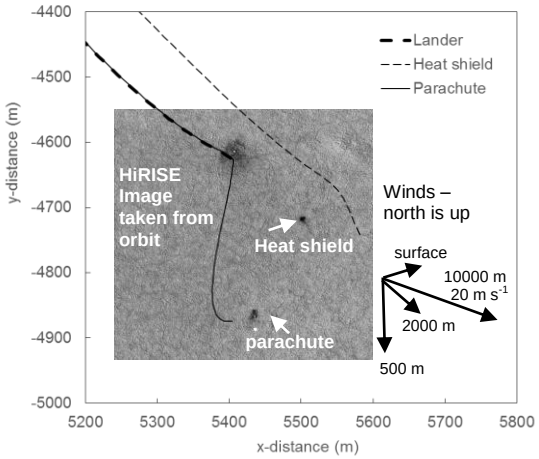

Figure 1. Trajectories of jettisoned Phoenix hardware.

References

[1] Paton, M.: Protection of surface assets on Mars from wind blown jettisoned spacecraft components, Acta Astronautica, Vol. 136, pp. 395-406, 2017.

[2] Harri, A. -M., et al.: Mars MetNet Mission Status, EGU, 12-17 April, 2015 in Vienna, Austria, 2015.

[3] Paton, M., Harri, A. –M., Savijärvi, H.: Properties of Martian winds as determined from trajectory modelling of jettisoned spacecraft parts, American Astronomical Society, DPS meeting #48, 2016.

EPSC Abstracts
Vol. 11, EPSC2017-519, 2017
European Planetary Science Congress 2017

Study of gravity waves propagation in the thermosphere of Mars based on MAVEN/NGIMS density measurements

M. Vals (1), F. Forget (1), A. Spiga (1), E. Millour (1)
(1) Laboratoire de Météorologie Dynamique, Paris, France (margaux.vals@lmd.jussieu.fr)

Abstract

By measuring regular oscillations of the density of CO_2 in the upper atmosphere (between 120 and 190km), the mass spectrometer MAVEN/NGIMS (Atmosphere and Volatile EvolutioN/Neutral Gas Ion Mass Spectrometer), reveals local effects of gravity waves, and conversely, yields precious information on the conditions for propagation and activity of gravity waves.

Using these datasets, and combined to the Mars Climate Database (MCD: www-mars.lmd.jussieu.fr), we study some possible interpretations of the observed variability in the activity of gravity waves.

1. Introduction and background

Gravity waves can be responsible for significant dynamical and thermal perturbations of the mean flux, as they transfer their momentum and energy by breaking ([3]). They also alter local profiles of the meteorological variables as they propagate. They originate from perturbations of the stratified atmospheric fluid, which makes gravity and buoyancy forces compete to restore equilibrium. Sources for such perturbations include topography, convection, fronts or jet-streams.

Gravity waves amplitude increases with altitude, as the density decreases. Their amplitude at a given atmospheric level are controlled by two factors at lower levels: obviously the sources that trigger gravity waves, but also the occurrence of breaking and dissipation while the emitted gravity wave propagates upward. Gravity waves can break and/or dissipate either when they reach a critical level (where the ambient wind equals the phase speed c, first Eliassen-Palm theorem, see [3] and [2]) or when they reach convective instability (considering the mean plus the perturbed atmospheric state). This means that the upward propagation of gravity waves is impacted both by the horizontal wind and static stability; for instance in weak horizontal winds conditions, stationary gravity waves (c=0) vanish.

The aim of our study is to propose an interpretation of the influence of these different background parameters on the gravity waves observed by MAVEN/NGIMS.

2. Data processing

For each orbit, the wandered longitude, latitude, solar longitude, local time, altitude, CO_2 density, as well as the elapsed time from the periapsis were extracted (NASA PDS archives). The distance from the periapsis is deduced from the latitude and longitude displacement. The density deviation is calculated by subtracting the instantaneous density, $dens_{1s}$, to the mean density, $dens_{40s}$, taken here to be the 40-second sliding averaged density (see 1). The perturbations are then normalized to this same mean density over 40-seconds (i.e. about 120km horizontally) to provide an estimate of the relative density perturbation $dens_{rel}$, i.e. $dens_{rel} = \frac{dens_{1s} - dens_{40s}}{dens_{40s}}$. The analysis of the relative density instead of the absolute value allows a direct view of the effect of the gravity waves on the unperturbed meteorological variable, estimated by the average on 40 seconds. We distinguish different altitude levels to study the datasets: between 170 and 200km altitude (each side of the periapsis: ingress and egress data) and under 170km (near to the periapsis). Figures 2 and 3 display the seasonal variability respectively of the mean latitude, and of the root mean square of the relative density of each orbit for the three datasets.

3. Discussion and current state

The seasonal variability of gravity waves reveals a clear tendency of strong peaks and off-peaks activity. This pattern doesn't seem to depend on the considered altitude range.

The MCD allows to obtain the wind velocity, and other meteorological variables at the considered

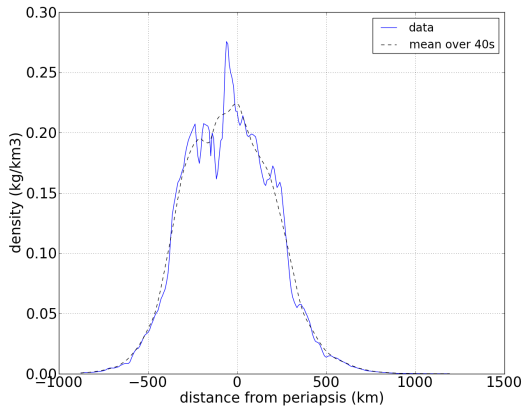

Figure 1: Example of density variations in function of the distance from periapsis in kilometers for orbit 3606 with Ls (Solar Longitude) = 198.22°

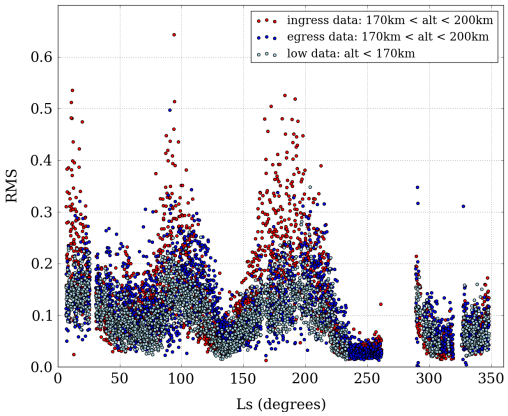

Figure 3: Root Mean Square (RMS) of the relative density calculated for each orbit along the solar longitude for the different altitude datasets (ingress, egress, periapsis)

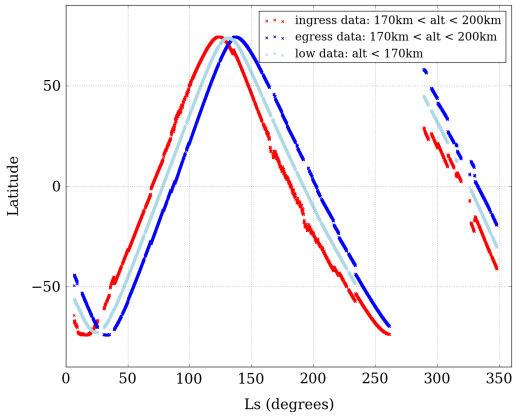

Figure 2: Mean latitude wandered by each orbit along the solar longitude for the different altitude datasets (ingress, egress, periapsis)

locations, seasons and local times, and this from the ground, up to the considered altitudes. Observations don't display strong correlation with the horizontal wind extracted from the MCD. However, the temperature seems to present a good anti-correlation to the observed amplitude variability.

4. Summary and Perspectives

We discussed the atmospheric properties controlling the activity of gravity waves in the thermosphere. The next step, which is ongoing and will be presented in the frame of the conference, consists in an analysis at pressure levels of the data.

References

[1] Forget et al.: Improved general circulation models of the Martian atmosphere from the surface to above 80 km, *J. Geophys. Res.*, 104:24,155–24,176, 1999.

[2] A. Hauchecorne, M. L. Chanin, and R. Wilson: Mesospheric temperature inversion and gravity wave breaking, *Geophys. Res. Lett.*, 14:933–936, 1987.

[3] R. S. Lindzen:Turbulence and stress owing to gravity wave and tidal breakdown, *J. Geophys. Res.*, 86:9707–9714, 1981.

[4] F. Lott and M. Miller.: A new sub-grid scale orographic drag parametrization: its formulation and testing, *Q. J. R. Meteorol. Soc.*, 123:101–128, 1997.

[5] Millour et al.: The Mars Climate Database (MCD version 5.2), *European Planetary Science Congress 2015*, 10:EPSC2015–438, 2015.

[6] A. Spiga, F. González-Galindo, M.-Á. López-Valverde, and F. Forget:Gravity waves, cold pockets and CO_2 clouds in the Martian mesosphere, *Geophys. Res. Letters*, 39:L02201, 2012.

EPSC Abstracts
Vol. 11, EPSC2017-525, 2017
European Planetary Science Congress 2017

Akatsuki (space based cloud-tracking) and TNG/HARPS-N (ground based Doppler velocimetry) coordinated wind measurements of cloud top Venus' atmosphere

R. Gonçalves (1), P. Machado (1), J. Peralta (2), Y. J. Lee (2), T. Widemann (3), A. Harutyunyan (4)
(1) Institute of Atrophysics and Space Science IA, Lisbon Portugal, (2) Japanese Aerospace Exploration Agency JAXA, Japan (3) LESIA - Laboratoire d'Études Spatiales et d'Instrumentation en Astrophysique and Observatoire de Paris, Université Paris-Diderot, Meudon, France (4) Telescopio Nazionale Galileo, TNG, and Italian Instituto Nazionale di Astrofisica (INAF) (rgoncalves@oal.ul.pt)

Abstract

We present wind velocity results based in the measurements of the horizontal wind field at the cloud top level of the atmosphere of Venus, near 70 km altitude in the visible range on the dayside. The purpose is to characterize the zonal and meridional wind latitudinal behavior and profiles on hour and day timescales, to study wind variability and to constrain the effect of large scale planetary waves, as is the case of the Y shape Venus' wave [2].

The observations (28-29 January 2017) were carried out at the "Telescopio Nazionale Galileo" (TNG) with the spectrograph "High Accuracy Radial velocity Planet Searcher" (HARPS-N). The ground based observations were coordinated with the Japan Aerospace Exploration Agencie's (JAXA) Akatsuki satellite. Venus Climate Orbiter (VCO) "Akatsuki" is currently the only spacecraft operating in Venus' orbit. The ground observations probed the cloud top layer (70km altitude) using the Doppler velocimetry method, enabling a cross-validation with Akatsuki cloud-tracking technique.

HARPS-N is the most stable and precise high resolution spectrograph observing the northern skies in the world, and it was especially made for extrasolar planet searches. However, the stability of the HARPS-N spectrograph provided unprecedented high quality spectra at Venus atmosphere, which allow us to retrieve wind velocities with an unmatched precision and spatial and temporal accuracy. With the data obtained now, we would contribute to better constrain the zonal wind, the meridional wind flow and detect and characterize mesoscale atmospheric waves on Venus' atmosphere. With this project, TNG and HARPS-N opened a new window for Planetary Systems atmospheric characterization. The 3.58-meter Telescopio Nazionale Galileo (TNG) and the Visible Spectrograph HARPS-N provide a highly resolved (115.000) spectrum in the visible range (0.38-6.9 µm). The sequential technique of visible Doppler velocimetry (fine-tuned for CFHT/ESPaDOnS [5], [6] and adapted for the fiber-fed spectroscope HARPS-N) has proven a reference technique to measure instantaneous zonal and meridional winds and is the only technique to retrieve meridional wind profiles for both hemispheres simultaneously, with consistent results [5], [6]. These measurements are necessary to help validating Global Circulation Models (GCMs) [3], and to extend the temporal coverage of available datasets

The TNG observations focused on the zonal wind field near equator (latitudes between 10° S and 10° N) and meridional wind field between latitudes 60° S and 60° N (both hemispheres). The measured meridional wind flow will be compared with a model of a 20 ms-1 meridional wind flow. The zonal wind measures included various points of the dayside hemisphere, between 10° N and 10° S, by steps of 5°, and from sub-Earth longitude [ϕ - ϕE] = -23 to -56. We compared our measurements with simultaneous observations using the instrument from the Akatsuki mission (VCO).

1. Introduction

In the Venus' lower mesosphere (65-85 km), visible observations of Doppler shifts in solar Fraunhofer lines have provided the only Doppler wind measurements near the cloud tops in recent years [4], [5], [6], [7], [8]. The region is important since it constrains the global mesospheric circulation in which zonal winds generally decrease with height while thermospheric SS-AS (Subsolar-Antisolar)

winds increase [1]. On Akatsuki, atmospheric circulation at 70 km was measured with cloud tracking techniques. However, winds derived in this manner are mean velocities about time intervals or more than 30 minutes and do not reflect instantaneous wind velocity and its significant variability at shorter time scales.

2. Method and Results

With HARPS-N, the complete optical spectrum, from 383 to 690 nm, is collected over 40 spectral orders in a single exposure at a resolution of about 115,000. In the single scattering approximation, the Doppler shift measured in solar light scattered on Venus dayside is the result of two instantaneous motions: (1) a motion between the Sun and Venus upper clouds particles, which scatter incoming radiation in all directions including the observer's; this Doppler velocity is minimal near Venus sub-solar point; (2) a motion between the observer and Venus clouds, resulting from the topocentric velocity of Venus cloud particles in the observer's frame; this effect is minimal near Venus sub-terrestrial point. The measured Doppler shift is the sum of those two terms. It therefore varies with planetocentric longitude. The Doppler shift vanishes at the half phase angle meridian (see Figure 1), where both terms cancel each other [5], [6] and we use this meridian as "zero-Doppler-reference" to check for instrumental or calibration drifts. The Doppler velocities are modelled using two kinematical templates for the zonal wind: (1) solid rotation with v zonal = v (equator) x cos(latitude), (2) uniform retrograde velocity, v zonal = v (equator). Both models are explored within latitudinal range 60S-60N. Once the best fit is obtained, we define the acceptable domain at 2-sigma.

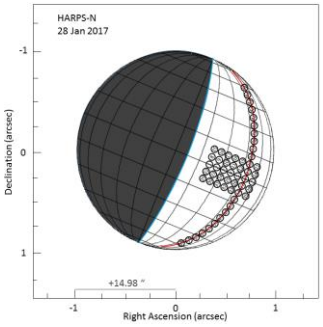

Figure 1: Schematic of Venus observations from TNG/HARPS-N. The black solid circles represent the instrument FOV (1") and each respective pointing along Venus disc. The red solid line is located at the half phase angle, which measures are used to retrieve the meridional wind. Each solid black line in the planetary grid has a step of 15º in both latitude and longitude. The axis units are set to the angular diameter of Venus, which is 14,98".

Acknowledgements

We gratefully acknowledge the collaboration of the TNG staff at La Palma (Canary Islands, Spain). We thank the Akatsuki team for support with coordinated observations. We acknowledge support from Fundação para a Ciência e a Tecnologia, projects FCT (ref. UID/FIS/04434/2013 and ref. PD/BD/128019/2016) through national funds and by FEDER through COMPETE2020 (ref. POCI-01-0145-FEDER-007672).

References

[1] Hueso, R., Peralta, J., Sànchez-Lavega, A., Icarus, Vol. 217, pp. 585-598, 2012.

[2] Imai M. et al., Icarus Vol. 278, pp 204–214, 2016

[3] Lebonnois, S. et al., J. Geophys. Res., Vol. 115, E06006, 2010.

[4] Machado, P., Luz, D. Widemann, T., Lellouch, E., Witasse, O, Icarus, Vol. 221, pp. 248-261, 2012.

[5] Machado, P., Widemann, T., Luz, D., Peralta, J., Icarus, Vol. 243, pp. 249-263, 2014.

[6] Machado, P., Widemann T., Peralta J., Gonçalves R., et al., Icarus, Vol. 258, pp. 8-26, 2017.

[7] Widemann, T. et al., Planetary and Space Science, Vol. 55, pp. 1741-1756, 2007.

[8] Widemann, T. et al., Planetary and Space Science, Vol. 56, pp. 1320-1334, 2008.

EPSC Abstracts
Vol. 11, EPSC2017-530, 2017
European Planetary Science Congress 2017

A test case: new retrievals of ozone at the terminator on Mars

A. Piccialli (1), A. C. Vandaele (1), S. Robert (1), F. Daerden (1), S. Viscardy (1), L. Neary (1), S. Aoki (1,2), V. Wilquet (1), F. Lefèvre (3), A. Määttänen (3), F. Montmessin (3)
(1) Planetary Aeronomy, Belgian Institute for Space Aeronomy, 3 av. Circulaire, 1180 Brussels, Belgium; (2) Fonds National de la Recherche Scientifique, Brussels, Belgium, (3) LATMOS/IPSL, UVSQ Université Paris-Saclay, UPMC Univ. Paris 06, CNRS, Guyancourt, France. (arianna.piccialli@aeronomie.be, Twitter: @**apic79**)

Abstract

ASIMUT, the BIRA-IASB radiative transfer code, was modified in order to take into account the changes in the atmospheric composition and structure across the martian day/night terminator. Here, we will discuss the impact of this implementation on the retrievals of ozone profiles derived from SPICAM solar occultations in the ultraviolet.

1. Introduction

The martian atmosphere at the day-night terminator is a region of great interest characterized by gradients of density and temperature, driven by differences in the solar illumination, and by sharp transitions in the chemical regime. Ozone, in particular, displays rapid changes due to photolysis across the terminator [1]. Nowadays, most of the retrieval algorithms for solar and stellar occultations rely on the assumption of a spherically symmetrical atmosphere. In order to handle concentration gradients along the line of sight it is necessary therefore to improve the retrieval scheme used to analyse occultation observations.

2. Observations

SPICAM (SPectroscopie pour l'Investigation des Caractéristiques Atmosphériques de Mars), on board the ESA's mission Mars Express, is a remote sensing spectrometer observing in the ultraviolet (118–320 nm) and in the near infrared (1–17 μm) [2]. In the solar occultation mode, the UV sensor is particularly well suited to measure the vertical profiles of O_3 and aerosols of the martian atmosphere [3]. Figure 1 displays transmission spectra obtained at different altitudes for the observation 05555A02. The signal below 200 nm has a poor S/N ratio due to the low emission of the Sun at those wavelengths. The ozone absorption band (Hartley band) is clearly visible around 250 nm.

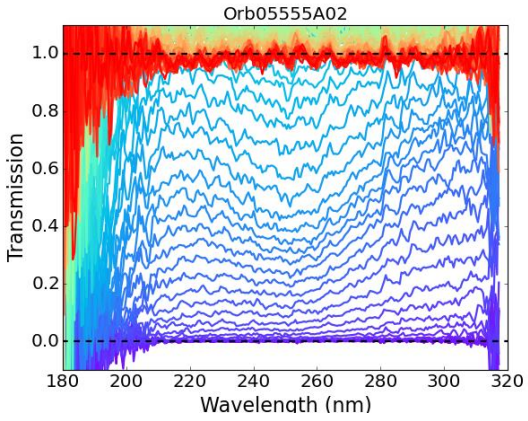

Figure 1: Example of SPICAM transmission spectra at different altitudes: (blue) low altitudes; (red) high altitudes.

3. Retrieval technique

SPICAM-UV spectra are simulated using the line-by-line radiative transfer code ASIMUT-ALVL developed at IASB-BIRA [4]. ASIMUT has been modified in order to take into account the atmospheric composition and structure at the day-night terminator. Three different gradients along the line of sight (LOS) can be considered: temperature, total density gradients and the variations of the concentration of specific species. As input for ASIMUT, we used gradients predicted by a 1D model with high temporal resolution [5] driven by the 3D GEM-Mars v4 Global Circulation Model (GCM) [6,7]. Figures 2 and 3 show examples of temperature and density profiles obtained around the terminator by the GEM-GCM.

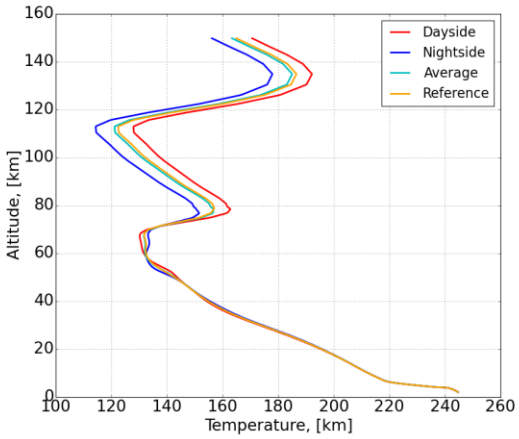

Figure 2: Vertical temperature profiles obtained by the GEM-GCM. The reference profile (yellow) is obtained at the terminator; the average profile (green) is the mean of the day (red) and night (blue) side profiles.

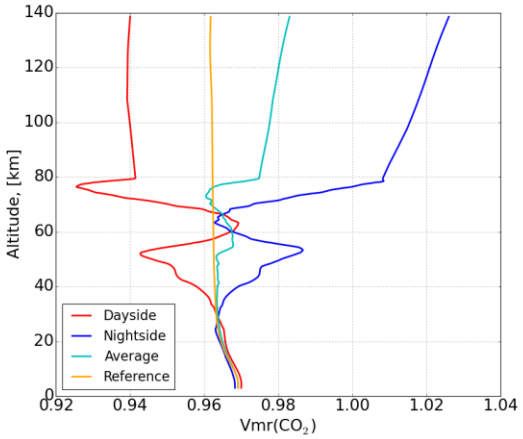

Figure 3: Vertical CO_2 mixing ratio profiles obtained by GEM-GCM. Colours code as in Fig. 2

4. Summary and Conclusions

We will apply the ASIMUT improved retrieval scheme to SPICAM-UV solar occultation data, focusing on ozone (O_3). The main objective is to test the impact of these gradients on ozone retrievals. Results of this study will then be used for the analysis of the data expected from the NOMAD instrument on the ExoMars 2016 Trace Gas Orbiter.

Acknowledgements

The research leading to these results has received funding from the European Union's Horizon 2020 Programme (H2020-Compet-08-2014) under grant agreement UPWARDS-633127. SA has been supported by the FNRS "CRAMIC" project under grant agreement n° T.0171.16

References

[1] Lefèvre, F., Bertaux, J.L., Clancy, R. T., Encrenaz, T., Fast, K., Forget, F., Lebonnois, S., Montmessin, F., Perrier, S., Aug. 2008. *Heterogeneous chemistry in the atmosphere of Mars.* Nature 454, 971–975.

[2] Bertaux, J., Korablev, O., Perrier, S., Qu´emerais, E.,Montmessin, F., Leblanc, F., Lebonnois, S., Rannou, P., Lef`evre, F., Forget, F., Fedorova, A., Dimarellis, E., Reberac, A., Fonteyn, D., Chaufray, J. Y., Guibert, S., Oct. 2006. *SPICAM on Mars Express: Observing modes and overview of UV spectrometer data and scientific results.* JGR (Planets) 111 (E10), 10–+.

[3] Määttänen, A., Listowski, C., Montmessin, F., Maltagliati, L., Reberac, A., Joly, L., Bertaux, J.L., Apr. 2013. *A complete climatology of the aerosol vertical distribution on Mars from MEx/SPICAM UV solar occultations.* Icarus 223, 892–941.

[4] Vandaele, A.C., M. De Mazière, R. Drummond, A. Mahieux, E. Neefs, V. Wilquet, O. Korablev, A. Fedorova, D. Belyaev, F. Montmessin, and J.L. Bertaux, *Composition of the Venus mesosphere measured by SOIR on board Venus Express.* J. Geophys. Res., 2008. 113 doi:10.1029/2008JE003140.

[5] García Muñoz, A., J.C. McConnell, I.C. McDade, and S.M.L. Melo, *Airglow on Mars: Some model expectations for the OH Meinel bands and the O2 IR atmospheric band*, Icarus 176 (2005) 75–95.

[6] Daerden, F.; Whiteway, J. A.; Neary, L.; Komguem, L.; Lemmon, M. T.; Heavens, N. G.; Cantor, B. A.; Hébrard, E.; Smith, M. D. *A solar escalator on Mars: Self-lifting of dust layers by radiative heating.* GRL, 2015, Vol. 42, Issue 18, pp. 7319-7326.

[7] Neary, L. and F. Daerden, *The GEM-Mars General Circulation Model for Mars: Description and Evaluation*, Icarus, 2017, in review.

EPSC Abstracts
Vol. 11, EPSC2017-557, 2017
European Planetary Science Congress 2017

Characterising gravity waves in the Martian thermosphere using MAVEN accelerometer data

A. Siddle, I. C. F. Mueller-Wodarg

Blackett Laboratory, Imperial College London, Prince Consort Road, London SW7 2AZ, UK

Abstract

Gravity waves (GW's) are ubiquitous in the Martian atmosphere and sources of such waves include topography disturbing wind flow near the surface and shear flow in the atmosphere. GW's can have profound effects on the atmosphere as they carry momentum from their source in the lower atmosphere into the upper atmosphere (mesosphere/thermosphere) [1]. More accurate theoretical descriptions of the atmosphere are possible only when the effects of GW's are included in models, so studying their properties and characteristics is vital for gaining a full understanding of the Martian atmosphere [2][3]. GW's in Mars' upper atmosphere (140-160 km) have been studied using accelerometer data from MAVEN. Waves have been extracted from density profiles by deriving an unperturbed background density model. The relative density perturbations (amplitudes) and wavelengths of the GW's have been characterised with extensive Fourier analysis. Wave amplitudes of atmospheric mass densities are found to be mostly below 10%. Apparent horizontal wavelengths are found to range from 10's to 100's of km. Temperature profiles have been derived from density measurements and temperature waves have been extracted. Temperature perturbations are found to be mainly below 10 K and wavelengths are comparable to those of density waves. Improvements to temperature extraction techniques will be discussed.

The relationship between GW properties and conditions within the atmosphere has been studied and a clear trend is seen with temperature. Both wave amplitude and wavelength increase with decreasing temperature; which is consistent with recent findings from MAVEN's Neutral Gas and Ion Mass Spectrometer (NGIMS) data [4]. Our study shows that both density amplitudes and wavelengths can vary by nearly a factor 2 over a 200 K temperature range. A positive correlation between solar zenith angle and both amplitude and wavelength has also been found, however this correlation is weakened by the removal of the temperature dependence. Waves extracted from MAVEN accelerometer data are compared to those determined from MAVEN's NGIMS dataset as well as Mars Global Surveyor accelerometer data [5]. We find consistency between the results obtained using the three datasets.

Using data from MAVEN's accelerometer and NGIMS instrument, global background temperature structures will be determined. Improved temperature extraction techniques developed using models will also be implemented

References

[1] Forbes, J. M. (2002) Wave Coupling in Terrestrial Planetary Atmospheres, in Atmospheres in the Solar System: Comparative Aeronomy (eds M. Mendillo, A. Nagy and J.H. Waite), American Geophysical Union, Washington, D. C..

[2] Barnes, J. R. (1990), Possible effects of breaking gravity waves on the circulation of the middle atmosphere of Mars, J. Geophys. Res., 95(B2), 1401–1421

[3] Angelats i Coll, M., F. Forget, M. A. López-Valverde, P. L. Read, and S. R. Lewis (2004), Upper atmosphere of Mars up to 120 km: Mars Global Surveyor accelerometer data analysis with the LMD general circulation model, J. Geophys. Res., 109, E01011

[4] Terada, N., et al. (2017), Global distribution and parameter dependences of gravity wave activity in the Martian upper thermosphere derived from MAVEN/NGIMS observations, J. Geophys. Res. Space Physics, 122, 2374–2397

[5] Withers, P. (2006), Mars Global Surveyor and Mars Odyssey Accelerometer observations of the Martian upper atmosphere during aerobraking, Geophys. Res. Lett., 33, L02201

EPSC Abstracts
Vol. 11, EPSC2017-614, 2017
European Planetary Science Congress 2017

Atmospheric Mars Entry and Landing Investigations & Analysis (AMELIA) by ExoMars 2016 Schiaparelli Entry Descent Module

F. Ferri (1), O. Karatekin (2), A. Aboudan (1), B. VanHove (2), G. Colombatti (1), C. Bettanini (1), S. Debei (1), S. Lewis (3), F. Forget (4) and the AMELIA team
(1) Università degli Studi di Padova, Centro di Ateneo di Studi e Attività Spaziali "Giuseppe Colombo" (CISAS) (francesca.ferri@unipd.it / Fax +39-049-8276855), (2) Royal Observatory of Belgium (ROB), Brussels, Belgium, (3) School of Physical Sciences, The Open University, Walton Hall, Milton Keynes MK7 6AA, UK, (4) Laboratoire de Météorologie Dynamique, UPMC BP 99, 4 place Jussieu, 75005, Paris, France

1. Introduction

The Entry, Descent and Landing System (EDLS) of an atmospheric entry probe or lander requires measurements in order to trigger the events of the descent sequence. These measurements besides being aimed at guaranteeing a safe landing, could provide essential information for the study of planetary atmosphere. The ESA *ExoMars* program, with the Schiaparelli Entry Demonstrator Module (EDM) in 2016 and the entry module containing the Surface Platform and Rover in 2020 provides the rare (one-per-mission) opportunity for new direct *in situ* measurements over a wide altitude range and with resolution not achievable over the full altitude range by remote sensing observations.
The Atmospheric Mars Entry and Landing Investigations & Analysis (AMELIA) experiment aimed at exploiting the EDLS engineering measurements for scientific investigations of Mars' atmosphere and surface. The data recorded during the different phases can be used for an accurate trajectory and attitude reconstruction and for the retrieval of the atmospheric profile to study the atmospheric structure, dynamics and static stability and to characterize the landing site context [1].

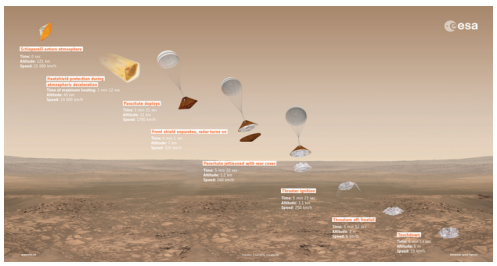

Figure 1: ExoMars 2016 Schiaparelli EDL scenario.

2. ExoMars 2016 Schiaparelli mission

On 19th October 2016, Schiaparelli entered into the martian atmosphere. Although it did not complete a safe landing on Mars, it transmitted data throughout its descent to the surface, until signal was lost about 1 minute before the expected touch-down on Mars' surface. The EDL sequence (Fig. 1) should have lasted for 6 minutes starting with a hypersonic atmospheric entry protected by an instrumented heatshield, followed by a passive descent under parachute and an active proximity phase during which retrorockets are activated in order to slow down and ensuring a final horizontal position of the Schiaparelli platform at touch down, and finally a landing on a crushable structure for damping the impact [2].

The atmospheric entry and the majority of the descent phases were performed nominally: the aerobraking under the frontshield occurred as expected, the parachute deployed normally, and the heatshield, having served its purpose, was released 40 seconds after (as programmed). The unexpected dynamics of the vehicle at parachute inflation resulted in the saturation of one of the gyroscope that caused the fatal error in the guidance and control system. The erroneous information in the attitude generated a negative altitude estimation that in turn successively triggered a premature release of the parachute and backshell, a too brief firing of the retrorockets and finally the activation of the on-ground systems (including DREAMS) as if Schiaparelli was landed. In reality Schiaparelli was still at an altitude of around 3.7 km, therefore it continued in free fall to the crash landing on the surface of Mars (33 seconds later at a velocity of 150 m/s) (Fig. 2).

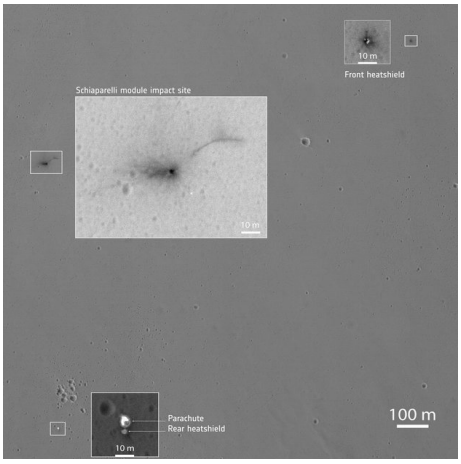

Figure 2: HIRISE image of Schiaparelli crash landing

Schiaparelli continuously transmitted telemetry that was received from the TGO (Trace Gas Orbiter) while the signal carrier was recorded by the Giant Metre-wave Radio Telescope (GMRT) in Pune (India) and by ESA MarsExpress orbiter until the loss of signal.

The radio signal and the telemetry data set, although limited, are essential to investigate the anomaly that caused the crash landing, but also for the achievement of AMELIA experiments scientific objectives. At the time of writing, these data are still under analysis to investigate the reasons for the Schiaparelli's landing failure and are under embargo.

3. AMELIA simulations and reconstructions

The measurements transmitted during entry and descent have been used for the reconstruction of the Schiaparelli EDM trajectory and attitude determination and for the retrieval of an atmospheric profile of parameters such as density, temperature and pressure along the entry and descent trajectory. Within the AMELIA team, different algorithms, methods and data sets are used to simulate and reconstruct the EDM dynamics in order to retrieve and validate the most accurate atmospheric profile [1]. A strong effort was also put into atmospheric modelling and data assimilation in order to improve predictions and weather forecasts, monitoring weather conditions and to assess the atmospheric context at entry, so as to forecast the environmental conditions that Schiaparelli was going to face, but also in view of scientific analysis and interpretation of the AMELIA results.

The flight data of Schiaparelli, besides providing a technical assessment of the EDL, allowed for sounding the atmosphere along its trajectory, so as per the seven atmospheric profiles retrieved by previous successful Mars entry probes [3, 4, 5, 6, 7, 8]. These *in situ* measurements are fundamental for studying the martian atmospheric structure and dynamics, and also for the investigation of the meteorology and the planetary boundary layer on Mars.

4. Conclusions

Despite the ultimate failure of Schiaparelli to land safely, sufficient EDL data was returned in order to reconstruct the trajectory and attitude of the EDM and retrieve atmospheric profiles over the altitude range from 121 km to 4 km above the surface.
We will report the results on the atmospheric reconstruction in terms of the assessment of the atmospheric science.

Acknowledgements

AMELIA is an experiment for scientific investigations of Mars' atmosphere and surface by means of the Schiaparelli measurements during its entry, descent and landing on Mars. The International AMELIA team built under the joint coordination of Principal Investigator: Francesca Ferri (Italy) and 3 Co-Principal Investigators (CoPIs): Özgür Karatekin (Belgium), Stephen R. Lewis (United Kingdom), François Forget (France) (*Interdisciplinary Scientist*). The team included scientists from Italy, France, UK, Belgium, Finland, Germany, Australia and USA.

References

[1] F. Ferri et al. (2017) submitted to *Space Science Rev.*
[2] T. Blancquaert et al., (2017) *14th International Planetary Probe Workshop*, The Hague, NL.
[3] Seiff, A., D.B. Kirk, (1977) *J. Geophys. Res* **82**, 4364.
[4] Schofield, T., et al. (1997) *Science* **278**, 1752-1758.
[5] Magalhães, J.A., J.T. Schofield, A. Seiff, (1999) *J. Geophys. Res*.**104**, 8943-8945.
[6] Withers, P. and M. D. Smith (2006) *Icarus* **185**.
[7] Withers, P., Catling, D.C. (2010) *Geophys. Res. Lett.* **37**.
[8] Holstein-Rathlou, C., A. Maue, and P. Withers (2016) *Planet. Space Scie.* **120**: 15-23.

EPSC Abstracts
Vol. 11, EPSC2017-629-1, 2017
European Planetary Science Congress 2017

Water vapour in the middle atmosphere of Mars by SPICAM/MEX

A.Fedorova (1), D. Betsis (1), J.-L. Bertaux (2,1), O. Korablev(1), F. Montmessin (2)
(1) Space Research Institute(IKI), Moscow, Russia (fedorova@iki.rssi.ru), (2) LATMOS-UVSQ, Guyancourt, France

Abstract

While the H_2O column density in the Martian atmosphere is well known now and has been monitored by different missions for last decades the behavior of water in the middle atmosphere, its interannual and seasonal variability, is still opened question due to an absent of observational material. We present here long-term observations of the H_2O vertical distribution in the Martian atmosphere by SPICAM on Mars-Express for a period of several Martian years and study the seasonal and spatial variations of the H_2O density and mixing ratio at different altitudes as well as interannual variations connected to such special event as the 2007 global dust storm.

1. Introduction

The Martian atmospheric water vapor is trapped close to the surface by condensation and its vertical distribution is variable with season and location. In the aphelion season when the atmosphere is colder, water is located near the surface and blocked in the Northern hemisphere by the aphelion cloud belt [1]. The hygropause (condensation level) altitude is as low as 10-15 km. During warmer perihelion season this altitude could reach 40-50 km.

Recent observations of the Martian hydrogen corona reported a rapid change of the hydrogen escape rate for weeks/months during the global dust storm and on the seasonal scale during the Martian year [2-4]. One proposed explanation of observed changes in coronal emission is that water vapor can be transported to higher altitudes (up to 80 km) where the rate of photodissociation by near-UV sunlight increases, providing an additional source of hydrogen for the upper atmosphere. Recent photochemical model has supported a contribution of high-altitude water in the hydrogen escape on the short time scale [5]. Based on the SPICAM/MEX observations we study seasonal variations of water at altitude from 20 to 80 km during several Martian years.

2. Observations

Since 2004 the SPICAM IR spectrometer on Mars-Express [6] carries out measurements of the vertical distribution of water vapor in the 1.38 μm band, the CO_2 density in the 1.43 μm band and aerosol properties in the middle atmosphere of Mars by means of solar occultations. The observations cover now 7 Martian Years with 2 occulation campaigns for a year (Figure 1). In this work we present vertical distribution of water vapor observed for several years including the global dust storm in MY28 (observations at Ls = 250-310°).

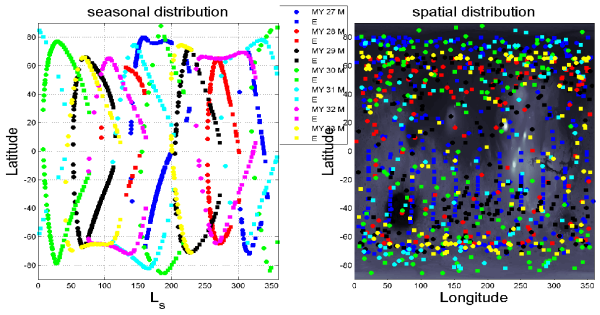

Figure 1: Seasonal and spatial coverage of SPICAM/MEX solar occultations

3. The interannual variations

Despite the solar occultation campaigns are not completely repeatable in spatial distribution and time, the interannual comparison and a seasonal trend can be obtained. Figure 2 shows a comparison of the H_2O density at 60 and 70 km for MY 28, 29, 32 and 33. In

the Northern hemisphere observations in MY28,29,32 don't show prominent increase of the water content as it was during the MY28 global dust storm. This difference can not be completely related to the difference in latitudinal coverage. The increase of the water density above 60 km in the northern hemisphere looks like special case of the global storm on Mars. In the Southern hemisphere MY28, 29, 32 show the increase of the density with higher values for MY28. MY33 at Ls=199-230° didn't show the prominent increase of the density.

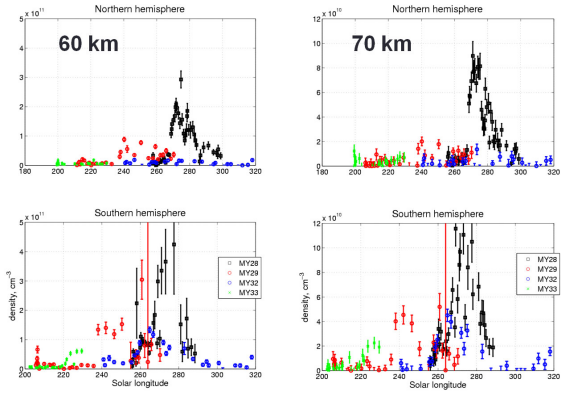

Figure 2: H_2O density for MY28, MY 29, MY32 and MY33.

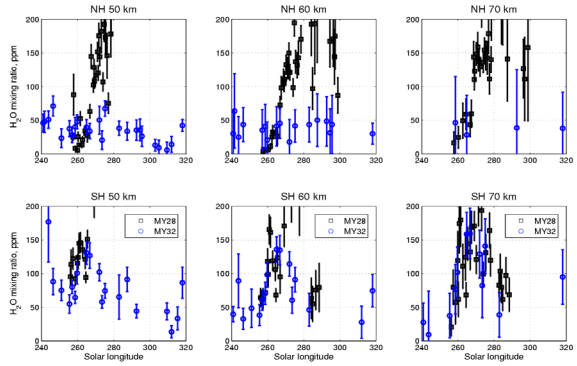

Figure 3: Evolution of the H_2O mixing ratio at the altitudes of 50, 60 and 70 km during MY28 and MY32 shown for the Northern and Southern hemispheres separately.

Using the CO_2 density from 1.43 μm band we can obtain the vertical distribution of H_2O mixing ratio. Figure 3 presents the H_2O mixing ratio for two Martian years (28 and 32) at 50, 60 and 70 km respectively. These figures also support the global dust storm was a really unique event where the water vapor reaches altitude up to 70 km with mixing ratio higher than 100 ppm in the northern hemisphere. Meanwhile the MY32 observations show a high value of H_2O 40-100 ppm at altitude of 50-70 km than could give a seasonal feedback to the hydrogen escape rate.

Acknowledgements

This work has been supported by the Russian Government grant №14.W03.31.0017.

References

[1] Clancy, R.T., Grossman, A.W., Wolff, M.J., James, P.B., Rudy, D.J., Billawala, Y.N., Sandor, B.J., Lee, S.W., Muhleman, D.O., 1996. Water Vapor Saturation at Low Altitudes around Mars Aphelion: A Key to Mars Climate? Icarus 122, 36-62.

[2] Clarke, J. T., et al., 2014. A rapid decrease of the hydrogen corona of Mars, Geophys. Res. Lett., 41, 8013–8020, doi:10.1002/2014GL061803.

[3] Chaffin, M. S., et al., 2014. Unexpected variability of Martian hydrogen escape, Geophys. Res. Lett., 41, 314–320, doi:10.1002/2013GL058578.

[4] Bhattacharyya, D. et al., 2015, A strong seasonal dependence in the Martian hydrogen exosphere, Geophys. Res. Lett., 42, 8678–8685, doi:10.1002/2015GL065804.

[5] Chaffin, M. S., et al. (2017). "Elevated atmospheric escape of atomic hydrogen from Mars induced by high-altitude water." Nature Geosci 10(3): 174-178.

[6] Korablev, O. et al., 2006. SPICAM IR acousto-optic spectrometer experiment on Mars Express. J. Geophys. Res. 111, E09S03.

EPSC Abstracts
Vol. 11, EPSC2017-642, 2017
European Planetary Science Congress 2017

Synergistic atmospheric retrievals : Using OMEGA and PFS to retrieve martian CO

S. Robert (1), **S. Aoki** (1, 2), A. Piccialli (1), J. Audouard (3), F. Montmessin (3), S. Ferron (4), F. Altieri (5), G. Bellucci (5), A. Geminale (5), M. Giuranna (5), G. Sindoni (5) and A.C. Vandaele (1)
(1) Royal Belgian Institute for Space Aeronomy, Brussels, Belgium, (2) Fonds National de la Recherche Scientifique, Brussels, Belgium, (3) LATMOS, Guyancourt, France, (4) ACRI-ST, Sophia-Antipolis, France, (5) Istituto di Astrofisica e Planetologia Spaziali, Rome, Italy. severine.robert@aeronomie.be

Abstract

Recently, a theoretical study was published showing how science return can benefit from synergistic retrievals [1]. The same approach is here applied to experimental data. OMEGA and PFS instruments, both on Mars Express spacecraft, have collected high-quality data enabling us to retrieve CO volume mixing ratio, among others. The synergy between OMEGA and PFS channels will be presented and the benefits of the synergy will be described by comparing synergistic spectral retrievals and non-synergistic ones.

Introduction

Since 2004, the European mission, Mars Express [2], has delivered a tremendous quantity of data concerning the surface and the atmosphere of Mars. Hopefully so will the ExoMars Trace Gas Orbiter [3] (EMTGO) which was inserted into orbit around Mars in October 2016. The datasets are generally studied separately and that is a necessary first step. However, because each of the spectral regions and geometries has its advantages and disadvantages, the combination of different types of measurements in a synergistic way enables us to better exploit the available data and increase the science return. Tools and methodology have been developed in a previous theoretical study [1]. Simulated spectra based on the characteristics of the two InfraRed instruments onboard EMTGO were used and enabled us to demonstrate the usefulness of synergistic retrievals and to pave the way to more collaborative studies.The expertise built during the theoretical study was used to analyze experimental data in a study associating PFS and OMEGA data, both instruments onboard Mars Express. Carbon monoxide was chosen as test-molecule. CO is a non-condensable gas present in the atmosphere of Mars, varying from 300 to 1500 parts per million in volume mixing ratios, depending on the season [4]. The remote sensing of CO can be performed in different spectral domains and with different geometries of observation.

OMEGA and PFS datasets

We focused on experimental data using the datasets of two infrared instruments on board Mars Express, OMEGA [5] and PFS [6].

Table 1: Characteristics of the instruments' channels. Name of the instrument ; geometry ; type of instrument ; instrumental line shape ; name of the channel ; spectral range and spectral resolution are given.

OMEGA		PFS	
nadir		nadir	
Mapping spectrometer		Fourier transform spectrometer	
Gaussian ILS		PFS ILS	
SWIR-C	SWIR-L	SWC	LWC
0.93-2.69 μm 14 nm	2.52-5.09 μm 20 nm	1.2-5 μm 1.3 cm^{-1}	5-45 μm 1.3 cm^{-1}

We selected datasets in the Hellas Planitia region (30-55°S ; 45-90° E) during Southern winter. These conditions should be advantageous when aiming for a successful retrieval of CO. Therefore, we chose to test the orbits 1186 and 3234, as it was used by Encrenaz et al. [7] and Sindoni et al. [8] and as a high abundance of CO has been retrieved from these orbits in both studies. Two channels of OMEGA and two of PFS were taken into account in order to retrieve surface temperature and CO abundances and if possible,

surface emissivity and surface albedo. The characteristics of the channels are given in Table 1.

Spectral retrievals

We used ASIMUT-ALVL, an home-made Radiative Transfer code [9] which was modified in order to treat OMEGA and PFS data separately and altogether. In the spectral ranges of the considered instruments, two bands of CO can be observed: 1–0 centered at 4.65 μm and the 2–0 band at 2.35 μm. Non-synergistic retrievals were performed in a first step to evaluate the assets of each dataset. For instance, the 2–0 band depth exhibits less than 1% absorption in the SWIR-C channel of OMEGA while the 1–0 band absorption is strong in the SWIR-L OMEGA channel.

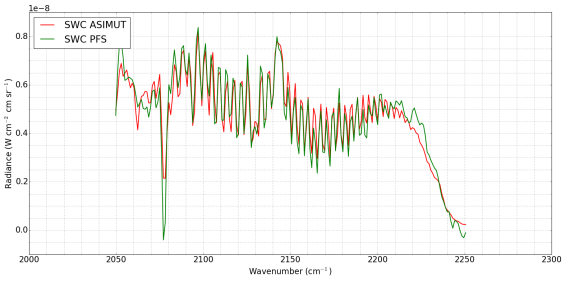

Figure 1: CO 1-0 band fitted with ASIMUT for the orbit 1186 considering PFS instrument. Surface temperature was retrieved using the 400-520 cm^{-1} range. 2550 ppm of CO were retrieved.

CO_2, H_2O and aerosols content were fixed using the results of the BIRA-IASB GCM, GEM-Mars [10]. HITRAN 2012 [11] was used for the spectroscopic parameters and the Sun spectrum was taken from ACE the solar irradiance data were collected from the ACE – FTS data [12] in the IR.

Summary and Conclusions

The previous theoretical study showed how science return can be increased when benefiting from spectral synergies. The demonstration suggested here is made based on experimental data. Considering the quantity of data obtained around Mars, the field of applications of this approach is promising. The retrievals will be presented altogether with the strategy of the synergy and the diagnostic tools developed.

Acknowledgements

The research was performed as part of the "Interuniversity Attraction Poles" programme financed by the Belgian government (Planet TOPERS) and a BRAIN research grant BR/143/A2/SCOOP. This work has been supported by the FNRS "CRAMIC" project under grant agreement n° T.0171.16. The research leading to these results has received funding from the European Union's Horizon 2020 Programme (H2020-Compet-08-2014) under grant agreement UPWARDS-633127. J.A. work is funded by the French government through the excellence laboratory Exploration Spatiale des Environnements Planétaires, Labex ESEP N 2011-LABX-030.

References

[1] S. Robert et al. *Journal of Quantitative Spectroscopy and Radiative Transfer*, 189:86–104, 2017.

[2] A. Chicarro et al. *Eur. Space Agency Spec. Publ.*, 1240:3–13, 2004.

[3] J. Vago et al. *Solar System Research*, 49(7):518–528, 2015.

[4] M.D. Smith et al. *Journal of Geophysical Research*, 114:E00D03, 2009.

[5] J.-P. Bibring et al. *Eur. Space Agency Spec. Publ.*, 1240:37–49, 2004.

[6] V. Formisano et al. *Eur. Space Agency Spec. Publ.*, 1240:71–94, 2004.

[7] Th. Encrenaz et al. *Astronomy & Astrophysics*, 459:265–270, 2006.

[8] G. Sindoni et al. *Planetary and Space Science*, 59:149–162, 2011.

[9] A.C. Vandaele et al. *Journal of Geophysical Research*, 113:E00B23, 2008.

[10] L. Neary and F. Daerden. *Icarus (in revision)*, 2017.

[11] L.S. Rothman et al. *Journal of Quantitative Spectroscopy and Radiative Transfer*, 130:4–50, 2013.

[12] F. Hase et al. *Journal of Quantitative Spectroscopy and Radiative Transfer*, 111:521–528, 2010.

EPSC Abstracts
Vol. 11, EPSC2017-652, 2017
European Planetary Science Congress 2017

How does the latitudinal dependency of the cloud structure change Venus' atmosphere's general circulation?

I. Garate-Lopez and S. Lebonnois
Laboratoire de Météorologie Dynamique (LMD/IPSL), Sorbonne Universités, UPMC Univ Paris 06, Paris, France
(itziar.garate@lmd.jussieu.fr / Fax: +33 (0)1 44 27 62 72)

Abstract

Differently to the previous simulation of the LMD/ IPSL Venus GCM [5], we now take into account the latitudinal variation of the clouds' structure described by [2], and we analyze its impacts on the general circulation of Venus atmosphere. Both solar heating rates and the infrared net-exchange rate matrix used in the radiative transfer code have been modified in that sense. Additional tuning below the clouds has also been performed.

The current results show a better agreement with observations in both mean zonal wind and average temperature fields. Moreover, taking into account the latitudinal variation of the clouds has brought along with it the formation of a well defined cold collar poleward of 60º at cloud level.

Besides, we have reanalyzed the wave activity present in Venus atmosphere and found new baroclinic mid-latitude waves. However, we do not obtain the gravity waves present in the deep atmosphere in the previous model [5].

1.Introduction

The model used here is based on that presented in [5]. This previous simulation reproduced Venus' atmosphere's superrotation and obtained mid-latitude and equatorial zonal wind jets. However, the vertical shear of the zonal wind below the clouds was not completely consistent with the measurements performed by different probes, and the modeled equatorial jet was too intense comparing with the mid-latitude jets.

The average temperature structure obtained with the previous simulation was also good, since it was quite close to the reference VIRA model [6] and it showed a wide cold polar region with some inner structure. Nevertheless, the modeled temperatures were warmer than the VIRA values above the clouds and colder below the clouds, and the obtained cold polar region was located higher than the observed cold collar.

In the previous model, polar barotropic and mid- to high-latitude baroclinic waves were present in the cloud region, while in the middle cloud a Kelvin type and a Rossby-gravity type waves were obtained.

2.Modifications to the model

In Venus, the cloud top altitude decreases and the particles' size increases towards the poles [2]. In the present simulation, we take into account these latitudinal variations of the cloud structure when using look-up tables of the solar heating rates based on [3] and when computing the infrared net-exchange rate matrix [1] used in the radiative transfer code.

Moreover, in order to better fit the vertical profile of the modeled mean temperature to the VIRA reference profile [6], we multiply by a factor of 3 the solar heating rates of [3] between 30 and 48 km where the lower haze is observed. We also consider an additional extinction below the clouds by adding a continuum in the IR spectra used for the computation of the cooling rates. This additional continuum is divided in two; a value of 1.3×10^{-6} cm^{-1} $amagat^{-2}$ at 30 - 48 km altitude and a value of 4×10^{-7} cm^{-1} $amagat^{-2}$ at 16 - 30 km where the transition between stability and instability against convection is observed. This additional continuum plays a key role in the windows present between 3 and 7 μm, but has no influence in the rest of the spectrum.

3.Results

The present vertical profiles of the mean zonal wind are more consistent with the probes' measurements between 40 and 60 km altitude (see Figure 1), probably due to a new baroclinic wave activity found at low and mid latitudes at these altitude range. However, below 40km the present zonal winds are slower than the previous ones, which were more

consistent with the vertical profiles obtained by the Venera and Pioneer Venus probes. The gravity waves present in the deep atmosphere in the previous model [5] are no longer seen, which might be the reason why the deep zonal winds decreased speed, as they played a significant role in angular momentum transport.

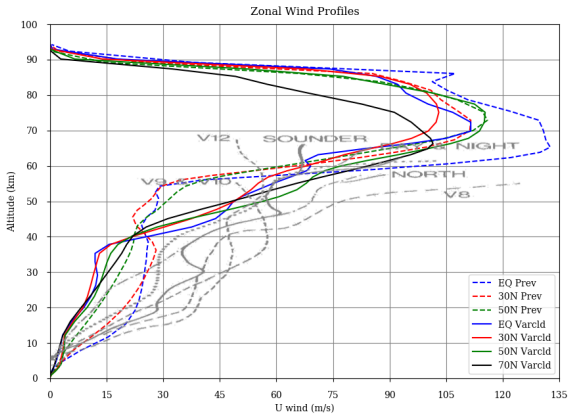

Figure 1: vertical profiles of the mean zonal winds for the previous (dashed line) and new (continuous line) IPSL VGCM models. Different probes' measurements are added in grey.

The equatorial jet is less intense that in the previous model while the mid-latitude jets have increased velocity, being the present latitudinal profile of the wind more consistent with observations [4]. This improvement is mainly related to the meridional transport of angular momentum by the intense wave activity present in the atmosphere. The different types of waves obtained by the present IPSL VGCM model are: diurnal and semi-diurnal tides, barotropic and baroclinic waves, and low-latitude Rossby-type and equatorial Kelvin-type waves.

The present zonally averaged temperature structure is also more consistent with observations than in the previous model. The temperature values above the cloud have decreased and the values below the clouds have increased due to the modifications in the solar heating and IR cooling rates, so the mean vertical profiles fits better now the VIRA profile.

Moreover, the zonally and temporally averaged temperature field (altitude vs. latitude cross section) obtained from the present model shows a cold feature at ~62km altitude and poleward of 60º that resembles the observed cold collar [2] (see Figure 2).

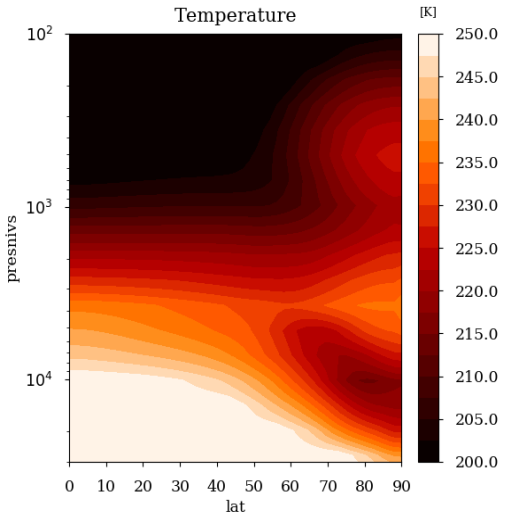

Figure 2: zonally and temporally averaged temperature field of the new IPSL VGCM model.

References

[1] Eymet, V., Fournier, R., Dufresne, J.-L., et al.: Net-exchange parameterization of the thermal infrared radiative transfer in Venus' atmosphere, J. Geophys. Res, Vol. 114, E11008, 2009.

[2] Haus, R., Kappel, D., Arnold, G.: Atmospheric thermal structure and cloud features in the southern hemisphere of Venus as retrieved from VIRTIS/VEX radiation measurements, Icarus, Vol. 232, pp. 232–248, 2014.

[3] Haus, R., Kappel, D., and Arnold, G.: Radiative heating and cooling in the middle and lower atmosphere of Venus and responses to atmospheric and spectroscopic parameter variations, Planet. Space Sci., Vol. 117, pp. 262–294, 2015.

[4] Hueso, R., Peralta, J., Garate-Lopez, I., et al.: Six years of Venus winds at the upper cloud level from UV, visible and near infrared observations from VIRTIS on Venus express, Planet. Space Sci., Vol. 113–114, pp. 78–99, 2015.

[5] Lebonnois, S., Sugimoto, N., and Gilli, G.: Wave analysis in the atmosphere of Venus below 100-km altitude, simulated by the LMD Venus GCM, Icarus, Vol. 278, pp. 38–51, 2016.

[6] Seiff, A., Schofield, J.T., Kliore, A.J., et al.: Model of the structure of the atmosphere of Venus from surface to 100km altitude, Adv. Space Res., Vol. 5, pp. 3-58, 1985.

EPSC Abstracts
Vol. 11, EPSC2017-659, 2017
European Planetary Science Congress 2017

Long Term Science Planning for the ExoMars Trace Gas Orbiter

B. Geiger (1), M. Ashman (2), A. Cardesín Moinelo (3), D. Frew (4), J. García Beteta (1) and M. Muñoz Fernández (5)
(1) Aurora Technology, (2) Telespazio Vega, (3) Serco, (4) ESA, (5) HE Space; all: ESAC, Villanueva de la Cañada, Spain

Abstract

In preparation for the science planning of the ExoMars Trace Gas Orbiter mission, the Science Operations Centre performs an analysis of geometric conditions and the resulting observation opportunities and constraints.

1. Introduction

ExoMars is a joint programme of the European Space Agency (ESA) and the Russian space agency Roscosmos. The ExoMars Trace Gas Orbiter (TGO) spacecraft was launched on 14 March 2016 and entered Mars orbit on 19 October 2016. In the current aerobraking phase the orbital period will be reduced to approximately 2 hours before ultimately achieving a quasi-circular orbit at a distance of ~400km from the surface. The primary science phase of the mission is planned to start in April 2018.

The scientific payload of the TGO spacecraft comprises the following 4 instruments:

- The Atmospheric Chemistry Suite (ACS), [1].
- The Colour and Stereo Surface Imaging System (CaSSIS), [4].
- The Fine Resolution Epithermal Neutron Detector (FREND), [2].
- The Nadir and Occultation for MArs Discovery (NOMAD) instrument [3], [5].

2. Long Term Planning

In preparation for the primary science phase of the mission, the Science Operations Centre (SOC) based at the European Space Astronomy Centre (ESAC) is currently preparing the Long Term Planning (LTP) of science operations. In this process the SOC devises a feasible science observation strategy based on the mission's science priorities and the instrument team requests. In this contribution we show a few examples of the studies carried out for this purpose.

2.1 Data Volume

On long time scales in the order of one year, the mission profile is mainly conditioned by the variability of the available data volume resources. Based on the bitrate evolution shown in Figure 1, conservative estimates for the available data volume range between ~20 Mbit/day at minimum Mars-Earth distance and ~1 Mbit/day close to solar conjunction.

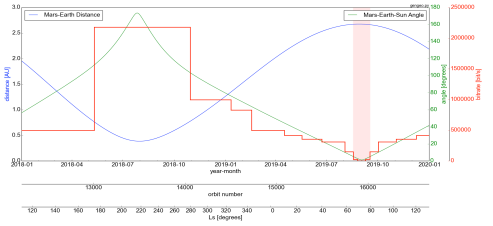

Figure 1: Evolution of the Mars-Earth distance (blue) and Mars-Earth-Sun angle (green) during the years 2018 and 2019. The red line indicates the bitrate for telemetry data downlink.

2.2 Occultation Opportunities and Timelines

On time scales in the order of weeks, the variation of the orientation of the spacecraft orbital plane with respect to the direction of the Sun is decisive for the occurrence and characteristics of solar occultations. These are the most important measurements for the detection and quantification of trace gases in the

atmosphere of Mars and are therefore essential for achieving the mission's science objectives.

Figure 2 depicts the typical temporal evolution of the β-angle, which is commonly used to describe the orientation of the orbital plane. Finally, Figure 3 illustrates occultation event and pointing timelines within one orbit as well as their evolution with time over a period of six months.

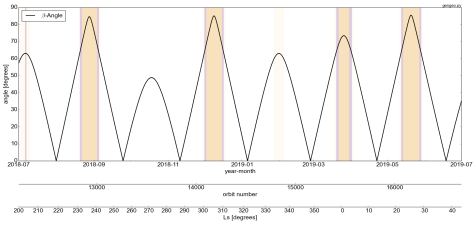

Figure 2: Evolution of the β-angle during a period of one year. The purple shaded periods are intervals with β between 63° and 68° roughly corresponding to the occurrence of "grazing occultations", and the yellowish colour indicates periods with β larger than 68° without occultations.

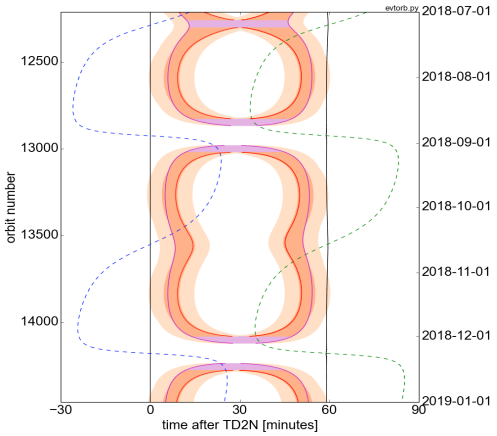

Figure 3: Event and occultation pointing timeline. Event times are depicted relative to the terminator crossing from day to night (TD2N). Black lines: terminator crossing. Red line: Sun at Mars limb. Purple line: Sun at 250km limb height. Dashed blue line: ascending node. Dashed green line: descending node. The red and purple shaded areas, respectively, correspond to the pointing block intervals for normal and grazing solar occultations. The light-red shaded areas indicate the required time for spacecraft slew blocks.

References

[1] Korablev, O., et al.: Three infrared spectrometers, an atmospheric chemistry suite for the ExoMars 2016 trace gas orbiter, Journal of Applied Remote Sensing, Vol. 8, 2014.

[2] Mitrofanov, I., et al., FREND experiment on ESA's TGO mission: science tasks, initial space data and expected results, Geophysical Research Abstracts, EGU General Assembly 2017.

[3] Thomas, I. R., et al.: Optical and radiometric models of the NOMAD instrument part II: the infrared channels – SO and LNO, Optics Express, Vol. 24, pp. 3790-3805, 2016.

[4] Thomas, N., et al.: The Colour and Stereo Imaging System (CaSSIS) for ESA's ExoMars Trace Gas Orbiter, Publikationen der DGPF, Vol. 25, 2016.

[5] Vandaele, A.C., et al.: Optical and radiometric models of the NOMAD instrument part I: the UVIS channel, Optics Express, Vol. 23, pp. 30028-30042, 2015.

EPSC Abstracts
Vol. 11, EPSC2017-673-1, 2017
European Planetary Science Congress 2017

CONSTRAINING THE MSL-SAM METHANE DETECTED SOURCE LOCATION THROUGH MARS REGIONAL ATMOSPHERIC MODELING SYSTEM (MRAMS)

Jorge Pla-García[1,2,3], Scot C.R. Rafkin[2] and the REMS and MSL Science teams

[1]Centro de Astrobiología (CSIC-INTA), 28850 Torrejón de Ardoz, Madrid, Spain, [2]Southwest Research Institute, Boulder CO 80302, USA, [3]Space Science Institute, Boulder CO 80301, USA (jpla@cab.inta-csic.es)

Abstract

The detection of methane by SAM instrument [1] has garnered significant attention. There are many major unresolved questions regarding this detection: 1) Where is the release location? 2) How spatially extensive is the release? 3) For how long is methane released? In an effort to better address the potential mixing and remaining questions, atmospheric circulation studies of Gale Crater were performed with MRAMS mesoscale model, ideally suited for this investigation. The model was focused on rover locations using nested grids with a spacing of 330 meters on the innermost grid that is centered over the detection site. In order to characterize seasonal mixing changes throughout the Martian year, simulations were conducted at Ls0, 90, 180 and 270. The rise in methane concentration was reported to start around Ls336, peaked shortly after Ls82, and then dropped to background prior to Ls103. The aim of this work is to establish the amount of mixing during all seasons and to test whether methane releases inside or outside of Gale crater are consistent with SAM observations.

1. Experiment configuration

Four different scenarios were considered for this research: punctual methane release inside Gale crater (scenario 1#), punctual METHANE release outside -100km NW- crater (scenario 2#), continuous METHANE release outside -100km NW- crater (scenario 3#) and continuous methane release inside crater (scenario 4#). In the punctual releases scenarios (1#, 2#), experiments were designed injecting four tracers into the model to simulate the transport of methane and to understand the mixing of air inside and outside the crater. Tracer #1 mimics methane release and the other three tracers are placed in different elevations (vertical discriminator), due to the three dimensional nature of mixing and transport. In this two first scenarios, tracer #2 is placed from 200 to 500 meters AGL inside Gale crater, tracer #3 from 500 to 2,000 meters AGL inside Gale crater, and tracer #4 elsewhere (outside and above Gale crater, see Figure 1). In the continuous release scenarios (3# and 4#) just one tracer (methane continuous release) was considered and MRAMS code was modified to do so mimicking different clathrates emissions [4]. In all scenarios, the release is assumed to take place near the season when the rise of concentration was first noted (Ls336). This is a transitional time at Gale Crater, when the flushing winds are giving way to a rapid mixing scenario but slower compared to Ls270.

2. Results

As expected [2, 3], Ls270 was shown to be a faster mixing season when air within and outside the crater was well mixed by strong, flushing, northerly flow and large amplitude breaking mountain waves: air flowing downslope (buoyancy and dynamical forcing) at night penetrate all the way to the surface. In the experiments, all inside mass is gone from crater after just 10 hours. At other seasons only ~50% of inside mass stays in crater after 10 hours and simulations indicate that the air flowing down the crater rims does not easily make it to the crater floor. Instead, the air encounters very cold and stable air pooled in the bottom of the crater, which forces the air to glide right over the colder, more dense air below. Thus, the mixing of near surface crater air with the external environment in these seasons is potentially rapid but slower than Ls270. Atmospheric circulation is strongly 3-D, not just 2-D, so in order to constrain a source air mass location is important to take into account vertical motion instead of just horizontal wind speed and direction. Timescale of mixing in MRAMS model is on the order of 1 sol regardless of season, much faster than previously estimated. Duration of methane peak observed by SAM is ~100 sols (assuming no high frequency variations). In the scenario 2# (punctual methane release outside Gale crater), methane arriving rover location from outside crater is diluted by approx. 6 orders of magnitude

after just 12 hours (Figure 2). Therefore, either there is a continuous release inside the crater (more likely) to counteract mixing, or the methane is widely distributed so that mixing doesn't matter, or a local release outside the crater have to be continuous and very large magnitude (unlikely). Continuous release experiments (scenarios 3# and 4#) are being performed both inside and outside the crater. The calculations of methane fluxes are being performed mimicking clathrates emissions at different depths and formed from a gas phase containing 90%, 50% and 10% of methane [4]. Preliminary results of scenario 3# show that timing for SAM measurements is important due to the mixing (increases and drops) of methane inside crater (Fig. 4) and can be seen here:https://data.boulder.swri.edu/jpla/EPSC17/CH4_Ls270_AGL_14M.gif. Scenario 4# experiment is being performed.

3. Figures

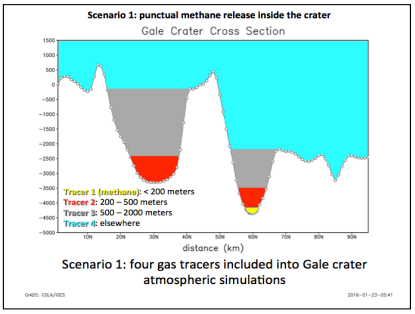

Figure 1: Tracers configuration for scenario 1#. Note tracer 1 is outside the crater in scenario 2#

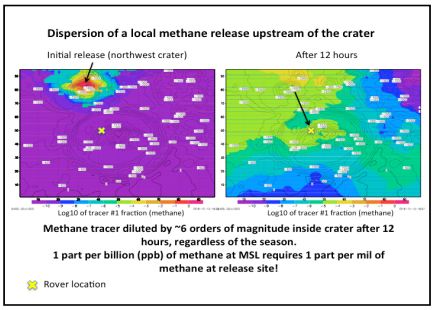

Figure 2: ***Punctual*** methane released outside crater is diluted by approx. 6 orders of magnitude after just 12 hours when arriving to rover location

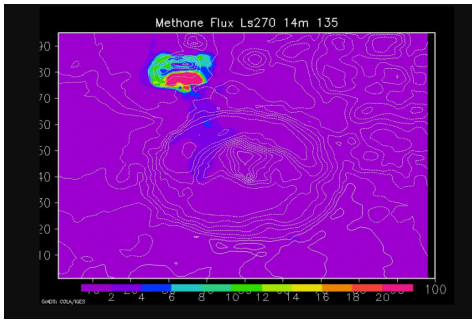

Figure 3: Scenario 3#: methane ***continuous*** release outside crater. Some methane make it to the rover location during nighttime.

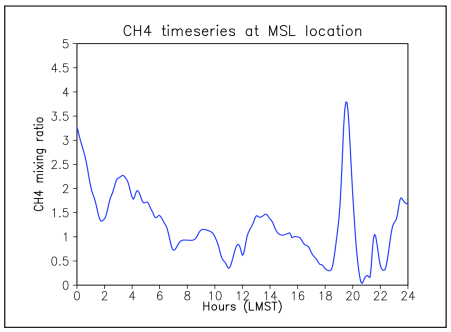

Figure 4: Methane time series at rover location for scenario 3#. Although methane ***continuous*** release is outside crater, some methane make it to the rover location due to atmospheric circulation, so timing of SAM measurements is critical. Nighttime (dynamic) downslope flows entering through north crater rim (moreover at ~1800-2000LMST in the seven sols that methane is releasing in the simulation) have an impact into the methane levels.

References

[1] Webster et al. Science, 2015 [2] Pla-Garcia et al, Icarus 2016. [3] Rafkin et al., Icarus, 2016 [4] Gloesener et al. 6th MAMO conference, 2017

EPSC Abstracts
Vol. 11, EPSC2017-695, 2017
European Planetary Science Congress 2017

Model study of the methane photochemistry in the atmosphere of Mars in the context of the upcoming ExoMars mission

S. Viscardy (1), F. Daerden (1), L. Neary (1), A. García Muñoz (2)

(1) Belgian Institute for Space Aeronomy (BIRA-IASB), Brussels, Belgium, (2 Technische Universität Berlin, Germany (sebastien.viscardy@aeronomie.be)

Abstract

In the context of the upcoming ExoMars mission [1, 9], we present a model study of the distribution of organic species produced by the photochemical destruction of methane (CH_4) released from the surface. Moreover, we reinvestigate the theoretical lifetime of methane in the light of recent model results predicting the formation of layers of methane at high altitude during a few weeks after surface release [10].

1. Introduction

In the past decade, the detection of methane in the atmosphere of Mars has been reported several times [2, 3, 5, 8, 11]. These observations have strongly drawn the attention of the scientific community and triggered a renewed interest in Mars as their implications for the geochemical or biological activities are remarkable. However, given that methane is expected to have a photochemical lifetime of several centuries, the relatively fast loss rates of methane estimated from Earth-based measurements remain unexplained [6]. Although this gave rise to objections against the validity of those observations [13], recent in situ measurements [10] confirmed that methane is being occasionally released into the atmosphere from an unknown source (possibly from the ground). In addition, The NOMAD instrument on board the ExoMars Trace Gas Orbiter [9] is thus expected to provide key information and make one able to better understand the fate of methane and its by-products on Mars. This is in this context that we present a model study of the behaviour of methane plumes and some preliminary results on the chemistry of methane in the atmosphere of Mars.

2. 3D-GCM (GEM-Mars)

The model study presented here is based on the General Circulation Model for the atmosphere of Mars [10]. It is a grid-point model based on the Canadian Global Environmental Multiscale (GEM) model for weather forecasting on Earth. For the present study it was operated at 4°×4° horizontal resolution and with 102 vertical levels reaching from the surface to 8×10^{-6} Pa (~150 km). The standard chemistry [4] and the photochemistry of organic species [12] are described online using a time step of 30 minutes.

3. Photochemistry of CH_4 after surface release

Using a 3D General Circulation Model for the atmosphere of Mars (called GEM-Mars), we recently payed specific attention to the evolution of the vertical distribution of methane after different surface release scenarios […]. We showed that, a few days after its release from the ground, methane is not uniformly dispersed into this atmosphere but can rather form layers at altitudes as high as 50 km (see Figure 1).

The upcoming European Space Agency (ESA)/Roskosmos ExoMars Trace Gas Orbiter mission carries two instruments that are designed to measure the first vertical profiles of methane and derived organic species with high sensitivity and to do so in a mode of systematic diurnal monitoring throughout a full Mars year. These are the Nadir and Occultation for Mars Discovery (NOMAD) spectrometer suite [9], with expected detection limit for methane of 25 parts per trillion by volume and a vertical resolution of ~1 km, and the Atmospheric Chemistry Suite (ACS). They are thus expected to

provide key information of the methane production and destruction in the atmosphere of Mars.

In this context, in order to anticipate the future observations by those two instruments, we will present preliminary results of a model study of the distribution of the methane and other organic species produced by the photochemical destruction of CH_4 after surface release.

Furthermore, as the methane released from the ground is expected to be lifted quickly high in the atmosphere, we here investigate how this fundamental result impacts the fate of CH_4 in the atmosphere of Mars, more precisely its lifetime.

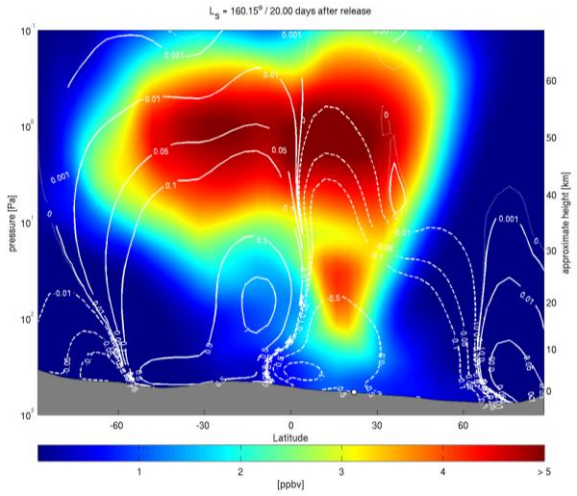

Figure 1: Zonal mean of methane mixing ratio 20 days after an instantaneous release at the equator. Contours in white represent the so-called Hadley cells.

References

[1] Drummond, R., Vandaele, A.-C., Daerden, F. Fussen, D., Mahieux, A., Neary, L., Neefs, E., Robert S., Willame, Y., and Wilquet, V., Studying methane and other trace species in the Mars atmosphere using a SOIR instrument, Planetary and Space Science, Vol. 59, pp. 292-298 (2011).

[2] Fonti, S. and Marzo, G. A., Mapping the methane on Mars. Astronomy and Astrophysics, Vol. 512, A51 (6 p.) (2010).

[3] Formisano, V., Atreya, S., Encrenaz, T., Ignatiev, N., and Giuranna, M., Detection of methane in the atmosphere of Mars, Science, Vol. 306, pp. 1758-1761 (2004).

[4] García Muñoz, A., McDonnell, J. C., McDade, I. C., and Melo, S. M. L., Airglow on Mars: Some model expectations for the OH Meinel bands and the O_2 IR atmospheric band, Icarus, Vol. 176, 75-95 (2005).

[5] Krasnopolsky, V. A., Maillard, J. P., and Owen, T. C., Detection of methane in the Martian atmosphere: Evidence for life? Icarus, Vol. 172, pp. 537-547 (2004).

[6] Lefèvre, F. and Forget, F., Observed variations of methane on Mars unexplained by known atmospheric chemistry and physics, Nature, Vol. 460, pp. 720-723 (2009).

[7] Mischna, M. A., Allen, M., Richardson, M. I., Newman, C. E., and Toigo, A. D., Atmospheric modeling of Mars methane surface releases, Planetary and Space Science, Vol. 59, pp. 227-237 (2011).

[8] Mumma, M. J., Villanueva, G. L., Novak, R. E., Hewagama, T., Bonev, B. P., Disanti, M. A., Mandell, A. M., and Smith, M. D., Strong release of methane on Mars in northern summer 2003, Science, Vol. 323, pp. 1041-1045 (2009).

[9] Vandaele, A. C., et al., Science objectives and performances of NOMAD, a spectrometer suite for the ExoMars TGO mission, Planet. Space Sci., Vol. 119, 233–249 (2015).

[10] Viscardy, S., Daerden, F., and Neary, L., Formation of layers of methane in the atmosphere of Mars after surface release, Geophys. Rev. Lett., Vol. 43 (2016).

[11] Webster, C. R. *et al.*, Mars methane detection and variability at Gale crater. Science, Vol. 347, pp. 415-417 (2015).

[12] Wong, A.-S., Atreya, S., and Encrenaz, T., Chemical markers of possible hot spots on Mars, Journal of Geophysical Research , Vol. 108, 5026 (7 p.) (2003).

[12] Zahnle, K., Freedman, R. S., and Catling, D. C., Is there methane on Mars?, Icarus, Vol. 212, pp. 493-503 (2011).

EPSC Abstracts
Vol. 11, EPSC2017-740, 2017
European Planetary Science Congress 2017

How to interpret the temperature variability in Titan's upper atmosphere?

J. Cui (1,2,3)
(1) School of Atmospheric Sciences, Sun Yat-Sen University, Zhuhai, China, (2) Lunar and Planetary Science Laboratory, Macau University of Science and Technology, Macau, China, (3) Key Laboratory of Lunar and Deep Space Exploration, National Astronomical Observatories, Chinese Academy of Sciences, Beijing, China (cuijun7@mail.sysu.edu.cn / Fax: +86-0756-3668292)

Abstract

Over the past 12 years, the Cassini Ion Neutral Mass Spectrometer (INMS) observations have revealed a highly variable neutral temperature in Titan's upper atmosphere, with a mean temperature of 150 K but a variability of more than 70 K. No systematic horizontal or diurnal variations could be identified, and the observed temperature variability is more likely to be temporal in nature rather than spatial. At least three scenarios have been investigated so far to identify the driving force of the variable thermal structure, including the solar-driving scenario, the plasma-driven scenario, and the cooling-driving scenario. However, no scenario is able to interpret properly the observations.

1. Introduction

Over the past 12 years, the implementation of the Cassini-Huygens mission has greatly improved our understanding of Titan, the largest moon of Saturn and the only moon within the Solar System that possesses a permanent and extended atmosphere. As revealed by the Cassini Ion Neutral Mass Spectrometer (INMS) data, one of the intriguing characteristics identified in Titan's atmosphere is the large variability of more than 70 K in neutral temperature at altitudes above 1000 km (around a mean temperature of 150 K), which has sometimes been termed as the problem of energy crisis in Titan's upper atmosphere (e.g., Snowden & Yelle 2014 and references therein). This article is devoted to a description of such a problem and our continuous efforts towards understanding properly both the nature and the driving force of the observed temperature variability.

2. What is the nature of the observed temperature variability?

The first Cassini flyby with Titan, denoted as TA, revealed a neutral temperature of around 150 K in Titan's upper atmosphere (Waite et al. 2005, Yelle et al. 2006), which is consistent with the early Voyager observations made by the Ultraviolet Spectrometer (UVS) (Vervack et al. 2004). Later, a comparison between the TA and T5 flybys showed surprisingly that the nightside temperature is higher than the near-terminator temperature by more than 10 K (De La Haye et al. 2007). By combining the INMS data from 13 flybys covering exclusively Titan's northern hemisphere, both Mueller-Wodarg et al. (2008) and Cui et al. (2009) showed a tendency of decreasing neutral temperature from the equator towards the north pole, despite that no systematic diurnal variations could be identified. Finally, with the aid of 32 Titan flybys, Snowden et al. (2013) confirmed that any horizontal variations in neutral temperature, either meridional or diurnal, that had been previously reported were simply observational bias and the thermal structure of Titan's upper atmosphere appeared to be irregular and sporadic. The above observations suggest that the temperature variability is more likely to be temporal in nature rather than spatial. In such a scenario, the upper regions of Titan's atmosphere are more or less spatially uniform but expand or shrink as time evolves in response to certain externally driving forces. This scenario is also supported by the observation of H_2 density variability above Titan's exobase, which could only be reproduced by assuming an exbase density variability characterized by an infinitely large scale length (Cui et al. 2011). Since the scale length has to be finite, the above observation naturally implies that the exospheric density variability is likely temporal in nature.

The scenario of time-varying thermal structure in Titan's upper atmosphere led to the study of Westlake et al. (2011), who found that the mean temperature above 1000 km varied with the ambient plasma environment (especially in terms of the intensity of magnetospheric electron precipitation), being higher under plasma-sheet conditions as compared to lobe-like conditions (Rymer et al. 2009).

3. What is the driving force of the observed temperature variability?

The absence of any diurnal variation in neutral temperature (e.g., Snowden et al. 2013) clearly implies that the thermal structure of Titan's upper atmosphere cannot be solar-driven. This is also supported by the absence of correlation between neutral temperature and solar EUV flux (Snowden et al. 2013). In addition, Snowden & Yelle (2014) have predicted that with the variability in solar EUV flux over the period of Cassini observations, the temperature variability is no larger than 5 K, far insufficient to account for the observed variability.

The apparent correlation between neutral temperature and electron precipitation identified by Westlake et al. (2011) suggests that the thermal balance in Titan's upper atmosphere is likely plasma-driven. However, the typical heating/cooling timescale is about 10 Earth days (Snowden & Yelle 2014) whereas the duration for Cassini observations made in the vicinity of Titan during one Titan flyby is typically 10 minutes. The large difference in the above two timescales makes the accessing the significance of Westlake et al.'s correlation difficult (Snowden & Yelle 2014).

The seminal work of Yelle (1991) indicated that the thermal balance in Titan's upper atmosphere was strongly influenced by the abundance of the minor constituent, HCN, as the main coolant (through its rotational line emission) at altitudes above the homopause. In Cui et al. (2016), the so-called cooling-driven scenario was tested, showing that the neutral temperature could be different by more than 70 K at a similar level of $\sim 3\times10^{-4}$ in HCN mixing ratio. Therefore the variation in HCN abundance in Titan's upper atmosphere cannot account for the observed temperature variability either.

4. Conclusions and prospects

Over the past 12 years, the Cassini INMS observations have revealed a highly variable neutral temperature in Titan's upper atmosphere, with a mean temperature of 150 K but a variability of more than 70 K (e.g., De La Haye et al. 2007, Mueller-Wodarg et al. 2008, Westlake et al. 2011, Cui et al. 2011, Snowden et al. 2013). No systematic horizontal or diurnal variations could be identified, and the observed temperature variability is more likely to be temporal in nature rather than spatial (Cui et al. 2011). At least three scenarios have been investigated so far to identify the driving force of the variable thermal structure of Titan's upper atmosphere, including the solar-driving scenario, the plasma-driven scenario, and the cooling-driving scenario. However, no scenario is able to interpret properly the observations (e.g., Snowden & Yelle 2014, Cui et al. 2016).

There are other scenarios that have not been examined in detail. Extensive signatures of wave-like structures have been identified in the INMS data and characteristic values of basic wave parameters have been estimated (Cui et al. 2013, 2014). Therefore one of the scenarios likely responsible for the observed temperature variability is the wave-driven scenario in which the thermal structure of Titan's upper atmosphere is strongly modulated by the dissipation of waves of different modes (e.g., Matcheva & Strobel 1999, Hickey et al. 2000, Schubert et al. 2003).

Alternatively, it would also be interesting to examine rigorously the functional form and intensity of the missing energy source/sink in Titan's upper atmosphere for each flyby available. Such an examination has to be made with the aid of the observed N_2, CH_4 and HCN density profiles, which can be used to infer the solar heating rate, the HCN cooling rate, as well as the contribution from conductive heat flow. Comparing various energy source/sink terms would then allow the assessment of the detailed energetics in Titan's upper atmosphere and the derivation of any extra terms required to force thermal balance. Information on the vertical profile of solar heating efficiency appropriate for each individual flyby is crucial for such an examination.

Acknowledgements

The author acknowledges supports from the National Science Foundation of China (NSFC) through grants

41374178 and 41525015. This work is also supported by the Science and Technology Development Fund of Macau SAR (039/2013/A2 and 082/2015/A3).

References

[1] Cui, J., et al.: Analysis of Titan's neutral upper atmosphere from Cassini Ion Neutral Mass Spectrometer measurements, Icarus, Vol. 200, pp. 581-615, 2009.

[2] Cui, J., et al.: The implications of the H_2 variability in Titan's exosphere, J. Geophys. Res., Vol. 116, A11324, 2011.

[3] Cui, J., et al.: Compositional effects in Titan's thermospheric gravity waves, J. Geophys. Res., Vol. 40, pp. 43-47, 2013.

[4] Cui, J., et al.: Density waves in Titan's upper atmosphere, J. Geophys. Res., Vol. 119, pp. 490-518, 2014.

[5] Cui, J., et al.: The variability of HCN in Titan's upper atmosphere as implied by the Cassini Ion Neutral Mass Spectrometer measurements, Astrophys. J., Vol. 826, L5, 2016.

[6] De La Haye, V., et al.: Cassini Ion and Neutral Mass Spectrometer data in Titan's upper atmosphere and exosphere: Observation of a suprathermal corona, J. Geophys. Res., Vol. 112, A07309, 2007.

[7] Hickey, M.P., et al.: Gravity wave heating and cooling in Jupiter's thermosphere, Icarus, Vol. 148, pp. 266-281, 2000.

[8] Matcheva, K.I., & Strobel, D.F.: Heating of Jupiter's thermosphere by dissipation of gravity waves due to molecular viscosity and heat conduction, Icarus, Vol. 140, pp. 328-340, 1999.

[9] Mueller-Wodarg, I.C.F., et al.: Horizontal structures and dynamics of Titan's thermosphere, J. Geophys. Res., Vol. 113, E10005, 2008.

[10] Rymer, A.M., et al.: Discrete classification and electron energy spectra of Titan's varied magnetospheric environment, Geophys. Res. Lett., Vol. 36, L15109, 2009.

[11] Schubert, G., et al.: Heating of Jupiter's thermosphere by the dissipation of upward propagating acoustic waves, Icarus, Vol. 163, pp. 398-413, 2003.

[12] Snowden, D.S., et al.: The thermal structure of Titan's upper atmosphere, I: Temperature profiles from Cassini INMS observations, Icarus, Vol. 226, pp. 552-582, 2013.

[13] Snowden, D.S., & Yelle, R.V.: The thermal structure of Titan's upper atmosphere, II: Energetics, Icarus, Vol. 228, pp. 64-77, 2014.

[14] Vervack, R.J., et al.: New perspectives on Titan's upper atmosphere from a reanalysis of the Voyager 1 UVS solar occultations, Icarus, Vol. 170, pp. 91-112, 2004.

[15] Waite, J.H., et al.: Ion Neutral Mass Spectrometer results from the first flyby of Titan, Science, Vol. 308, pp. 982-986, 2005.

[16] Westlake, J.H., et al.: Titan's thermospheric response to various plasma environments, J. Geophys. Res., 116, A03318, 2011.

[17] Yelle, R.V.: Non-LTE models of Titan's upper atmosphere, Astrophys. J., Vol. 383, pp. 380-400, 1991.

[18] Yelle, R.V., et al.: The vertical structure of Titan's upper atmosphere from Cassini Ion Neutral Mass Spectrometer measurements, Icarus, Vol. 182, pp. 567-576, 2006.

EPSC Abstracts
Vol. 11, EPSC2017-754, 2017
European Planetary Science Congress 2017

Influence of Suprathermal Atoms on the Escape and Evolution of Mars' CO2 Atmosphere

H. Lichtenegger (1), U. V. Amerstorfer (1), H. Gröller (2), F. Tian (3), H. Lammer (1), L. Noack (4), C. Johnstone (5), and L. Tu (5)

(1) Space Research Institute, Austrian Academy of Sciences, Schmiedlstrasse 6, 8042 Graz, Austria (herbert.lichtenegger@oeaw.ac.at), (2) Lunar and Planetary Laboratory, University of Arizona, Tucson, AZ, USA, (3) Ministry of Education Key Laboratory for Earth System Modeling, Center for Earth System Science, Tsinghua University, Beijing, China, (4) Royal Observatory of Belgium, Brussels, Belgium, (5) Department of Astrophysics, University of Vienna, Vienna, Austria.

Abstract

Loss rates of hot oxygen and hot carbon from Mars are presented for an EUV flux of 1, 3, 10, and 20 times the present one which correponds to different epochs in the past. Moreover, the contribution of different chemical processes to the loss rates at different times is shown and the evolution of the martian CO2 atmosphere is discussed.

1. Introduction

The escape of hot oxygen and carbon from the martian atmosphere for 1, 3, 10, and 20 times the present solar EUV, corresponding to different epochs in Mars' evolution, is studied. Based on simulated 1D profiles for neutrals and ions of the upper atmosphere for the various EUV fluxes [2], the stochastic motion of hot O and C produced via different chemical reactions is calculated by means of a 3D Monte Carlo modell [1]. From the obtained energy distribution of the suprathermal particles at the exobase, the escape rates of O and C corresponding to the different EUV fluxes can be estimated.

2. Results

We discuss different sources of hot oxygen and carbon atoms in the martian thermosphere and their changing importance with the EUV flux. The increase of the production rates due to higher densities resulting from the higher EUV flux competes against the expansion of the thermosphere and corresponding increase in collisions. We find that the escape due to photodissociation continuousely increases with increasing EUV level, while other processes show a different behaviour. E.g., the escape of particles due to dissociative recombination of O2+ reaches a maximum at the $\sim$ 10 EUV level and starts to decrease again for higher values (Fig. 1).

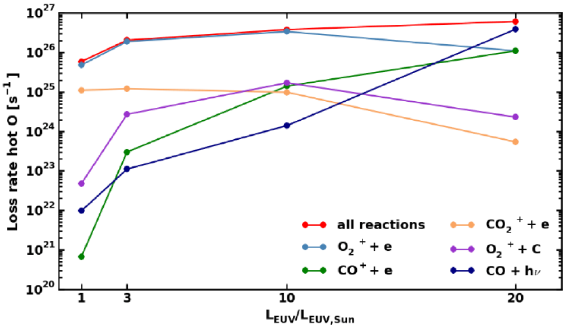

Figure 1: Loss rates of hot O as a function of EUV flux normalized to the present solar EUV flux for various production processes.

Depending on the initial rotation rate of the Sun and its rotational evolution, the different EUV fluxes can be related to different times in the past of the martian history by comparing a sample of solar like stars of different age and rotation rate [3]. If we assume that the Sun has been a slow rotator in the past, our findings show that Mars could not have had a dense atmosphere at the end of the Noachian epoch, since such an atmosphere would not have been able to escape until today. In the pre-Noachian era, most of a magma ocean and volcanic activity related outgassed CO2 atmosphere could have been lost thermally until the Noachian epoch, when non-thermal loss processes such as suprathermal atom escape became dominant. Assuming a 2:1 relation for lost hot O to lost hot C, our results suggest that not more than an equivalent of some hundred millibar of CO2 could have been

removed since the Noachian epoch by suprathermal atom escape.

Acknowledgements

U.V. Amerstorfer and H. Lichtenegger acknowledge the supported by the Austrian Science Fund (FWF): P24247-N16.

References

[1] Gröller, H., V. I. Shematovich, H. I. M. Lichtenegger, H. Lammer, M. Pfleger, Y. N. Kulikov, W. Macher, U. V. Amerstorfer, and H. K. Biernat (2010), Venus' atomic hot oxygen environment, *J. Geophys. Res.*, *115*, E12017, doi:10.1029/2010JE003697.

[2] Tian, F., J. F. Kasting, and S. C. Solomon (2009), Thermal escape of carbon from the early Martian atmosphere, *Geophys. Res. Lett.*, *36*, L02205, :doi10.1029/2008GL036513.

[3] Tu, L., C. P. Johnstone, M. Güdel, and H. Lammer (2015), The extreme ultraviolet and X-ray Sun in Time: High-energy evolutionary tracks of a solar-like star, *Astron. Astrophys.*, *577*, L3, doi:10.1051/0004-6361/201526146.

EPSC Abstracts
Vol. 11, EPSC2017-779, 2017
European Planetary Science Congress 2017

Mars Express science highlights and future plans

D. Titov (1), J.-P. Bibring (2), A. Cardesin (3), T. Duxbury (4), F. Forget (5), M. Giuranna (6), F. González-Galindo (7), M. Holmström (8), R. Jaumann (9), A. Määttänen (10), P. Martin (3), F. Montmessin (10), R. Orosei (11), M. Pätzold (12), J. Plaut (13), and MEX SGS Team (3).

(1) ESA-ESTEC, 2200 AG Noordwijk, The Netherlands; (2) IAS-CNRS, Orsay, France; (3) ESA-ESAC, Madrid, Spain; (4) George Mason University, Fairfax, VA, USA; (5) LMD, Paris, France; (6) IAPS-INAF, Rome, Italy; (7) IAA, Granada, Spain; (8) IRF, Kiruna, Sweden; (9) IPF-DLR, Berlin, Germany; (10) LATMOS/ IPSL, CNRS, Guyancourt, France; (11) IRA-INAF, Bologna, Italy; (12) RIU-Uni Cologne, Cologne, Germany; (13) JPL, Pasadena, CA, USA; (dmitri.titov@esa.int)

Mars Express remains one of ESA's most scientifically productive missions whose publication record now exceeds 1000 papers. Characterization of the geological processes on a local-to-regional scale by HRSC, OMEGA and partner experiments on NASA spacecraft has allowed constraining land-forming processes in space and time. Recent results suggest episodic geological activity as well as the presence of large bodies of liquid water in several provinces (e.g. Eridania Planum, Terra Chimeria) in the early and middle Amazonian epoch and formation of vast sedimentary plains north of the Hellas basin. Mars Express observations and experimental teams provided essential contribution to the selection of the Mars-2020 landing sites. More than a decade-long record of the atmospheric parameters such as temperature, dust loading, water vapor and ozone abundance, water ice and CO_2 clouds distribution, collected by SPICAM, PFS and OMEGA spectrometers as well as subsequent modeling have provided key contributions to our understanding of the martian climate. ASPERA-3 observations of the ion escape covering complete solar cycle have revealed important dependencies of the atmospheric erosion rate on parameters of the solar wind and EUV flux. The structure of the ionosphere sounded by the MARSIS radar and the MaRS radio science experiment was found to be significantly affected by the solar activity, the crustal magnetic field, as well as by the influx of meteorite and cometary dust. MARSIS and ASPERA-3 observations suggest that the sunlit ionosphere over the regions with strong crustal fields is denser and extends to higher altitudes as compared to the regions with no crustal anomalies. The ionospheric plasma expands to higher altitudes where it contacts with the solar wind plasma. Reconnection of solar magnetic field lines carried by the solar wind with field lines of crustal origin opens channels through which the ionospheric plasma escapes to space, producing strong and narrow cavities in the density. The situation is very different on the night side where the ionosphere has patchy structure. Such patchy ionizations are observed in the regions where field lines have a dominant vertical component. Through these patches the ionospheric plasma from the dayside penetrates and supplies the nightside ionosphere.

Mars Express has fully accomplished its objectives set for 2015-2016. The mission provides unique observation capabilities amongst the flotilla of spacecraft investigating Mars. The mission has been confirmed till the end of 2018. The science case for the mission extension until the end of 2020 has been submitted to the ESA Science Program Committee. The observation program proposed for 2019-2020 includes both augmenting the coverage and extending long-time series, as well as new elements and potentially new opportunities for discoveries. It will be boosted by collaboration and synergies with NASA's MAVEN, ESA-Roscosmos Trace Gas Orbiter and other missions. The talk will give the mission status, review the recent science highlights, and outline future plans.

EPSC Abstracts
Vol. 11, EPSC2017-788-2, 2017
European Planetary Science Congress 2017

Short-period planetary-scale waves found in a Venus GCM

M. Takagi (1), N. Sugimoto (2), H. Ando (1), and Y. Matsuda (3)
(1) Kyoto Sangyo University, Kyoto, Japan (takagi.masahiro@cc.kyoto-su.ac.jp / Fax: +81-75-705-1714), (2) Keio University, Yokohama, Japan, (3) Tokyo Gakugei University, Koganei, Japan

Abstract

Short-period waves or disturbances at the cloud levels in the Venus atmosphere are investigated using a GCM. Preliminary results show that two kinds of waves with periods of about 5.5 and 7.5 Earth days are found at 40–80 km levels. At 68 km, vortical motions and disturbances with remarkable zonal winds are predominant at mid-latitudes at 40°–70° and low-latitudes equatorwards of 30°, respectively. The structure of the low-latitude disturbances are similar to that of the equatorial Kelvin wave. Because phase speeds of these waves are the same, it is suggested that they form a planetary-scale coherent structure symmetric about the equator.

1. Introduction

In previous observations of the Venus atmosphere, it has been pointed out from the cloud motions that the so-called Kelvin and Rossby waves exist at the cloud top levels whose periods are about 4 and 5 Earth days, respectively [2, 4]. However, their structures and/or generation mechanisms remain unclear at present. New observational results on the atmospheric superrotation and various waves are being provided from the Akatsuki mission which has started observations from December 2015, by which the three-dimensional structures and wave activities of the Venus atmosphere at the cloud levels will be elucidated in the forthcoming future.

In order to interpret the observational results in terms of dynamics, and elicit as much information from them as possible, the Venus atmospheric dynamics should be investigate theoretically and numerically. In the present study, the short-period waves with periods shorter than 10 Earth days found at the cloud levels are investigated using a Venus GCM named VAFES [7].

2. Model

VAFES is a full nonlinear GCM with simplified physical processes for the Venus atmosphere based on the primitive equations on the sphere, which enables us reproduce realistic structures of the Venus upper atmosphere at the cloud levels such as the baroclinic instability waves, the cold collar, the thermal tides, and so on [8, 1]. The model atmosphere extends from the ground to about 120 km, and 120 levels are taken at a regular spacing of 2 km. The horizontal resolution is T63 (192×96 grid points in longitude and latitude). The vertical eddy viscosity with a constant coefficient of 0.15 $\mathrm{m^2\,s^{-1}}$ is used. The horizontal eddy viscosity is represented by the second-order hyper-viscosity, whose damping time for the maximum wavenumber is approximately 0.1 Earth days. The value of physical parameters are set adequately for the Venus atmosphere. The solar heating is based on the previous observation [9]; but it is neglected above 80 km in the present study. The temperature field is relaxed to a prescribed horizontally uniform field, $T_0(z)$, which is taken from the Venus international reference atmosphere (VIRA) [6]. See our previous work [8] for more details of the model.

The initial condition is an idealized superrotating state. The zonal wind is assumed to be in the solid body rotation; its velocity increases linearly with altitude from the ground to 70 km, which is 100 $\mathrm{m\,s^{-1}}$ at the equator at 70 km, and constant above this level. It is assumed that the planet rotates from west to east, as the Earth, and eastward is positive. The initial temperature distribution is cyclostrophically balanced with the initial zonal wind.

Using this initial state, we perform a nonlinear numerical integration for more than 5 Earth years. The model atmosphere reaches a quasi-equilibrium state within about 1 Earth year, in which the wind and temperature fields are stably maintained for more 4 Earth years, as shown in the previous studies [8]. In the present study, we analyze the data obtained for the last 1 Earth year in the quasi-equilibrium state. The sampling rate is every 6 hours.

3. Preliminary results

It has been shown from the Fourier analysis that two kinds of waves are found with periods of about 5.5 and 7.5 Earth days at broad vertical levels of 40–80 km. The

5.5-day and 7.5-day waves have significant amplitudes in the zonal winds at low-latitudes and latitudes from mid-latitudes to the polar region, respectively. On the other hand, in the meridional winds, they have at mid-latitudes and the polar region, respectively. It is thought that the 5.5-day wave is related to the baroclinic instability waves [8].

Figure 1 shows a horizontal structure of the short-period wave observed at 68 km. The short-period components are extracted by a high-pass filter with a cut-off period of 10 Earth days. It is found that vortex motions dominate at mid-latitudes, whose horizontal wind velocity is about 40 $\mathrm{m\,s^{-1}}$. In low-latitudes equatorwards of 30°, zonal winds with a zonal wavenumber of 1 are predominant, whose velocity is about 20 $\mathrm{m\,s^{-1}}$. Phase velocities of these waves observed at mid- and low-latitudes are the same. The present result suggests that a planetary-scale coherent structure which is symmetric about the equator and extends from the equator to mid-latitudes exists at the cloud top levels asociated with these waves. The symmetry about the equator has also been observed in UV cloud images and brightness temperatures at the cloud top levels [5]. Its generation mechanism remains unclear, but it may be related to the shear instability found in a shallow water system [3].

In the lower cloud levels (50–60 km), it is found that vortical motions with a zonal wavenumber of about 5 dominate at low-latitudes. It is also pointed out that streak structures extending to down-stream regions are found in the vertical winds at mid- and high-latitudes. These streak structures are associated with remarkable divergence and convergence of the horizontal winds. It is suggested that these structures are similar to recent nightside cloud images obtained by the IR2 camera onboard Akatsuki.

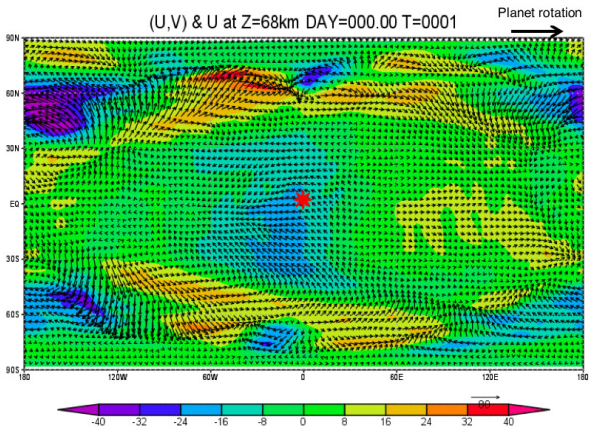

Figure 1: Horizontal structure of the short-period disturbances obtained at 68 km: horizontal winds (vectors) and zonal wind velocity (colors). Note that the subsolar point is located at (0°E, 0°N), the center of the figure.

References

[1] Ando, H., N. Sugimoto, M. Takagi, H. Kashimura, T. Imamura, and Y. Matsuda (2016), The puzzling Venusian polar atmospheric structure reproduced by a general circulation model, Nat. Commun., 7:10398, doi:10.1038/ncomms10398.

[2] Del Genio, A. D., and W. B. Rossow (1990), Planetary-scale waves and cyclic nature of cloud top dynamics on Venus, J. Atmos. Sci., 47, 293–318.

[3] Iga, S., and Y. Matsuda (2005), Shear Instability in a Shallow Water Model with Implications for the Venus Atmosphere, J. Atmos. Sci., 62, 2514–2527.

[4] Kouyama, T., T. Imamura, M. Nakamura, T. Satoh, and Y. Futaana (2015), Vertical propagation of planetary-scale waves in variable background winds in the upper cloud region of Venus, Icarus, 248, 560–568.

[5] Sato, T. M., H. Sagawa, T. Kouyama, K. Mitsuyama, T. Satoh, S. Ohtsuki, M. Ueno, Y. Kasaba, M. Nakamura, and T. Imamura (2014), Cloud top structure of Venus revealed by Subaru/COMICS mid-infrared images, Icarus, 243, 386–399.

[6] Seiff, A., J. T. Schofield, A. J. Kliore, F. W. Taylor, S. S. Limaye, H. E. Revercomb, L. A. Sromovsky, V. V. Kerzhanovich, V. I. Moroz, and M. Ya. Marov (1985), Adv. Space Res., 5, 3–58.

[7] Sugimoto, N., M. Takagi, and Y. Matsuda (2014), Baroclinic instability in the Venus atmosphere simulated by GCM, J. Geophys. Res. Planets, 119, 1950–1968, doi:10.1002/2014JE004624.

[8] Sugimoto, N., M. Takagi, and Y. Matsuda (2014), Waves in a Venus general circulation model, Geophys. Res. Lett., 41, 7461–7467, doi:10.1002/ 2014GL061807.

[9] Tomasko, M. G., L. R. Doose, P. H. Smith, and A. P. Odell (1980), Measurementsof the flux of sunlight in the atmosphere of Venus, J. Geophys. Res., 85, 8167–8186.

EPSC Abstracts
Vol. 11, EPSC2017-809, 2017
European Planetary Science Congress 2017

Ground based mid-IR heterodyne spectrometer concept for planetary atmospheres observations

O.V. Benderov (1), **V.V. Garamov** (1), V.M. Semenov (1), M.V. Spiridonov (1,3), A.V. Rodin (1,2), B. Stepanov (4)
(1) Moscow institute of physics and technology, Russia, (2) Space Research Institute, Russia, (3) Prokhorov General Physics Institute, Russia, (4) G.G. Devyatykh Institute of Chemistry of High-Purity Substances, Russia (garamov@phystech.edu)

Abstract

We present a heterodyne spectrometer concept based on distributed feedback (DFB) quantum cascade lasers (QCL) operated in midle infrared region (MIR). The instrument is assumed to be mount on the Russian infrared observatories. The core features of the concept are compact design, utilizing a novel mid-IR fiber optical components and dynamic local oscillator frequency locking using reference molecule absorption line. The instrument characteristics are similar to modern heterodyne devices THIS (Cologne University, Germany) and MILAHI (Tohoku University, Japan) in terms of fundamental parameters, including spectral resolution, spectral coverage in a single observation.

1. Introduction

During last decades geology and internal structure of planets, their satellites and small bodies attract increasingly more attention. But planetary atmospheres remain most efficient sources of knowledge about planets and their evolution. The key advantage of high spectral resolution in the analysis of the outgoing radiation spectra of planets is concerned with the capability to retrieve detailed information about composition, structure, and photochemical kinetics of their atmospheres[1],[2]. Ultra-high spectral resolution ($\lambda/\Delta\lambda \sim 10^8$) provided by a heterodyne detection of the infrared radiation, allows for Doppler wind measurements at different altitudes[3]. The most valuable problems to be solved are vertical temperature and wind profiles on Mars and Venus, integral and vertical concentration measurements of minor constituents on Mars and Venus, wind and temperature on Titan. This provides information for heat balance and global atmospheric dynamics recovery, which is essential for comparison with 3D general circulation models.

To date direct wind measurements on planetary scale are only possible by means of ground-based telescopic observations with ultra-high resolution heterodyne spectrometers in the infrared and microwave spectral ranges. Such instruments are unique, being developed by only a few groups worldwide and upgraded slowly relative to the progress in infrared photonic technology. The development of heterodyne infrared spectroscopy for planetary astronomy based on modern technology would provide continuous air flow monitoring by means of modest meter-class telescopes. Such monitoring would provide data for numerical models verification and assimilation, required to step forward from climate models to prognostic ones.

2. Middle IR fiber devices development

MIR fiber application is still very limited due to absence of commercially available MIR fiber based devices, e.g. couplers. However, in past few years significant progress in developing of chalcogenide and fluoride fiber based devices were firstly presented[4]. Our group created theoretical model for chalcogenide fused fiber couplers and experimental setup for its fabrication and characterization. Optimal geometrical parameters for achieving required coupling ratio were studied with computer simulation. A custom workstation with NiCr electric heater to reach temperature of 100 – 350°C in heated region was developed.

3. MIR heterodyne spectrometer

The principal sketch of the MIR heterodyne spectrometer is presented on the Fig. 1. Incoming signal from a planet is received by IR telescope and then passes to the spectrometer's input aperture. After that this signal is being mixed with MIR QCL radiation via a free-space Pellicle beam splitter or

MIR fiber coupler and detected with a photo-detector (PD). In present work we used 7.8μ, 5.6μ and 10μ QCLs as local oscilators (LO) and TEC-cooled mercury-cadmium telluride (MCT) photodiodes with a bandwidth up to 1 GHz. Due to PDs nonlinear response with the respect to the electrical field, incoming signal is being down-converted form IR-frequency range to the radio-frequency range, so it is possible to retrieve its spectrum using high-frequency spectrum analyzer. In order to achieve extremely high level of LO frequency stability (~MHz) without long term temperature drifts we utilized frequency locking technique using QCL wavelength modulation and reference gas cell to record reference gas absorption line simultaneously with heterodyne measurements. In addition we used two black bodies for intensity calibration purposes and Fabry-Perot etalon for QCL frequency scale calibration.

For the purpose of miniaturisation, mass reduction and optical alignment simplification MIR fiber couplers are supposed to be used in the optical scheme of the instrument instead of the beam splitters. Single mode chalcogenide fiber of IHPS RAS was used for fiber coupler fabrication technique. First results were demonstrated for 3 um range[5].

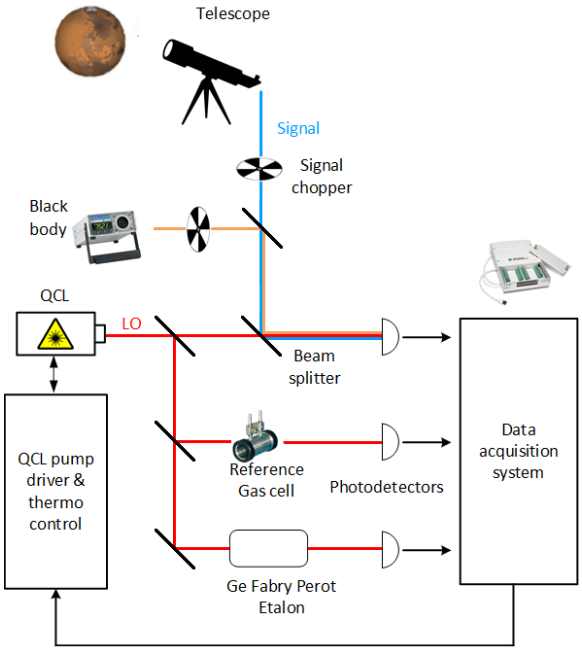

Figure 1: Scheme of mid-IR heterodyne spectrometer concept. Free-space beam splitter are planned to be replaced with mid-IR fiber couplers.

4. Summary and Conclusions

At present moment we created laboratory setup including all necessary elements of MIR heterodyne spectrometer that have been mentioned above. We have studied different components of noises of our system and found optimal value of LO power. The measured signal to noise ratio (SNR) with MCT PD was about 10 times greater than LO's shot noise (theoretical limit of heterodyne technique SNR) and limited by QCL relative intensity noise (RIN). However, applying additional filtering it is possible to reduce this value better than 5 shot noise level, which is typical to TEC cooled MCT PD[6]. Also we demonstrate heterodyne signal measurements using laboratory black body with temperature of 400 °C.

Acknowledgements

This work is supported by Russian Science Foundation grant #16-12-10559.

References

[1] Sornig, Manuela, et al.: Investigations of Dynamics and Temperatures in the Venusian Upper Atmosphere by Infrared Heterodyne Spectroscopy, 2011.

[2] Wirtz, Daniel, Guido Sonnabend, and Rudolf T. Schieder.: THIS: a tuneable heterodyne infrared spectrometer, Spectrochimica Acta Part A: Molecular and Biomolecular Spectroscopy, T. 58, № 11, pp. 2457-2463, 2002.

[3] Kostiuk T. et al.: Titan's stratospheric zonal wind, temperature, and ethane abundance a year prior to Huygens insertion, Geophysical research letters, T. 32, № 22, 2005.

[4] G. Stevens and T. Woodbridge: Mid-IR fused fiber coupler, Proc. of SPIE Vol. 9730 973007-7, 2016

[5] Dianov et al.: Singlemode optical fiber based on AsS gss, Rus. Nonorgan. Mater., vol 39, №6, pp. 741-745.

[6] Weidmann, Damien, et al.: Hollow waveguide photomixing for quantum cascade laser heterodyne spectro-radiometry, Optics express, T. 19, № 10, pp. 9074-9085, 2011.

EPSC Abstracts
Vol. 11, EPSC2017-855, 2017
European Planetary Science Congress 2017

Modelling the effects of gravity waves in the GEM-Mars GCM

L. Neary, F. Daerden and S. Viscardy
Royal Belgian Institute for Space Aeronomy, Brussels, Belgium (lori.neary@aeronomie.be)

Abstract

Parameterizations for orographic and non-orographic gravity waves are included in the GEM-Mars general circulation model (GCM) for low-resolution simulations. The impacts of these parameterizations on the temperature and winds in the upper atmosphere are examined and sensitivity studies are discussed.

1. Introduction

Gravity waves have been observed in the Martian atmosphere (e.g. Creasey et al., 2006, England et al., 2017) and are considered to have an important impact on the temperature and dynamics of the upper atmosphere.

The waves can be produced by flow over topography and propagate upwards to break in the upper atmosphere. This has the effect of depositing energy and momentum into the mean flow, altering the general circulation patterns. Other sources of gravity waves include wind shears and instabilities (called non-orographic). As it is computationally expensive and impractical to run a GCM at a horizontal resolution high enough to resolve gravity waves, it is necessary to parameterize their effects on the grid-scale winds in the model.

For Earth, it has been shown that the inclusion of a parameterization for both orographic and non-orographic wave drag in climate models is necessary to properly reproduce the extratropical stratospheric/mesospheric circulation. It has become increasingly accepted that the effects of these types of waves should also be included in Martian GCMs.

Here we evaluate the results of simulations made with the GEM-Mars GCM (Neary and Daerden, 2017) including parameterizations for both orographic and non-orographic gravity wave drag. A comparison of temperatures with those observed by the Mars Climate Sounder (MCS) (McCleese et al., 2007; Kleinböhl et al., 2009) help to assess the impact of these schemes.

2. Methods

We use the GEM-Mars GCM at a horizontal resolution of 4°×4° with 103 vertical levels up to a height of ~150 km to test the parameterizations. A brief description of the model is given here, as well as a description of the experiments performed.

1.1 Model description

GEM-Mars is grid-point model with a semi-Lagrangian advection scheme and a two-time-level semi-implicit integration method. For the 4°×4° horizontal resolution presented here, we use an integration time step of 1/48th of a Martian sol.

The model simulates interactive carbon dioxide-, dust-, water- and atmospheric chemistry cycles. Dust and water ice clouds are radiatively active. Size distributed dust is lifted by saltation and dust devils. The model includes 16 chemical species and has fully interactive photochemistry and gas-phase chemistry.

For the effects of orographic gravity wave drag, we use the scheme described by McFarlane (1987). The sub-grid scale parameters are derived from the high resolution MOLA topography. A low-level blocking scheme is also incorporated (Zadra et al., 2003). The gravity wave drag (GWD) scheme relies on the saturation concept of Lindzen (1981) to calculate the vertical structure of the wave drag force. The changes in the horizontal wind due to GWD depend on the sub-grid scale orographic variance, the atmospheric stratification, local density height scale and a tunable parameter defined as the product of a representative value of horizontal wavenumber and an efficiency factor less than one. For Mars, this parameter was reduced from the terrestrial value. In the wave

saturation regions, the wave amplitude is set according to a critical Froude number that is set to $\sqrt{0.5}$. This number is also considered a tuning parameter, but kept unchanged here.

For the effects of non-orographic gravity waves, we use the scheme of Hines (1997a,b). This method uses the Doppler-spread theory of gravity wave saturation where breaking is represented by imposing an upper limit to the range of vertical wavenumbers in the spectrum that can propagate above some altitude considered. The wavenumber upper limit at some azimuth j at a given altitude is given by:

$$m_j = \frac{N_0}{\Phi_1 \hat{\sigma}_j + \Phi_2 \hat{\sigma}_h + V_j - V_{0j}}$$

where N_0 is the buoyancy frequency at the source level, $\hat{\sigma}_j$ is the gravity wave wind standard deviation in direction j at altitude z, $\hat{\sigma}_h$ is the total gravity wave wind standard deviation at altitude z, V_j is the background wind in direction j at the source altitude and Φ_1 and Φ_2 are tunable parameters.

1.2 Scenarios/Experiments

Comparisons are made between simulations performed with orographic GWD only and with both orographic and non-orographic GWD.

There are several parameters to be set in the non-orographic GWD scheme. The initial simulation shown here uses a source level of ~10 km, 8 equally spaced azimuths, Φ_1 = 1.5, Φ_2 = 0.3, an equivalent horizontal wavenumber k^*, which represents the mean horizontal wavelength of the gravity wave spectrum of 200 km and a lower bound vertical wavenumber m_{min} which imposes a limit on the allowable maximum vertical wavelength of 12 km. For the orographic GWD scheme, we use a value 5×10^{-6} for the tunable parameter.

3. Results

The top row of Figure 1 shows the difference in zonal mean temperatures between the two simulations for the two equinox seasons. In the winter pole between 1 and 0.01 Pa, there is a cooling effect, on the order of ~20 K. Compared with MCS, the run with non-orographic GWD (bottom row in Figure 1) reduces the warm bias seen in the run with orographic GWD only (2nd row in Figure 1). The results are encouraging, but further tests are required to examine the sensitivity to parameters in both parameterizations.

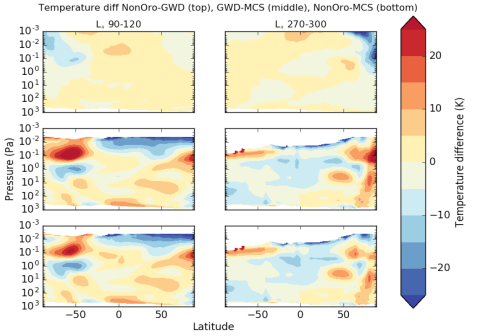

Figure 1 Temperature differences between 2 model simulations and MCS observations for 2 seasons: Left column is northern summer solstice (L_s=90-120°), right column is northern winter solstice (L_s=270-300°). The top row is the difference between the run with both orographic and non-orographic GWD (NonOro) and with orographic only (GWD). Middle row is NonOro-MCS, bottom row is GWD-MCS.

4. Summary and Conclusions

Initial tests with the non-orographic GWD parameterization included in GEM-Mars indicate that the strongest effects on temperature are seen in the solstice periods at L_s = 90° and 270° in the upper atmosphere of the winter polar region. Between 1 and 0.01 Pa, a cooling on the order of 20 K is seen in the winter pole, giving better agreement with MCS temperatures. There is little change during the equinox periods (not shown here).

As GEM-Mars has the capability of running at a much higher resolution, it is possible to make a reference simulation where gravity waves are resolved to help quantify their effects and constrain the values used in the parameterizations.

Acknowledgements

This work received funding from the ESA PRODEX Office under the Exo-Mars NOMAD project.

References

Creasey, J.E., Forbes, J.M., Hinson, D.P., 2006. Global and seasonal distribution of gravity wave activity in Mars' lower atmosphere derived from MGS radio occultation data. Geophysical Research Letters 33. doi:10.1029/2005GL024037

England, S.L., Liu, G., Yiğit, E., Mahaffy, P.R., Elrod, M., Benna, M., Nakagawa, H., Terada, N., Jakosky, B., 2017. MAVEN NGIMS observations of atmospheric gravity waves in the Martian thermosphere: Gravity Wave Observations at Mars. Journal of Geophysical Research: Space Physics. doi:10.1002/2016JA023475

Hines, C., 1997a. Doppler-spread parameterization of gravity-wave momentum deposition in the middle atmosphere. Part 1: Basic formulation. Journal of Atmospheric and Solar-Terrestrial Physics 59.

Hines, C.O., 1997b. Doppler-spread parameterization of gravity-wave momentum deposition in the middle atmosphere. Part 2: Broad and quasi monochromatic spectra, and implementation. Journal of Atmospheric and Solar-Terrestrial Physics 59, 387–400.

Kleinböhl, A., Schofield, J.T., Kass, D.M., Abdou, W.A., Backus, C.R., Sen, B., Shirley, J.H., Lawson, W.G., Richardson, M.I., Taylor, F.W., Teanby, N.A., McCleese, D.J., 2009. Mars Climate Sounder limb profile retrieval of atmospheric temperature, pressure, and dust and water ice opacity. Journal of Geophysical Research 114. doi:10.1029/2009JE003358

Lindzen, R.S., 1981. Turbulence and stress owing to gravity wave and tidal breakdown. J. Geophys. Res 86, 9707–9714. doi:10.1029/JC086iC10p09707

McCleese, D.J., Schofield, J.T., Taylor, F.W., Calcutt, S.B., Foote, M.C., Kass, D.M., Leovy, C.B., Paige, D.A., Read, P.L., Zurek, R.W., 2007. Mars Climate Sounder: An investigation of thermal and water vapor structure, dust and condensate distributions in the atmosphere, and energy balance of the polar regions. Journal of Geophysical Research 112. doi:10.1029/2006JE002790

McFarlane, N.A., 1987. The effect of orographically excited gravity wave drag on the general circulation of the lower stratosphere and troposphere. Journal of the Atmospheric Sciences 44, 1775–1800.

Neary, L. and Daerden, F., 2017. The Gem-Mars General Circulation Model for Mars: Description and Evaluation, Icarus (in review).

Zadra, A., Roch, M., Laroche, S., Charron, M., 2003. The subgrid-scale orographic blocking parametrization of the GEM Model. Atmosphere-Ocean 41, 155–170. doi:10.3137/ao.410204

EPSC Abstracts
Vol. 11, EPSC2017-861, 2017
European Planetary Science Congress 2017

Mars Radiative Balance including high altitude water

JT Erwin (1,2), RV Yelle (2)
(1) The Royal Belgian Institute for Space Aeronomy, Brussels, Belgium, (2) The Lunar and Planetary Laboratory, University of Arizona, Tucson, USA (jt.erwin@aeronomie.be)

Abstract

Recent spacecraft mission (e.g. Mars Express and Maven) have greatly expanded our understanding of the composition, structure, and dynamics of the Martian atmosphere. And with the ExoMars Trace Gas Orbiter recent arrival and soon to begin its scientific phase, it is necessary to have an updated model of Mars atmospheric structure and IR radiative balance. In this presentation, we acknowledge and adapt previous modeling and update their results to accommodate the most recent observational and modeling results, including recent high altitude water.

1. Introduction

Recent spacecraft missions have probed the atmospheric structure to gain understanding of many processes. Some of the observations relevant to this study are discussed below.

These observations justify a re-evaluation of the compositional and thermal structure derived from modeling efforts. Also, by considering the results in the lower and upper atmosphere together, we can remove many assumption and gain a consistent understanding of the atmospheric structure.

1.1 Recent Observation and Models

Observations of enhanced and variable hydrogen escape has been performed by the Hubble Space Telescope and Mars Express. This loss rate could explain the loss of water from an ancient Mars. But the upward flux is larger then the lower atmosphere can support, and modelling has so far been unable to explain this discrepancy. The SPICAM instrument aboard Mars Express has observed water vapor in the upper atmosphere that is in excess of the saturation limit [1,2].

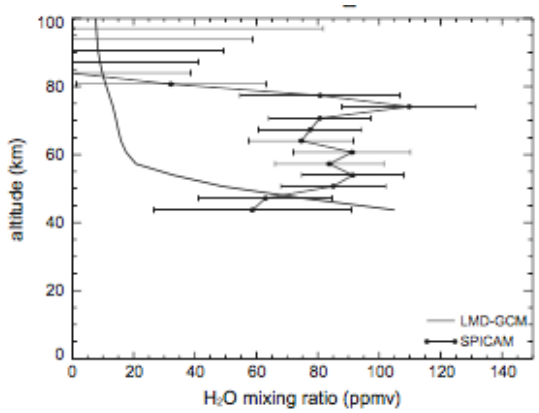

Figure 1: Example observed water vapor from [2].

Water in the upper atmosphere has import ramifications as a source of escaping hydrogen. Water vapor as a source of odd hydrogen is an import species in the photochemical recycling of CO2, and can affect the abundance of many species throughout the atmosphere, and therefore their ability to escape the atmosphere or be absorbed onto the surface [3].

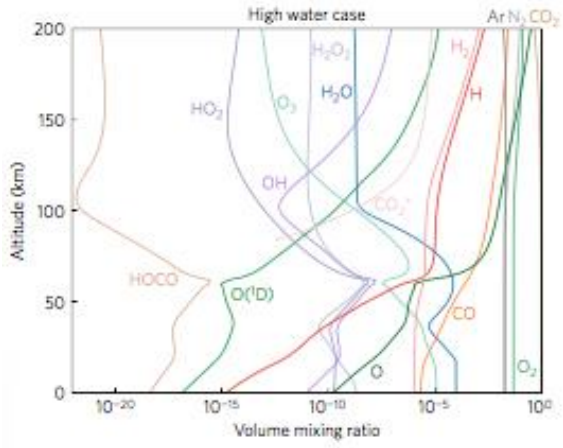

Figure 2: Example converge photochemical solution from [3] including an artificial water vapor peak.

The MAVEN spacecraft has been performing UV occultations and in situ density measurements to better our understanding of the current structure and rates of escape of the Martian atmosphere, which in turn help us infer the history of the atmosphere. It has shown there is an enhanced rate of escape of hydrogen that needs to be better explained by modeling.

1.2 Non-LTE Radiative Transfer

Many of the species in the above photochemical results are import to the IR radiative balance in the upper atmosphere, which is important for the temperature and structure of the stratosphere. This can in turn affect the diffusion and escape of atoms and molecules through the thermosphere.

Carbon dioxide is the dominant component of the atmosphere, and as a strong greenhouse gas it is essentially to the IR radiative balance in the atmosphere. It has a complicated vibrational structure, and the non-LTE populations have been investigated extensively in the Martian atmosphere [4,5], as well as in the Venusian atmosphere. In addition, water vapor is a strong radiator, and its presence in the upper atmosphere suggests it may have an important effect on the thermal structure.

2. Summary and Conclusions

In preparation for the next set of spacecraft observations of the Martian atmosphere, this work aims to concurrently model the radiative-thermal balance with updated non-LTE rates, photochemistry, and diffusion and escape. This is used to evaluate our understanding principal processes that determine the structure of the atmosphere, and to provide base case on which to plan future observations.

Acknowledgements

This work had been supported in part by the Belgian Education Exchange Foundation.

References

[1] Maltagliati, L., Montmessin, F., Fedorova, A., Korablev, O., Forget, F., & Bertaux, J. L. Evidence of Water Vapor in Excess of Saturation in the Atmosphere of Mars. *Science*, 2011.

[2] Maltagliati, L., Montmessin, F., Korablev, O., Fedorova, A., Forget, F., Määttänen, A., et al. Annual survey of water vapor vertical distribution and water–aerosol coupling in the martian atmosphere observed by SPICAM/MEx solar occultations. *Icarus*, 2013.

[3] Chaffin, M. S., Deighan, J., Schneider, N. M., & Stewart, A. I. F. Elevated atmospheric escape of atomic hydrogen from Mars induced by high-altitude water. *Nature Geoscience*, 2017.

[4] López-Valverde, M. A. & López-Puertas, M. A non-local thermodynamic equilibrium radiative transfer model for infrared emissions in the atmosphere of Mars: 1. Theoretical basis and nighttime populations of vibrational levels. *Journal of Geophysical Research*, 1994.

[5] López-Valverde, M. A. & López-Puertas, M. A non-local thermodynamic equilibrium radiative transfer model for infrared emission in the atmosphere of Mars. 2: Daytime populations of vibrational levels. *Journal of Geophysical Research,* 1994.

EPSC Abstracts
Vol. 11, EPSC2017-885, 2017
European Planetary Science Congress 2017

Investigating circular patterns in linear polarization observations of Venus

G. Mahapatra (1), D.M. Stam (1), Loïc Rossi (1), Michiel Rodenhuis (2), Frans Snik (2) and C.U.Keller (2)
(1) Faculty of Aerospace Engineering, Delft University of Technology, Kluywverweg 1, 2629HS Delft, The Netherlands
(2) Sterrewacht Leiden, Leiden Observatory, Leiden, The Netherlands

Abstract

In this work, we analyse linear polarization data of the planet at a distance, obtained with the Extreme Polarimeter (ExPo) on the William Herschel Telescope on La Palma. These spatially resolved, high-accuracy polarization observations of Venus show faint circular patterns centered on the sub-solar point that are absent in the flux observations. So far, careful analyses have ruled out instrumental effects which leaves us to wonder about atmospheric properties on Venus as the cause of the circular patterns. Using numerical simulations of the flux and polarization of sunlight that is reflected by Venus, we have investigated the relation between the observed patterns and several atmospheric properties, such as variations in particle sizes, composition, density and altitude. We discuss the plausibility of the possible causes in the view of the current knowledge of the composition and dynamical processes in Venus's atmosphere.

1. Introduction

The dynamic nature of Venusian climate has been a source of constant study due to its dense CO_2 atmosphere combined with sulphuric acid clouds and hazes. Gravity waves of various shapes and sizes have been observed on the clouds starting with Mariner 10 and Pioneer Venus ([3]), the Venera mission and the Magellan spacecrafts. The European VEx mission has studied such waves in great detail and has reported the fluctuations to be in temperature and cloud layers ([1]). Recently planetary wide gravity waves were detected by the Japanese Akatsuki mission ([2]).

Photopolarimetry as a tool, has played a vital role in constraining the cloud and haze particle properties of Venus as was shown by [4]. In this work we present the ground-based observations of Venus using the Extreme Polarimeter (ExPo) instrument at the William Herschel Telescope on La Palma at different wavelengths in visible, using both narrow and broad-band filters. We also present our modelling efforts to explain the observed fluctuations in polarized flux using our doubling-adding radiative transfer code (see [8]) which accounts for multiple scattering of light from the Venusian atmosphere and computes all the components of polarized light for a spatially resolved disk with multiple layers of cloud and gas with definable particle properties.

2. Observations of Venus

Our Venus observations have been carried out with the ExPo imaging polarimeter installed at the William Herschel Telescope on La Palma. This instrument has been designed for the observation of faint, linearly polarized light scattered by circum-stellar material. The instrument is very sensitive to linearly polarized light, capable of reaching a sensitivity of 10^{-4} provided enough photons are available. At the time of observations, the Venus phase angle was 48.7° and its angular diameter 12.5". Six different filters were used, four narrow-band and two broadband. The results we report are not suspected to be caused by physical effects in the corresponding spectral lines.

In all our observations we see increased polarization in regions near both poles. A second feature, observed only in the narrowband images, is an intriguing structure consisting of several thin rings extending across the illuminated disk of Venus. Calibrated polarized intensity images are shown for two filters in Fig. 1.

3. Model simulations

We describe the sunlight that is incident on a planet and the scattered light by the planet by Stokes vectors I, Q, U and V ([9]). Our radiative transfer code computes all the components of polarized flux for a wavelength of choice from a spatially resolved planet with a horizontally homogeneous but vertically inhomogeneous atmosphere (see [8]). It assumes a plane-parallel approximation.

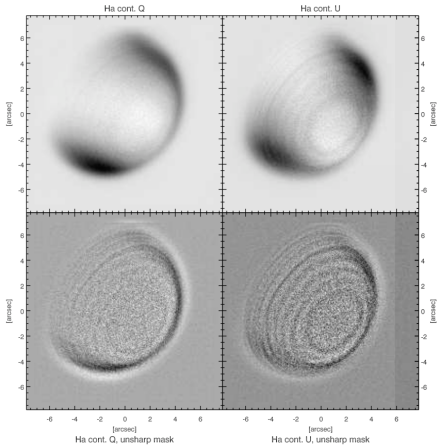

Figure 1: Calibrated Stokes Q and U images (top) and with an unsharp mask subtracted (bottom).

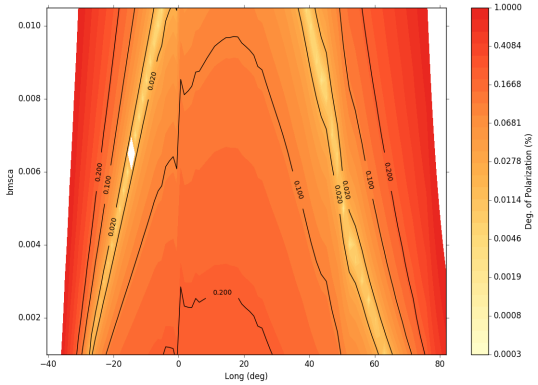

Figure 2: Contour plot showing fluctuations degree of polarization with increasing scattering optical thickness for a model Venus atmosphere. The spikes around 0° longitude are a numerical effect.

We carry out our simulations for a model Venus CO_2 atmosphere with cloud layers of aerosol optical thickness, b_{aer}=256, to simulate a semi-infinite cloud layer. The haze layers above the cloud deck has a scattering optical thickness, b_{aer}=0.1. Finally we set our model with another gas layer above the haze layer to simulate Venus conditions, with a standard molecular scattering optical thickness, b^m_{sca}=0.005. Since the observations show planet-wide faint fluctuations in polarized flux, we rule out the possibility of variations observed to be caused by clouds and hazes. Fig. 2 shows the simulations of increasing b^m_{sca} above the base cloud+haze+gas layer model with respect to the standard value, along the longitude.

Our model simulations show the sensitivity of changes in b^m_{sca} to the resulting polarized flux. We find that slight changes in b^m_{sca} (in the order of 10^{-3}) results in significant changes (in the order of 10^{-1}) in polarized flux. Such changes might be explained due to the density variations in the gas layer above the clouds and haze.

References

[1] Piccialli, Arianna, et al. "High latitude gravity waves at the Venus cloud tops as observed by the Venus Monitoring Camera on board Venus Express." Icarus 227 (2014): 94-111.

[2] Fukuhara, Tetsuya, et al. "Large stationary gravity wave in the atmosphere of Venus." Nature Geoscience 10.2 (2017): 85-88.

[3] Rossow, William B., et al. "Cloud morphology and motions from Pioneer Venus images." Journal of Geophysical Research: Space Physics 85.A13 (1980): 8107-8128.

[4] Hansen, James E., and J. W. Hovenier. "Interpretation of the polarization of Venus." Journal of the Atmospheric Sciences 31.4 (1974): 1137-1160.

[5] Kawabata, K., et al. "Cloud and haze properties from Pioneer Venus polarimetry." Journal of Geophysical Research: Space Physics 85.A13 (1980): 8129-8140.

[6] Knibbe, Willem JJ, et al. "Analysis of temporal variations of the polarization of Venus observed by Pioneer Venus Orbiter." Journal of geophysical research 103 (1998): 8557-8574.

[7] Rossi, Loïc, et al. "Preliminary study of Venus cloud layers with polarimetric data from SPICAV/VEx." Planetary and Space Science 113 (2015): 159-168.

[8] Stam, D. M., and J. W. Hovenier. "Errors in calculated planetary phase functions and albedos due to neglecting polarization." Astronomy & Astrophysics 444.1 (2005): 275-286.

[9] Hansen, James E., and Larry D. Travis. "Light scattering in planetary atmospheres." Space science reviews 16.4 (1974): 527-610. APA

EPSC Abstracts
Vol. 11, EPSC2017-886-1, 2017
European Planetary Science Congress 2017

Planetary-scale streak structures produced in a high-resolution simulation of Venus atmosphere

H. Kashimura (1), N. Sugimoto (2), M. Takagi (3), Y. Matsuda (4), W. Ohfuchi (1), T. Enomoto (5), K. Nakajima (6), M. Ishiwatari (7), T. M. Sato (8), G. L. Hashimoto (9), T. Satoh (8), Y. O. Takahashi (1), Y.-Y. Hayashi (1)
(1) Department of Planetology/Center for Planetary Science, Kobe University, Kobe, Japan (hiroki@gfd-dennou.org), (2) Keio University, (3) Kyoto Sangyo University, (4) Tokyo Gakugei University, (5) DPRI, Kyoto University, (6) Kyushu University, (7) Hokkaido University, (8) ISAS, JAXA, (9) Okayama University

Abstract

Planetary-scale streak structures captured by the IR2 camera onboard AKATSUKI was reproduced in a high-resolution simulation of Venus Atmosphere. We have found that the streak structures are extending from the polar vortices and synchronized in both hemispheres. Our experiments suggest that a low-stability layer is a key for forming the planetary-scale streak structures.

1. Introduction

Night-side images of Venus taken by the IR2 camera onboard the Venus Climate Orbiter/AKATSUKI has shown many features of the lower cloud layer. One prominent feature is a bright planetary-scale streak structure extending from high-latitudes to low latitudes on both hemispheres. IR2 night-side images capture infrared radiated from the near-surface atmosphere, and the infrared can be blocked by clouds. Therefore, bright regions indicate thin-cloud regions.

2. Numerical model and set up

We have performed a high-resolution simulation of the Venus atmosphere by a simplified general circulation model, which is based on AFES: the Atmospheric general circulation model For the Earth Simulator. The horizontal resolution is T159 (i.e., about 0.75 deg x 0.75 deg grids) and the vertical resolution is about 1 km with the model top at 120 km. In the model, the atmosphere is dry and simply forced by the solar heating with the diurnal change and Newtonian cooling that relaxes the temperature to the horizontally uniform basic temperature which has a virtual static stability of the Venus atmosphere. In the basic temperature profile, we have introduced a low-stability (0.1 K/km) layer from 55 km to 60 km, which is suggested by the recent radio occultation observation.

3. Results

In this study, we have found that a planetary-scale streak structure similar to that observed by the IR2 night-side image is produced in the vertical velocity field above the low-stability layer in the simulated atmosphere. Large streaks are shown by strong downward flow. This is consistent with the observation because the downward flow can decrease cloud amounts and make a thin-cloud region. Seen from above the pole, the simulated streak structure shapes a huge spiral extending from the polar vortex to low latitudes. Such spiral may correspond to that observed by VIRTIS onboard Venus Express. The streak structures on both hemispheres are synchronized, that is the streak structures located in the same longitude.

We have also performed numerical experiments with increasing the static stability of the "low-stability layer". The streak structure does not appear in the case that the stability is set to 2.0 K/km. Our results suggest that the neutral stability layer plays an important role on the formation of the planetary-scale streak structure. The fact that our simplified atmospheric GCM has produced the structure similar to the cloud pattern observed in the Venus atmosphere implies that the cloud pattern is dominated by the atmospheric circulation.

Acknowledgements

We thank the all members related to the AKATSUKI project. This study was conducted under the joint research project of the Earth Simulator Center with title “Simulations of Atmospheric General Circulations of Earth-like Planets by AFES.” This study was supported by JSPS KAKENHI 16H02225 and 16K17809, and also by MEXT as "Exploratory Challenge on Post-K computer" (Elucidation of the Birth of Exoplanets [Second Earth] and the Environmental Variations of Planets in the Solar System).

EPSC Abstracts
Vol. 11, EPSC2017-938, 2017
European Planetary Science Congress 2017

Trace gas retrievals for the ExoMars Trace Gas Orbiter Atmospheric Chemistry Suite mid-infrared solar occultation spectrometer

K. S. Olsen (1), F. Montmessin (1), A. Fedorova (2), A. Trokhimovskiy (2), O. Korablev (2) and the ExoMars TGO Science Working Team
(1) Laboratoire Atmosphères, Milieux, Observations Spatiales (LATMOS/CNRS), Paris, France, (2) Space Research Institute (IKI), Moscow, Russia (kevin.olsen@latmos.ipsl.fr)

Abstract

ExoMars is a two-part mission to Mars jointly led by ESA and Roscosmos. The first phase was launched in March 2016 and consisted of the Trace Gas Orbiter (TGO) and Schiaparelli lander. The TGO successfully entered orbit around Mars in October 2016 and has since begun a crucial aerobreaking campaign to circularize its orbit with a nominal 400 km altitude and 2 hr period. There are four scientific instruments on TGO: the Atmospheric Chemistry Suite (ACS), the Nadir and Occultation for Mars Discovery (NOMAD) spectrometer, the Colour and Stereo Surface Imaging System (CaSSIS), and the Fine-Resolution Epithermal Neutron Detector (FREND). This presentation will focus on trace gas retrievals for the mid-infrared (MIR) channel of the ACS instrument operating in solar occultation mode.

ACS is a set of three spectrometers that are designed to better characterize the atmosphere of Mars with unprecedented accuracy. It aims to detect and quantify unknown trace gases diagnostic of active geological or biological processes, to map their distribution and attempt to identify sources, and to refine our knowledge of the vertical distribution of major and minor atmospheric gases. It has three channels: near-infrared (NIR), thermal-infrared (TIRVIM) and MIR. The NIR channel is combination of an echelle grating and an acousto-optical tunable filter (AOTF), and is similar to the Ultraviolet and Infrared Atmospheric Spectrometers for Mars and Venus (SPICAM/V) on Mars Express and Venus Express (Korablev et al., 2006; Bertaux et al., 2007). It has a spectral range of 0.73–1.6 μm and operates in nadir mode. It is intended to provide mapping support to solar occultation measurements. TIRVIM is a small Fourier transform spectrometer with a spectral range of 2–17 μm and resolution of 0.2 cm^{-1}. It has heritage from the Mars Express Planetary Fourier Spectrometer (PFS), operates in both nadir and solar occultation mode, and will be able to measure the physical state of the atmosphere (vertical profiles of temperature, pressure and dust opacity). NOMAD is also a multi-channel spectrometer with complimentary objectives to ACS. It consists of a pair of combination echelle-AOTF spectrometers, much like SPICAM/V and ACS NIR, that operate in both nadir and solar occultation mode. In its original configuration, TGO carried a high-resolution Fourier transform spectrometer (FTS) covering a wide spectral range to detect trace gases (Wennberg et al., 2011), supported by the nadir-viewing NOMAD instrument capable of carrying out trace gas mapping studies. The ACS MIR channel aims to reproduce the capabilities of the FTS using a novel concept for atmospheric studies: a cross-dispersion spectrometer combining an echelle grating with a wide blaze angle and secondary, steerable diffraction grating (Korablev et al., 2017). It is capable of finer resolution than its echelle-AOTF counterparts, but is limited in its instantaneous spectral range compared to its FTS predecessor.

The ACS MIR block is thermally isolated from TIRVIM and coupled to NIR, but shares a common electronics block. It consists of an entry telescope and collimator, a large echelle grating (107×240 mm, 3.03 grooves per mm), a steerable pair of secondary grating mirrors, and a Sofradir MCT array detector The low-density echelle grating at a high blaze angle (63.43°) provides overlapping spectra at high orders. The secondary grating separates the orders and the resulting spectra are recorded by the detector with 640 pixels in the x direction corresponding to wavelength, and 512 pixels in the y direction corresponding to order. Several spectra are recorded for each order on sequential pixel rows. The secondary grating has two reflective gratings mounted side-by-side that can rotated. We

will use ten secondary grating positions, each with an instantaneous spectral width of around 16 cm^{-1} between 2380 and 4350 cm^{-1}. The spectral orders and range covered by each position are given in Table . During the acquisition of a set of solar occultation spectra, the grating position can be changed between each measurement, allowing for the retrieval of vertical profiles for several trace gases and major species at the same time.

Table 1: Spectral ranges and orders of secondary grating positions.

Grating angle	Diffraction orders	Minimum wavelength	Maximum wavelength
7.5°	205–213	2.790 µm	2.899 µm
5.7°	214–223	2.665 µm	2.790 µm
3.9°	224–235	2.529 µm	2.665 µm
2.1°	236–248	2.397 µm	2.529 µm
0.3°	249–258	2.304 µm	2.397 µm
-3.3°	142–149	3.984 µm	4.209 µm
-5.1°	150–161	3.688 µm	3.984 µm
-6.9°	162–174	3.414 µm	3.688 µm
-8.7°	175–190	3.127 µm	3.413 µm
-10.5°	191–208	2.857 µm	3.127 µm

Raw spectral images will be processed by ESA at the European Space Operations Centre (ESOC), calibrated spectra will be produced by Roscosmos at the Space Research Institute (IKI), and there are two parallel trace gas retrieval operations: at IKI, based on SPICAV retrievals, and at LATMOS, presented here. All three channels of the ACS instrument, and the other TGO instruments have been switched on and checked out on several occasions between launch and orbit capture.

1. ACS MIR Retrievals

The LATMOS ACS MIR retrievals will be based on software prepared for the high-resolution solar occultation FTS from the original TGO configuration. We will use the GGG software suite maintained at NASA's Jet Propulsion Laboratory. GGG is derived from early versions of the Occultation Display Spectra (ODS) software developed or the ATMOS spectrometer flown on the space shuttles (Norton and Rinsland, 1991). It is designed to be a multipurpose and robust spectral fitting suite and is currently used for the MkIV balloon FTS missions (Toon, 1991) and the Total Carbon Column Observing Network (TCCON) of ground-based FTSs (Wunch et al., 2011).

The main component of GGG is GFIT, which computes volume absorption coefficients for each gas in the fitting spectral range, computes a spectrum line-by-line, and fits the computed spectrum to the measured spectrum using a non-linear Levenberg-Marqhardt minimization. The state vector contains the continuum level and tilt, and volume mixing ratio (VMR) scaling factors (VSFs) for each target gas. GFIT is capable of fitting multiple gases at the same time. The VSF is a multiplicative scaling factor applied to the *a priori* VMR vertical profile. In principle, GFIT only modifies the magnitude, and not the shape of, the *a priori* VMR vertical profile. However, in solar occultation mode, the *a priori* can be scaled for each observed spectrum at each tangent altitude.

The computed spectrum is calculated using the HITRAN 2012 spectral line list (Rothman et al., 2013), with modifications provided by JPL for the TCCON collaboration. Line broadening coefficients for CO_2 need to be modified to reflect the lower pressure and colder temperatures of the Martian atmosphere, and collisional-induced broadening in 95% CO_2 atmosphere. We are implementing new broadening parameters from Brown et al. (2007) and Lavrentieva et al. (2014). In theory, the retrievals done with GGG are independent of the VMR *a priori*. For consistency, a single set of *a priori* VMR vertical profiles will be used. These will be refined as our knowledge of the Mars atmosphere increases. The VMRs of major interfering species, CO_2 and H_2O, may be updated for each occultation.

Temperature and pressure are vital parameters for accurately computing absorption line depths. A first attempt at spectral fitting will be done using climatological models from the Mars Climate Database. New observations of temperature and pressure made by the Mars Reconaissance Orbiter's Mars Climate Sounder and the TIRVIM channel will be assimilated into the LMD General Circulation Model. When a more accurate assimilation is ready, the retreivals will be reprocessed using the updated *a priori* vertical profiles of temperature, pressure, CO_2 VMR, and H_2O VMR.

Much work is being done to investigate the limits of the retrieval algorithm by generating synthetic spectra for different atmospheric conditions (temperature, pressure, dust loading, and trace gas abundances). To test our ability to resample the spectra, very high resolution spectra are computed first, then resampled to the realistic, non-uniform spacing of an MIR order. Noise is added to the spectra, they are resampled to a uni-

form fitting grid, and spectral fitting is performed using generic *a priori* to see how well the trace gas VMR vertical profiles used to create the synthetic spectra are reproduced.

We will introduce the ExoMars TGO mission, the ACS instrument and summarize the results of pre-science-operations instrument check-outs. The GGG software suite will be introduced, as will be the work done to adapt it for use at Mars with ACS MIR, such as modelling the ACS MIR instrument line shape. We will show our simulations of solar occultation transmission spectra, and present results of our effort to fit these spectra and retrieve vertical profiles of trace gas VMRs.

References

Bertaux, J.-L., Nevejans, D., Korablev, O., Villard, E., Quémerais, E., Neefs, E., Montmessin, F., Leblanc, F., Dubois, J. P., Dimarellis, E., Hauchecorne, A., Lefèvre, F., Rannou, P., Chaufray, J. Y., Cabane, M., Cernogora, G., Souchon, G., Semelin, F., Reberac, A., Van Ransbeek, E., Berkenbosch, S., Clairquin, R., Muller, C., Forget, F., Hourdin, F., Talagrand, O., Rodin, A., Fedorova, A., Stepanov, A., Vinogradov, I., Kiselev, A., Kalinnikov, Y., Durry, G., Sandel, B., Stern, A., and Gérard, J. C.: SPICAV on Venus Express: Three spectrometers to study the global structure and composition of the Venus atmosphere, Planet. Space Sci., 55, 1673–1700, doi:10.1016/j.pss.2007.01.016, 2007.

Brown, L. R., Humphrey, C. M., and Gamache, R. R.: CO_2-broadened water in the pure rotation and ν_2 fundamental regions, J. Mol. Spectrosc., 246, 1–21, doi:10.1016/j.jms.2007.07.010, 2007.

Korablev, O., Bertaux, J.-L., Fedorova, A., Fonteyn, D., Stepanov, A., Kalinnikov, Y., Kiselev, A., Grigoriev, A., Jegoulev, V., Perrier, S., Dimarellis, E., Dubois, J. P., Reberac, A., Van Ransbeeck, E., Gondet, B., Montmessin, F., and Rodin, A.: SPICAM IR acousto-optic spectrometer experiment on Mars Express, J. Geophys. Res., 111, E09S03, doi:10.1029/2006JE002696, 2006.

Korablev, O., Montmessin, F., Trokhimovskiy, A., Fedorova, A. A., Shakun, A. V., Grigoriev, A. V., Moshkin, B. E., Ignatiev, N. I., Forget, F., Lefévre, F., Anufreychik, K., Kozlova, T. O., Semena, N., Ivanov, Y. S., Kungurov, A., Kalinnikov, Y. K., Titov, A. Y., Stepanov, A. V., Zharkov, A., Semenov, A., Patsaev, D., Martynovich, F., Sidorov, A., Viktorov, A., Timonin, D., Sazonov, O., Shashkin, V., Santos-Skripko, A., Maslov, I., Dzuban, I., Stupin, I., Merzlyakov, D., Makarov, V., Nikolskiy, Y., Altieri, F., Arnold, G., Belyaev, D. A., Betsis, D. S., Bertaux, J. L., Duxbury, N., Encrenaz, T., Gerard, J. C., Guerlet, S., Grassi, S., Fouchet, T., Hartogh, P., Kasaba, Y., Khatuntsev, I., Krasnopolsky, V. A., Kuzmin, R. O., Lellouch, E., Lopez-Valverde, M. A., Luginin, M., Määtänen, A., Marcq, E., Martin Torres, J., Medvedev, A., Millour, E., Shematovich, V. I., Olsen, K. S., Patel, M., Quantin-Nataf, C., Rodin, A. V., Thomas, I. Thomas, N., Vazquez, L., Vincendon, M., Wilquet, V., Wilson, C., Zasova, L. V., Zelenyi, L. M., and Zorzano, M. P.: The Atmospheric Chemistry Suite (ACS) of three spectrometers for the ExoMars 2016 Trace Gas Orbiter, Space Sci. Rev., *in press*, 2017.

Lavrentieva, N. N., Voronin, B. A., Naumenko, O. V., Bykov, A. D., and Fedorova, A. A.: Linelist of $HD^{16}O$ for study of atmosphere of terrestrial planets (Earth, Venus and Mars), Icarus, 236, 38–47, doi:10.1016/j.icarus.2014.03.037, 2014.

Norton, R. H. and Rinsland, C. P.: ATMOS data processing and science analysis methods, Appl. Opt., 30, 389–400, doi:10.1364/AO.30.000389, 1991.

Rothman, L. S., Gordon, I. E., Babikov, Y., Barbe, A., Chris Benner, D., Bernath, P. F., Birk, M., Bizzocchi, L., Boudon, V., Brown, L. R., Campargue, A., Chance, K., Cohen, E. A., Coudert, L. H., Devi, V. M., Drouin, B. J., Fayt, A., Flaud, J.-M., Gamache, R. R., Harrison, J. J., Hartmann, J.-M., Hill, C., Hodges, J. T., Jacquemart, D., Jolly, A., Lamouroux, J., Le Roy, R. J., Li, G., Long, D. A., Lyulin, O. M., Mackie, C. J., Massie, S. T., Mikhailenko, S., Müller, H. S. P., Naumenko, O. V., Nikitin, A. V., Orphal, J., Perevalov, V., Perrin, A., Polovtseva, E. R., Richard, C., Smith, M. A. H., Starikova, E., Sung, K., Tashkun, S., Tennyson, J., Toon, G. C., Tyuterev, V. G., and Wagner, G.: The HITRAN2012 molecular spectroscopic database, J. Quant. Spectrosc. Radiat. Transfer, 130, 4–50, doi:10.1016/j.jqsrt.2013.07.002, 2013.

Toon, G. C.: The JPL MkIV interferometer, Opt. Photonics News, 2, 19–21, doi:10.1364/OPN.2.10.000019, 1991.

Wennberg, P. O., Hipkin, V. J., Drummond, J. R., Dalhousie, U., Toon, G. C., Allen, M., Blavier, J.-F., Brown, L. R., Kleinböhl, A., Abbatt, J. P. D., Sherwood Lollar, B., Strong, K., Walker, K. A., Bernath, P. F., Clancy, R. T., Cloutis, E. A., Desmarais, D. J., Eiler, J. M., Yung, Y. L., Encrenaz, T., and McConnell, J. C.: MATMOS: the Mars atmospheric Trace Molecule Occultation Spectrometer, in: Mars Atmosphere: Modelling and observation, edited by Forget, F. and Millour, E., pp. 480–481, 2011.

Wunch, D., Toon, G. C., Blavier, J. L., Washenfelder, R. A., Notholt, J., Connor, B. J., Griffith, D. W. T., Sherlock, V., and Wennberg, P. O.: The Total Carbon Column Observing Network, Phil. Trans. R. Soc. A, 369, 2087–2112, doi:10.1098/rsta.2010.0240, 2011.

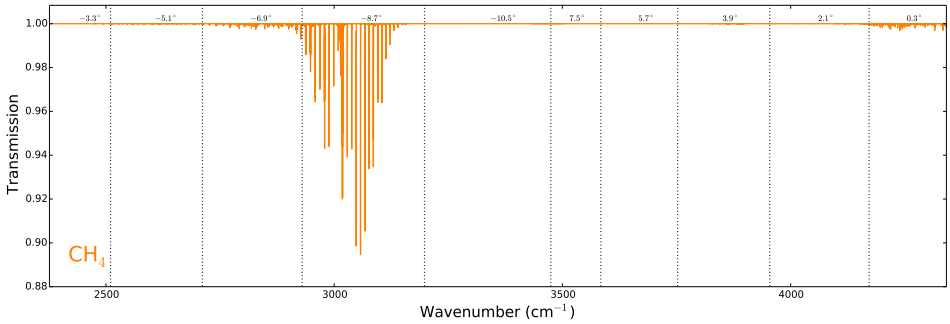

Figure 1: An excerpt from the ACS MIR spectral atlas showing the contribution from methane to the solar occultation transmission spectra. This spectrum shows all secondary grating positions, but the ACS MIR instrument can only record a spectrum for one position instantaneously. The dashed vertical lines show the range of each position. To search for methane, the $-8.7°$ secondary grating position will be used. This spectrum represents a tangent altitude of 20 km and a peak methane abundance of 6 ppmv.

EPSC Abstracts
Vol. 11, EPSC2017-962-1, 2017
European Planetary Science Congress 2017

A new method to analyze UV stellar occultation data

D. Evdokimova (1, 2), L. Baggio (2), F. Montmessin (2), D. Belyaev (1). J.-L. Bertaux (1,2)
(1) Space Research Institute of RAS, Moscow, Russia, (2) LATMOS, Paris, France (evd.dar@yandex.ru)

Abstract

SPICAV stellar occultation measurements in the UV composed a huge dataset concerning vertical distributions of CO_2, SO_2 and O_3 abundances on the night side of Venus mesosphere (80-130 km). Beside those absorption features the instrument was also sensitive to emissions from different extended sources in addition to a star light in spectral range from 110 to 320 nm. These emissions, hereafter «stray light», result in systematic errors when retrieving gaseous abundances from transmission spectra. In this paper we present a new method of data processing and a classification of different types of stray light at SPICAV UV stellar occultations. The method was developed on a basis of Richardson-Lucy algorithm including: (a) deconvolution process of measured star light and (b) separation of extra emissions registered by the spectrometer.

1. Introduction

Chemistry and dynamics of Venus CO_2-atmosphere are greatly affected by vertical distribution of trace gases (SO_2, O_3, HCl, H_2O, etc.). The most powerful method to achieve high vertical resolution in atmospheric profiles is occultation. Stellar occultation experiment onboard the ESA's Venus Express mission allowed to study night Venus atmosphere within altitude range of 80-130 km that was being observed by an imaging UV spectrometer SPICAV in 2006-2014 [1]. The instrument's spectral range of 118-320 nm was sensitive to absorption bands of CO_2, SO_2, SO and O_3 [5, 6].

SPICAV simultaneously records 5 spectra binned within neighbor pixel lines on the CCD matrix. The light from a point star mainly comes to the central bin, while it is spatially and spectrally distributed by the instrument point-spread function (PSF) over the CCD. When star is occulted in the atmosphere some additional light (hereafter "stray light") will come to those five spectral bins from different altitudes on 80-130 km. The present work is devoted to the stray light extraction from the stellar occultation spectra to improve the atmospheric transmission retrieval.

2. Stray light registering in stellar occultations

Nitric oxide (NO) glow, Lyman-alpha emission and reflected sun light are main sources of the stray light.

NO emission in the spectral range of 180-280 nm is formed at altitudes about 110 km at night [2]. It is the most intense and well defined type of stray light. Its spatial distribution within the FOV makes the CCD illumination vary as a function of the relative position of the bright limb in the FOV.

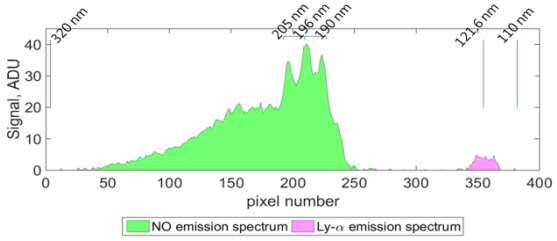

Figure 1: NO emission and atmospheric Lyman-a in the shadow of the atmosphere (40-60 km), orbit 2721A05. Observation was done with slit.

Lyman-a emission is produced by interplanetary and Venusians hydrogen at 121,6 nm [3,4]. Lyman-a distorts star signal at altitudes where CO_2 absorption is weak. The Lyman-a line is well distinguishable in spectra measured with slit. For others it is integrated in large FOV and spread over about 250 pixels.

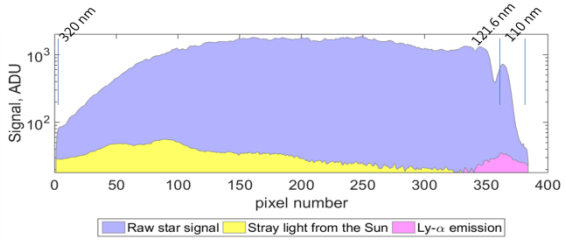

Figure 2: Star signal above 200 km with separated sun and Lyman-a illumination, orbit 2721A05.

The third type of stray light is sun light reflecting on Venus crescent or spacecraft surfaces. Its intensity is noticeable in the spectral range of 200-300 nm that overlaps the range of NO emission.

3. A new data processing algorithm

Taking into account the PSF distribution and stray light pollution [5] the spectra of five bands are

$$S_{expi} = \alpha_i S_{ref} T + S_{straylighti}, i = 1 \dots 5 \quad (1)$$

where α_i is the fraction of the PSF in the i-th band, S_{ref} is the star signal outside the atmosphere, T is atmospheric transmission determined by gases.

The gaseous profiles are retrieved by modeling the atmospheric transmission in the observing layers (see in details [5]). Equation (1) shows the need to add stray light as additional parameter in the synthetic spectra of transmission.

The new method allowed separating the partly absorbed star light (S_{orig}) and stray light emissions before the retrieving process of gas concentration. The star signal is restored using a damped Richardson-Lucy iterative algorithm [7]. Equation (2) describes deconvolution iteration process of observing spectrum from the known PSF function (f_{PSF}) and binning factor (f_{bin}). The process starting from approximation $S_{orig} = S_{obs}$ gives original stray light ($S_{str.\ light}$) spectra in the end.

$$S_{obs} = f_{bin}\left(f_{psf} S_{orig} + S_{str.light}\right) \quad (2)$$

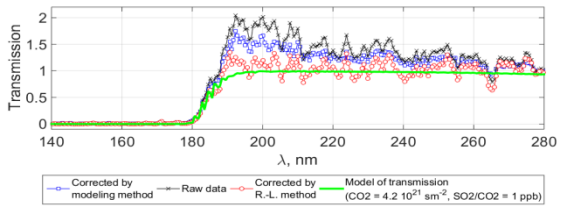

Figure 3: Example of the observation where R.-L. algorithm improves the result (2111A01, 109 km).

It takes ~40 iterations (with acceleration techniques) to reach the good estimation of original spectrum without adding any hypothesis of atmosphere composition and structure.

4. Summary and Conclusions

The new method of data processing allowed distinguishing the different sources of stray light in transmission spectra at UV stellar occultations. Thanks to this method one can extract UV emissions independently on gaseous absorption features.

Extra light illuminated the matrix of the SPICAV instrument had 3 distributed sources: NO and Lyman-a emissions and sun illumination. That provides more data with good vertical resolution to study behaviors of the emissions.

Acknowledgements

D. Evdokimova and D. Belyaev acknowledge support of the RSF grant #16-12-10453. We would like to thank our LATMOS colleagues for their kind collaboration. J.-L. Bertaux acknowledges support of the Russian government grant #14.W03.31.0017

References

[1] Bertaux J.-L. et al.: SPICAV on Venus Express: Three spectrometers to study the global structure and composition of the Venus atmosphere. Planet. Space Sci., Vol. 55, pp. 1673-1700, 2007.

[2] Royer, E., Montmessin, F., Bertaux, J.-L. : NO emissions as observed by SPICAV during stellar occultations. Planet. Space Sci., Vol. 58, pp. 1314–1326, 2010.

[3] Chaufray, J.-Y., et al.: Hydrogen density in the dayside venusian exosphere derived from Lyman-a observations by SPICAV on Venus Express. Icarus, Vol. 217, pp. 767–778, 2012.

[4] Chaufray, J.-Y., et al.: Observations of the nightside venusian hydrogen corona with SPICAV/VEX. Icarus, Vol. 262, pp. 1–82, 2015.

[5] Belyaev, D., et al.: Night time distribution of SO2 content in Venus' upper mesosphere. Icarus, Vol. 294, pp. 58-71, 2017.

[6] Montmessin, F., et al.: A layer of ozone detected in the nightside upper atmosphere of Venus. Icarus, Vol. 216, pp. 82–85, 2011.

[7] Richard L. White.: Image restoration using the damped Richardson-Lucy method. The Restoration of HST images and spectra II. Space Telescope Science Institute, 1994.